THE GROWTH OF FATIGUE CRACKS IN A TURBINE SHAFT STEEL UNDER MIXED MODE I AND III

BY

RIADH ABDULLA MOHAMMED

A Dissertation Submitted to the University of Sheffield for the Degree of Doctor of Philosophy in the Faculty of Engineering

Department of Mechanical and Process Engineering

University of Sheffield

January 1993

To the memory of my late friend

Emad Al-Jadder

PREFACE

The work presented in this dissertation is based on the findings of research performed in the Mechanical and Process Engineering Department of the University of Sheffield.

The content of this dissertation is original except where specific references are made to other work. No part of this thesis has been submitted to any other University for a degree.

R.A.Mohammed

January 1993

Acknowlegdements

I would like to thank The Ministry of Oil, Baghdad, Iraq, for their financial support and scholarship, for without it this research would not have been possible.

My thanks are due to the Head of Department of Mechanical and Process Engineering for the use of departmental facilities. My thanks are also due to NEI Parsons Ltd., Newcastle-upon Tyne and IRD, Newcastle Upon Tyne for the supply of the specimens.

I would like to express my gratitude to my supervisor Dr. J. R. Yates for his invaluable help, encouragement, guidance and fruitful discussions during the time of this research. I am also grateful to Professor K. J. Miller for his encouragement, attitude and valuable advice and also for the use of equipment in the SIRIUS laboratories.

I would like to express my gratitude to Dr. M. W. Brown for the several sessions of discussion, advice and for devoting his time to answer any query or question. My thanks are also to Dr. E. R. de los Rios for his help in the fractography work.

My thanks are also due to all secretarial and technical staff for their help, especially Mr. J. Smith for manufacturing specimens, Mr J. Goodliffe for his electrical work and Mr. M. Wild for his photographic work.

I am indebted to my close friend Dr. M. A. Kamala for his infinite support and help in all difficulties, and to all my friends and postgraduate students for their support and lively discussions.

My greatest gratitude goes to those who suffered most and sacrified for this research, my loving wife Layla and my children Ashraf and Zina, whose support was most needed and granted in the hardest of times.

SUMMARY

Low pressure steam turbine shafts and other rotating machinery invariably contain design stress concentration features, such as notches, grooves and slits. These shafts are subject to selfweight bending and steady state torque during operation. Some of these manufacturing features could initiate fatigue cracks which may cause failure if left to propagate.

In this research, fatigue crack growth of 3.5%NiCrMoV steel was studied on specimens taken from a low pressure steam turbine shaft. Three point bend specimens were used to establish the threshold for fatigue crack growth of this material under slit and precracked conditions. Circumferentially slit round specimens have been used to study the mode III fatigue threshold and crack growth behaviour. Angled slit rectangular specimens were used to study and investigate the failure conditions in mixed mode I & III loadings.

Three different stress ratios were used to determine the effect of R ratio on the threshold and fatigue crack growth in mode I, mode III and mixed mode I & III loadings. Two slit angles 45° & 60° were used to investigate the effect of the $\frac{K_{III}}{K_I}$ ratio on the threshold and crack growth rates in mixed mode I & III.

The results of these tests were analysed to achieve the previously stated aims of this study and lead to the conclusion that crack propagation in mixed mode I & III occurred by a mode I mechanism when the mode I threshold stress intensity factor has been exceeded. A new procedure to analyse the mode I crack growth in the mixed mode I & III tests was established by, first, finding equations to calculate the value of the changing crack angle with respect to the crack length and, second, to use these values in calculating the local mode I stress intensity

factor to establish the threshold conditions and to achieve equations to represent the whole crack growth rate. Finally the threshold stress intensity factor was linked to crack growth behaviour to devise empirical equations that represent crack growth under mixed mode I & III conditions.

A new model to predict the crack path from the crack length was developed, and the effect of the slit angle on the crack initiation and growth rate in mixed mode I & III was established.

Contents

List of Tables

Nomenclature

a	Crack length
B	Thickness
d	Mode III specimen diameter
$\frac{da}{dN}$	Crack growth rate
E	Young modulus
G	Strain energy releases rate
K_{cl}	Stress intensity factor at which crack starts to open
K_{eff}	Effective stress intensity factor
K_I	Mode I stress intensity factor
K_{Ith}	Mode I threshold stress intensity factor
K_{II}	Mode II stress intensity factor
K_{III}	Mode III stress intensity factor
K_{max} and K_{min}	Maximum and minimum stress intensity factors
ΔK	Stress intensity factor range
K_{Ith}	Mode I threshold stress intensity factor
K_{th0}	Threshold stress intensity factor at R = 0
K_{IIIth}	Mode III threshold stress intensity factor
l	Separation of p.d. reference leads
m	Exponent in Paris crack growth equation
M	Bending moment
N_c	Number of cycles
r_p	Radius of plastic zone
r_N	Radius of notch root
r_y	Plastic zone depth

R	Stress ratio
s	Separation of p.d. leads across the crack
t	Thickness of three point bend specimen
T and T_L	Applied and limit torques
V_r	Reference potential drop
w	Width of three point bend specimen
α	Crack growth angle
γ	Shear strain
γ	Material constant
Γ	Plastic strain intensity
ϵ_e	Strain
τ_y	Ultimate shear stress
υ_e	Elastic Poisson's ratio
υ	Poisson's ratio
θ	Slit angle of three point bend specimen
σ	Stress
σ_1	Maximum principal stress
σ_y	Yield stress
β	Aspect ratio
ϕ	Twist angle of branch crack

Subscript

$max.$	Maximum
$min.$	Minimum

Abbreviations

CTD	Crack tip displacement

CTS	Compact tension specimen
CTOD	Crack tip opening displacment
EDM	Electric discharge machine
EPFM	Elastic plastic fracture mechanics
LEFM	Linear elastic fracture mechanics
PSBs	Persistent slip bands
TPB	Three point bend specimen
UTS	Ultimate tensile stress

Chapter 1

Introduction

Rotating shafts such as turbo-generator rotors are very complex and heavy equipment. They are used to drive large pumps to push oil in main transfer lines, which travels for several thousands of miles through many stages. They are also utilized for electrical power generation and transmission shafts for automotive use.

Each large gas or steam turbine set with its attached pump or generator set may be up to 60 metres long and rotate at more than 6000 rpm to produce a high pressure inside the oil main pipelines, or a 50 Hz electrical current supply. A typical gas or steam turbine would consist of several rotors and stators. The rotors are attached to the main shaft which has to support its own weight as well as the weight of the rotors. The shaft itself is supported by two journal bearings and kept in place by thrust bearings. Each turbine consists of a high pressure (HP), an intermediate pressure (IP) and several low pressure (LP) turbines, see Fig.(1.1). These machines are often subjected to transient high amplitude torsional oscillations which may severely limit the useful life of the equipment.

Metal fatigue, which could be defined as fracture by progressive growth of a crack under variable cyclic loads, is one of the main concerns of the turbine designer, manufacturer and operator. It is considered as one of the main causes of failure of components during operational life, and can determine the life of many components. Cracks will be initiated and developed when the fatigue threshold conditions have been exceeded.

In the oil pumping and the electricity generating industries there is a great demand for a better understanding of the possible fatigue failure of the turbine shaft or other rotating parts; it is also a very costly business. The cost of the failure can run into millions of dollars. During normal operation, the shaft is subjected to self-weight bending and a steady state torque. However immediate high speed closure after an electrical fault may cause large transient torques in the shaft. Also the shaft will have to supports its own and other rotating disc weights which are attached to it during shut down periods.

1.1 Objectives of this research

The aim of this research is to have a better understanding of fatigue failure in rotating machinery due to the effects of cyclic torsion and bending load. The material used in these tests was $3.5\%NiCrMoV$ steel taken from an actual LP rotor shaft steel provided by NEI Parsons Ltd. of Newcastle upon Tyne.

A series of tests were conducted to provide and establish in order to determine the following objectives:

- The threshold conditions of the material used.

- The effect of stress ratio (R) on the thresholds of mode I, mode III and mixed mode I & III.
- A method and/or a procedure capable of studying the crack growth rate in mixed mode (I & III).
- The effect of the slit angle on the initiation and growth of a crack in mixed mode (I & III).
- The changes in crack growth angle with respect to crack extension or length.

A rectangular cross section specimen with a central slit was used for pure mode I tests. A cylindrical specimen with a slit in the centre was used for mode III tests. A rectangular cross-section specimen with an angled slit was used to determine the failure conditions in mixed mode (I & III) loading.

1.2 Thesis layout

Previous work and a literature review of theories of fatigue failure conditions concerned with this research, such as the threshold conditions, crack growth rate and the effect of stress ratio on the threshold reported by other researchers are discussed in Chapter Two. Failure criteria are also reported in Chapter Two.

The present authors research programme is described in Chapter Three. The experimental equipment and test rigs, used for this research, are described in Chapter Four. The material, specimen geometry and experimental procedure are also reported in that chapter. Results and observations are given in Chapter Five which also include some of the fractographic studies of the broken specimens.

The results are analysed in Chapter Six and discussed fully in Chapter Seven. Previous research results were compared to the data obtained from this study and different failure criteria were considered.

Chapter Eight contains the summary of the conclusions drawn from this research while Chapter Nine describes proposals for further work.

Chapter 2

Literature Review

2.1 Historical background

Ever since the beginning of the industrial revolution, which transferred Britain from an agricultural nation to a mainly industrial one, mechanical failure was considered to be one of the main obstacles in running and maintaining the machinery. Some engines could run smoothly for long periods with hardly any problem, and suddenly fail for no apparent reason, due to fracture in one of its components. It was first reported to be caused by ageing or tiredness, and since then, the word fatigue was used to describe a metal that fails due to repeated or cyclic load which causes the material to change gradually till failure takes place resulting in losses financially as well as in human terms.

Research in the topic of failure due to fatigue started as early as 1820s and still going on with some drastic failures still occurring such as the Comet aircraft in 1950s, the D.C 10 airliner in 1979 and the twin engine transport heli-

copter in Scotland in the late 1980s.

2.2 Crack initiation and propagation

Two of the most likely areas where a crack might initiate are the surface and region with mechanical and metallurgical defects. The surface grains are the only grains which are not supported by neighbouring grains and also they are more susceptible to the environmental attack than any other group of grains. So it is clear that any area that combines the above two weak points could be the starting point for a crack to initiate, such as a notch at the surface.

Metallurgical defects in a metal could cause initiation which leads to failure of the component. During cyclic stressing fatigue tests, crack initiation is generally preceded by localization of plastic strain (Brown and Miller 1973). This gives rise to the slip planes which form within surface grains and whose weakest slip planes are favourably oriented with respect to the applied stress system. As cycling continues, these slip lines widen and form slip bands, which were first noticed by Ewing and Humphrey (1903). Microscopic discontinuities or slip steps on the surface are created as a result of the presence of these slips bands. Lynch (1978) observed that in the case of uniaxial loading, if these planes intersect the free surface at 45°, intrusion and extrusion may occur.

As the test proceeds, some slip bands become more important than others due to their persistent occurrence and that is where a fatigue crack may

eventually initiate Fig.(2.1) (Wood 1958).

Although slip bands are not the only source of crack initiation, other metallurgical defects could be more favourable such as non-metallic inclusions which could cause the crack to initiate due to either the inclusion itself suffering fatigue before the actual grains of the metal or it may cause a debonding of the inclusion from the surrounding grains (Broek 1978).

Cracks may also initiate at grain boundaries where they are likely to be more susceptible to environmental effects, also they could be the weakest point where the grain boundaries are defected due to their incompatibility (Guiu et al 1982).

Finally, most of the cracks are formed due to more than one active defect, but this defect is dependent on the microstructure of the metal and the amount of local plastic strain to which the grain or inclusions are subjected to.

For a crack to initiate and propagate due to fatigue damage, cyclic plastic deformation is essential. Since elastic deformation is fully reversible and therefore can cause no damage, only plastic deformation can cause irreversible damage to the material which is essential for a fatigue crack.

Normally a fatigue process consists of three stages a) cyclic softening b) crack initiation and finally c) crack propagation till failure of the material takes place. It is normal to divide fatigue life time into the following stages:

1) Initiation or birth of fatigue crack.

2) Stage 1 crack growth, where the cracks lie along the active slip planes,

which generally coincide with the maximum shear plane which lies at 45° to the loading direction.

3) Stage II crack propagation which takes place after the crack extends across two or three grains and it is normally accompanied by a change of direction from the initial 45° to a direction perpendicular to the maximum tensile stress Fig.(2.2) (Brown 1988).

4) The final failure or rupture which takes place after the crack has extended so much that the material can not take the load any more which causes it to fail suddenly causing drastic losses if not detected earlier.

2.3 Linear Elastic Fracture Mechanics (LEFM)

Propagating cracks are divided into two types, short and long cracks. In this research our concern is mainly with long cracks which are defined to be of length which is more than 0.5 mm long and therefore LEFM can be applied in the assessment of the crack growth (Miller 1982). For LEFM it is important that elasticity conditions in the crack tip zone dominate, i.e. the plastic zone does not greatly perturb the crack tip elastic stress field.

The conditions of LEFM must be satisfied and its limitations must be avoided. It is a well known practice that LEFM can not be applied to cracks initiated at notch roots and on physically short (micro and macroscopic) cracks. Another limitation to the LEFM application is that it can not model situations where plasticity is appreciable. Therefore the main requirements for a valid LEFM - type test is the plastic zone which is created by the singularity condition at the

crack tip must be very small in relation to the elastic state Fig.(2.3)

i.e $r_p \leq \frac{a}{50}, \frac{w}{50}, \frac{B}{50}$

where

r_p is the plastic zone depth.

a is the crack length.

w is the width of the specimen.

B is the thickness of the specimen.

This condition may be satisfied by the limitations imposed on the slit depth of the specimen compared to the diameter of the mode III specimen and the width of the three point bend specimen.

The application of the LEFM has provided an empirical basis for describing the phenomenon of fatigue crack propagation. In a situation, above the threshold, when a load is applied to a sharp precracked or slit specimen (crack tip radius is zero), the crack will open and a plastic zone is created at the crack tip causing the crack to blunt and claiming a new surface at the tip of the crack. When the load is removed, the crack will close and the new claimed surface will be the new extension of the crack.

LEFM analysis of the crack growth permits a direct and advantageous comparison between small laboratory specimens and large structures when the stress intensity factor terms (which incorporates the geometry factor and the loading factor) are identical in both cases. If two cracked bodies with different loads have the same stress intensity factors then the crack tip stress fields are identical.

2.4 Stress intensity factor

There are three basic modes of relative displacement of the cracked surface, which can occur, these are shown in Fig.(2.4). The preferred mode of crack growth depends on the type of loading. These modes were identified by Irwin (1957) as:

Mode I which is called the opening mode in which the crack surfaces move directly apart and loads are applied perpendicular to both the crack front and faces. It is related to stage II of the fatigue crack extension.

Mode II which is a shear loading, which relates to stage I of fatigue crack extension and it is produced when the load is applied perpendicular to the crack front in the plane of the crack.

Mode III is the antiplane shear loading in which crack surfaces remain in the crack plane, but move parallel to the crack front.

For each crack surface displacement mode there is a particular elastic stress field associated with the crack in the vicinity of its tip. This stress field is best explained by a term known as the stress intensity factor (K) which was first introduced by Irwin (1957). The suffix I,II,III represent the modes of the stress intensity factor. In mode I, when a remote stress (σ) is applied to a crack of length (2a) located in the centre of an infinite body, will cause the stress intensity factor K_I to rise to a value given by the relationship

$$K_I = F(\frac{a}{b})\sigma\sqrt{\pi a} \tag{2.1}$$

where $F(\frac{a}{b})$ is a correction factor depending on the geometry of the specimen. This relationship is only approximate as it is only the first term of a long expres-

sion.

Investigation of the crack growth in an elastic field was started in 1953 by Head and then by Frost and Dugdale (1958) and continued by McEvily and Illg (1958) and then by Liu (1963). It was Paris and Erdogan (1963) who brought their works together and concluded that the stress intensity factor which provides a complete description of the stress field around a crack tip, should control the rate of fatigue crack propagation. This relationship was expressed in the equation known as the Paris Law, which confirms that the crack growth increment per cycle ($\frac{da}{dN}$) is principally a function of the alternating stress intensity factor ΔK

$$\frac{da}{dN} = A(\Delta K)^m \qquad (2.2)$$

where $\Delta K = K_{max} - K_{min}$ and A and m are constants dependent on the material, temperature, microstructure and stress ratio. The value of m is usually $2 \leq m \leq 5$. This relationship is widely used since it exposes the most important fact of the self similarity of the fatigue crack growth process. However it is only valid in the linear part of the fatigue kinetic diagram Fig.(2.5) (Ritchie 1979).

In Fig (2.5), the curve is divided into three regions. In region C, there is a large effect of microstructure which explains the deviation of the curve from linearity and by the time the component reached this stage of crack growth, its life is nearly at the end, while in region B, the straight line could be adequately described by the Paris Law. In the first stage, stage A the crack extension rate falls to around one atomic distance per cycle (i.e 10^{-7} $mm/cycle$). Due to the low level of the applied stress, crack growth in this region is reported to be intermittent (Stanzl and Tschegg 1980) which gives support to the Hornbogen & Gatz (1976) theory that cracks are subject to the microstructural variation.

Other workers did not agree that the stress intensity factor is the best parameter to describe the stress field around the crack or to be used as a parameter to monitor the initiation and the growth of the crack at different states. Hay and Brown (1986) in their work on the initiation and early growth of fatigue cracks from a circumferential notch loaded in torsion, claimed that the mode III stress intensity factor can not provide a unifying parameter for crack propagation at different temperatures and reasonable correlation was obtained by using an elasto-plastic strain intensity factor that characterizes mode III deformation close to the crack tip.

2.5 Fatigue threshold behaviour

In simple terms we can define the fatigue threshold as the boundary between no crack growth and crack growth. In practice the threshold is determined from the highest stress intensity factor at which the detectable crack growth rate is less than 10^{-10} m/cycle i.e less than one atom spacing per cycle (Ritchie 1979). Pook (1985c) defined the fatigue crack growth threshold as 'the minimum value of ΔK_I needed for continued stage II of fatigue crack growth under steady state conditions'. The steady state conditions means that the crack must have grown for some distance, this will restrict the definition to long cracks. A better definition was given by Pook (1985c) as 'the value of ΔK_I corresponding to a steady - state crack growth rate of 10^{-11} m/cycle' which is slightly less than one lattice spacing per cycle.

Little is known from a mechanistic or metallurgical point of view about the micro-mechanisim of the crack propagation at near threshold growth rates,

and furthermore there is still a substantial lack of reliable engineering data. This information is extremely important for design purposes when determining the life time of a component which can withstand an extremely high frequency with low amplitude loading for a life time of 10^{10} cycles over 20 years. In a high speed rotor of a steam turbine operating at 3000 r.p.m, a crack growth rate of the seemingly insignificant near threshold growth rate of 3×10^{-12} m/cycle could produce a crack length of 30 mm during the life time of the rotor, which could clearly result in catastrophic failure. In fact knowledge of low growth rate fatigue crack propagation data and in particular, information regarding the existence of the threshold stress intensity factor, has been shown to be essential in the analysis of such problems as cracking in turbine blades, turbine shafts and alternator rotors(Tschegg 1982).

2.5.1 Fatigue threshold under mode I

Lindley (1981) and Ritchie (1979) stated that threshold may be defined as the value of mode I stress intensity factor range (ΔK_{th}) below which fatigue crack remains dormant or grows very slowly at an experimentally undetectable speed.

Mode I fatigue thresholds are usually approached using a load shedding technique as recommended by ASTM standard E647. This procedure involves successive load reductions of not more than 10%. Larger reductions in load are liable to give premature crack arrest from retardation effects owing to residual plastic deformation. The crack is allowed to grow a distance equal to several times the plastic zone generated at the previous (higher) load level to minimise these retardation effects caused by changes in load.

Ritchie (1979) stated that the threshold intensity (ΔK_{th}) should represent the alternating stress intensity where the growth rate is infinitesimal and went on to review the factors that could influence the near threshold growth rate such as mean stress which does not influence the midrange growth rate (growth rate which follows Paris Law) while near threshold propagation is generally extremely sensitive to load ratio R or mean stress. He concluded that near threshold behaviour is particularly sensitive to microstructural factors such as cyclic strength grain size, grain boundary composition and structure.

2.5.2 Fatigue threshold under mode III

Experimental studies on fatigue crack threshold and propagation in mode III (antiplane shear) are rather rare in the literature especially if they are to be compared to the vast amount of research published for fatigue crack growth under mode I (tensile opening) conditions.

Most research on mode III fatigue is carried out using circumferentially notched round bar specimen under torsional loading (Hourlier et al 1978 and 1982). Although this specimen is simple in geometry, it is extremely prone to misalignment problems which induce undesired bending moments and hence cause asymmetrical crack growth. Ritchie et al (1985) avoided this problem through a specially designed torsional Woods metal grip in their study of mode III fatigue crack growth in various metals. It was concluded that mode III crack growth rates are related to the cyclic crack tip displacement (ΔCTD_{III}) or plastic strain intensity range ($\Delta\Gamma_{III}$) provided friction abrasion and interlocking between sliding fracture surfaces was minimised by the application of small superimposed tensile mean loads.

The crack front in a pure mode III loading is a closed curve and this means that the crack front can not rotate and remains continuous. In a macroscopic sense the crack remains confined (Tschegg 1982) to its initial plane Fig.(2.6). Pook (1985a) stated that for pure mode III a 'twist' fracture surface is sometimes observed, at zero mean load (R = -1) this consists of intersecting mode I facets on a complementary planes at ($\pm 45°$) to the macroscopic crack plane Fig.(2.7).. True mode III crack growth in which the fracture surfaces have a rubbed, featureless appearance is otherwise observed. It is not clear whether mode I facets do not form, or they form and then destroyed by rubbing; the former is assumed in Ritchie et al (1982), Hurd and Irving (1982) and Tschegg (1982).

For a given applied loading, the growth rates of both types of crack diminish rather than increase with increasing crack length due to interference between the crack faces, and a transition commonly occurs from a microscopically flat to factory roof type of fracture surface. This transition has been taken to define false mode III threshold for macroscopically flat fatigue crack growth, the value of which is in general considerably higher than the fatigue threshold which corresponds to the factory roof cracking. Hellier et al (1985), Pook and Sharples (1979) suggested that from consideration of mode I branching at a mode III crack the ratio of this latter mode III threshold to the mode I threshold for a given material should be 1.35 theoretically.

Hay and Brown (1985) applied a 3.0 $MPa\sqrt{m}$ mode I stress intensity factor to reduce the crack flank interference and to achieve the maximum crack growth for the applied load. In their constant angular deflection condition tests, they found that cracks were initiated in the form of a 'factory roof' by a mode

I mechanism at approximately 45° to the plane of the notch. The factory roof cracks propagated radially in these 45° planes until the applied stress intensity factor increased to a value where the mode of cracking changed to a mode III type, which gave a flat fracture surface. If the initial applied load was high enough, a flat fractured surface would have been produced across the entire cross section. The application of the axial load did not affect the major features of the fracture surfaces, but reduced the amount of surface rubbing.

The same results were obtained in their tests of constant stress intensity factor conditions, where the applied torque was reduced as the cracks propagate. The fractured surfaces were flat when the stress intensity factor was high and it was a factory roof facet shape when the stress intensity factor was low. The change from flat to a factory roof was accompanied by a reduction in crack growth rate, which gives the indication of a crack face rubbing preventing the full effect of the applied load being felt at the tip of the long crack. A similar procedure was used by Ritchie et al. (1985) in their mode III tests on AISI 4340, 4140, ASTM A469,and A470 Fig.(2.8). It was found that in pure mode III tests, the sliding crack surfaces remain in contact to such an extent that the broken ligament of the specimen is still able to carry torque and that is why they superimposed small static axial loads onto the cyclic torsional loads to separate the sliding crack surfaces. It was found that no interpretation was obtained from the results of a mode III test on annealed 4140 steel using the stress intensity factor as a parameter versus the fatigue crack growth rate as shown in Fig (2.9a), while the same test when repeated with the use of the small axial loading and using a plastic strain intensity range($\Delta\Gamma_{III}$) as a replacement to the stress intensity factor, a better interpretation was obtained that falls within a certain range as shown in Fig (2.9b). A unique relationship between mode III propagation rates

and ($\Delta\Gamma_{III}$) was found with minimum scatter over a wide range of growth rates when the same tests were performed on A469 and A470. A relationship was also found between crack tip displacement CTD_{III} and the plastic strain energy Γ_{III} for small scale yielding and is given as

$$CTD_{III} = 2\Gamma_{III} \tag{2.3}$$

At high crack fatigue growth rates and short crack lengths, the fatigue surfaces were observed to be microscopically flat (pure mode III) and as the cracks grow, the crack growth rate is reduced and a transition takes place from the microscopically flat surface to the factory roof surface. This transition process is claimed by Ritchie et al (1985) to be irreversible, as the torque is increased to the previous levels, the factory roof mode does not revert to the microscopically flat mode. They concluded that if the crack tip displacement is taken as a base for comparison, mode I cracks were propagating at higher rate than the mode III. Crack extension was considered to occur via the coalescence of voids initiated at inclusions in the immediate vicinity of the mode III crack tip by mode II shear parallel to the crack front. Hourlier et al (1985) used notched round bar at load ratio equal to zero resulted in fatigue crack inclined in one direction at an angle (α) joined by regions of ductile fracture surfaces and concluded that fatigue crack propagates in a direction in which the crack growth rate is maximum.

Although determination of mode I fatigue threshold is widely accepted, mode III threshold condition determination is not as readily defined as mode I. Tschegg (1982) considered the true mode III threshold to be the lowest stress intensity factor range at which mode III flat crack growth occurred. At lower applied ΔK_{III} value crack propagation occur by mode I facets. Hellier et al

(1985) defined the mode III threshold as the boundary between no crack growth and facetted crack growth.

2.5.3 Fatigue threshold under mixed modes I and III

There is no generally accepted definition of fatigue threshold under mixed mode loading. The investigation of fatigue threshold under mixed modes has been carried out under four different methods, Pook (1979) investigated it using a three point bend specimen with an angle slit. The angle was varied in order to obtain different ratios of $\frac{\Delta K_I}{\Delta K_{III}}$. Yoshioka et al (1984) used a centre cracked plate specimen having an inclined crack ($\beta = 0, \frac{\pi}{8}, \frac{\pi}{4}$) as shown in Fig.(2.10), while Yates and Miller (1988) used a circumferentially slit round bar with a special loading frame Fig. (2.11) that allows specimens to be loaded in four point bending with two outer loading points displaced either side of the specimen axis. The distance of the outer loading points from the specimen centre line governs the applied torque and the separation of the two centre supports governs the ratio of torque to bending moment. Full details of the frame is given in Yates (1987). Nayeb-Hashimi et al (1982) investigated fatigue thresholds under mixed modes I and III using circumferentially notched cylindrical specimens subjected to cyclic torsion with a superimposed static loading. They claimed that the superimposed K_I values did not influence crack growth rates of mode III as long as the super imposed K_I does not exceed 70% of the K_{Ith}.

Hourlier and Pineau (1981) in their work on mixed modes I and III used a notched round bar with a cyclic mode and steady mode III loading on fatigue precracked specimens. They stated that ridges were observed running radially towards the centre of the specimen. These features correspond to the formation

of fairly regular sets of inclined facets connected by longitudinal radial planes. The inclined facets fractographic features are similar to those observed in mode I loading, while the longitudinal radial planes exhibit the features associated with ductile rupture and rubbing. Also a decrease in the fatigue crack growth rate in mixed mode I and III was reported compared to mode I growth rate and this decrease can reach two orders of magnitude. This decrease was associated with the crack closure phenomenon. They concluded that under complex mode loading a fatigue crack propagates in the direction in which the crack growth is maximum and that the crack growth rate is assumed to be controlled only by the local mode I component.

Hay (1983) used a notched bar specimen in his constant angular displacement test at high torque and reported the transition from the small factory roof facet to the flat mode III fractured surfaces which gives reason to believe that flat fractured surfaces are formed by pure mode III mechanism rather than rubbed mode I facets due to interface friction in the facet surfaces.

It is a known fact that the cracks in a mixed mode loading tend to grow in mode I. This observation can not be proved in the strict sense of the word. Pook (1985a) confirmed this tendency for proportional loading at both macroscopic (1 mm) scale and a smaller (0.1 mm) scale. At the macroscopic scale the tendency appears to be suppressed if the crack front is a closed curve.

The results of these methods did not coincide with each other as the crack in a circumferentially slit round bar would tend to be confined to the plane of the slit which means that the crack can not rotate and remains continuous, while the crack in the angle slit specimen can easily twist to the preferred mode I orientation. The path of this last orientation has not been predicted firmly yet.

Pook (1985a) concluded that the fracture surfaces of the mixed mode I and III test specimen showed that the initial crack growth was achieved by the formation of small mode I branch cracks which developed into a 'twist fracture'. This consisted of narrow mode I facets connected by irregular cliffs of predominantly mode III as crack growth proceeds. These facets tend to merge as the cracks grow. Pook (1985a) also stated that the event which controls the failure of the specimen is the propagation of mode I branch cracks.

Yoshioka et al (1984) who used several types of specimen to find ΔK_{Ith} concluded that the same value of ΔK_{Ith} was achieved for compact tension specimen with a fine saw cut as that of the electrical discharge machined slit as well as that of specimens with long fatigue cracks. They also found that the value of ΔK_{Ith} was approximately the same as the threshold value for mode III for a stress ratio of $R \simeq 0$.

Yates and Miller (1987) used the crack opening displacement of the inclined branch cracks to describe the mixed mode I and III fatigue threshold and concluded that the magnitude of the crack opening displacement in mode I direction governs the mode I crack growth in mixed mode I and III fatigue and that this failure criterion is independent of the specimen geometry.

So far, no single fracture mechanics parameter can describe the experimental mixed mode I and III threshold conditions satisfactorily on its own. However, ways of combining mode I and mode III fracture mechanics parameters might give a better understanding.

2.6 The effect of stress ratio on threshold fatigue

The effect of mean stress is often expressed in terms of the stress or load ratio (R). Stress ratio is defined as the minimum stress divided by maximum stress during the stress cycle (R= $\frac{\sigma_{min}}{\sigma_{max}}$.)

The effect of R ratio on crack growth is explained in terms of LEFM. Two categories could be used to explain the effect of mean stress on the threshold and crack growth. First is that if the amplitude of stress intensity factor is kept constant during the test and the mean tensile stress is increased, it will cause the maximum stress level to increase causing an increase in the crack growth. In terms of stress intensity factor a high stress ratio will lead to a high maximum stress intensity factor which means that the crack is more likely to propagate under the high value of the maximum stress intensity factor than a lower value.

The second category is the crack closure effect on the crack growth, and this is explained in the fact that it was noticed that some cracks remain closed even at stress intensity factors which are higher than the minimum value, causing the actual effective range of stress intensity factor to be reduced. If the effective range of stress intensity factor is to be considered as the only factor that controls the initiation and propagation of the fatigue crack growth, this will mean that the mean stress intensity factor level has nothing to do with the crack growth behaviour as long as the effective stress intensity factor range is kept constant through out the test. But experimental results have shown that the level of crack

closure is related to the level of the mean stress intensity factor, i.e

$$\Delta K_{eff} = K_{max} - K_{cl} \ = \text{function of } (K_{max}, K_{mean})$$

where K_{cl} is the stress intensity factor at which the crack starts to open. This means that the mean stress or R plays an important influence in the changing of the level of crack closure level. This subject will be taken in detail in the next section.

Numerous investigations of the influence of mean stress on the fatigue threshold and long life fatigue strength have been made. Ritchie (1979) indicated that although little influence can be seen for the midrange of growth rates, near threshold propagation is generally extremely sensitive to the load ratio. Studies in a wide range of steels and non ferrous alloys, tested in ambient temperature air, indicated that the value of ΔK_{th} is markedly decreased, and that propagation rates are increased, as the load ratio is raised within a range of R from 0 to 0.9.

Ibrahim (1989) in his work on 2024 -T3 aluminium alloy concluded that the threshold stress intensity range, ΔK_{th} decreases linearly as the positive stress ratio increases and as the magnitude of compressive peak stress decreases and that the intermediate crack growth rate, for a given value of ΔK, increases as the stress ratio increases and as the magnitude of the compressive peak stress decreases. He introduced a new formula for the crack opening stress level as a function of stress ratio, the R ratio values he used were 0, 0.2, 0.5, although his results did not coincide with similar equations proposed earlier by Schijve (1988) or Elber (1970) he managed to normalize the crack growth curves for various R to a single curve which made him believe that 2024-T3 aluminium alloy has a unique $\frac{da}{dN}$ vs ΔK_{eff} curve.

The influence of grain size and stress ratio combined together were studied by Cadman and Brook (1983) and Priddle (1978). Cadman during his tests on the effects of grain orientation and stress ratio R on ΔK_{th} in low alloy steel stated that the threshold decreased as the ratio increased, for both transverse and longitudinal cracks along the rolling direction. The threshold value for the transverse crack at values of R between 0.1 and 0.6 was lower than for the longitudinal crack. This was due to roughness induced closure while at higher R ratio, the longitudinal crack showed a lower threshold value than the transverse crack. This was caused by manganese sulphide stringers, because stringers represented an easy path for crack growth compared with the metal matrix. Priddle in his study on the influence of grain size on ΔK_{th} in 316 stainless steel at different R ratio found that ΔK_{th} was dependent on R ratio and grain size. When the same R ratios were used for coarse and fine grain materials it was found that ΔK_{th} was higher in the coarse grain than the fine grain material.

Yoshioka et al (1984) stated that ΔK_{th} under mode III is not affected by stress ratio R and is approximately constant, and can be regarded approximately equal to ΔK_{th} under mode I of the same material at stress ratio $R \simeq 0$. Their work on mixed mode I and III brought them to the conclusion that the value of ΔK_{th} is greatly affected by the mixed mode conditions.

Tschegg (1983) stated that in cylindrical circumferentially notched AISI 1018 steel specimens the fatigue crack growth rates based on effective mode III strain intensity values are not influenced by changing R values in the range from (-1) to (-0.02). However, the sliding crack closure influence increases, if the R ratios exceeds (-0.2). Nayeb-Hashemi et al (1983) in their study of torsionally loaded circumferencially notched cylindrical bars of A469 and A470 commercial

rotor steel stated that mode III fatigue crack growth rates were observed to be independent of R ratio at R = -1 and -0.5.

The relationship between ΔK_{th} and R could be represented as in Fig.(2.12). It is seen by many researchers that ΔK_{th} can not be a material constant. Schmidt and Paris (1973) explained the R dependence of ΔK_{th} by the mechanism of crack closure (see fig.2.13); they proposed to subtract from ΔK_{th} that part which is needed to open the crack. The stress intensity factor which just opens a crack during the loading part of the cycle K_{cl}, is taken as the transition point between excursions of compressive stresses and strains and excursions of tensile stresses and strains in the region near the crack front.

In recent years several methods were established to measure the crack closure, the most common method is the measurement of specimen compliance (Fleck 1990) using either a crack mouth gauge or back face strain gauge. This method assumes that crack closure actually takes place at certain stress intensity factor called K_{cl}. Taylor (1992) states that it is now well established that the crack closes gradually over a range of K during unloading. He goes on to say that the use of ΔK_{eff} which is defined as

$$\Delta K_{eff} = K_{max} - K_{cl}$$

is in fact equivalent to a simplified use of the energy balance method. He uses ΔK_{true} parameter which is calculated directly from the energy change with the load. It was concluded that ΔK_{true} remains constant with R ratio and appears to be the 'intrinsic' value of the threshold.

The crack closure was not measured in this research as it is impossible

to measure it in mode III tests and it is very hard to measure it accurately in mixed mode I & III. Also mode I tests were performed mainly on slit specimens, in order to establish mode I thresholds conditions essential for comparison purposes.

Schmidt and Paris (1973) proposed two equations to describe the relation between stress ratio and threshold value of stress intensity factor, one for a high value of R and the other for a low value. In general it was observed that ΔK_{th} decreases linearly as R increases, till R reaches a certain critical value, after which the threshold remains constant. Schmidt and Paris attributed this to the crack closure effect. If the stress intensity needed to open a crack ΔK_{cl} is assumed constant, then one might expect that there must be a certain portion of the stress intensity range above ΔK_{cl} called ΔK_o, necessary to produce crack growth at the threshold. If ΔK_o is assumed constant with changes in load ratio two distinct situation arise [see Fig.(2.14)].

For low load ratio - if $K_{min} \leq K_{cl}$, then

$K_{max} = K_{cl} + K_o$

Since R $= \frac{K_{min}}{K_{max}}$

then $\Delta K_{th} = K_{max} - K_{min} = K_{max}(1 - R) = (K_{cl} + \Delta K_o)(1 - R)$

i.e $\Delta K_{th} = \Delta K_{tho}(1 - R)$

where ΔK_{tho} is the threshold stress intensity at R = 0

For high load ratio, if $K_{min} \geq K_{cl}$ then

$K_{th} = \Delta K_o$ =constant

and $K_{max} = \frac{\Delta K_{th}}{1-R} = \frac{K_o}{1-R}$

therefore $\Delta K_{th} = K_o$

These two relations would predict forms of ΔK_{th} versus R and K_{max} versus R as shown in Fig.(2.14).

Other empirical equations describing the effect of R on ΔK_{max} have been proposed by other researchers such as Klensil and Lukas (1972) which is widely used for steels

$$\Delta K_{th} = \Delta K_{tho}(1 - R)^{\gamma}$$

where ΔK_{tho} is the threshold stress intensity at $R = 0$ and γ is a material constant its value ranges 0 - 1.

A relationship similar to Schmidt and Paris previous equation was suggested by Beevers (1981).

$$\Delta K_{th} = \Delta K_{ith} + \Delta K_{cth}$$

where $\Delta K_{ith} = \Delta K_{max} - \Delta K_{cl}$

$$\Delta K_{cth} = \Delta K_{cl} - \Delta K_{min}$$

ΔK_{ith} is essentially ΔK_o for $\Delta K_{min} \leq \Delta K_{cl}$

and for $K_{min} \geq K_{cl}$

$$\Delta K_{th} = \Delta K_o$$

Xiaopeng (1990) derived a relationship different to the previous one in value of ΔK_{th} but similar in the expression. This general expression, for the variation of ΔK_{th} with R is given as :

$$\Delta K_{th} = \Delta K_{tho}(1 - R)^{\frac{1}{2}}$$

The values of ΔK_{th} obtained from this equation were compared to the

results obtained via a practical experiment, it was found that a good agreement exists between the two values for metal such as EN3A, En24 and D6C while a slight difference was shown for Ti-6Al-4V plate as shown in Fig(2.15 a & b). This equation coincides with Klensil and Lucas if the value of γ was taken to be 0.5. Lindley (1981) gave the values of γ for several types of steel in his research on threshold. Another equation was derived by McEvily and Gregor (1977) and given as :

$$\Delta K_{th} = \left(\frac{1-R}{1+R}\right)^{\frac{1}{2}} \Delta K_o$$

The effect of stress ratio R on the crack growth was considered by the Japanese Welding Engineering Society (JWES) and are given in their standard 2805 which offers a formula to substitute for the Paris law (Allen 1980)

$$\frac{da}{dN} = C\left(\frac{1+R}{1-R}\right)(\Delta K)^m$$

$$= \frac{C}{2} K_{mean}(\Delta K)^{m-1}$$

This formula indicates that the crack growth depends on the mean stress value.

As much as some workers insist that R has a great effect on the threshold of fatigue cracks, others such as Maddox (1975) concluded that crack propagation in steel are not greatly affected by changes in mean stress provided that stresses are always tensile. Others showed a K_{Imax} dependency at R ratios. This dependency is not universal, Beevers et al (1975) results showed a clear dependency on K_{Imax} at R ratios for medium carbon - manganese steel as long as R ratio is below 0.5, also Suresh and Ritchie (1983) and Ritchie et al (1980) found that for a pressure vessel steel, the fatigue crack growth threshold changes with mean stress depended on the environment such as oxide induced crack closure.

It is clear from most of the published data and work on the effect of load ratio on the crack growth that there is no clear criterion of any load ratio as most the data are not sufficient to determine this criterion.

2.7 Effect of crack closure

The concept of crack closure was first described by Elber (1970) who proposed that premature contact between the crack faces can occur even during the tensile portion of the fatigue cycle because of the permanent residual displacements, arising from prior plastic zones left in the wake of growing fatigue crack. Since the crack can not propagate while it remains closed, the net effect of closure is to reduce the applied ΔK value to some lower effective value (ΔK_{eff}) actually experienced at the crack tip.

Therefore $\Delta K_{eff} = K_{max} - K_{cl}$

Where K_{cl} is the stress intensity factor at which the two fractured surfaces first come into contact during the unloading portion of the fatigue cycle.

The stress intensity factor range is given by

$$\Delta K = K_{max} - K_{min}$$

Elber (1971) postulated that fatigue crack propagation rate is governed by the effective value of the stress intensity factor range ΔK_{eff} such that

$$\frac{da}{dN} = C(\Delta K_{eff})^m$$

$$= C(U\Delta K)^m$$

where $U = \frac{\Delta K_{eff}}{\Delta K} = \frac{K_{max} - K_{cl}}{K_{max} - K_{min}}$

which is the fraction of the cycle during which the crack is fully open.

Elber suggested the following relationship to determine the value of U.

$$U = 0.5 + 0.4R \qquad \text{for} \quad -0.1 \leq R \leq 0.7$$

Smith, Watson and Topper (1970) proposed their so called SWT parameter which describes the relationship between the effective stress intensity factor range and the stress ratio, based on Walker's parameter (1970), and it is given as

$$\Delta K_{eff} = \frac{\Delta K}{[2(1-R)]^{\frac{1}{2}}}$$

If the value of ΔK is kept constant, and the value of stress ratio R is changed from R = 0 to R = -1, the value of ΔK_{eff} for R = 0 is greater than that of R = -1 by a factor of $(\sqrt{2})$. It also follows that the crack growth rate for R=0 is twice that of R = -1. This result is in agreement with some experimental results by Qingzhi (1984) and some finite element analyses by Newman (1976).

Suresh and Ritchie (1983) discussed the factors that introduce crack closure among them are, as shown in Fig.(2.16), the following factors:

2.7.1 Oxide induced crack closure

The concept of oxide induced crack closure, according to Ritchie et al (1980), Stewart (1980) and Suresh et al (1982), is based on the phenomenon that at low load ratios, near threshold growth rates are significantly reduced in moist environments compared to dry environments, due to the presence of corrosion deposits on crack faces. Such oxide debris provides a mechanism for enhanced

closure by resulting in an earlier contact between the fractured surfaces through an increased closure stress intensity (K_{cl}). The formation of corrosion deposits and its process is promoted by:

a) Small crack tip opening displacements (CTOD) (Suresh and Ritchie 1982).

b) Highly oxidizing media, such as water (Suresh and Ritchie 1983)

c) Low load ratio, which facilitate repeated contact between the fractured surfaces through small CTOD values (Suresh and Ritchie 1982).

d) Rough fracture surfaces, which at low ΔK values, promote relative sliding and rubbing between mating crack surfaces (Suresh and Ritchie 1982).

e) Lower strength material (Ritchie et al 1980)

Ignoring any other effect, such as plasticity and hysteresis losses, Suresh and Ritchie (1983) developed an expression to evaluate the crack closure stress intensity K_{cl} at the crack tip for plane strain conditions as shown in Fig (2.17) to be

$$\Delta K_{cl} = \frac{d_o E}{4\sqrt{\pi l}(1-\upsilon^2)}$$

where d_o is the maximum excess oxide thickness, $2l$ the location behind the tip corresponding to the oxide formation and $\frac{E}{1-\upsilon^2}$ is Young's modulus in plane strain. However this expression is capable of providing a crude description of the extent of oxide - induced closure.

2.7.2 Roughness induced crack closure

The roughness of a crack is caused by the extension of the crack through several grains. Near threshold crack growth proceeds by propagation along slip bands

on active slip planes (Venables, Hicks and King 1983). The sharp changes in the crack path which this necessitates on reaching grain boundaries produces rough fracture surfaces, the roughness depends on the grain size. The mode of growth involves both tensile (mode I) and shear displacement (mode II) components in the slip band in which the crack is propagating. As seen in Fig.(2.18), when the cycle is at K_{min} the crack is wedged open by non mating fracture facets. Large compressive stresses are generated across regions in contact, leading to fracture surface damage. When the forces applied are just above ΔK_{cl} the fracture surfaces have separated and the crack propagates in the slip band by a mixture of mode I and mode II opening. By K_{max} some irreversible deformation will have taken place in the slip band. When the load is reduced to just below K_{cl}, the crack is again wedged open with compressive stresses across the mating regions just starting to build up, preventing the surfaces from sliding over each other. The crack tip remains in the same state for the part of the cycle from K_{cl} through K_{min} and back to K_{cl} so it experiences only a reduced $\Delta K = K_{max} - K_{cl}$.

Suresh and Ritchie (1982) developed a simple, two dimensional geometric model in order to estimate the influence of mode II displacement and fracture surface roughness on closure stress intensity level.

$$\left(\frac{K_{cl}}{K_{max}}\right) = \sqrt{\frac{2\gamma x}{1+2\gamma x}}$$

where γ is a non dimensional surface roughness parameter taken as the height, h, to the width, w, of the asperities and x is the ratio of mode II to mode I crack tip displacements. The value of this expression, as claimed by Suresh and Ritchie is that it shows a reasonably good agreement with experimental results derived from data on a 1018 mild steel and fully pearlitic rail steel (Minakawa

and McEvily et al (1981) and Gray et al (1983)).

2.7.3 Plasticity induced crack closure

Plasticity - induced crack closure takes place due to the elastic constraint in the wake of the crack tip of material elements permanently stretched within prior elastic zones which leads to interference between mating crack surfaces (Elber 1970).

Elber proposed an empirical relationship between the load ratio and the ratio $\frac{K_{cl}}{K_{max}}$ which was stated as.

$$\frac{K_{cl}}{K_{max}} = 0.5 + 0.1R + 0.4R^2$$

This was modified later by Schijve (1976) to account for load ratio effect at the higher ΔK values by incorporating higher order terms of R such that

$$\frac{K_{cl}}{K_{max}} = 0.45 + 0.2R + 0.25R^2 + 0.1R^3$$

Schmidt and Paris (1973) used a crack closure concept to account for the dependence of ΔK_{th} on R where ($\Delta K_{th} = K_{max} - K_{min}$). If the following two assumptions were made [Fig.(2.13)]

a) K_{cl} which is the closure stress intensity, at the threshold is independent of R ratio.

b) ΔK_o, i.e the effective threshold stress intensity range necessary to produce fatigue crack growth is constant.

At low R ratios, where $K_{min} \leq K_{cl}$

$$K_{max} = K_{cl} + \Delta K_o. \quad \text{for} \quad K_{min} \leq K_{cl}$$

while at high R ratio where $K_{min} \geq K_{cl}$

$$\Delta K_{th} = \Delta K_o \quad \text{for} \quad K_{min} \geq K_{cl}$$

It can be seen from these equations that a critical value of load ratio exists (R_{cl}) above which the crack closure has no effect. This value of R is obtained when $K_{min} = K_{cl}$ such that $K_{th} = K_o$.

Finally to conclude the discussion about R ratio and crack closure effect, some researchers have utilised the closure concept to explain the load ratio effect on the assumption that as the mean load is raised, the crack will remain open for a longer period of the cycle, thereby increasing ΔK_{eff} and hence the crack growth rate. This argument has been applied to the threshold conditions on steel, titanium and aluminium alloys with little or no experimental evidence. This argument does not stand for the intermediate crack growth rate in the linear part of the $\frac{da}{dN}$ versus ΔK curve in which the load ratio has no effect and yet closure is equally likely to occur, other researchers have observed that the level of crack closure effect in inert environments is greater than the level in air (Buck et al 1975, Irving et al 1973). If the effect of load ratio is due to crack closure, this will mean that near threshold growth rates would be more sensitive to the load ratio in inert atmospheres which is in contradiction to all experimental observation by Priddle et al (1978), McEvily and Greger (1977) and many others. From all these it can be concluded that models based on this concept to explain crack-growth

behaviour patterns at near threshold levels must be regarded as questionable.

2.8 Failure criteria for fracture

2.8.1 Strain energy release rate

Generally speaking there are two approaches to the study of fracture mechanics, the energetic treatment and the stress parameter approach. The stress parameter in the form of stress intensity factor was discussed earlier. In the Griffith theory (1921 and 1924), the crack system is treated as a whole by assuming that cracks will propagate if the elastic energy release by their growth is greater than the energy required to create a new fracture surfaces. Therefore the crack will extend in a direction in which the strain energy release rate is at its maximum value.

Lawn and Wilshaw (1975) showed that the mechanical energy released during incremental crack extension is independent of loading configuration, i.e no difference was noticed between constant force (dead weight loading) and a constant displacement (fixed grip loading). Even though this conclusion is considered only for two specific loading geometries, vigorous analysis showed this conclusion to be quite general. They defined the strain energy release rate (G) as the derivative of the mechanical energy release with respect to crack length and is given by

$$G = -\left(\frac{dU_E}{da}\right)_u \tag{2.4}$$

where dU_E is the strain potential energy and da is the crack increment.

Broek (1978) showed that the strain energy release rate (G) for mode

I is given by the equation

$$G_I = \frac{K^2{}_I}{E}\left(1 - v^2\right) \tag{2.5}$$

where v is the Poisson's ratio and E is Young's modulus.

The same was applied to mode II and III such that

$$G_{II} = \left(1 - v^2\right)\frac{K^2{}_{II}}{E} \tag{2.6}$$

and

$$G_{III} = (1 + v)\frac{K^2{}_{III}}{E} \tag{2.7}$$

He also stated that the total energy release rate in a combined mode cracking can easily be obtained by adding the energies from the different modes, i.e

$$G = G_I + G_{II} + G_{III} = \frac{1 - v^2}{E}\left(K^2{}_I + K^2{}_{II} + \frac{K^2{}_{III}}{1 - v}\right) \tag{2.8}$$

Lawn and Wilshaw (1975) considered the strain energy release rate in a combined mode cracking with tilt and twist configuration and stated that

$$G(\theta, \phi) = K^2{}_I(\theta, \phi)\frac{(1 - v^2)}{E} + K^2{}_{II}(\theta, \phi)\frac{(1 - v^2)}{E} + K^2{}_{III}(\theta, \phi)\frac{(1 + v)}{E} \tag{2.9}$$

where θ is tilt angle and ϕ is the twist angle of the crack extension as shown in Fig (2.19). For pure mode I loading the functions $G(\theta)$ and $G(\phi)$, are plotted in Fig.(2.20) for $v = \frac{1}{3}$ which shows that the maximum values of the maximum strain energy release rate for $G(\theta)$ and $G(\phi)$ occur at the value of $\theta = 0$ *and* $\phi = 0$

respectively. It is then concluded that the crack is favoured to continue in its original plane. Thus the plane crack in mode I loading may be said to have directional stability and that the predicted orientation of the crack growth is directly ahead of and in the plane of the initial crack.

For a mixed mode I and III, the mode III component will tend to twist the crack out of its original plane. A consideration of Fig (2.19) shows that while a θ - rotation of the crack plane can be accommodated by a continuous adjustment of the front, a ϕ -rotation can not. In the later case the crack overcomes the accommodation problem by segmenting into 'partial fronts' separated by cleavage steps. A plot of the normalised strain energy release rate in mixed mode I and III is given in Fig.(2.21) (Lawn and Wilshaw 1975) which indicates that the preferred orientation of the crack is that which minimises the shear loading on the crack, i.e in the direction of pure mode I. The plot also shows that as the ratio of the $\frac{K_{III}}{K_I}$ increases from the value of (0) to (4) the maximum value of the curve of the strain energy release rate is not defined sharply which means that the crack path is not defined closely.

Now, if we consider the fatigue crack extension in respect of the strain energy release rate, it can be stated that crack extension can occur when the strain energy release rate (G) is equal to the energy required for the crack growth (Broek 1978).

$$\Delta G = \Delta K^2{}_{Ith} \frac{1 - \upsilon^2}{E} \tag{2.10}$$

Lawn and Wilshaw (1975) showed that for mixed mode I and III, the maximum strain energy release rate takes place when $\theta = 0$

i.e

$$G(\phi) = K^2{}_I(\phi)\frac{(1-v^2)}{E} + K^2{}_{III}(\phi)\frac{(1+v)}{E} \tag{2.11}$$

From the combination of the equations (2.10) and (2.11) we can deduct that the general condition for failure is

$$\left(\frac{\Delta K_I(\phi)}{\Delta K_{Ith}}\right)^2 + \frac{1}{1-v}\left(\frac{\Delta K_{III}(\phi)}{\Delta K_{Ith}}\right)^2 = 1 \tag{2.12}$$

Other workers such as Nuismer (1975), Hussain (1974), Wang (1977) discussed in their work the strain energy release rate and reached the same results as Lawn and Wilshaw except they did not consider the variation of the strain energy release rate with the twist angle.

2.8.2 The strain-energy density concept

The search for a quantity that provides a more realistic description of material and structure failure has led Sih (1974,1973) to a consideration of the energy concentrated in the crack tip region where fracture takes place for an elastic material, the criterion is expressed in terms of the strain energy density factor (S) where S is given by the equation

$$S = a_{11}K_I^2 + 2a_{12}K_IK_{II} + a_{22}K^2{}_{II} \tag{2.13}$$

Where $a_{ij}(i,j = 1,2)$ describes the angular variation of (S) around the crack tip and they are given by the following expressions:

$$a_{11} = (\frac{1}{16\mu})(3 - 4v - \cos\theta)(1 + \cos\theta) \tag{2.14}$$

$$a_{12} = (\frac{1}{16\mu})(2\sin\theta)(\cos\theta - (1-2\upsilon)) \tag{2.15}$$

$$a_{22} = (\frac{1}{16\mu})\,(4(1-\upsilon)(1-\cos\theta) + (1+\cos\theta)(3\cos\theta - 1)) \tag{2.16}$$

Where μ and υ are the shear modulus and Poisson ratio respectively, θ is the angle of the initial direction of the crack.

The application of the (S) factor to predict crack propagation is based on two hypotheses which can be stated as follows:

1) Crack initiation occurs when the strain energy density factor reaches a critical value, i.e

$$S = S_{cr} \quad \text{for} \quad \theta = \theta_0$$

Where θ_0 marks the angle of crack extension. Fig (2.22).

2) The initial crack growth takes place in the direction along which the strain energy factor is minimised i.e

$$\frac{ds}{d\theta} = 0 \quad \text{at which } \theta = \theta_0$$

Maiti and Smith (1984 a and b) claimed that the strain energy density criteria could not predict the crack path and that some difficulties are found on applying this criteria to some situations. They used the criteria of maximum tangential stress (MTS), maximum tangential principal stress (MTPS) and maximum tangential strain (MTSN). They compared their results with those obtained from the strain energy density criteria (SED) and they claimed that the unstable crack paths based on SED criteria are different from those based on other three in many cases. While the critical loads given by the four criteria can be made very close provided the loads are calculated on the same basis.

2.8.3 Maximum normal crack tip stress

Lawn and Wilshaw (1975) discussed the crack tip stresses of a sharp slit and gave the expressions to evaluate the components of stress and displacement directly from the stress function for different modes I, II and III. The relevant functions are stated below in terms of co-ordinate system of Fig(2.23)

Mode I

$$\sigma_{xx} = \frac{K_I}{2\pi r^{\frac{1}{2}}}\left(\cos(\frac{\theta}{2})[1 - \sin(\frac{\theta}{2})\sin(\frac{3\theta}{2})\right) \tag{2.17}$$

$$\sigma_{yy} = \frac{K_I}{2\pi r^{\frac{1}{2}}}\left(\cos(\frac{\theta}{2})[1 + \sin(\frac{\theta}{2})\sin(\frac{3\theta}{2})\right) \tag{2.18}$$

$$\sigma_{xy} = \frac{K_I}{2\pi r^{\frac{1}{2}}}\left(\sin(\frac{\theta}{2})\cos(\frac{\theta}{2})\cos(\frac{3\theta}{2})\right) \tag{2.19}$$

$$\sigma_{zz} = \upsilon(\sigma_{xx} + \sigma_{yy}) \tag{2.20}$$

Mode III

$$\sigma_{xz} = \left(\frac{K_{III}}{2\pi r^{\frac{1}{2}}}\right)\left(-\sin(\frac{\theta}{2})\right) \tag{2.21}$$

$$\sigma_{yz} = \left(\frac{K_{III}}{2\pi r^{\frac{1}{2}}}\right)\left(\cos(\frac{\theta}{2})\right) \tag{2.22}$$

Where υ is Poisson's ratio.

Erdogan and Sih (1963) indicated that in ideal brittle materials, the so called 'sliding' and 'tearing' modes of crack extension do not take place. The mode of fracture seems to be always a crack opening. They proposed that a mixed mode I and II fracture takes place when the maximum normal crack tip stress exceeds its critical value for mode I and the crack does not grow till the mode I fatigue threshold stress intensity factor is exceeded.

Yates (1987) extended the above work of Lawn and Wilshaw further to include the mixed mode I and III fatigue by considering both tilt and twist crack configuration and gave failure conditions for stresses to be .

$$\Delta\sigma_{yy} = \Delta\sigma_{crit} = \Delta\sigma_{yy}\cos^2\phi + \Delta\sigma zz\sin^2\phi + \Delta\sigma_{yz}\sin 2\theta = \frac{\Delta K_{Ith}}{\sqrt{2\pi r}} \qquad (2.23)$$

where ϕ is the twist angle.

Combining the equations evaluating the stresses in mode I and III given by Lawn and Wilshaw with the previous Yates failure conditions for $\theta = 0$ will give us

$$\frac{\Delta K_I}{\Delta K_{Ith}}\left(\cos^2\phi + 2\upsilon\sin^2\theta\right) + \frac{\Delta K_{III}}{\Delta K_{Ith}}\sin 2\phi = 1 \qquad (2.24)$$

Yates (1987) concluded that the maximum occurs when

$$\phi = \frac{1}{2}\tan^{-1}\left(\frac{2}{1-2\upsilon}\frac{\Delta K_{III}}{\Delta K_I}\right) \qquad (2.25)$$

and finally failure is expected to take place in the direction which minimises the mode II (shear) component of the stress field.

The same results were reached by Pook (1985c) through using a branch crack analysis, in which he assumed that the crack starts to propagate when the stress intensity factor of the branch crack exceeds that of mode I threshold value. Yates (1987) gave an approximate solution for the stress intensity factors of a twisted branch crack at an angle (ϕ) in a mixed mode I and III loading to be

$$K_I(\phi) = K_I(\cos^2\phi + 2\upsilon\sin^2\phi) + K_{III}\sin 2\phi \tag{2.26}$$

$$K_{III}(\phi) = K_I - (\frac{2\upsilon - 1}{2})\sin 2\phi + K_{III}\cos 2\phi \tag{2.27}$$

and later stated that the failure locus is given by the equation (2.24)

Yoshioka et al (1984) used the theory which assumes that the crack branches in a three-dimensional direction and does not continuously grow along the extension of the main crack, which is the same analysis as that used by Pook. The failure envelope proposed by Yoshioka et al is the same as that of Pook and is given by the equation

$$\frac{1}{2}\left(K_I(1+2\upsilon) + \left(K^2{}_I(1-2\upsilon)^2 + 4K_{III}^2\right)^{\frac{1}{2}}\right) = constant \tag{2.28}$$

Other investigators such as Hourlier and Pineau (1981) used the facet stress intensity factor in their work to predict crack path under cyclic mode I loading with superimposed steady mode III loading. It was shown that under complex mode loading a fatigue crack propagates in the direction in which the crack growth is maximum. The crack growth rate was assumed to be controlled by the local mode I component. The rate of fatigue crack growth of a facet inclined at an angle (α) was calculated using the mode I cyclic and the maximum value of the stress intensity factors.

$$\frac{da}{dN} = C(\Delta K_I)^{\beta}(K_{max})^{\gamma} \tag{2.29}$$

where (C) is constant and (β *and* γ) are given for each material. It was observed that the fatigue crack growth rate in the superimposition of the constant torque (mode III loading) to the alternating tensile load (mode I loading) was decreased compared to that of the mode I loading only. This is believed to be associated with the closure phenomenon which was discussed earlier. A good agreement was found between the calculated facet angle and the measured ones for the three materials used by Hourlier and Pineau.

2.8.4 Maximum normal crack tip strain

A theory of strain failure criteria similar to the stress failure criteria was proposed by Wu (1974) and developed by Chang (1981) which depends on the principal that in brittle fracture, the cleavage fracture would take place when the maximum tensile strain around a crack tip exceeds a critical value.

Yates (1987) took this theory further by assuming that fatigue crack growth is controlled by mode I maximum tensile strain around the crack tip and that the crack will grow when the value of the maximum tensile crack tip strain exceeds that of mode I threshold value. He developed a fatigue failure locus for mixed mode I and III and it is given by

$$\frac{\Delta K_I}{\Delta K_{Ith}} cos^2\phi + \frac{\Delta K_{III}}{\Delta K_{Ith}} \frac{sin2\phi}{(1-2v)} = 1 \tag{2.30}$$

The maximum will occur when

$$\phi = \frac{1}{2} tan^{-1} \left(\frac{2}{1-2v} \frac{\Delta K_{III}}{\Delta K_I} \right) \tag{2.31}$$

which will give the value of the threshold stress intensity factor.

Chapter 3

Research Programme

A study has been made of fatigue crack threshold and propagation in mode I, mode III and mixed mode I and III; i.e under cyclic and bending loads, for different stress ratios R, to provide a basis for estimating fatigue life in large rotating generator shafts subject to transient oscillation. Most of the previous work has been conducted for mode I loading, but only recently studies for non-mode I have been taken up and most of these researches were conducted for fixed stress ratio R. The research programme was divided into three stages:

3.1 Mode I tests

Three point bend specimens were used to establish the near threshold growth characteristics and threshold stress intensity factor. Twenty two tests were carried out to establish the threshold value of ΔK under mode I loading for different values of load ratio R equal to 0.06 (for R=0), 0.17, 0.37 and 0.5.

3.2 Mode III tests

Fifteen tests were performed on the pure mode III loading situation using a straight circumferentially slit round bar in torsion. Four different load ratios R were used, the usual (-1) ratio as well as (0), (0.17) and (0.5). These tests were performed to establish the behaviour of the material near or at the threshold condition for mode III loading.

3.3 Mixed mode I & III tests

Once the threshold values of the stress intensity factors for mode I and mode III were established, three point bending specimens with slit angle of (45°&60°) were used to get two ratios of $\frac{\Delta KI}{\Delta KIII}$ equal to 1 and 1.73 respectively. Tests at different R ratio (0.06, 0.17 and 0.5) were carried out to investigate the effect of R ratio on the fatigue crack growth and to establish the mixed mode behaviour of the crack, the fatigue crack direction and path and finally the crack growth rate and its correlation with that of pure mode I tests. The material, specimen geometry and experimental procedure are discussed in detail in Chapter 4. In all tests a constant current potential drop system was used to detect and monitor the initiation and extension of the crack in all the three stages of this research. Fracture surfaces were broken open using liquid nitrogen then examined under an optical microscope and photographed in a scanning electron microscope. The experimental results and analyses are reported and discussed in Chapters 5, 6 & 7.

Chapter 4

Material, test machines and experimental procedure

4.1 Introduction

In this research a single material was used throughout all the tests. The chemical and mechanical properties, specimens geometry, test rigs, crack measuring techniques, crack calibration equations, stress intensity factor calibrations and experimental procedure are discussed in this chapter.

4.2 Material specification

The material used for this research was supplied by NEI Parsons Ltd., Newcastle upon Tyne, and was taken from an 8 inch thick section of an L.P. rotor of turbine used in the electricity generating power plant as shown in Fig.1.1 and Fig.4.1.

The material is a 3.5 %NiCrMoV steel, the thermo-mechanical treatment of the steel consists of heat treatment of the rotor forging by the forgemaster. In the final treatment the rotor had been austenitized at $825°C$, mist quenched to $200°C$, tempered at $625°C$ for 32 hours and then furnace cooled. This final process is designed to stress relieve and ensure vanadium carbide precipitation. No other heat treatment was given to the raw material or the specimen.

The composition of the material used in this research consist of the elements given in Table 1.

Fig.(4.2) shows the microstructure which is lower bainite with small complex carbide precipitates. The average austenite grain size was 150 μm $\pm 30\mu m$ (Yates 1987). Tensile strength impact toughness data from various positions in the forging were supplied. The mean value of the 0.2% proof stress was 682 MPa ($\pm 4MPa$) and the mean value of the ultimate tensile stress was 832 MPa ($\pm 6MPa$). The mechanical properties are given in Table 2.

4.3 Specimen geometry

Several types of specimens have been used by different investigators to study mode I, mode III and mixed modes I & III. The geometry of the specimen used in these tests are governed by the capacity of the existing chucks and the dimension of the raw materials.

4.3.1 Mode I test specimen

Three point bending specimens were used to carry out tests to determine the mode I fatigue threshold condition. The geometry of the specimen is shown in Fig.(4.3). Its design was based on several considerations, it should be a standard fracture mechanics specimen so that accurate stress intensity factors would be available and it should be suitable for the development of baseline mode I threshold data. It should be thick so that the transition to slant (45°) crack growth, sometimes observed in thin sheets, would not occur.

A spark machined slit was used to avoid difficulties associated with machining. In pure mode I tests the angle of slit was 90°. A 0.1 mm wire was used to slit the specimen on the electric discharge machine to a depth of 5mm in the centre of the specimen and a width of less than 0.2 mm.

The spark eroded slit was introduced to the original specimens which were machined to size without the slit by the supplier NEI Parson Ltd. The 6mm tapped holes at the end of the specimen were used to connect the leads from the D.C. supply for the p.d. required to monitor the crack. All dimensions such as slit depth, width were measured on a co-ordinate measuring machine.

Some precracked specimens were used to determine the crack growth threshold conditions and to compare the results with those from slit specimens.

4.3.2 Torsion test specimen

For torsion tests, a round specimen with a spark eroded slit was used. As the chucks could only accept a maximum specimen diameter of 7/8 inch, the diameter

of the specimen was chosen to be 19 mm, the length was limited by the thickness of the disc cut from the rotor and therefore the length was chosen to be 85 mm.

Fig.(4.4) shows the dimension of the specimens used in torsion, the specimens were machined to the dimensions given, the ends of the specimens were flattened at 90° to each other to accommodate the cotter pins which hold the specimen in place.

The slitting was carried out using a spark eroding machine, firstly using 0.2 mm diameter wire and then 0.1 mm diameter wire for the last 1.5 mm of the slit to reach a depth of 3.5 mm. A special geared rotation assembly was used to turn the specimen during the spark machining process in order to ensure an even slit. All measurement of the depth and width of the slit and the diameter of the specimen were taken using a coordinate measuring machine.

4.3.3 Mode I & III test specimen

For the mixed mode I & III tests, a rectangular three point bending specimen, similar to those used for mode I tests, with an angled slit were used. The specimens were supplied by NEI Parsons Ltd.

The dimensions and geometry of the specimen are shown in Fig (4.5). The working section of the surface was hand polished using 800, 1000 and 1200 grit silicon carbide paper to get a good surface finish for study of the crack extension under the microscope.

Two series of tests were carried out using the same batch of 3.5%NiCr-MoV steel with slit angle (θ) values of 45° and 60° giving the mixed mode ratio

of $\frac{\Delta K_I}{\Delta K_{III}}$ to be 1.00 and 1.73 respectively.

4.4 Test Rigs

Two rigs were used in this research, a displacement controlled torsion machine was used for mode III tests and a Mayes ESHE 100 servo-hydraulic test machine was used for mode I and mode I & III tests.

4.4.1 Mode III test machine

A simple displacement controlled torsion fatigue testing machine, which was originally designed by Zachariah (1973) was used to carry out mode III tests.

The general layout and arrangement of the rig is given in Fig.(4.6) and (4.7) which consists of three sub-assemblies, the specimen load cell assembly, the high speed drive unit and the low speed drive unit, which was not used in this work. The full description of the rig is given by Zachariah (1973). The crack initiation and extension inside the specimen were monitored by measuring p.d.

The machine which consists of a variable speed d.c motor with an adjustable disc throw crank and an adjustable length conrod which is connected to another adjustable disc throw crank fitted on the headstock chuck. The conrod length and disc throw could be adjusted for a wide range of mean and cyclic angular displacements that could be applied to the specimen.

The specimen was held in place using tapered cotters, the other side of the specimen is connected in series with the load cell which is calibrated to give

the required torque.

4.4.2 Mode I and mixed mode I and III tests machines

All tests were carried out using the Mayes ESHE 100 servo-hydraulic fatigue machine. Three point bending specimens were used, two supports were provided by the two rollers fixed at a distance of 12 cm apart in the existing loading frame. The third point was provided by the roller attached to the machine cross head.

The machine was operated under the control of a load cell with a sinusoidal wave form in the frequency of 40 Hz over a 0-10 KN load range. This load cell was calibrated by Mayes engineer regularly. The layout of the rig is shown in Fig.(4.8).

The crack was monitored by two methods. The first was two travelling microscopes to monitor the surface crack length from both sides of the specimen. This was compared to the second method which used a d.c. current supply to provide a potential drop across the slit. Three p.d readings were taken, two positions across the crack and one as a reference potential drop. These three reading with maximum and minimum loads were collected at different intervals on a Solartron data logger which had the accuracy of $1\mu V$ and then printed on an attached telex type printer.

4.5 Crack measuring techniques

One single method was used to monitor crack initiation and extension in mode III tests while two methods were used in the mode I and mixed modes I & III tests.

4.5.1 Direct current potential drop technique

This technique employs the fact that any discontinuity in a current carrying conductor will cause a disturbance in the electrical potential field in that conductor. In this method, a constant current is supplied through the specimen from a direct current (D.C) power supply. As the crack length increases, the cross section of the specimen is reduced which causes the p.d. to be increased across the specimen. The change in this p.d. is of the order of a few micro-volts, which could be detected by a sensitive voltmeter. A constant current of 20 Amps was supplied from a constant current source to the leads on the end of the specimen. This current was sensitive enough to register any changes and small enough not to heat the specimen.

Four pairs of p.d leads were spot welded at the shoulder of the slit in the mode III specimen while two pairs were spot welded for the three point bending test with an extra pair of leads for the reference point in both cases,which were further apart. The leads for measuring the p.d. were made of pure ferrous material to minimise thermo-electric effects. These leads were attached, in the case of the three points bending tests, to copper wires which were placed in a temperature controlled chamber to minimise any thermal e.m.f. interference

which would arise from a temperature difference between a pair of junctions.

The p.d. was measured using a Solartron data logger which was attached to a telex type printer to record the data at preset intervals.

4.5.2 The optical travelling microscope

The other method which was used to monitor the crack initiation and extension was using two travelling microscopes at either side of the three point bending specimen. This method is not suitable for the round specimen, as the cracks were internal. The handicap of this method is that only the surface cracks of a plane specimen can be monitored and there is evidence that the crack does not always grow uniformly across the whole crack front through the thickness of the specimen. Therefore an optical method is not able to monitor crack growth in the centre of the specimen and that is where the D.C. potential drop technique can be used in conjuction.

4.6 P.d. crack calibration equations

Two equations were used to calibrate the crack length, one for the round specimen of mode III tests and the other one was for the three point bending test specimens.

4.6.1 P.d. calibration for round specimen

To find an expression which could express the relationship between the voltage reading and the crack length, an equation of the form given below was derived :

$$\frac{a}{D} = 0.35\left(1 - e^{\alpha(\frac{\Delta V}{V_r})^{\beta}}\right) \tag{4.1}$$

where:

a is the fatigue crack length

D is the initial uncracked diameter.

ΔV is the difference of voltage reading at two successive readings.

V_r is the reference voltage reading.

As $\frac{\Delta V}{V_r} \Longrightarrow 0.3 \quad \frac{a}{D} \Longrightarrow 0.35$

since $a \Longrightarrow 6.0$ mm (maximum value of crack)

also as $\frac{\Delta V}{V_r} \Longrightarrow 0 \quad \frac{a}{D} \Longrightarrow 0$

The values of α and β were found by changing the above equation to the form

$$\ln\left\{-\ln(1 - \frac{a}{0.35D})\right\} = \ln\alpha + \beta \ln\frac{\Delta V}{V_r} \tag{4.2}$$

A graph of $\ln\ \{-\ln\ (1 - \frac{a}{0.35D})\}$ versus $\ln\frac{\Delta V}{V_r}$ was plotted and the values of α and β were found to be $\alpha = -30.557$ $\beta = 1.553$ as shown in Fig.(4.9), correlation coefficient was found to be 0.994. A calibration curve was plotted as shown in Fig.(4.10)

The verification of this curve was assured by comparison of the measured final crack length of the specimens after breaking open and the calculated length, and they were found to be in good agreement.

4.6.2 P.d. calibration for the three point bending specimen

Gilbey and Pearson (1966) developed an equation that is used widely for the measurement of crack length in a cracked three point bending specimen and it is expressed as :

$$\cosh(KV) = \cosh\frac{\pi h}{2w}\sec\frac{\pi a}{2w} \tag{4.3}$$

This equation was developed later by Brown (Private communication) and used for contact points across the slit and reference points Fig (4.11) and given as:

$$cosh(KV_1) = \cosh\frac{\pi h_1}{2w}\sec\frac{\pi a}{2w} \tag{4.4}$$

$$\cosh(KV_2) = \cosh\frac{\pi h_2}{2w}\sec\frac{\pi a}{2w} \tag{4.5}$$

dividing (4.4) by (4.5)

$$\frac{V_1}{V_2} = \frac{\cosh^{-1}\left(\cosh\frac{\pi h_1}{2w}\sec\frac{\pi a}{2w}\right)}{\cosh^{-1}\left(\cosh\frac{\pi h_2}{2w}\sec\frac{\pi a}{2w}\right)} \tag{4.6}$$

where

V_1 = p.d. across the crack

V_2 = reference point p.d.

$2h_1$ = distance separating the leads across the crack

$2h_2$ = distance separating the leads across the reference points

a = crack length, w = width of the specimen

Since h_1 and h_2 are fixed and could be considered as constants

therefore $\cosh\frac{\pi h_1}{2w} = A$ and $\cosh\frac{\pi h_2}{2w} = \mathrm{B}$

leading us to

$$\frac{V_1}{V_2} = \frac{\cosh^{-1}\left(A \sec \frac{\pi a}{2w}\right)}{\cosh^{-1}\left(B \sec \frac{\pi a}{2w}\right)} \tag{4.7}$$

A simplified version of the equations (4.4) and (4.5) could be obtained by assuming a = 0

From equation (4.5)

$\cosh(KV_2) = \cosh \frac{\pi h_2}{2w}$

therefore

$$K = \frac{\pi h_2}{2wV_2} \tag{4.8}$$

From(4.8) into (4.4)

$$\cosh \frac{\pi h_2 V_1}{2wV_2} = \cosh \frac{\pi h_1}{2w} \sec \frac{\pi a}{2w} \tag{4.9}$$

$$\cosh \frac{\pi h_2 V_1}{2wV_2} = \cosh \frac{\pi h_1}{2w} \frac{1}{\cos \frac{\pi a}{2w}} \tag{4.10}$$

leading to

$$\cos \frac{\pi a}{2w} = \frac{\cosh \frac{\pi h_1}{2w}}{\cosh \frac{\pi h_2 V_1}{2wV_2}} \tag{4.11}$$

therefore

$$\frac{a}{w} = \frac{2}{\pi} \cos^{-1} \left(\frac{\cosh \frac{\pi h_1}{2w}}{cosh \frac{\pi h_2 V_1}{2wV_2}} \right) \tag{4.12}$$

This last equation was used to calculate the length of the crack as the p.d. increases. A ratio of $\frac{V_1}{V_2}$ was used rather than the individual values of V_1 and

V_2 to accommodate any long term drift in the constant supply of the current.

The accuracy of the above equation could be verified using an aluminium foil model cut to 4 times the size of the specimen with the slit. Three pairs of leads were then connected to the model at distances four times those in the specimen and a current is then passed through the specimen. The results of the two readings were then compared and found within a good agreement and also checked against microscope readings [see Fig(4.12)].

4.7 The stress intensity factor calibration

Values of the stress intensity factors for mode III, mode I and mixed modes I & III were calculated using different formulae in LEFM. The slit used in all the specimens was achieved using a 0.1 mm diameter wire on an spark erosion machine. The radius of the slit is 3.5 mm in torsion specimens and 5 mm in three point bending specimens. The argument of whether this slit is a crack or a notch could be settled using Taylor's argument (Taylor 1992). Taylor's method is based on the concept that relatively sharp notches can be considered to be crack like and therefore analysed by LEFM approach and that the notch concentration factor K_t indicates the degree to which the local stress is raised, implying an equal decrease in the applied fatigue limit. K_t was calculated for the torsion and three point bending specimens and found to be 16.3 and 19.3 respectively. Taylor stated that "in practice this prediction is resonably accurate in high cycle fatigue for blunt notches (e.g. if $K_t = 1.5$) but gives a very great underestimate of the behaviour of sharper notches". Since the notch used in this research has a stress concetration factor $K_t = 16 - 19$, it can be stated clearly that the slit used in

this research should be treated as a crack and not as a notch.

4.7.1 Mode III specimen

The calculation of stress intensity factor for a round specimen used in mode III test with a circumferential slit was taken from Tada, Paris and Irwin(1985).

$$\Delta K_{III} = F(\frac{a}{b})\tau_N\sqrt{\pi a} \tag{4.13}$$

where

$$\tau_N = \frac{2T}{\pi a^3}$$

$$F(\frac{a}{b}) = G(\frac{a}{b}) \times \sqrt{\frac{a}{b}}$$

and

$$G(\frac{a}{b}) = \frac{3}{8}\left(1 + \frac{1}{2}\frac{a}{b} + \frac{3}{8}(\frac{a}{b})^2 + \frac{5}{16}(\frac{a}{b})^3 + \frac{35}{128}(\frac{a}{b})^4 + 0.208(\frac{a}{b})^5\right)$$

where $2b$ is the specimen diameter, $b - a$ is the slit depth and $2a$ is the diameter of the non-slit part of the specimen as shown in Fig.(4.4)

T = torque

τ_N = net section shear stress

This calibration was given by Benthem and Koiter (1972) to an accuracy better than 1% according to Tada, Paris and Irwin (1973). Method used is Asymptotic Approximation.

4.7.2 Mode I specimen

The three point specimen used in this test is of rectangular shape with thickness (b) and a slit (a) in the centre. The stress intensity factor was calibrated using the equation given by Tada, Paris and Irwin (1985)

$$\Delta K_I = F(\frac{a}{b})\sigma\sqrt{\pi a} \tag{4.14}$$

where $F(\frac{a}{b})$ is given by the equation

$$F(\frac{a}{b}) = 1.090 - 1.735(\frac{a}{b}) + 8.2(\frac{a}{b})^2 - 14.18(\frac{a}{b})^3 + 14.57(\frac{a}{b})^4$$

and

$$\sigma = \frac{6M^2}{b}$$

where M is given by :

$$M = \frac{\Delta Pl}{4}$$

where l = support span

ΔP= the applied load

σ= stress

The calibration was given by Brown and Srawley (1966). The accuracy given by Tada et al. (1985) as 1% while the same calibration given by Rooke and Cartwright (1976) suggested an overall accuracy to be better than 1% for $\frac{a}{b} \leq 0.6$.

4.7.3 Mixed mode I & III specimen

The specimen used for mixed mode I & III is the same as that of pure mode I except for the angle of slit (θ) where it is 90° for mode I and variable for mixed mode I & III depending on the ratio of K_I/K_{III}. In this research, the angles were limited to 45° and 60° only.

For $\theta \neq 90$, the apparent values of K_I (K_A) were first calculated using equation (4.14) and K_I and K_{III} values were then calculated using the expressions (Pook 1985a):

$$K_I = K_A \sin^2 \theta$$
$$K_{II} = 0$$
$$K_{III} = K_A \sin \theta \cos \theta$$

Giving the ratio of $K_I/K_{III} = \tan \theta$

4.8 Experimental procedure

All tests were conducted in air at room temperature (average 21°C). Two different test procedures were adopted. The first one was for mode III tests while the other one was for mode I and mixed mode I & III tests.

4.8.1 Mode III tests

The first thing to be done before installing the specimen was to calibrate the load cell. This was achieved by attaching dead weight loads to pair of arms bolted to the tail stock chuck and recording the voltmeter reading for each load. This was repeated for the other side of the test rig. A relationship between the torque and voltage readings was established as given in Fig.(4.13) and the equation of this relationship is expressed as :

$$V = 0.4036T + 0.0036 \tag{4.15}$$

where V is the voltage in mV, and T is the torque in Nm.

The test procedure in mode III depended on using several specimens with one tested for each load. The load reduction method was used to determine the threshold stress intensity factor for the specific stress ratio (R). Starting with a chosen value of ΔK_{III}, a crack growth rate in mode III was found. The load was then reduced and applied on another specimen until a threshold value of ΔK_{III} was obtained for which the crack growth rate was below 10^{-8} mm/cycle.

4.8.2 Mode I and mixed mode I & III tests

All tests were conducted at frequency of 40 Hz. In most cases a load was implemented on the specimen which initiates a crack that extends beyond the growth rate of 10^{-8} mm/cycle. A stress intensity factor higher than that of the threshold, was applied to produce the required fatigue crack. This was followed by periodically decreasing the load range by not more than 10%. At each step the

crack was allowed to grow a distance of several times the previous plastic zone size to minimise any possible effect of residual stress resulting from the unloading sequence. This process was carried out till the crack rate of growth was less than 10^{-8} mm/cycle. In some tests (mode I) the load was increased by 10% after the crack stopped propagating in order to find ΔK_{Ith} for a precracked specimen which was found to be different from that of a pre-slit specimen.

The loading arrangement as shown in Fig.(4.14) is very simple. It includes placing the specimen in the centre of the 120 mm span between two circular fixed support attached to the servo-hydraulic actuator with the slit being aligned with the centre line of the loading frame. The load was applied through a single roller attached to the machine cross head. A pair of current leads were connected to the specimen ends to supply the d.c. constant current with two mobile traveling microscopes, one at each side of the specimen to monitor the crack initiation and extension visually, p.d. leads were spot welded in the appropriate positions to monitor the crack electrically.

Chapter 5

Results and observations

5.1 Introduction

In this chapter the experimental results of all tests are presented. The tests are divided into three main categories, mode I, mode III and mixed mode I & III tests.

The stress ratio was changed in order to find its effect on the fatigue threshold value of the stress intensity factor. The values of R were taken to be 0.06, 0.17 and 0.5. The results will be considered into two categories, failed and unfailed specimens. The data readings of unfailed specimens will not be given, as no change in any reading was recorded.

The experimental details were given earlier in Chapter Four. The crack growth rate under mode I, mode III and mixed mode I & III will be discussed in sections (5.2.2,5.3.1 & 5.4.2) respectively, fractography will be dealt with in

sections (5.2.4,5.3.2 & 5.4.3).

5.2 Mode III tests

All mode III tests were performed on the displacement controlled torsion machine which was described earlier in Chapter Four. The first tests to be carried out were for stress ratio (R) = -1, and then for R = 0.06 and 0.17. Tests for R = 0.5 could not be carried out on this rig as it was beyond the capacity of the machine and it could not take the load. The slit was extended beyond the 3.5 mm depth and to the limit of the LEFM condition of $\frac{r_y}{a} \leq \frac{1}{50}$, but still the torque was above the limit of the machine. Another similar modern rig was used to carry out the tests at R = 0.5 and it was successful (see Table 5).

The results of ΔK_{III} for R = -1 are not to be used for comparison with those of mode I and mixed mode I & III since the specimen used for mode I and mixed mode I & III is a three point bending specimen and the stress ratio implemented on it can not be less than zero, i.e in the negative value.

The fracture surfaces in mode III tests were all factory roof type, as some of them can be seen in the fractography section. Higher stress intensity factors were not implemented as the threshold value of the mode III tests is considered to be the initiation of mode I cracks in the form of a factory roof fractured surface.

5.2.1 P.d. calibrations

To monitor the initiation and extension of the crack in the cylindrical mode III specimen, the p.d. system across the slit was used. No equation was available to express the relationship between the crack length and the p.d. readings. An equation had to be derived to define this relationship. As the crack extended due to fatigue a record of the p.d. across four contact points was kept throughout the test. When the crack had extended a sufficient distance, the test was stopped and the specimen removed, cooled in liquid nitrogen and broken open. The crack depth was then measured at the four monitoring contact points using a travelling microscope and an enlarged photograph of the cracked surface. Ten specimens were used to plot a graph of p.d versus actual crack length in mm.

A calibration curve of $\frac{\Delta V}{V_r}$ versus $\frac{a}{D}$ was plotted as shown in Fig.(4.10). To verify this equation six specimens were used to compare between the calculated crack length and the actual measured one. They were found to be in good agreement with each other. It is a known fact that as the crack extended further, the error in measurement was greater due to the fact that no axial load was used to separate any contact points of the factory roof surfaces that might cause a shorting in the electrical p.d readings.

The values of V_r were of the order of 0.7 - 0.8 mV, therefore any change in p.d. reading = 7 μV will represent a change of 1% in $\frac{V}{V_r}$ and a change in $\frac{a}{D}$ of approximately 0.01%.

The major problem experienced in implementing this method of measuring the crack length is the sliding contact imposed by pure cyclic torsional loading giving rise to marked crack surface interaction effect. This is evident

from sign of heating, abrasion and fretting oxidation on mode III surfaces causing the electrical potential measurements of crack length to suffer from severe shorting problems (Ritchie et al 1985).

5.2.2 Initiation and propagation of cracks in mode III

In some of the tests, initiation of cracks started within the first few cycles as in the test for specimen RD1 when the range of the applied stress intensity factor was 15 $MPa\sqrt{m}$ for R = -1. The initiation of the crack occurred within a few hundred cycles from the start of the test. Initiation of the crack took place simultaneously all round the specimen. Some deviations in crack length were evident and that was clear from the p.d. reading, which will only be recording local events in the vicinity of the spot welded probes.

From the first 1 mm of the crack growth, deviation out of the mode III plane took place and the crack extended in a plane inclined by 45° to the slit plane forming the factory roof crack. When R was = -1, the crack was extended in ±45° planes, but when R is changed to 0 or 0.06 the crack planes were single set and inclined at 45° only. This is due to the fact that the maximum stress in the first case was $\frac{\pm\Delta\sigma}{2}$, ie $\frac{\Delta\sigma}{2}$ in tension and $-\frac{\Delta\sigma}{2}$ in compression while in the second case where R $\simeq$ 0 it is given as $\Delta\sigma$ if the same ΔK_{III} values were used.

Since the nature of the crack is the factory roof type, the crack growth under pure cyclic torsion is strongly influenced by torsional crack closure, especially as the crack increases in length, where the effective torque on the unbroken ligament is severely reduced from the nominal applied value by rubbing and in-

terlocking between adjacent crack surfaces.

5.2.2.1 Crack growth rates

Crack growth rates in mode III specimens were calculated from the crack extension as the number of cycles increases.

Fig.(5.1) shows a graph of the potential drop readings with respect to the number of cycles elapsed. These potential drop readings were later converted to actual crack length in mm versus number of cycles and were plotted as shown in Fig.(5.2).

It can be seen from the above two graphs, the p.d. readings and the corresponding crack lengths that some fluctuations exist in these graphs and it looks as if the crack length has dropped down instead of extending, this is mainly due to the nature of the crack which is a factory roof, and shorting takes place between the two sliding surfaces of the factory roof crack.

From the graph of crack length versus numbers of cycles, the crack growth was calculated using a tangent method, where two points could be taken and crack growth rate is given as:

$$\begin{aligned} \frac{da}{dN} &= \frac{\textit{increase in crack length}}{\textit{number of cycles between the two points}} \\ &= \frac{a_2 - a_1}{N_2 - N_1} \end{aligned}$$

As the crack increases in length, the crack growth rate is reduced due

to the frictional forces. The fluctuation was quite high and the crack growth rate did not show consistent behaviour, some cracks continue to accelerate, but others could show a constant or decreasing growth rate. In general the crack growth increase at first and then decreases. In the actual calculation of the crack growth rate a seven point method was used as recommended by ASTM E647 (E647 - 88a).

5.2.2.2 Undetected crack length

The potential drop method for measuring the crack length can not detect very small cracks. This is due to the fluctuation of the instrumentation used and the error introduced by such instruments can lead to some cracks being undetected. When the test starts, no crack could be detected and the p.d. readings seems to be set to a certain value with a small fluctuation. This fluctuation is what decides the length of the undetected cracks. If the maximum and minimum values of the p.d. readings are taken over a range of number of cycles = Nc, it is converted to crack length using equation 4.1. We can use the following expression to measure the undetected crack length.

$$\frac{da}{dN} = \frac{maximum\ undetectable\ crack\ length - minimum\ undetectable\ crack\ length}{N_c} \tag{5.1}$$

For example in specimen RD8 test the minimum detectable crack growth rate was

$$\frac{da}{dN} = 3 \times 10^{-8} mm/cycle.$$

This method is shown in Fig.(5.3).

Another method to measure the undetectable crack length is to calculate the

crack length (a_1) for a corresponding value of $\frac{V_1}{V_2}$ using equation (4.1). Then applying the same formula to calculate (a_2) for a corresponding $\left(\frac{V_1}{V_r} + \Delta(\frac{V_1}{V_r})\right)$ as shown in Fig.(5.4) where $\Delta \frac{V_1}{V_r}$ is the fluctuation in the p.d. readings, then

$$\frac{da}{dN} = \frac{a_2 - a_1}{N_c}$$

5.2.3 Effect of mean stress on mode III threshold

Fig.(5.5) shows the effect of stress ratio (R) on the value of ΔK_{IIIth}. Several tests were carried out to decide the value of ΔK_{IIIth} for the 3.5%NiCrMoV at different values of R = -1, 0.06, 0.17 and 0.5. The method used depends on the use of several specimens. Each specimen was used for a specific value of ΔK_{III}. A decreasing value of ΔK_{III} was reached that just initiated a crack and this was regarded as the ΔK_{IIIth}. It can be seen from the above figure that the effect of (R) on the threshold of ΔK_{th} under mode III is seen as $R = -1$, $\Delta K_{th} = 7.5\ MPa\sqrt{m}$, $R = 0.06$ gives $\Delta K_{IIIth} = 6.8\ MPa\sqrt{m}$, $R = 0.17$ gives $\Delta K_{IIIth} = 6.6 MPa\sqrt{m}$ and for $R = 0.5$, $\Delta K_{IIIth} = 6.35 MPa\sqrt{m}$

The difference in the value of ΔK_{IIIth} for $R = -1$ and $R = 0.5$ is $1.25 MPa\sqrt{m}$ which is 16% of the value of ΔK_{IIIth} for $R = -1$. The expected experimental error is 5%, so it can be decided that for $3.5\% NiCrMoV$ the effect of the stress ratio (R) on the value of ΔK_{th} under mode III loading is not all that significant, even though it follows the general rule that ΔK_{th} decreases as R increases.

5.2.4 Fractography

All fractured specimens under mode III tests were broken open after cooling in liquid nitrogen. Some specimens were prepared for fractographic analysis. The scanning electron microscope (SEM) was used for the examination of the fatigue fracture surface. The surfaces were prepared by cutting them using a slow diamond electric saw with coolant so that it did not damage the fractured surface. The surface was then cleaned using detergent followed by ultrasonic cleaning in methanol.

Examination of the fatigue fractured surfaces showed similar features. For pure mode III tests obtained using a slit round specimen in torsion, the crack front formed is a closed curve. Mode I facets emerged on complementary planes from the root of the slit and continue inwards towards the centre of the specimen. At zero mean load (R = -1), the facets were inclined at approximately $\pm 45°$to the mode III crack plane as shown in Fig.(5.6). Some rubbing in parts of the cracked surfaces were noticed where some spots of featureless cracked surfaces exist. The direction of the crack growth is shown by studying the flow lines (striation) on the whole of the fatigue crack surface.

No microscopically flat surfaces were noticed for $\Delta K_{III} \leq 15 MPa\sqrt{m}$ in all the specimens tested, only factory roof type were observed. These facets grew parallel to the crack front and they tended to merge as the crack grew while in some specimens these facets were separated and they did not merge as the crack grew further as shown in Fig.(5.7).

As ΔK_{III} was reduced from 15 to 6 $MPa\sqrt{m}$, in order to find the threshold value of ΔK_{III}, these facets were noticed to get smaller as ΔK_{III}

decreases until they disappear in the unfailed specimens where no facets were formed.

5.3 Mode I Tests

All mode I tests were carried out on rectangular three point bending specimens with a slit at the middle of the specimen at an angle = 90° to the axis of the specimen.

Tests in mode I were undertaken for four different stress ratios (R = 0.06, 0.17,0.37 and 0.5) in order to find the threshold values of ΔK_I for these R ratios. Five tests on precracked specimens were completed for the above four values of stress ratios (see Tables 3 & 4). It was found that there is a significant difference in the values of ΔK_{Ith} between precracked and slit specimens for the same R ratios. This will be discussed in Chapter Six. No stress relief process was carried out after the slitting of the specimens as the high temperature attained in melting and vaporizing metal from the specimen during spark erosion process affect a shallow layer (0.0001 - 0.005 in.) of the surface machined (Metal Handbook Vol.3, 8th edition) and the plastic zone depth at the crack tip is found to be much higher than the residual stresses layer depth. The SIRIUS workshop ensured that the lowest current is used in the spark erosion process and the cooling of the material was very efficient.

5.3.1 Mode I crack growth

The crack growth was detected and monitored using a d.c potential drop system as well as two travelling microscopes. The measurements of crack length were taken on both sides and according to ASTM method E647 (ASTM E647-88a). These two measurements are invalid if the reading at the front varies by more than 0.025w or by more than 0.25B whichever is less from the reading at the back. Through out the test these readings were within the ASTM standard limit.

The value of the stress intensity factor for pure mode I was calculated using the equation (4.14) given by Tada et al (1985). The mode I threshold results for different (R) ratios are given in Table (3) and fig. 5.8. The results show some effect of R ratio on the threshold, but they do not show that as R increases ΔK_{Ith} decreases. ΔK_{Ith} for R = 0.06 was equal to $8.1 MPa\sqrt{m}$ while when R increases to 0.17 ΔK_{Ith} increases to $8.4 MPa\sqrt{m}$, but it starts to decrease and reaches a value of $7.14 MPa\sqrt{m}$ as R increases to 0.37. It then increases to $8.25 MPa\sqrt{m}$ when R = 0.5. For precracked specimens (see Table 4) the results are clearer. For R = 0.06, $\Delta K_{Ith} = 7.1$ and decreases to 6.7 for R = 0.17. It is then increased to $7.1 MPa\sqrt{m}$ for R = 0.37 and decreased to the value of $5.7 MPa\sqrt{m}$ for R = 0.5.

All the results obtained from mode I and mixed mode I & III were processed using a Fortran 77 program on Sheffield University Prime 9950 computer. The raw data was taken from the data logger in addition to some of the specimen dimensions. The data logger recorded five readings, these were, the minimum and maximum load applied to the specimen at that moment and the specimen front and back p.d. readings as well as that of the p.d. reference point. The

number of cycles were calculated from the time elapsed and the frequency given by the Mayes servohydraulic test machine. These readings were recorded at certain intervals such as every five or ten minutes depending on the test. Additional data supplied to the program were the test number, the width and thickness of the specimen, the distance between the reference p.d. probes and the number of readings put into the data file.

The program calculated the crack length using equation (4.12) taking v_1 as the average between front and back sides of the specimen p.d. readings. Once the crack length was calculated, the stress intensity factor could be calculated using equation (4.14) making use of the minimum and maximum load readings to calculate the applied load range. A graph of crack length versus the number of cycles was then plotted and from the information on this graph, the fatigue crack growth was then calculated using a seven point fit routine given in ASTM E647. A graph of crack growth rate versus stress intensity factor was then plotted which shows the threshold value of ΔK_{Ith} for that particular test.

5.3.1.1 Crack initiation and crack growth in regime A or near threshold

Two types of tests were performed, one on slit specimens while the other was performed on fatigue precracked specimens. For R = 0.17, the starting stress intensity factor for the threshold tests was $7.0 MPa\sqrt{m}$ after more than 5×10^6 cycles, no crack was detected. The load was increased on HRE 26 to 7.76 $MPa\sqrt{m}$ and no crack was detected after more than 10^7 cycles. A higher load was applied on HRE25 specimen so that ΔK_I was calculated to be 8.24 $MPa\sqrt{m}$ and still no crack could be detected after more than 7×10^6 cycles. The lowest

undetectable crack length was calculated in all these tests and was found to be 1×10^{-11} m/cycle. The threshold value of ΔK_I for R = 0.17 was found to be $8.3 MPa\sqrt{m}$ as the specimen HRE28 failed when $\Delta K_I = 8.44 MPa\sqrt{m}$ was applied and the crack was initiated after less than 10^6 cycles. The same test was repeated on HRE27 with the value of $\Delta K_I = 8.4 MPa\sqrt{m}$ a crack was initiated and extended to failure.

For R = 0.5 the tests started with a value of $\Delta K_I = 5 MPa\sqrt{m}$ and kept on increasing it by an average of 10% to obtain a value of ΔK_I = 5.5, 6.0, 6.6, 7.2 and 8.0 $MPa\sqrt{m}$, but no crack was detected in all these tests till ΔK_I was increased to the value of $8.8 MPa\sqrt{m}$, then a crack was detected after 0.5×10^6 cycles. These tests were later repeated with different values of ΔK_I starting with $\Delta K_I = 6.25 MPa\sqrt{m}$ and increased to 6.8 and 7.5 $MPa\sqrt{m}$ and after 10^7 number of cycles, no crack could be detected till ΔK_I was increased to $8.25 MPa\sqrt{m}$ and the crack was initiated and extended to 7.2 mm when the number of cycles were just less than 2×10^6.

It is noticeable that when the value of ΔK_I is less than the threshold value, the crack can not be detected even after 10^7 cycles, while when the value of ΔK_I is above the threshold, the crack was initiated and extended to a reasonable length in less than 10^6 cycles.

As the cracks were initiated in those slit specimen tests, the test was stopped in each case and the crack length was measured on both sides of the specimen using the travelling microscope and the p.d. calibration to reach an accurate value of crack length. The load was then reduced by steps of 10% till the crack did not extend any further, even though the number of cycles elapsed from the last reduction of load was more than 10^7 cycles. The value of ΔK_{Ith} for

a fatigue precracked specimen was found to be much lower than the slit specimen. In HRE25 specimen for R = 0.17, this ΔK_{Ith} was found to be $6.7MPa\sqrt{m}$, while for HRE76 precracked specimen ΔK_{Ith} was equal to 5.7 $MPa\sqrt{m}$ for R = 0.5 and for the same R value in HRE80 specimen it was found to be equal to $6MPa\sqrt{m}$.

The difference between the stress intensity factor for a slit specimen and a fatigue precracked specimen was found to be quite large and it was within 20% of the threshold value of the slit specimen, i.e. the precracked specimen threshold value of ΔK_I is less than the slit specimen by an average of 20% .

5.3.1.2 Crack growth in the linear region of regime B

In this region, fatigue crack growth, could be described by Paris law. The crack length in this regime was calculated by the Fortran computer program based on a program given in ASTM E647.

In this region the effect of R is diminished and it can be seen from the crack growth rate for different R values tests that R effect is hardly noticeable. This will be dealt with in Chapter Six in figures (6.2 & 6.3).

The relationship between fatigue crack growth rate ($\frac{da}{dN}$) and the mode I stress intensity factor for this linear region could be described by this following equation:

$$\frac{da}{dN} = 0.45 \times 10^{-11} \Delta K^3{}_I \qquad (5.2)$$

Where growth rate in m/cycle and stress intensity factor in $MPa\sqrt{m}$

If these results are to be compared with the previously published results of Lindley & Richards (1982), they will be found in good agreement. Also Lindley & Richards found the threshold stress intensity factor of the $3.5\%NiCrMoV$ rotor forging steel to be 8.6 $MPa\sqrt{m}$ for R = 0.1 which is in good agreement with the 8.3 $MPa\sqrt{m}$ found in this research for R = 0.17.

5.3.2 Fractography

Two mode I specimens were broken open and examined under the scanning electron microscope, HRE28 (R = 0.06) and HRE80 (R = 0.5). The first one was tested under constant load till the final fracture took place. In the second specimen a crack was initiated and extended by 8 mm from the bottom of the slit, the load was then reduced by 10% and the process was repeated until the crack stopped extending and after 10^7 cycles no crack extension was recorded. The load was then increased by 10% and the crack started extending again. The stress intensity factor (ΔK_I) for HRE28 was equal to 8.44 $MPa\sqrt{m}$ at R = 0.06. The fracture surface had no identity except for the appearance of crystallographic facets and they existed in high density and they kept on increasing as ΔK_I was increased due to the extension of the crack.

Fig.(5.9) shows the fracture surface of HRE80 with R = 0.5 at constant load just above threshold value when the crack extended to a length of 3mm and the plastic zone was small. Failure takes place in one of the slips planes causing the facets to appear in different places in the fracture surfaces. The surface is featureless and does not show any particular pattern or striations and shows a typical mode I fracture surface. The crack was allowed to extend to a length of 9 mm before the test was stopped and the load reduced by 10%. The nature of

the fracture surface is of crystallographic facets. As the load is reduced further till the crack stops extending, the surface changes from crystallographic facet nature to a flat plane fracture due to the very low crack growth rate, where the crack changes direction in step wise pattern inside the layers of one grain, and the same things happen when the crack extends from one grain to another neighbouring one leading to the illumination of the crystallographic facets and to the existence of a predominantly flat fracture surface as shown in Fig.(5.10) where stress intensity factor (ΔK_I) and crack growth rates ($\frac{da}{dN}$) are both low.

5.4 Mixed mode I and III tests

Several tests were carried out for different $\frac{\Delta K_I}{\Delta K_{III}}$ ratios in order to determine the threshold value of the stress intensity factor under mixed mode I & III. The load shedding technique which was used for mode I tests can not be used in the mixed mode I & III conditions due to the increasing load dissipation as the crack extends since the crack is a factory roof type. Also the crack path is not defined since the crack angle will change with the crack extension causing the ratio $\frac{\Delta K_I}{\Delta K_{III}}$ to change, and there is no reliable method to calculate these changes as they take place. It was found that the method using several specimens was the most practical one in determining the threshold value of ΔK for these conditions. The problems associated with the slit specimens could be avoided in the future if the conclusions of this research were to be used in calculating the value of the crack angle as the crack extends.

The results of mixed mode I & III of fatigue tests for different R ratios are shown in Fig.(5.11) and given in Tables 6 & 7. The results are divided into two

parts, one for failed specimens and the other for unfailed specimens, where cracks could not be detected with the equipment used in these tests. These figures also include pure mode I and mode III tests results. The results were then normalised by mode I threshold stress intensity factor which was determined earlier from the slit three points tests at $\theta = 90^o$ for each R value as shown earlier in Table 3.

5.4.1 Fatigue crack growth rate in mixed mode I & III

As the crack is initiated when the conditions stated above are met, the crack will start extending till it reaches the steady state. The branch crack growth rate is governed by the Paris equation and the crack keeps on extending till the fracture point where the specimen is broken open.

The crack length was measured using the two travelling microscopes and the p.d. system using equation (4.12). The crack growth rate was calculated using the seven point curve fitting as proposed by ASTM E647. As it was not possible to use any precracked specimen due to the load dissipation process, all tests carried out were for slit specimens.

Three stress ratios (R) were used, these were R = 0.06, 0.17 and 0.5, two slit angles were used 45° and 60° only which gives a value of $\frac{\Delta K_I}{\Delta K_{III}} = 1$ and 1.73 respectively.

Readings of p.d. across the crack and the applied load were taken every five or ten minutes depending on the test conditions which gathered hundreds of readings in order to have a good source of data to be used at later stages.

The graphs of fatigue crack growth rates versus the crack length will be

produced and discussed in Chapters Six and Seven. In general the crack growth was slow or discontinuous at the beginning of the test and increased with the number of cycles.

5.4.2 Fractography of mixed mode I & III

All mixed modes specimens were broken open and seven specimens were prepared for fractographic analysis and were analysed using the scanning electron microscope (SEM). These specimens had different slit angles (45°&60°) and their R ratios were 0.06, 0.17 and 0.5. The other specimens which were broken open were not analysed under the SEM as they kept to the same pattern of the fatigue fractured surfaces as those used in this section of the study.

5.4.2.1 Specimens with slit angles of 45°

Three specimens HRE29, HRE31 and HRE78 were used in this analysis, they had R ratios of 0.06, 0.17 and 0.5 respectively and stress intensity factor ranges were 11.55, 12.16 and 9.9 $MPa\sqrt{m}$.

The facets started to appear at the slit root once the threshold value of ΔK_I was exceeded. These facets were all along the slit root. A difference in the length existed and that depended on the facet initiation place. The longest of these facets were found to be at the centre of the fracture surface and they get shorter nearer the edges of the specimen.

For R = 0.5, a unique pattern of the cracked surface was observed in all the test specimens used for this ratio. A border facet was initiated at spots

very close to the edges of the cracked surfaces, these two facets extended in a parabolic shape curve until they met each other at the centre of the lower part of the fracture surface where ΔK_I and the crack growth rate are very high as shown in Fig.(5.12).

In HRE78 the crack direction seems to vary from one spot to another. On different sides of the slit cliff the direction of the crack growth seems to be 180^o to one another. As the crack extended beyond the facet area it seemed to have a well defined crack front and in the area outside the meeting point of the two parabolic border facets, the crack seemed to extend so fast that what used to be striations are now small cracks themselves.

Fig.(5.13) shows a mixed mode fatigue crack surface where some rubbing is clearly shown causing the surface to be flat while next to it a striation can be seen which shows the existence of mode I fatigue. As the crack grows, the mode changes from mixed mode to practically mode I only. The rubbing effect of mode III is clearly shown in Fig.(5.14) where the top of what could have been a factory roof facet is made flat and featureless due to the rubbing between the two faces.

For R = 0.06 and 0.17 the pattern of the crack surfaces changes from that of R=0.5, the factory roof facets start at the slit root just as before and the facet in the middle of the fatigue crack face is longer than any other facet. Facets become shorter nearer the sides of the specimen, but there is no border facet surrounding the facetted area as existed for R=0.5. Those facets are initiated at a certain angle to the slit and along the whole slit length. When the crack has extended so much, the centre part in between the two facets has not grown at the same rate and as the crack extends even further, the centre part is broken

open showing that the fracture is brittle and not a fatigue one where the fracture surface is very coarse.

As the crack front advances further the mode changes towards mode I, where the crystallographic facets are dominant.

5.4.2.2 Specimens with slit angle of 60°

Four specimens HRE24, HRE73, HRE83 and HRE74 with stress intensity factor ranges equal to 10.8,10.48,9.8 and 9.6 $MPa\sqrt{m}$ respectively were prepared for inspection using the SEM. Their R ratios were 0.06 for the first two specimens and 0.17 and 0.5 for the other two specimens respectively. The general appearance of the fracture surface is similar for all of them. For HRE24 and 73 where R=0.06, it was noticed that as ΔK_A was reduced from 10.8 to 10.48 $MPa\sqrt{m}$, the length of the factory roof facets was reduced too, almost to half the length as shown in Fig.(5.15).

Considering any mode I graph of fatigue crack growth rate versus the stress intensity factor, e.g Fig.(2.5), the part of the curve from the threshold till it reaches the steady growth rate is called the structure sensitive area, and this is where most of the facets start. In all these specimens facets grew together due to fatigue. These facets are either joined together by plastic deformation and ductile tearing of the intervening ligaments or they stay independent or separated. The thickness of these facets increases with the crack depth and then decreases till it reaches a continuous crack front where all the facets had disappeared. A lot of rubbing takes place at the facets stage as was shown earlier.

As the crack extends and the facets disappear, the fatigue cracked sur-

face becomes coarse and crystallographic facets start to appear. As the crack extends further and the stress intensity increases, some striations appear expressing the steady state crack growth of mode I. As the crack extends even further with the increases of the stress intensity factor (ΔK_A), voids or dimples start to appear due to plastic deformation of the material showing that the fracture surface is over loaded as shown in Fig.(5.16). These dimples or voids coalesce with each other causing the material to break open.

5.4.3 The effect of mean stress on threshold behaviour in mixed mode I & III

The effect of R on the threshold value of ΔK_A could be studied from the figures (5.17) and (5.18). In the case of the 60° slit, it can be said that as R increases ΔK_{th} decreases, but the effect is not noticeable as R increases further towards the 0.5 value, since the difference between the threshold value for R=0.06 and 0.17 is 2.7% of the higher value while the difference between ΔK_{th} for R=0.17 and 0.5 is only 1.6% of the threshold value of ΔK for R= 0.17.

In the case of the 45° slit, the effect of the load ratio (R) is not very well defined, since ΔK_{Ath} is equal to 11.5 $MPa\sqrt{m}$ for R=0.06 while it increased to 12.1 $MPa\sqrt{m}$ when the load ratio increased to 0.17 and it started to decrease rather quickly to 9.1 $MPa\sqrt{m}$ for R=0.5.

It can be concluded that on the whole, increasing R ratio will result in a decrease in the apparent threshold value of stress intensity factor (ΔK_{Ath})

Chapter 6

Analysis

6.1 Mode I tests

6.1.1 Precracked and slit specimens

In the mode I tests three point bend slit specimens were used to determine the fatigue stress intensity threshold. The crack was allowed to grow to a length of 5 - 6 mm beyond the slit length, the test was then stopped and the crack length was measured. A 10% load reduction process was started to estimate the threshold value of the stress intensity factor of the fatigue precracked specimen. This test was repeated with different R ratios of 0.06, 0.17, 0.37 and 0.5 in order to consider its effect on the threshold.

For R = 0.17 ΔK_{Ith} for the slit specimen was 8.4 $MPa\sqrt{m}$, while the crack stopped extending when the applied ΔK_I was 7.00 $MPa\sqrt{m}$ for the precracked specimen. Fig.(6.1) shows the fatigue crack growth rate versus ΔK_I

for HRE 25 specimen where it was used as a slit specimen and then as a fatigue precracked specimen.

For both precracked and slit specimens tests, the fatigue crack growth rate at the threshold was 10^{-7} mm/cycle. This rate was increasing till it reaches 2.5×10^{-6} mm/cycle, while the stress intensity factor hardly changes its value. The two graphs cross one another at 2.5×10^{-6} mm/cycle. After this value the slit specimen fatigue crack growth rate was higher than that of the precracked specimen until it reached 4×10^{-6} mm/cycle. After that the crack growth rate seems to be the same till the specimen reaches its fracture point where the value of the crack growth rate reaches a value much higher than 8×10^{-6} mm/cycle.

Figures (6.2) and (6.3) show the fatigue crack growth rates versus ΔK_I for the slit specimens and the precracked ones for different R ratios.

A general comparison of the threshold values between the slit specimens and the fatigue precracked ones could be found from the data given in Tables (3) and (4), where it is clear that the threshold value of ΔK_I for the precracked specimens is lower than the slit specimens.

6.1.2 Crack growth rates in the linear region of mode I tests

It is previously reported that the fatigue crack growth in the mid regime or in the linear region of the $(\frac{da}{dN})$ against (ΔK_I) graph, where striation formation predominates and growth rates of 10^{-8} - 10^{-6} mm/cycle typically occur, has been found by many workers to obey the Paris - Erdogan law. Lindley and Richards

(1982) claim that fatigue crack growth rate in the region is relatively insensitive to microstructure and mean stress.

It can be seen from Fig.(6.1) that the fatigue crack growth rate in this region can be described by the following equation

$$\frac{da}{dN} = 0.45 \times 10^{-11}\ \Delta K_I{}^3 \tag{6.1}$$

where $\frac{da}{dN}$ is in m/cycle and stress intensity factor (ΔK_I) in $MPa\sqrt{m}$.

To compare this result with other previously published ones, Lindley and Richards (1982) gave the following equation as an upper bound growth rate for many steels in the mid ΔK_I regime

$$\frac{da}{dN} = 1 \times 10^{-11}\ \Delta K_I{}^3 \tag{6.2}$$

Other workers such as Yates and Miller (1989) expressed the fatigue crack growth rates in the linear region for the steel used in these tests, as

$$\frac{da}{dN} = 5 \times 10^{-12} \Delta K_I{}^3 \tag{6.3}$$

Elsender (1982) gave an average fatigue crack growth rate for tests performed on the HRE steel at normal room temperature to be

$$\frac{da}{dN} = 3.1 \times 10^{-12}\ \Delta K_I{}^3 \tag{6.4}$$

with the same upper bound equation as that given by Lindley and Richards.

6.1.3 Effect of stress ratio on the crack growth rate in the linear region

Lindley and Richards, as stated earlier, believe that the crack growth rate in this linear region is relatively insensitive to the R ratio effect. In this study the Paris equation for the linear part of the crack growth rate was deduced for several specimens each with different R ratio. These equations are given as follows:

For R = 0.06

$$\frac{da}{dN} = 0.45 \times 10^{-11}\ \Delta K_I{}^3 \tag{6.5}$$

Where da/dN is in m/cycle and ΔK_I is in $MPa\sqrt{m}$.

For R =0.17

$$\frac{da}{dN} = 0.87 \times 10^{-11}\ \Delta K_I{}^3 \tag{6.6}$$

and for R = 0.5

$$\frac{da}{dN} = 1.0 \times 10^{-11}\ \Delta K_I{}^3 \tag{6.7}$$

All these tests were performed on slit specimens.
Figures (6.4) to (6. 6) show the actual derivations of these equations.

Many workers such as Maddox (1975), Pearson (1972), James (1973), Frost, Marsh and Pook (1977) and Nishioka and many others generally indicated an increase in growth rates as R increases positively. In general, the reported increase in growth rates are factors of 3 or less (for R increasing from 0 to 0.7),

unless yielding or transition to plane stress conditions occurs at the crack tip in which case more significant increase in growth rate ($\times 10$) have been reported.

The fatigue crack growth at the linear region of the crack growth for different R ratios could be represented by the equation with respect to that for R = 0

For positive R ratio

$$\frac{da}{dN} = (\frac{da}{dN})_{R=0}(1.2 + 2R) \tag{6.8}$$

This equation seems to agree with the previous reported fatigue crack growth for R = 0.17 and 0.5. In order to verify this equation further fatigue crack growth tests are required.

6.1.4 Effect of R on mode I threshold prediction

It is convenient for comparative purposes to present previously published data showing ΔK_{th} as a function of stress ratio (R). It was reported earlier in Chapter Two that there are several prediction theories for the effect of R ratio on the mode I fatigue threshold. These relations were stated as empirical equations. The values of the threshold stress intensity factors achieved in this study are imposed on these empirical equations as shown in Figures (6.7) to (6.9).

The first prediction theory is proposed by Schmidt and Paris (1973) which describes the relationship between stress ratio and threshold value of the stress intensity factor for two different R ratios, one for high value of (R) and the other for low value. This theory depends on the crack closure argument as explained earlier in the literature review chapter and it is given as:

$$\Delta K_{Ith} = \Delta K_{tho}\,(1 - R) \tag{6.9}$$

For low R ratio, if $K_{min} \leq K_{cl}$, where K_{cl} is the stress intensity factor which just opens the crack during the loading part of the cycle.

and as

$$\Delta K_{Ith} = \Delta K_0 = constant \tag{6.10}$$

For high load ratio, if $K_{min} \geq K_{cl}$, where ΔK_0 is the effective threshold stress intensity range.
which leads to

$$\Delta K_0 = K_{max}\,(1 - R) \tag{6.11}$$

Figure (6.7a) shows the experimental threshold stress intensity factor for both the slit and the precracked specimens. Yates and Miller results (1987) are plotted in figure (6.7b). It can be seen that the threshold stress intensity factor for the slit specimens is above the predicted failure line of the previously stated relationship, while those of the precracked specimens are closer to the failure lines predicted in this theory. The same can be said about Yates and Miller's results.

The second theory to describe the effect of R ratio on ΔK_{Ith} was proposed by Klensil and Lukas (1972) which is widely used in analysing threshold data and it is given as:

$$\Delta K_{th} = \Delta K_{tho}\,(1 - R)^{\gamma} \tag{6.12}$$

where γ is a material constant and could be determined experimentally. Its value for the $3.5\%NiCrMoV$ is estimated by Paris and Erdogan (1963) and also reported by Lindley (1982) to be 0.6 for positive R ratios. Fig.(6.8a & b) show the threshold values of the stress intensity factor obtained in this study as well as those of Yates and Miller with respect to equation 6.12. The fatigue cracked specimens are in good agreement with this theory while slit specimens results are considerably higher than the predicted failure line. .

The third expression to describe the relationship between stress ratios and ΔK_{Ith} is given by McEvily and Gregor (1977) and it is stated as

$$\Delta K_{th} = \left(\frac{1-R}{1+R}\right)^{\frac{1}{2}} \Delta K_0 \qquad (6.13)$$

The same relationship is given by Kaisand and Mowbray (1979) for positive R values, while for negative R values

$$\Delta K_{th} = \frac{1-R}{1-\frac{R}{3}} \Delta K_0 \qquad (6.14)$$

The explanation for the negative value in the above equation is based upon the assumption that one third of the compressive part of the applied cycle is effective in propagating cracks. Figures (6.9a & b) show the experimental data obtained in this research and Yates & Miller (1987) results in comparison with equation (6.14).

6.1.5 Prediction of threshold for fatigue precracked specimens

All the previously discussed predictions were for slit specimens in respect to the stated empirical relationship. It is noticed that the threshold stress intensity

factor for all the failed slit specimens in this study are higher than the predicted failure equations. A comparison might be made between the failure of the slit specimens and the fatigue precracked ones in the light of the stated failure loci. It is a result of this study that the value of the ΔK_{Ith} of the fatigue precracked specimens is lower than that of the slit ones and it is closer to the failure lines stated earlier.

6.2 Mode III tests

In this section, the threshold stress intensity factor under mode III loading is investigated. Also the effect of the stress ratio on the threshold and the crack growth rate has been studied.

Fig.(6.10) shows a graph similar to the S-N curve with the S being replaced by ΔK_{III}. It can be seen from this graph that the threshold stress intensity factor (ΔK_{IIIth}) for R = -1 is 7.4 $MPa\sqrt{m}$.

The method used to determine ΔK_{IIIth} is that proposed by Pook (1975) which has the advantage of being used on very simple test equipment, using simple testing routines, but expensive on specimens as it requires many specimens for each set of tests.

In pure mode III tests, where round slit specimens were used, stress intensity factors for pure mode III tests were calculated using a formula given by Tada, Paris and Irwin as stated in Chapter Four equation (4.13).

Four R ratios were considered, R=-1, 0, 0.17 and 0.5. The failure mode considered in these tests is of the factory roof type and not the macroscopically

flat structure mode, which is normally of a higher threshold value than the previously mentioned failure. The fractured surface of the failed specimens showed the characteristic facets, indicating that the failure was that of a mode I nature. This suggest that low ranges of ΔK_{III} favour 45° cracking over shear cracking.

Table (5) gives the threshold stress intensity factor for the mode III tests for different R ratios. The threshold stress intensity factor recorded for the four investigated stress ratios were as stated below

R = -1 $\Delta K_{IIIth} = 7.4\ MPa\sqrt{m}$

R = 0 $\Delta K_{IIIth} = 7.2\ MPa\sqrt{m}$

R = 0.17 $\Delta K_{IIIth} = 6.8\ MPa\sqrt{m}$

R = 0.5 $\Delta K_{IIIth} = 6.35\ MPa\sqrt{m}$

It can be seen from the above results that as the stress ratio (R) increases ΔK_{IIIth} decreases.

For specimen RD1 a torque range of 49 Nm was applied for R = -1. Deviation out of the mode III plane occurred in the form of fatigue cracks which were initiated at the slit root. This generally occurred within a few hundred cycles from the start of the test. Initiation took place simultaneously, to a certain

extend, all round the specimen cross section. Very little crack asymmetry was evident, as can be seen from Fig.(5.6). Therefore the potential drop given by the four poles, which will only be recording local events in the vicinity of the spot welded probes, could be taken as representative of the whole of the crack front.

6.3 Crack growth in mode III

The main features which are considered in this section are:
The relation between the crack growth rates and the crack length.
The relation between crack growth rates and the stress intensity factor.
The effect of stress ratio (R) on the crack growth rates.

Fig.(6.11) shows the crack length versus the crack growth rates $\frac{da}{dN}$ for R = -1. It can be seen that the growth rate starts at 10^{-7} mm/cycle, it then increases to 1.74×10^{-6}, where it reaches the peak. When crack length is less than 0.5 mm the growth rate starts to decrease. As the crack extends even further, the growth rate decreases even further. A close study of the crack growth rates shows that the rate does not decrease or increase continuously. The shape of the graph is a zigzag, which is due to fluctuation in the effective applied force. This is the result of the interlocking of mode I facets on complementary planes and the friction between the opposite crack surfaces as well as the shorting in the crack detection circuit. Both of these effects are difficult to quantify. It can be deduced from Fig.(6.11) that for R = -1 the crack growth rate decreases with increasing crack depth.

The crack growth rate under different loads for the same R ratio is shown in Fig.(6.12). It can be deduced from this graph that increasing the applied load causes an increase in mode I fatigue crack growth rate. In both of these specimens the maximum growth rates recorded were when the crack lengths were less than 0.5 mm long. One might argue that the maximum growth rate recorded is due to the crack being a short crack. This is not true as plotting the Kitagawa - Takaheshi diagram for the material under research showed that the length of short crack for this material is less than .14 mm. The fluctuation in the crack growth rates seems to increase as the crack increases in depth. This is due to reasons explained earlier.

The effect of R ratio on the crack growth rate is considered in Fig.(6.13). It can be seen that the average crack growth rate increases as R increases. The average crack growth rate for R = -1 is less than 1×10^{-6} mm/cycle, while it increases to 2×10^{-6} mm/cycle when $R = 0$. The average value of the crack growth rate is further increased to 3×10^{-6} mm/cycle when R is 0.17. Therefore tests at R = -1 could be conducted at lower growth rates, involving larger number of cycles than those tests for R = 0 or R = 0.17. The crack growth rate increases for R = 0.06 to 0.5 while it decreases for R = -1.

6.3.1 Crack growth rates with respect to stress intensity factor

Figs.(6.14), (6.15) and Fig.(6.16) show the crack growth rates in three specimens for three different R ratios (-1, 0 and 0.17) respectively. In all three graphs, the fluctuation in the crack growth rate is very clear. The fluctuation is high. This is mainly due to shorting in the crack detecting circuit, as a result of the contacts between points on the opposite faces of the crack in the initial stages of its extension, and due to the interlocking and frictional effects between the crack facets which reduces the stress intensity factor. Measurements of the effective stress intensity factor is hard to achieve.

For R = 0, 0.17 and 0.5 it is clear that the average crack growth rate increases as the stress intensity factor increases, while it decreases as the stress intensity factor increases for R = -1. This could be due to the crack profile difference for R = -1 and when R > 0.

The average crack growth rate for R = -1 is less than 1×10^{-6} mm/cycle. It increases to 1.5×10^{-6} for R = 0 and it is 3×10^{-6} mm/cycle for R = 0.17. These results shows that as R increases from -1 to 0.17 the average crack growth rate is increased too.

The reason for this could be due to the fact that for R = 0 or above, the torsional cycling with a cyclic minimum of 0 (for R = 0)or above will result in a single set of 45 deg. tension planes being subjected to a tensile stress amplitude of $\Delta\sigma$. For R = -1, the mean cycling effect is zero, with the same torque range as

before, the shear planes will experience the stress as previously, but the 45-deg planes will individually only experience $\frac{\Delta\sigma}{2}$ in tension and $\frac{\Delta\sigma}{2}$ in compression. Hence the tensile stress on any particular 45-deg planes has been halved, causing the crack growth in this mode to be reduced.

Fig.(6.17) shows a comparison between mode I and mode III for crack growth rate. It can be seen that the mode III crack growth rate is much slower than the mode I. The mode I crack growth rate is almost 10 times higher than that of mode III for the same value of ΔK_{III}.

6.4 Mixed mode I and III

6.4.1 Mixed mode threshold prediction theories

6.4.1.1 Pook's theory

In an angled slit specimen, similar to those used in this research, Pook (1980) predicted that fatigue crack threshold takes place when the stress intensity factor of the mode I facets (Δk_I), formed at the tip of the initial crack or slit exceeds that of the threshold.

i.e

$$\Delta k_I = \Delta K_{Ith} \tag{6.15}$$

For slit angle $\theta \neq 90^o$, the apparent values of the K_I, known as (K_A),

is the stress intensity factor of a conventional three point bending specimen calculated using Tada, Paris and Irwin (1985) method.

K_I and K_{III} were calculated using the approximate expression proposed by Pook (1985A)

The mode I facet stress intensity factor was then calculated using Pook's expression

$$k_I = \frac{1}{2}\left(K_I(1 + 2\upsilon) + \left(K_I{}^2(1 - 2\upsilon)^2 + 4(K_{III})^2\right)^{\frac{1}{2}}\right) \qquad (6.16)$$

where K_I and K_{III} are the macroscopic stress intensity factors in mode I and III respectively and υ is taken as $(\frac{1}{3})$.

6.4.1.2 Mixed mode (I & III) model

This model was proposed by Yates (1991) is a combination of Pook's and Yates and Miller (1989) models. It depends on the calculation of $\Delta K_I \& \Delta K_{III}$ of an angled slit specimen given earlier by Pook's theory (1985)

$$K_I = K_A \sin^2\theta$$

$$K_{III} = K_A \sin\theta\cos\theta$$

where θ is the angle of inclination of the original slit.

It also uses the crack opening displacement proposed by Yates & Miller (1989) as the parameter to describe the field at the tip of the crack. It was considered

(Yates 1991) that in an angled slit specimen the mode I direction for crack growth is perpendicular to the specimen long axis, such that $\phi = 90 - \theta$. The Tresca yield criterion is used to derive the condition for growth of fatigue cracks to reach the proposed locus of failure of

$$\left(\frac{\Delta K_I}{\Delta K_{Ith}}\right)^2 \sin\theta + 2.6\left(\frac{\Delta K_{III}}{\Delta K_{Ith}}\right)^2 \cos\theta = 1 \tag{6.17}$$

which leads to the result that the stress intensity factor of the crack in the mode I direction may be calculated using the equation

$$k_I = \left({K_I}^2 \sin\theta + 2.6\ {K_{III}}^2 \cos\theta\right)^{0.5} \tag{6.18}$$

The present research results and other relative data will be compared to the above failure prediction theories and other failure loci in Chapter Seven.

6.4.2 Threshold in mixed mode I & III loading

Tables 6 and 7 show the mixed mode I & III results which were performed using two different slit angles: 45° and 60°.

For 45° slit specimens the apparent threshold stress intensity factor (K_A) calculated using Tada, Paris and Irwin method (1985), where K_A is the stress intensity factor for a similar specimen with the same slit depth, but with 90° slit angle. It is found that the threshold stress intensity factor when $R = 0.06$ is 11.5 $MPa\sqrt{m}$. $K_I \& K_{III}$, calculated using Pook's method were 5.78 $MPa\sqrt{m}$

each. For R = 0.17, it was found that the crack started to grow when $\Delta K_A = 12.16 MPa\sqrt{m}$, i.e $\Delta K_I \& \Delta K_{III}$ were equal to 6.08 $MPa\sqrt{m}$ each. When R increases to 0.5, K_A at which fatigue threshold will take place was 9.1 $MPa\sqrt{m}$. $\Delta K_I \& \Delta K_{III}$ were 4.55 $MPa\sqrt{m}$ each.

For 60° slit specimens, ΔK_A threshold for R = 0.06 was 10.05 $MPa\sqrt{m}$ and ΔK_I & ΔK_{III} were 7.54 and 4.35 $MPa\sqrt{m}$ respectively. When R increases to 0.17, ΔK_A threshold decreases to 9.8 $MPa\sqrt{m}$ giving the values of 7.34 & 4.236 $MPa\sqrt{m}$ to ΔK_I & ΔK_{III} resp. As R increases to 0.5, K_A threshold decreases slightly to 9.5 $MPa\sqrt{m}$, giving 7.2 and 4.1 $MPa\sqrt{m}$ as ΔK_I & ΔK_{III} resp.

It can be argued that as R increases from 0 to 0.5 , for the 60 deg. slit angle specimens, the apparent stress intensity factor decreases from 10.05 to 9.5 $MPa\sqrt{m}$. This decrease is not all that significant but the specimen does follow the pattern that as R increases ΔK_{Ath} decreases.

The same can not be said about the 45° slit specimens. ΔK_{Ath} seems to increase first from 11.55 to 12.16 $MPa\sqrt{m}$ as R increases to 0.17. It then decreases drastically to 9.9 $MPa\sqrt{m}$ when R reaches 0.5 value.

6.4.3 Mixed mode I & III fatigue crack growth rates

From the figures concerned with this section, it is clear that the growth rate in general fluctuates. This is mainly due to the nature of the crack surfaces which causes shorting in the circuit used for detecting the crack length. It is noticeable that the fluctuation in the crack growth rate diminishes as the crack grows. This is due to the fact that the crack opening is larger at higher stress intensity factors and the mode of the loading changes towards mode I as the crack grows to failure point.

A comparison between mode I and mixed mode (I & III) for different R ratios and different slit angles will be discussed in Chapter Seven. It can be stated that the crack growth in mode I is higher than that in mixed mode I and III for the same stress intensity factor. Also as the crack grows, the mode of the loading changes from the mixed mode *I & III* to mode I, and at the last few millimetres of crack extension before the specimen is broken open, the mode of the crack growth is pure mode I, as it was shown earlier in Chapter Four, where fractography supported this fact. The slit angle also changes from 45° or 60° to 90° to the long axis of the specimen. The crack growth rate increases as the crack increases in length and the curve of the mixed mode grows nearer and nearer towards the mode I growth rate represented by the Paris equation, for each R ratio.

6.4.4 The effect of R ratio on crack growth

It can be seen from figure (6.18) that, for positive R ratios, as R increases, the crack growth rate increases too. The average crack growth rate for R = 0.06

increases from 0 to 4×10^{-6} mm/cycle, as the crack increases from 5mm (its original slit value) to 10 mm approximately, while for R = 0.17 the growth rate is increased from 0 to 6×10^{-6} mm/cycle for the same increase in crack growth. For R = 0.5, it is between $0 - 9 \times 10^{-6}$ mm/cycle. It is also clear that as the crack increases in length the crack growth rate increases too and the fluctuation in growth rate is reduced.

It can be said that as R increases from 0 to 0.5 the range of fatigue crack growth rates increases too from $0 - 4 \times 10^{-6}$ to $0 - 9 \times 10^{-6}$ mm/cycle.

6.4.5 The effect of slit angle on the crack growth rate

Fig.(6.19) shows a comparison in crack growth rate in mixed mode (I & III) loading for two different slit angles. The stress intensity factors have been normalised using mode I stress intensity threshold value. It can be seen that for the same value of stress intensity rate, the growth rate of the crack in the specimen with a 60° slit angle is higher than that with slit angle of 45° by 1×10^{-6} mm/cycle.

This is due to the fact that according to Pook's model the stress intensity factor in the 60° slit angle specimen is equivalent to $0.75K_A$, and the mode III stress intensity factor is equal to $0.433K_A$. In the 45° slit angle specimen, K_I is equal to K_{III} and it is $0.5K_A$.

It was established that mode I crack growth rate is much higher than that of mode III for the same value of stress intensity factor. It follows that the

crack growth rate in the specimen with slit angle of 60° must be higher than that in the specimen with the 45°, since K_I in the 60^O specimen is higher than that in the 45° specimen.

Chapter 7

Discussion

In this chapter the previously analysed results of mode I, mode III and mixed mode I & III will be discussed and compared to the previously mentioned fatigue threshold failure criteria. New equations to represent the whole crack growth behaviour in mode I and mixed mode I & III will be deduced. The crack growth in mixed mode I & III will be analysed according to a proposed new method which is based upon the change in the crack growth angle as the crack extends. Also a new model to predict the crack path using the crack length will be devised.

7.1 Mode I fatigue crack growth thresholds

Fatigue crack growth threshold stress intensity factors for the slit and precracked specimens (mode I) are presented in Tables (3) and (4). The results show that for the same material under the same stress ratio, the fatigue crack growth thresholds of the fatigue precracked specimens are lower than those of the slit specimens

under the same circumstances, even though if the crack closure mechanism is considered, the slit specimens should have lower threshold stress intensity factor due to the fact there is no crack closure in the slit specimen while in the precracked specimen the crack has extended few millimetres before the reduction in load process begins, in order to find the threshold stress intensity factor.

The reasons behind this could be due to stress distribution where slit specimens have compressive residual stresses caused by the spark eroding of the slit, while the precracked ones do not have any of these residual stresses, since the crack was allowed to grow for a distance at least ten times the maximum plastic zone of the previous load. It is also due to the fact that the slit specimens threshold was achieved by increasing the load till a crack was initiated, while for the precracked case it is done by load shedding method.

The other reason could be that in the slit specimen a crack has to be initiated due to high load while in the fatigue cracked specimens, the crack is propagating and it takes a higher load to start a crack than to extend it. This could be explained in terms of the fact that to initiate a crack from a slit specimen is similar to a crack initiation in a notch, while to extend a crack in an already fatigue cracked specimen is a crack propagation mechanism. Consider the stress - crack length graph at the crack tip, it can be stated that the stress at the crack tip is higher at a sharp crack tip compared to that in a notch or blunt crack tip. Also the above reasoning could be explained in terms of the stress concentration factor which is roughly calculated using the equation

$$K_T = 1 + 2\sqrt{\frac{D}{\rho}} \tag{7.1}$$

where

K_T is the stress concentration factor

D is the depth of the notch

ρ is the radius of the notch

Even though the factor is normally applied to notch specimens, the slit could be considered as a very small radius notch or as a blunt crack with root radius of 0.06 mm. This factor is larger for precracked specimen than slit one due to the fact that ρ is smaller by a factor of at least 10 for the precracked specimen than the slit ones (Taylor 1990).

7.2 Mode I fatigue crack growth equation

It was reported earlier in Chapter Six that the Paris equation for the linear region of mode I loading is given by the equation

$$\frac{da}{dN} = C\,\Delta K_I^m \tag{7.2}$$

Fig.(6.1) shows a graph of this equation for a slit and precracked specimens. In this section, the whole curve of the crack growth rate versus stress intensity factor will be considered.

The minimum crack growth rate that was considered as the crack started to grow was 1×10^{-7} mm/cycle. Also the linear region in figure (6.1) and

other figures representing similar equations starts when the value of crack growth is

$$da/dN = 2 \times 10^{-6} mm/cycle$$

The linear region of the crack growth rate continues beyond the value of

$$da/dN = 1 \times 10^{-4} \text{ mm/cycle}$$

The minimum crack growth rate considered was 10^{-7} mm/cycle. The linear region growth rate starts at a growth rate of 2×10^{-6} mm/cycle, giving a difference of 1.9×10^{-6} below the linear region.

An equation of the type

$$\frac{da}{dN} = C_1 \Delta K_I^{m1} - D \tag{7.3}$$

was considered to represent the whole curve of the crack growth. In this case D was equal to 1.9×10^{-6} mm/cycle.

If the maximum crack growth rate was taken to be 1×10^{-4} it will be found that

$$1 \times 10^{-4} - 1.9 \times 10^{-6} = 98.1 \times 10^{-6} \text{ mm/cycle}$$

which is nearly 100 times greater that the lowest crack growth rate in the linear region. The value of 1.9×10^{-6} mm/cycle was then added to the crack growth

rate and new values of C_1 and m_1 were found from the log - log graph to give the final crack growth rate equation.

$$\frac{da}{dN} = 4.6 \times 10^{-9}\ \Delta K_I^3 - 1.9 \times 10^{-6} mm/cycle \qquad (7.4)$$

Fig.(7.1) shows the above equation with respect to the experimental results. The equation is in a reasonable fit to the experimental data.

This crack growth rate equation is a development of the Paris equation which represent the linear part of the crack growth. It represents the crack growth for a certain specimen with a known threshold. Further development of this equation is shown in Chapter 7.8 by linking the value of D to the threshold stress intensity factor, by taking into consideration the effect of R ratio on threshold. This equation could describe the whole crack growth rate due to the fact that the effect of stress ratio on the crack growth in the linear region is small and the difference between the maximum and minimum crack growth rate is nearly 100 times the minimum value, where the effect of R ratio on the threshold might be considered.

7.3 Fatigue under mode III loading

Under pure cyclic torsion, the crack growth is strongly influenced by torsional crack closure. The effective torque on the unbroken ligament is severely reduced from the nominal applied value by rubbing and interlocking between adjacent crack surfaces. The fractured surface abrasion effect is critically dependent upon

the mode of the applied loading and the nature of the fractured surface. It is increased with increasing crack length and decreasing torque level.

In torsion, the crack will remain closed and confined to its own plane where the two sliding surfaces will then move parallel to one another. Whether the crack is a factory roof type or a macroscopically flat (at higher stress intensity factors), the two sliding surfaces will slide against each other causing friction, abrasion, smearing and fretting oxide formation. This will lead to reduction in the nominal value of the external stress to a lower value at the crack tip. This situation was similarly experienced by Tschegg et al (1991) and was called 'roughness - induced crack closure' or 'sliding mode crack closure'. This is the analogue to the mode I fatigue crack closure, where the stress intensity factor is reduced to some lower effective value at the crack tip by contact of mating surfaces under positive load.

In figure (6.11), the crack growth rate versus crack length for mode III was plotted. No sliding mode crack closure effect was considered in the calculation of these results. The crack growth rates observed in these experiments were lower than mode I crack growth rates by a factor of 10 at comparable stress intensity values, see figure (6.17). It is clear from figure (6.11) that for R = -1, the crack growth decreases with increasing crack length. This is due to the influence of the sliding crack closure on crack propagation, indicating the presence of some energy dissipating process that upset the theoretically expected scale with respect to the stress intensity factor.

The effect can be minimised by the application of an axial load, as in the case of Nayeb-Hashemi et al (1982) who showed that the sliding mode crack closure effect was reduced by opening the crack due to super imposing of a static

load to the specimen under torsion. However this method introduces a mixture of cyclic mode III and static mode I. It is uncertain to what extent friction can be eliminated using this method, since the roughness of the crack surface could exceed the static crack tip opening displacement.

It can be stated that the effective value of stress intensity factor at the crack tip is physically responsible for crack propagation, and not the normal external value which is partly dissipated by friction. It seems to be of great importance to attain more knowledge about the reduction in the applied torque which is effective at the crack tip. For this it does not make any difference whether the crack growth is considered as a function of ΔK_{III} (Hurd and Irving (1982), Suresh et al (1981), Tschegg (1983) and many others), the crack tip displacement ΔCTD_{III} (Suresh et al 1981) or the plastic strain intensity (McClintock et al 1981); only the effective value acting at the crack tip determines the resulting crack propagation. It can be further stated that as the diameter increases the sliding mode crack closure is increased. Also the roughness induced crack closure is obviously more effective at R = -1 than, say, at R = 0.

Closer examination of mode III loading test data showed that when the crack has extended a few millimetres in length, the uncracked cross section of the specimen could withstand a torque level higher than it would do normally if sliding mode crack closure does not exist, which means that the effective torque at the crack tip is less than the applied value.

7.4 A new method to analyse the crack growth in mixed mode I & III

It was discussed earlier that the actual growth of the crack in mixed mode (I & III) loading close to the fatigue threshold takes place in mode I. All previously reported methods were used to analyse the crack growth in the mixed mode conditions. The results did not satisfy the fact that the crack was growing in mode I and did not coincide with the mode I crack growth.

A comparison of pure mode I crack growth to the usage of ΔK_I in the mixed mode (I & III) as indicated by Pook's method which gave the value of ΔK_I as follows:

$$\Delta K_I = \Delta K_A sin^2\theta \tag{7.5}$$

Where θ is the slit angle in the rectangular specimen and K_A is the apparent stress intensity factor of a similar mode I specimen. Figures (7.2) and (7.3) show graphs of crack growth rate versus stress intensity factor range (ΔK_I) as calculated above for two specimens under mixed mode (I & III) loading with different slit angles but the same R ratios compared to the mode I crack growth rate equation. It can be seen that the curve representing the crack growth in the mixed mode does not match that of pure mode I. The growth rate in the mixed mode condition seems much higher than the mode I for the same (ΔK_I) which gives the indication that the calculated mode I stress intensity factor is much lower than the real value. The same results were obtained for all other R ratios.

The second method of analysis was to use ΔK_A to try and analyse the crack growth of the mode I branch in the mixed mode (I & III) loading. Figures (7.4) and (7.5) show the use of $\Delta \dot{K}_A$ as a parameter to represent the stress intensity factor of the mode I branch in the mixed mode (I & III) loading for two slit specimens with the same R ratios, but different slit angles. It is clear that the curve representing the branch crack growth does not match the pure mode I crack growth rate equation in any of the tests performed at different slit angles or different R ratios. The growth rate in the mixed mode (I & III) seems lower than that of pure mode I. This could be explained by considering K_A as the upper limit and K_I as the lower limit of the experimental data. This is based upon the fact that K_A is equal to K_I when the slit angle is 90^o as given earlier in equation 7.5. This explains the two previous calculation methods for K_I and K_A.

A new approach was taken to analyse the growth rates in the mixed mode (I & III) loading. In all previous methods the slit angle was kept constant and the initial value was considered through out the advance of the crack front. It was made clear above that as the crack grows the slit angle changes till it reaches 90^o and that is when the mode of the loading changes from the mixed mode (I & III) to the pure mode I loading. The change in value of the slit angle affects the local value of the mode I stress intensity factor.

Fig.(7.6) shows the changes in the angle as the crack grows. Fig.(7.7) shows the changes in the co-ordinates of the slit angle as the crack grows.
From Fig.(7.7)

$$\theta = tan^{-1}(\frac{w}{b}) \tag{7.6}$$

As the crack extends the crack front moves a distance equal to (c) on the horizontal axis in two opposite directions, as shown in fig.(7.7)

The new crack angle is given by the equation

$$\theta_1 = \tan^{-1}(\frac{w}{b-2c}) \tag{7.7}$$

A series of measurements were taken of the value of (c) and its coordinate value of the crack extension (a). The value of θ was calculated accordingly. This process was repeated several times for different specimens with different R ratios and slit angles. Graphs of the variable crack angle (θ) versus crack extension, were carried out and a relationship was found. This relationship was found to be different for the 45° and the 60° slit angles and are given by the equations:

For the 45° initial slit angle

$$\theta = 0.0026\ a^3 - 0.175\ a^2 + 4.87\ a + 45 \tag{7.8}$$

For the 60° initial slit angle

$$\theta = 0.004\ a^3 - 0.159\ a^2 + 3.17\ a + 60 \tag{7.9}$$

where θ is measured in degrees and a in mm.

Figure (7.8) shows the graph of the experimental values of θ versus

the measured crack extension (a) for different specimens with different R ratios and slit angles, using a Swiss SIP Universal measuring apparatus type mu-214B. The relationships represented by the above two equations are super imposed on the experimental results curve. It is clear that the relationship represented by equations (7.8) and (7.9) are in good agreement with the experimental data.

The above two equations could be represented in the non dimensional form using the thickness of the specimen (w) by substituting $\frac{a}{w}$ instead of a.
For equation 7.8

$$\theta = 0.0026\ (\tfrac{a}{w})^3 \times w^3 - 0.175\ (\tfrac{a}{w})^2 \times w^2 + 4.87\ (\tfrac{a}{w}) \times w + 45$$

For equation 7.9

$$\theta = 0.004\ (\tfrac{a}{w})^3 \times w^3 - 0.159\ (\tfrac{a}{w})^2 \times w^2 + 3.17\ (\tfrac{a}{w}) \times w + 60$$

substituting w = 30 mm will lead to the following two equations

For equation 7.8

$$\theta = 70.2\ (\tfrac{a}{w})^3 - 157.5\ (\tfrac{a}{w})^2 + 149.1\ (\tfrac{a}{w}) + 45$$

and for equation 7.9

$$\theta = 3.6\ (\tfrac{a}{w})^3 - 143.1(\tfrac{a}{w})^2 + 95.1\ (\tfrac{a}{w}) + 60$$

where a in all these equations is the crack extension measured from the bottom of the slit.

Once a relationship was established between the slit angle and the crack length, it could be used in calculating the actual mode I stress intensity factor of crack using the actual slit angle at that point.

$$\Delta K_I = \Delta K_A \sin^2 \theta$$

ie.

$$\Delta K_I = \Delta K_A \times f'(a)$$
$$\Delta K_I = Y \Delta \sigma \sqrt{\pi a}.f'(a)$$

where

Y is a calculated constant

σ is the applied stress

The value of the stress intensity factor was calculated accordingly using a small programme. Fig. 7.9 and fig. 7.10 show a comparison between the new crack growth in mixed mode (I & III) loading, calculated according to the new method and the experimental crack growth of pure mode I with the representation of pure mode I crack growth rates.

Figures (7.9) and (7.10) show that as the crack starts to extend, the growth rates moves immediately towards the pure mode I growth rates. As the

branch stress intensity range approaches that of the pure mode I, the growth rates coincide with that of mode I only. The two curves are very close to each other considering the error caused by the different stages of calculation and measurement.

7.5 A model to predict the crack path using the crack length

Fig.(7.7) shows a schematic crack path in mixed mode (I & III) test specimen. The crack growth angle (α) can be predicted using the crack length. The crack length considered in this model is the extension of the crack at the bottom of the initial slit.

The slit angle changes as the crack extends till it reaches the value of 90°, where the mode will be pure mode I only. In the 3.5 % NiCrMoV steel, mesurements showed that, in the slit type specimen, the initial crack growth angle is independent of the slit angles (i.e 45° *and* 60°). It was also noticed that it is not affected by the different R ratios.

The crack growth angle was measured using the SIP universal measuring apparatus type mu-214B at different crack length till failure point and the values of α were plotted versus crack length. This process was repeated for several specimens with different slit angles and different R ratios. It was found that the following equation represents the relation between the crack length and the value of the crack growth angle (α)

$$\alpha = c \log (b(a + 0.1)) \tag{7.10}$$

where

a = crack extension measured in mm from the bottom of the initial slit.

c and b are constants and given in this equation as:

c = 17.64

b = 3.142 $\times 10^3$

α is in degrees (see fig.7.7)

Percentage error in measuring the angle is 5%.

This relationship was applied to other broken specimens to find out how close it is to the practical results. Fig.(7.11) to fig.(7.14) show a comparison between the experimental values of the measured crack growth angle (α) versus the actual crack length (a) and the empirical relationship between them represented by equation (7.10). It can be seen that the empirical relationship is very close to the experimental results and the two results coincide with each other to a great extent. From this relationship it is easy to find out, from the crack length, for the metal under study, when the mixed mode (I & III) loading changes to pure mode I only.

7.6 Mixed mode I & III fatigue threshold failure criteria

In Chapter Two four failure criteria were discussed in the literature survey, two other failure criteria were reported in Chapter Six. In this section the failure locus of five of these criteria will be drawn and the stress intensity factors for all the failed and unfailed specimens will be compared to each criterion. Other previous research results such as Pook (1985 b), Yoshioka (1984) and Yates (1989) will be compared to the results of this study.

The stress intensity factor ranges were normalized by the threshold stress intensity factor range for mode I tests. Figure (7.15) shows all the mixed mode (I & III) res ults for different R ratios and different slit angles. Results are divided into those which led to failure and those which did not fail or show any sign of macroscopic cracking. The results also include those of pure mode I for the 90 degrees slit specimens and those of the mode III tests on circular slit specimens under torsion.

7.6.1 Strain energy release rate

Experimental fatigue results of this study are shown in fig. (7.15) in respect to the strain energy release rate failure locus predicted by equation 2.12. It can be seen that the failure results agree with the predicted failure locus for tests with slit angle of 45° while they differ for the tests with 60° slit angle.

Other research results are shown in figures (7.16) and (7.17). Fig.(7.16) shows the experimental results of this study with respect to equation 2.12 failure locus compared to Pook's (1985b) and Yoshioka et al (1984) results. Fig.(7.17) shows a comparison of the above results to those of Yates (1989).

In general equation 2.12 which is stated as

$$(\frac{\Delta K_I(\phi)}{\Delta K_{Ith}})^2 + \frac{1}{1-\upsilon}(\frac{\Delta K_{III}(\phi)}{\Delta K_{Ith}})^2 = 1 \qquad (7.11)$$

where (ϕ) is the twist angle of the branch crack and $\upsilon = \frac{1}{3}$, is considered to be a good fit to the current research results. These data are closer to the predicted failure locus than Yates (1989) experimental results. The results of Pook (1985b) are in a similar fit to the data obtained in this research. Yoshioka's two results are close to the failure locus.

7.6.2 The maximum normal crack tip stress

Earlier in Chapter Two, section (2.8.3), it was reported that Erdogan and Sih (1963) stated that failure in mixed mode actually takes place only when the maximum normal crack tip stress exceeded the mode I critical value of fracture and the crack does not grow until the mode I fatigue threshold stress intensity factor is exceeded. The failure locus of this condition was stated in equation 2.24 and it is as follows

$$\frac{\Delta K_I}{\Delta K_{Ith}}(\cos^2\phi + 2\upsilon\sin^2\phi) + \frac{\Delta K_{III}}{\Delta K_{Ith}}(\sin 2\phi) = 1 \qquad (7.12)$$

Fig.(7.18) shows the above failure locus in comparison to this study results.

Pook (1980) reached to the same failure locus through assuming that fatigue failure takes place when the stress intensity factor of the small branch exceeds that of the mode I threshold stress intensity factor and gave the following equation as the failure envelope

$$\frac{\Delta K_{III}}{\Delta K_{Ith}} = \left(1-(1+2\upsilon)\frac{\Delta K_I}{\Delta K_{Ith}} + 2\upsilon(\frac{K_I}{K_{Ith}})^2\right)^{\frac{1}{2}} \qquad (7.13)$$

Pook later in (1985b) claimed that in deriving the previous equation, no account was taken of the effect of the intervening cliffs and other irregularities. He stated the following equation as the new failure locus with the correction factor Y

$$\frac{\Delta K_{III}}{\Delta K_{Ith}} = Y\left(1 - (1 + 2\upsilon)\frac{K_I}{K_{Ith}} + 2\upsilon(\frac{K_I}{K_{Ith}})^2\right)^{\frac{1}{2}} \qquad (7.14)$$

Y was deduced to be = 0.74.

Fig.(7.19) shows the failure locus discussed above with comparison to the data obtained in this study and to the results of Pook (1985b) and Yoshioka et al (1984). Fig.(7.20) shows the same failure criterion compared to Yates (1989) and the current data.

Looking at the above three graphs, it can be seen that the equation (7.13) is in good agreement with the pure mode III data of this study, while it is non conservative with Yates's (1989), Pook's (1985b) and Yoshioka et al (1984) results. On the contrary the modified equation (7.14) is in better agreement with the other three studies than with data obtained in this research as far as pure mode III is concerned.

In mixed mode (I & III) tests, the modified equation (7.14) is a better match as a failure locus to the results of this study and to Pook's (1985b) and Yoshioka et al (1984). It is also a closer failure locus to Yates (1989) data than the original equation (7.13).

7.6.3 Maximum normal strain criterion

The original idea was proposed by St. Venant (Timoshenko 1953) in the 19th century. This theory contend that 'failure will occur whenever a principal strain reaches a limiting value, as determined by the standard tensile test'. In studying fracture of concrete Wu (1974) recognized the importance of strain to cleavage fracture who remarked that 'a meaningful criterion for cleavage fracture must be based on strain' and introduced the strain failure criterion that states 'cleavage fracture takes place when the maximum tensile strain around a crack reaches a critical value', and he presented evidence to support its use. Chang (1981) applied this theory to study of angled crack problem.

As far as fatigue is concerned, it could be stated that the maximum normal strain criterion could assume that fatigue crack growth will occur when the maximum tensile strain range exceeds that of mode I threshold. The fatigue failure locus for the mixed mode (I & III) for the above theory was given by equation 2.30 which states the following

$$\frac{\Delta K_I}{\Delta K_{Ith}}\cos\phi^2 + \frac{\Delta K_{III}}{\Delta K_{Ith}}\frac{\sin 2\phi}{1-2\upsilon} = 1 \tag{7.15}$$

where ϕ is the twist angle of the branch crack and the threshold stress intensity factors are found when

$$\phi = \frac{1}{2}\tan^{-1}\left(\frac{2}{1-2\upsilon}\frac{\Delta K_{III}}{\Delta K_{Ith}}\right) \tag{7.16}$$

It is clear from the above that the above criterion reveals that fracture occurrence depends on Poisson's ratio.

Fig.(7.21) shows the present research results with respect to the maximum normal crack tip strain criterion. Fig.(7.22) shows the same results compared to Pook's (1985b) and Yoshioka et al (1984) results with respect to the above criterion, while Fig.(7.23) shows the results of Yates's (1989) compared to the present research data for the same criterion.

It can be seen from the above three figures that the maximum normal strain criterion is not a very good representation for failure locus over the whole

range of stress intensity factor ratios obtained in this research and the other research fellows.

7.6.4 Crack opening displacement model

This model which was proposed by Yates (1991) was discussed earlier in Chapter Six. In this section the present research results will be compared to this failure prediction theory.

Fig.(7.24) shows the present research data for different R ratios compared to Yates's failure locus. It can be seen that the crack opening displacement failure locus (Yates 1991) represent the failure for these research results more than the branch crack model proposed by Pook. Pook's model indicates lower threshold conditions than that observed in this research. The reason for this could be that Pook assumes the direction of growth of the facet branch crack is based on the local crack tip conditions, while in Yates's model the direction of growth is given by the macroscopic mode I direction. Pook's model is better at indicating the fatigue threshold of the branch crack rather than the specimen failure.

Figures (7.25 & 7.26) show Yates's failure criteria compared to the present results, Pook's (1985b), Yoshioka's (1984) and Yates's (1989). A comparison between the three results show that the present research results are closer to Yates's failure model than the other mentioned research results. It can be deduced that the crack opening displacement failure criterion proposed by Yates (1991) is a close failure locus to present research results. The failure results

could be represented by this model, especially if the research data are compared separately in sets according to their R ratios.

7.7 The effect of mean stress on mixed mode I & III threshold

The effect of the mean stress of the mixed mode I & III fatigue threshold behaviour was reported earlier in Chapter Six. It was shown in figures (6.18 & 6.19) that there is little effect of R ratio on the threshold fatigue of the mixed mode I & III failure in the range of R = 0 to 0.5 for the slit three point bending specimen. This could be due to the fact that in the sharply slit specimen, there is no effect of the crack closure on the fatigue threshold as there is no oxide formation or surface roughness which are the dominant mechanism in the mean stress effect observed in the fatigue precracked specimens.

7.8 Mixed mode I & III fatigue crack growth equation

It was shown earlier that a crack in mixed mode I & III loading actually grows in mode I at low stress ranges, close to the threshold conditions. Therefore the mixed mode I & III crack growth equation will be similar to the mode I equation. The difference will be in the threshold stress intensity factor.

The procedure followed to represent the fatigue crack growth in the mixed mode I & III loading is similar to that described in section 7.2 for mode I crack growth and based on the following steps:

1. Pook's method (Pook 1985b) is used in analysing the crack growth in mixed mode I & III. Pook's method depended on the initial slit angle θ given as 45^o & 60^o in the specimens used in this research and 90^o for the pure mode I. The slit angle changes from its initial values of 45^o & 60^o to the pure mode I slit angle of 90^o as the crack extends.

2. The changes in the slit angle value with respect to the crack length is given by equations 7.8 & 7.9 for the 45^o & 60^o initial slit angles respectively which are stated as follows:

For the 45^o initial slit angle

$$\theta = 0.0026\ a^3 - 0.175\ a^2 + 4.87\ a + 45$$

For the 60^o initial slit angle

$$\theta = 0.004\ a^3 - 0.159\ a^2 + 3.17\ a + 60$$

where θ is measured in degrees and a in mm.

3. Once this relationship is established, it is possible to calculate the mode I stress intensity factor at that crack length and slit angle using Pook's above method given by the following equation

$$\Delta K_I = \Delta K_A \sin^2 \theta$$

Where K_A is the apparent stress intensity factor of a similar mode I specimen calculated using Tada et al method (1985) at different crack length and θ is the calculated slit angle with respect to the crack length.

4. Once the value of ΔK_I is established, an attempt was made to link the threshold stress intensity factor and the crack growth rate equation. This was achieved by considering an equation of the type:

$$\frac{da}{dN} = C\Delta K_I{}^m - (A\Delta K_{Ith} - D) \tag{7.17}$$

where $\frac{da}{dN} = C\Delta K^m$ is Paris equation of the linear region of the crack growth rate equation, D is the distance between the minimum growth rate considered in the linear region and the x- axis as explained previously in section 7.2.

The values of C & m were found from the best fit curve on the computer. These values represent the linear part of the crack growth rate equation which is similar to that of mode I. The values of A and D were found to be:

A = .968

D = 4.69

These values will give the following equation which define the crack growth rate at all stages.

$$\frac{da}{dN} = 0.62 \times 10^{-8}\Delta K_I{}^3 - (0.968\Delta K_{Ith} - 4.69) \times 10^{-6} \tag{7.18}$$

This equation gave a good representation of the crack growth rate for values of threshold stress intensity factor $\Delta K_{Ith} \geq 6$.

Figures (7.27) to (7.29) show the above equation compared to the mixed mode (I & III) crack growth for different R ratios and different slit angles using the pure mode I fatigue crack growth data.

For $\Delta K_{Ith} < 6$ the following equation was found to be the best to represent the crack growth equation:

$$\frac{da}{dN} = 0.62 \times 10^{-8} \Delta K_I{}^3 - (0.968(\Delta K_{Ith} + B) - 4.69) \times 10^{-6} \qquad (7.19)$$

where B is variable according to the value of ΔK_{Ith} and is given by the equation:

$$B = -0.5\Delta K_{Ith} + 3 \qquad (7.20)$$

i.e. for $\Delta K_{Ith} = 5$, B is 0.5

Fig.(7.30) shows the crack growth rate equation for $\Delta K_{Ith} < 6$. It can be seen that the two equations which represent the crack growth rates fit well to the experimental data given in the above mentioned graphs.

These equations are also, of course, suitable for mode I only loading, since the mixed mode I & III crack actually grows in mode I as it was shown earlier.

It can be deduced from the above four graphs that the new crack growth equations are very good representations of the crack growth in mode I and mixed

mode I & III loading as long as the threshold stress intensity is known. They are also in good agreement with Paris equation for the same test, which is mainly concerned with the linear region of the fatigue crack growth.

This method has combined the use of the changes in slit angle values with the threshold stress intensity factor. Once the threshold stress intensity factor is established, it is easy to predict the crack growth equation of an angled slit specimen under mixed mode I & III loading conditions.

The tendency for a crack to grow in mode I is considered to be an observation which does not appear to be capable of proof in the strict sense of the word (Pook 1985a). This method makes this observation more realistic and easier to prove. This method confirms that a crack in mixed mode I & III at low stress ranges, close to the threshold conditions, grows in mode I and its growth rate could be analysed using the above explained method.

Chapter 8

Conclusions

The fatigue crack threshold and crack growth behaviour in pure mode I, pure mode III and mixed mode (I & III) for a 3.5%$NiCrMoV$ rotor shaft steel was studied. A 90° slit rectangular cross-section three point bend specimen for mode I, a circumferentially slit round specimen in torsion was used for pure mode III loading and an angled slit three point bend rectangular cross-section specimen for the mixed mode (I & III) tests.

The effect of stress ratio (R) on the threshold was one of the main concerns of this research. Mode I and mode III tests were performed under different R ratios and the threshold stress intensity factor for each stress ratio (R) was found. Mixed mode (I & III) tests were carried out for two slit angles and three different R ratios. All tests were performed in laboratory air at room temperature. The main R ratios used for these tests were 0 (or 0.1 for mode I and mixed mode), 0.17 and 0.5. The mode I threshold stress intensity factor for the slit specimen condition was found by the load increasing method while

for the precracked specimen, the load shedding procedure was used. For mode III, several independent tests were performed until the threshold condition was reached for each R ratio. From this research the following conclusions were drawn:

8.1 Mode I tests

- A new crack growth equation was derived to represent the crack growth in mode I tests

$$\frac{da}{dN} = 0.46 \times 10^{-8}\ \Delta K_I^3 - 1.9 \times 10^{-6}$$

where $\frac{da}{dN}$ is in mm/cycle and ΔK_I *in* $MPa\sqrt{m}$.

- The crack measurement technique used in this research is a good and successful method for measuring the crack length in the 90^o and the angled slit three point bend specimen for the mode I and the mixed mode (I & III) tests respectively.

- Even though a different threshold stress intensity factor was found for each R ratio, it can not be said that its effect on the threshold is conclusive, but never-the-less it follows, in general, that the threshold stress intensity factor falls as R increases.

- The crack growth rate equations in the paris linear region were found for each different R ratio and it was clear that as R increases, the crack growth rate increases too. These equations are:

For R = 0.06

$$\frac{da}{dN} = 0.45 \times 10^{-11}\ \Delta K_I{}^3$$

Where da/dN is in m/cycle and ΔK_I is in $MPa\sqrt{m}$.

For R = 0.17

$$\frac{da}{dN} = 0.87 \times 10^{-11}\ \Delta K_I{}^3$$

and for R = 0.5

$$\frac{da}{dN} = 1.0 \times 10^{-11}\ \Delta K_I{}^3$$

- The threshold stress intensity factor for precracked specimens were lower than those for slit specimens, on the average, by 15% – 25%.

- Empirical equations proposed by Schmidt and Paris (1973), Klensil and Lukas (1972) and McEvily and Gregor (1977) to describe the threshold for mode I, failed to predict the threshold value of the stress intensity factor for different R ratios. In general, all previous predictions were closer to the precracked specimens data than the slit specimens data.

8.2 Mode III tests

- The d.c potential drop method was used to measure the crack length. An equation describing the calibration curve ralating the crack length to the d.c potential drop in a circumferentially slit round specimen under torsion

was determined and used successfully in this research. It is given as follows:

$$\frac{a}{D} = 0.35\left(1 - e^{-30.56(\frac{\Delta V}{V_r})^{1.55}}\right)$$

where

a is the fatigue crack length

D is the initial uncracked diameter.

ΔV is the difference of voltage reading at two successive readings.

V_r is the reference voltage reading.

- The crack growth rate under mode III loading is slower by a factor of 10 than that for mode I, under the same conditions.

- In the tests performed on the circumferentially slit round specimen under torsion, the effect of R ratio on the threshold stress intensity factor was more defined than that for pure mode I. It can be stated that for mode III, the threshold stress intensity factor decreases as R increases.

- For R = -1, the crack growth rate increases as the detected crack length increases and reaches its maximum when the crack length reaches the value of 0.5 mm. After that it starts to decrease as the crack extends in length.

- The crack growth rate increases as the stress ratio (R) increases.

- Crack surface interlocking and/or rubbing were identified as the main reason for the fact that the applied stress intensity factor is much higher than the effective stress intensity factor, thereby reducing the crack growth rate. It is also the reason for the fluctuation in crack length measurement. This fluctuation decreases as the crack increases in length.

- The crack surfaces interlocking or rubbing effect depends on the following:
  (a) The roughness of the crystallography of the precracked fractured surface that exist at that point.
  (b) The amount of wear debris existing as a result of the rubbing effect between the two fractured surfaces.

8.3 Mixed mode (I & III)

- The crack growth in mode I is higher than that in mixed mode (I & III) for the same stress intensity factor.

- The slit angle (θ) changes from 45° or 60° to 90° as the crack extends in length, changing the mode of the loading from mixed mode (I & III) to pure mode I.

- Some of the fatigue failure criteria discussed in this research such as Pook's (1984), Yates & Miller (1989), could not predict the mixed mode I & III threshold stress intensity factor. It was found that the crack opening dis-

placement model proposed by Yates (1991) was the best model to predict the threshold failure of the mixed mode test specimens.

- The actual growth of a crack in mixed mode (I & III) loading takes place in mode I and the fatigue threshold of the material is achieved when the stress intensity factor of the branch exceeds that of mode I for the same conditions

- All the discussed crack growth prediction models could not describe the crack growth in mixed mode (I & III) tests.

- A new method was derived to analyse crack growth in mixed mode (I & III) by calculating the crack angle as the crack extends. Once this crack angle is calculated for that particular length of crack, it can be used to calculate the mode I stress intensity factor using the method proposed by Pook (1984) for the angled slit rectangular specimen.

- New equations were derived to calculate the value of the slit angle as it changes with the crack length. The two equations were for the 45°&60° slit angle specimens respectively. They were stated as:

$$\theta = 70.2\,(\tfrac{a}{w})^3 - 157.5\,(\tfrac{a}{w})^2 + 149.1\,(\tfrac{a}{w}) + 45$$

$$\theta = 3.6\,(\tfrac{a}{w})^3 - 143.1(\tfrac{a}{w})^2 + 95.1\,(\tfrac{a}{w}) + 60$$

where w is the thickness of the specimen.

- A new equation was derived to calculate the crack growth angle (α) using the crack length which is independent of the original slit angle and the stress ratio (R),:

$$\alpha = 17.64 \times 10^3 log(3.142\ (a + 0.1))$$

where α is the crack growth angle in deg. and a is the crack length in mm.

- New crack growth equations were found to express crack growth in mixed mode I & III for the material used in this research.

The following equation gives a good representation of the crack growth rate for values of threshold stress intensity factor $\Delta K_{Ith} \geq 6\ MPa\sqrt{m}$.

$$\frac{da}{dN} = 0.62 \times 10^{-8} \Delta K_I{}^3 - (0.968 \Delta K_{Ith} - 4.69) \times 10^{-6}$$

where da/dN in mm/cycle and ΔK_I *and* ΔK_{Ith} *in* $MPa\sqrt{m}$

For $\Delta K_{Ith} < 6\ MPa\sqrt{m}$ the following equation was found to be the best

$$\frac{da}{dN} = 0.62 \times 10^{-8} \Delta K_I{}^3 - (0.968(\Delta K_{Ith} + B) - 4.69) \times 10^{-6}$$

where da/dN in mm/cycle and ΔK_I *and* ΔK_{Ith} *in* $MPa\sqrt{m}$
and B is variable given by

$$B = -0.5 K_{Ith} + 3 \qquad MPa\sqrt{m}$$

The above equation could be simplified mathematically to read

$$\frac{da}{dN} = 0.62 \times 10^{-8} \Delta K_I{}^3 - (0.484 \Delta K_{Ith} - 1.786) \times 10^{-6} \qquad mm/cycle$$

where da/dN in mm/cycle and ΔK_I *and* ΔK_{Ith} *in* $MPa\sqrt{m}$

Chapter 9

Suggestion for further work

The assumed value of the stress intensity factors in mixed mode I & III are not very accurate. More accurate values could be achieved using the finite element analyses method, which would provide better calculation of the fatigue crack growth rate and the threshold conditions.

An equation representing the effect of R ratio on the fatigue crack growth rates could be achieved if more tests with several R ratios could be carried out to collect enough data to derive the required equation.

Further experimental work on three point bend specimens with different slit angles will verify the effect of slit angle on the threshold and crack growth and may lead to a better understanding of mixed mode I & III crack growth.

Trying to eliminate the p.d. shorting, sliding and interlocking effects in

the mode III tests with out the introduction of mode I, will lead to more accurate results of these tests.

Changes in the design of torsion test rig to cater for higher values of R ratios, such as fitting bigger motor, will define, more precisely, the effect of R ratio on the threshold and crack growth rate in mode III tests.

A comparison between the 'macroscopically flat' and the 'factory roof' types of mode III fatigue failure and the possibility to interchange between the two types of failure (if possible) depending on load reduction or increase will give a better understanding of the mode III fatigue threshold and crack growth rate.

Element	C	Si	Mn	S	P	Ni	Cr	Mo	V	Fe
weight %	0.26	0.18	0.36	0.007	0.01	3.4	1.55	0.48	0.095	bal.

Table 1: Composition of the material

Test Position	Test direction	0.2% MPa	UTS MPa	El %	Reduction of Area %	FATT ($°C$)	Cv ft.lb
Top body (rim)	Radial	687	845	23	65.5	-40	124
Top body (rim)	Tangential	697	845	24	67.5		
Top body (core)	Longitudinal	697	865	22	58.5	+20	44
Mid body (core)	Tangential	680	834	20	50.5	+2	57
Bottom body (rim)	Radial	680	834	25	67.5	-40	124
Bottom body (rim)	Tangential	680	825	24	66.5		
Bottom body (core)	Longitudinal	676	814	23	66	-35	150
Mid Radius (CAP)	Tangential	669	808	19	68	-5	69
Mid Radius (CAP)	Radial	673	819	21	67	-20	82

Table 2: Tensile data from rotor HRE supplied by NEI Parsons Ltd.

specimen number	ΔK_I $(MPa\sqrt{m})$	stress ratio R	Failure
HRE27	6.8	0.06	No
HRE28	7.5	0.06	No
HRE27	8.1	0.06	Yes
HRE26	7.76	0.17	No
HRE25	8.24	0.17	No
HRE25	8.4	0.17	No
HRE28	8.44	0.17	Yes
HRE25	8.65	0.17	Yes
HRE26	6.08	0.376	No
HRE80	6.62	0.37	No
HRE26	7.14	0.37	Yes
HRE80	5.0	0.5	No
HRE76	5.5	0.5	No
HRE80	6.0	0.5	No
HRE76	6.6	0.5	No
HRE80	7.2	0.5	No
HRE80	8.0	0.5	No
HRE76	8.8	0.5	Yes
HRE80	6.25	0.5	No
HRE80	6.8	0.5	No
HRE80	7.5	0.5	No
HRE80	8.25	0.5	Yes

Table 3: Threshold stress intensity factors for mode I tests for slit specimens at different R ratios.

specimen number	ΔK_{Ith} $(MPa\sqrt{m})$	stress ratio R
HRE27	7.1	0.06
HRE25	6.7	0.17
HRE26	7.1	0.37
HRE76	5.7	0.5
HRE80	6.0	0.5

Table 4: Threshold stress intensity factors for fatigue precracked specimens in mode I tests at different R ratios.

specimen No.	RD1	RD2	RD3	RD4	RD5	RD6	RD6A	RD11	RD8A
stress ratio	-1	-1	-1	-1	-1	-1	-1	-1	-1
$\Delta K_{III}(MPa\sqrt{m})$	15.0	13.8	12.6	11.6	10.8	9.6	8.0	7.4	6.8
failed	Yes	Yes	Yes	Yes	Yes	Yes	Yes	Yes	No

specimen No.	RD7	RD8	RD10	RD9	RD12	RD13	RD14	RD14A
stress ratio	0	0	0	0	0.17	0.17	0.5	0.5
$\Delta K_{III}(MPa\sqrt{m})$	6.0	6.6	6.9	7.2	6.5	6.8	5.6	6.35
failed	No	No	No	Yes	No	Yes	No	Yes

Table 5: Threshold stress intensity factors for mode III tests for different R ratios.

stress ratio R	β deg	ΔK_A $(MPa\sqrt{m})$	ΔK_I $(MPa\sqrt{m})$	ΔK_{III} $(MPa\sqrt{m})$	$\Delta k_I Pook$ $(MPa\sqrt{m})$	$\Delta k_I Yates$ $(MPa\sqrt{m})$	Failure
.06	45	8.8	4.4	4.4	8.128	6.476	No
.06	45	10.4	5.2	5.2	9.606	7.653	No
.06	45	11.26	5.63	5.63	10.40	8.286	No
.06	45	11.55	5.78	5.78	10.668	8.499	Yes
.06	45	12.86	6.43	6.43	11.869	9.456	Yes
.017	45	9.95	4.975	4.975	9.19	7.332	No
.017	45	11.73	5.865	5.865	10.834	8.632	No
.017	45	12.16	6.08	6.08	11.831	8.948	Yes
.5	45	8.5	4.25	4.25	7.851	6.255	No
.5	45	9.1	4.55	4.55	8.405	6.696	Yes
.5	45	9.9	4.95	4.95	9.144	7.285	Yes

Table 6: Threshold stress intensity factors values for mixed mode I and III tests for 45° slit angle specimens at different R ratios.

stress ratio R	β deg	ΔK_A $(MPa\sqrt{m})$	ΔK_I $(MPa\sqrt{m})$	ΔK_{III} $(MPa\sqrt{m})$	$\Delta k_I Pook$ $(MPa\sqrt{m})$	$\Delta k_I Yates$ $(MPa\sqrt{m})$	Failure
.06	60	9.01	6.75	3.90	9.963	7.703	No
.06	60	9.2	6.90	3.98	9.897	7.865	No
.06	60	9.8	7.35	4.24	10.543	8.08	No
.06	60	10.05	7.54	4.352	10.812	8.592	Yes
.06	60	10.4	7.80	4.50	11.188	8.891	Yes
.06	60	10.8	8.1	4.676	11.619	9.233	Yes
.17	60	9.08	6.817	3.93	9.768	7.763	No
.17	60	9.783	7.34	4.236	10.524	8.364	Yes
.5	60	8.8	6.6	3.810	9.467	7.523	No
.5	60	9.00	6.75	3.897	9.682	7.694	No
.5	60	9.1	6.825	3.94	9.79	7.780	No
.5	60	9.5	7.20	4.157	10.328	8.207	Yes
.5	60	9.8	7.35	4.243	10.543	8.378	Yes
.5	60	10.1	7.575	4.373	10.865	8.635	Yes
.5	60	10.5	7.875	4.547	11.296	8.976	Yes
.5	60	10.8	8.10	4.675	11.619	9.233	Yes

Table 7: Threshold stress intensity factor values for mixed mode I and III tests for 60 deg. slit angle specimens at different R ratios.

References

1. ALLEN, R.J. 1980 - Fatigue crack growth characterization by LEFM - Part II. *Fatigue and Fracture of Engineering Materials and Structures.* **11**, 2, 71-108.

2. ASTM Standard E647, Tests for constant load amplitude fatigue crack growth rate above 10^{-8} m/c. *ASTM, Philadelphia, Pa.*

3. BEEVERS, C. J., 1981 - Some aspects of the influence of microstructure and enviroment on ΔK_{th} in fatigue thresholds. *EMAS, Warley, U.K, 1981*, 275 - 276.

4. BEEVERS, C. J., COOKE, R. J., KNOTT, J. F & RITCHIE, R. O., 1975 - Some considerations of the influence of subcritical cleavage growth during fatigue crack propagation in steels. *Metal Science*, 9, 119-126.

5. BENTHEM, J. P., & KOITER, W. T. 1972 - Asymptotic approximations to crack problems. In: Methods of analysis and solutions of crack problems (Sih, G. C., ed.). Noordhoft Int. Publishing, Leyden, the Netherlands, chapter 3.

6. BROEK, D., 1978 - Elementary engineering fracture mechanics, Sijthoft and Noordhoff International Publishers. The Netherlands.

7. BROWN, M. W., 1988 - Aspects of fatigue crack growth. Presented at the International Conference on Fatigue of Engineering Material and Structures. Sheffield 15 - 19 Sept. 1986. Published 1988. *Proc. Inst. of Mech. Eng.* **202**, 1, 19 - 29.

8. BROWN, M. W., & MILLER, K. J., 1973 - A theory for fatigue failure under multi-axial stress - strain conditions. *Proceedings of Inst. Mech. Eng.* **187**, 745 - 755.

9. BROWN, J. W. F. & SRAWLEY, J. E., 1966 - Crack toughness testing of high strength materials, American Soc. for Testing and Materials. *Philadelphia, ASTM STP.* **410**.

10. BUCKS, O. FRANDSEN, J. D & MARCUS, H. L. 1975, Crack tip closure and environmental crack propagation, *Eng. Fract. Mech. 1975*, **7**, 167.

11. CADMAN, A. J. & BROOK. R., 1983 - Influence of R ratio and orientation of the fatigue crack threshold and subsequent crack growth low alloy steel. *Proceedings of the International Symposium on Fatigue Crack Threshold Concepts AIME*, 281 - 298.

12. CHANG, K. J., 1981 - On the maximum strain criterion - a new approach to the angled crack problem. *Engineering Fracture Mechanics*, **14**, 107 - 124.

13. CLARK, G. & KNOTT, J. F., 1975 - Measurement of fatigue crack in notched specimen by means of theoretical electrical potential calibrations. *Journal of Mechanics and Physics of Solids*, **23**, 265 - 276.

14. ELBER, W., 1970 - The significance of fatigue crack closure in damage tolerance in aircraft structure. *ASTM STP* **486**, 230 - 242.

15. ELSENDER, A., 1982 - Fatigue crack growth rate for rotor and end ring forging steel. *Technical memorandum of Metallurgy Dept. No MET 79 - 183, NEI Parson LTD.*

16. ELSENDER, A. & BALTE A. D., 1983 - The cyclic Stress - Strain Behaviour of 3.5% NicrMoV L.P Rotor Steel, Technical memorandum (No MET 83 - 127) of Metallurgy Dept., NEI Parsons LTD.

17. ERDOGAN, F. & SIH, G. C., 1963 - On the crack extension in plates under plane loading and transverse shear. *Journal of Basic Engineering*, 519-527.

18. EWING, J. A., 1903 - The strength of materials. *Cambridge University Press*

19. EWING, J. A., & WILLIAMS, J. G., 1974 - The fracture of spherical shells under pressure and circular tubes with angled cracks in torsion. *International Journal of Fracture*, 10, 537-544.

20. FROST, N. E., & DUGDALE, D. S., 1958 - The propagation of fatigue cracks in sheet specimens. *J. Mech. & Phys. Solids.*, 6, 2, 92-110.

21. FROST, N. E., MARSH, K. J., & POOK, L. P., 1974 - Metal Fatigue, Clarendon Press, Oxford.

22. GILBEY, D. M., & PEARSON, S., 1966 - Measurements of the length of the central edge crack in a sheet of metal by an electrical resistance method. *Royal Aircraft Establishment, Farnborough, U.K. Technical Report*, 66402.

23. GRAY, G. T, THOMPSON, A. W., & WILLIAMS, J. C., 1983 - Roughness-induced crack closure: An explanation for microstructurally sensitive fatigue crack growth, *Met. Trans. A.*, **14a**, 421.

24. GRIFFITH, A. A., 1921 - The phenomena of rupture and flow in solids. *Phil. Trans. Royal Soc.*, **A221**,163-168.

25. GRIFFITH, A. A., 1924 - The theory of rupture. *Proceeding of 1st Int. Cong. Appl.* Mech Delft, 55 - 63.

26. GROSS, B., & SRAWLEY, J. E., 1965 - Stress intensity factors for three point bend specimens by Boundary Collocation. *NASA TN D - 3092.*

27. GUIU, F., DULNIAK, R. & EDWARDS, B. C. 1982 - "On the nucleation of fatigue cracks in pure polycrystalline α-Iron". *Fat. Eng. Mat. Struc.* . **5**, 311 - 321.

28. HAY, E., 1983 Fatigue at notches subject to torsion & axial loading. Ph.D. thesis. *Mechanical Engineering Department, University of Sheffield.*

29. HAY, E., & BROWN, M. W., 1985. Initiation and early growth of fatigue cracks from circumferential notch loaded in torsion. *The Behaviour of Short Fatigue Cracks, EGF*, pub. 1, (Edited by K.J. Miller and E.R. de los Rios) 1, *Mech. Eng. Publ.*, London, 309 - 321.

30. HEAD, A. K. 1953 - The growth of fatigue cracks. *Phil. Mag.*. **44**, 925 - 938.

31. HELLIER, A. K., CORDEROY, D. J. H. & McGIRR, M. B., 1985 - Some observations on mode III fatigue thresholds. *Int. Jour. of Fracture*, **29**, R45 - R48.

32. HOBSON, P. D., 1985 - "The growth of short fatigue cracks in a medium carbon steel". *Ph.D Thesis. Mech. Eng. Dept. Sheff. Univ.*.

33. HORNBOGEN, E., & GATZ, K. Z., 1976 - Microstructure and fatigue crack growth in a Fe-N-Al - alloy. *Acta. Met.*, **24**, 581 - 592.

34. HOURLIER, F., McLEAN, D & PINEAU, A., 1978 - Fatigue crack growth behavior of Ti-5AL-2.5Sn alloy under complex stress (mode I & steady mode III), *Metal Technology*, 154 - 185.

35. HOURLIER, F., & PINEAU, A., 1981 - Fatigue crack propagation behaviour under complex mode loading. In: Advances in Fracture Research, 5th Int. confer. on Fracture (ICF5), (Ed. D. Francois), Cannes, France, 1981. *Pergamon Press, Oxford U.K* 1833 - 1840.

36. HOULIER F & PINEAU, A., 1982 - Propagation of fatigue cracks under polymodal loading. *Fatigue of Engineering Materials and Structures,* **5**, 4, 287 - 302.

37. HOURLIER, F., D'H ONDT, H., TRUCHON, M. & PINEAU, A., 1985 - Fatigue crack path behaviour under polymodal fatigue. In: Multiaxial Fatigue. *ASTM STP* **853**, K. J. MILLER & M. W BROWN Eds. *American Society for Testing and Materials, Philadelphia* (1985),228 - 248.

38. HURD, N. J., & IRVING, P. E., 1982 - Factors influencing propagation of mode III fatigue cracks under torsional loading. *Design of Fatigue and Fracture Resistant Structures, ASTM STP 761, P.R ABELKIS & C. M. HUDSON, Eds, ASTM 1982,* 217 - 233.

39. HUSSAIN, M. A., PU, S.L. and UNDERWOOD, J., 1974 - Strain energy release rate for a crack under combined mode I & III. In: Fracture Analysis,

ASTM, Philadelphia, Pa., ASTM STP 560, 2 - 28.

40. IBRAHIM, F. K., 1989 - The effect of stress ratio, compressive peak, stress and maximum stress level on fatigue behaviour of 2024 - T3 aluminium alloy. *Fat. Frac. Engng. Mater. Struc.*, **12**, 1, 1 - 8.

41. IRVING, P. E., ROBINSON, J. L., & BEEVERS, C. J., 1973 - Fatigue crack closure in titanium alloys, *Int. Jour. of Fracture, 1973*, 9,105-108.

42. IRWIN, G. R., 1957 - Analysis of stresses and strains near the end of a crack transversing a plate. *Jour. of Appl. Mech, Trans. of the Amer. Soc. of Mech. Eng.*, **24**, 361 - 364.

43. JAMES, L. A., 1973 - The effect of stress ratio on the elevated temperture fatigue crack propagation of type 304 stainless steel. *Nuclear Technology.* **14**, May 1973, 163 - 170.

44. KAISAND, L. R., & MOWBRAY, D. F., 1979 - Relationship between low-cycle fatigue and fatigue crack growth rate properties, *Jour. of Testing and Evaluation*, **7**, 270-280.

45. KLENSIL, M., & LUKAS, P., 1972 - Effect of stress cycle asymmetry on fatigue crack growth. *Mat. Sci. and Eng.*, **9**, 231 - 240.

46. LAWN, B. R. & WILSHAW, T.R., 1975 - Fracture of brittle solids. Cambridge University Press, *Cambridge Solid State Science Series*

47. LINDLEY, T. C., 1981 - Near threshold fatigue crack growth Experimental methods, Mechanisms and Application, In: LARSSON, L. H., (ed.), Subcritical Crack Growth due to fatigue, stress corrosion and creep. *Lectures from a course held at the Joint Research Centre, Ispra (Italy)*, Oct. 19th - 23rd, 1981 in collaboration with the European Group on Fracture, 167 - 213.

48. LINDLEY, T. C., & RICHARDS, C. E., 1982 - Near threshold fatigue crack growth in materials used in the electricity supply industry. In: Fatigue thresholds, Fundamental and Engineering Applications. (Eds. BUCKLAND,A. BLOM & C. J. BEEVERS), *Proc. Inter. Confer. Stockholm, 1981, Engineering Materials Advisory Services, Ltd, West Midlands, U.K.*, 1087 - 1113.

49. LINDLEY, T. C. & STEWART, A. T., 1982 - Fatigue crack growth threshold applications. In: J. BUCKLAND, A. BLOM & C. J. BEEVERS, (Eds), Fatigue thresholds: Fundmental and Engineering applications. *Proc. Inter. confer.*, Stockholm, 1981 - Engineering material advisory services, Ltd., West Midlands. U.K., 967 - 987.

50. LIU, H. W. 1963 - "Crack propagation in thin sheet under repeated loading". *J. Bas. Eng., Trans. ASME Ser. D.*, **83**, 23 -31.

51. LYNCH, S. P., 1978 - "Mechanisms of Fatigue and enviromentally assisted fatigue". *ASTM STP*, **675**, 174 - 203.

52. MADDOX, S. J., 1975 - The effect of mean stress on fatigue crack propagation. A literature review. *Int. Jour. of Frac.*, **11**, 389 - 408.

53. MADDOX, S. J., GURNEY, T. R., MUMMERY, A. M., & BOOTH, G. S., 1978 - An investigation of the influence of applied stress ratio on fatigue crack propagation in structural steels. *The Welding Institute Report 72/1978/E,* Sept. 1978.

54. MAITI, S. K., & SMITH, R. A., 1984 a - Comparison of the criteria for mixed mode brittle fracture based on the preinstability stress - strain field. Part 1, slit and elliptical cracks under uniaxial tensile loading. *Int. Jour. of Frac.*, **23**, 1983, 281 - 295.

55. MAITI, S. K., & SMITH, R. A., 1984 b - Comparison of the criteria for mixed mode brittle fracture base on the preinstability stress - strain field. Part 2 Pure shear and uniaxial compressive loading. *Int. Jour. of Frac.*, **24**, (1984), 5 - 22.

56. MATAKE, I., IMAI, Y., & TAKASE, I. 1981 *Trans. ASME, Ser. A*, **48**, 1142.

57. McCLINTOCK, F. A., & RITCHIE R. O., 1981 - In: Mechanics of Fatigue. (Ed. T. MURA). *ASME Winter Annu. Meet. 1981 ASME*, New York.

58. McEVILY, A. J. & ILLG, W., 1958 - The rate of crack propagation on two Aluminium Alloys *NACA Tech. Note.* **4344**, Sep. 1958.

59. McEVILY, A. J., & GREGOR, J., 1977 - On the threshold for fatigue crack growth. Advances in Research on the Strength and Fracture of Materials, (Fracture 77) Ed. D. M. R., Taplin. *Pergamon Press, New York*, **2**, 1293 - 1298.

60. METALS HANDBOOK, Vol. 3 Machining, 8th Edition, Electrical Dischage Machining (EDM), page 231.

61. MILLER, K. J., An introduction to fracture mechanics. In: Mechanical and Thermal Behaviour of Metalic Metals, LXXXII *Corso Soc., Italiana di Fisica*, Bologna - Italy.

62. MINAKAWA, K. & McEVILY, A. J., 1981 - On crack closure in near threshold fatigue, *Scripta Met.* **15**, 633-636.

63. MUSUVA, J. K., & RADON, J. C., 1979 - The effect of stress ratio and frequency on fatigue crack growth . *Fat. Eng. Mat. and Struc.* **1**, 1979,

457 - 470.

64. NAYEB HASHEMI, H., McCLINTOCK, F. A., & RITCHIE, R. O., 1982 - Effect of friction and high torque on fatigue crack propagation in mode III, 1982 C, *Metallurgical Transaction A, Vol. 13A*, p. 2197-2204.

65. NAYEB HASHEMI, H., McCLINTOCK, F. A., & RITCHIE, R. O., 1983 Micro-mechanical modelling of mode III fatigue crack growth in rotor steels. *Int. Jour. of Fract.*, **23** (1983), 163 - 185.

66. NEWMAN, J. C. Jr., 1976 - Finite element of fatigue crack closure. *ASTM STP* **590**, 281 - 300.

67. NISHIOKA, K., HIRAKAWA, K. & KITAWA, Z., 1977 - Fatigue crack propagation behaviour of various steels. *Sumitomo Search, 17*, May, 1977, 39 - 55.

68. NUISMER, R. J., 1975 - An energy release rate criterion for mixed mode fracture. *International Journal of Fracture*, **11**, 245-250.

69. PARIS, P. C., & ERDOGAN, F., 1963 - A critical analyses of crack propagation Laws. *J. Bas. Eng.*, **85**, 528 - 534.

70. PEARSON, S., 1972 - The effect of mean stress fatigue crack propagation in half inch thick specimens of aluminium alloy of high and low fracture toughness. *Eng. Frac. Mech.*, **4**, 1, March, 1972, 9 - 24.

71. POOK, L. P., 1975 - Analysis and application of fatigue crack growth data, *Journal of Strain Analysis*, **10**, 242 - 250.

72. POOK, L. P., 1980 - Mode I branch cracks and their implications for combined mode failure. *National Engineering Laboratory Report 667*, East Kilbride, Glasgow.

73. POOK, L. P., 1983 - The role of crack growth in metal fatigue. In: Metal Society, London.

74. POOK, L. P., 1985a - Comments on fatigue crack growth under mixed mode I & III and pure mode III loading. In: Multiaxial Fatigue, ASTM STP 853, K. J., MILLER & M. W. BROWN Eds. *American Society for Testing and Materials, Philadelphia*, 249 - 263.

75. POOK, L.P., 1985b - The fatigue crack direction and threshlod behaviour of mild steel under mixed mode I & III loading. *Int. J. of Fatigue*, **7**, 21 -30.

76. POOK, L. P., 1985C - The significance of mode I branch cracks for mixed mode fatigue crack growth threshold behaviour. *Proc., 2nd Int confer. on*

Biaxial/Multiaxial Fatigue, Sheffield., Dec. 1985.

77. POOK, L. P., & SHARPLES, J. K., 1979 - The mode III crack growth threshold for mild steel. *Int. Jour. of Frac.*, **15**, R223 - R226.

78. PRIDDLE, K. E., 1978 - The influence of grain size on threshold stress intensities for fatigue crack growth in AISI 316 stainless steel. *Scri. Metall.*, **12**, 49 - 56.

79. QINZHI, H., 1984 - A model for calculating the fatigue crack opening load and its applications. *Fatigue of Engineering Materials and Structures*, **7**, 41 - 53.

80. RICHARDS, C. E. & LINDLEY, T. C., 1972 - The influence of stress intensity and microstructure on fatigue crack propagation in Ferretic materials, *Engineering Fracture Mechanics*,**4**, 951 - 978.

81. RITCHIE, R. O., 1979 - Near threshold fatigue crack propagation in steels. *Int. Met. Rev.*, **24**, 205 - 230.

82. RITCHIE, R. O., GARRETT, G. G., & KNOTT, J. F., 1971 - Crack Growth monitoring optimisation of the electrical P.d. technique using an analogue method. *Int. Jour. of Fracture Mechanics*, **7**, 462 - 467.

83. RITCHIE, R. O., SURESH, S., & MOSS, C. M., 1980 - Near threshold fatigue crack growth in pressure vessel steel in air and hydrogen. *Jour. of Eng. Mat. and Tech. Trans. of the Amer. Soc.of Mech. Eng., Series H*, **102**, 293 - 299.

84. RITCHIE R. O., McCLINTOCK, F. A., NAYEB - HASHEMI, H., and RITTER, M., A., 1982 *Metallurgical Transaction A, Vol. 13A 1982*, p. 101.

85. RITCHIE, R. O, McCLINTOCK, F. A., TSCHEGG, E. K., & NAYEB - HASHEMI, H., 1985 - Mode III fatigue crack growth under combined torsional and axial loading. In: Multiaxial Fatigue, ASTM STP 853, K. J., MILLER & M. W. BROWN Eds. *American Soc for Testing and Materials, Philadelphia* 1985, 203 - 227.

86. ROOKE, D. P. & CARTWRIGHT, D. J., 1976 - Compendium of stress intensity factors, HMSO, London.

87. SCHIJVE, J., & ARKEMA, W. J., 1976 *Dept. of Aerospace Eng. Report VTH - 217.* Delft University, The Netherlands.

88. SCHIJVE, J., 1981 - Some formulas for the crack opening stress level. *Engineering Fracture Mechanics*, **14**, 461 - 465.

89. SCHMIDT, R. A., & PARIS, P. C., 1973 - Threshold for fatigue crack

propagation and the effects of load ratio and frequency progress. In: Flaw Growth and Fracture Toughness Testing. *ASTM STP* **536**, (1973), 79 - 84.

90. SIH, G. C., 1973 - Methods of analysis and solutions of crack problems. *Noordhoff Intenational Publishing*, Leyden, 221-229.

91. SIH, G., C., 1974 - Strain energy density factor applied to mixed mode crack problems, *Int. J. of Fracture*, **10**, 305 - 321.

92. SMITH, R. N., WATSON, P. & TOPPER, T. H., 1970 - A Stress - Strain function for the fatigue of metals. *Transactions of ASME, Journal of Materials*, **5**, 4, 767 - 778.

93. STANZL, S., & TSCHEGG, E., 1980 Fatigue crack growth and threshold measured at very high frequencies (20KHZ). *Met. Sci.*, **14**, 137 - 140.

94. STEWART, A. T., 1980 - The infuence of environment and stress ratio on fatigue crack growth at near threshold stress intensities in low-Alloy steels. *Eng. Fract. Mech.* **13**, 1980 - 463 - 478.

95. SURESH, S., & RITCHIE, R. O. L., 1982 - A geometric model for fatigue crack closure induced by fracture surface roughness, *Met. Trans. A.*, **13A**, 1627 - 1635.

96. SURESH, S., & RITCHIE, R. O., 1983 - Some consideration on the modelling of oxide-induced fatigue crack closure using solutions for a rigid wedge inside a linear elastic crack, *Scripta Met.* **17**, 575-581.

97. SURESH, S., & RITCHIE, R. O., 1983 - On the influence of environment on the load ratio dependence of fatigue thresholds in pressure vessel steel. *Eng. Frac. Mech.*, **18**, 785 - 800.

98. SURESH, S., & RITCHIE, R. O., 1983 - Near Threshold fatigue crack propagation: A perspective on the role of crack closure.*Proceeding of the international symposium on fatigue crack growth threshold concepts*, Philadelphia, Pensylvania, Oct.(3 - 5) 1983. Edited by D.L.Davidson & S.Suresh. Publication of the Metallurgical Soc. of AIME.

99. SURESH. S., TOPLOSKY, J. & RITCHIE, R. O., 1981 - In fracture mechanics., 14th Symp., **1**. Theory and analysis, edited by Lewis, J. C., and Sines, G., *ASTM STP 791*, 1329.

100. SURESH, S., ZAMISKI, G. F. & RITCHIE, R. O., 1981 - Oxide induced crack closure: An explanation for near-threshold corrosion fatigue crack growth behaviour, Met. Trans. A, **12a**, 1435-1443.

101. TADA, H., PARIS, P. and IRWIN, G. R., 1985 - The Stress analysis of cracks handbook. St. Louis, Paris Production Inc., 2nd edition.

102. TAYLOR, D., 1989, Fatigue Thresholds, Butterworths, pp 27-44, and pp 159-181.

103. TAYLOR, D., 1990, Crack-Like Notches and Notch-Like Cracks, Proc. ECF-8, Turin, Italy.

104. TAYLOR, D., 1992 - Report No. TCD/Year 2/End of year report, Period 4, Project No. BR/EU 3051, Trinity College, Dublin.

105. TIMOSHENKO, S. P., 1953 - History of strength of materials. McGRAW - HILL, New York.

106. TSCHEGG, E. K., 1982 - A contribution to mode III fatigue crack propagation, *Mat. Sci. and Eng.*. **54**, No.1, 127 - 136.

107. TSCHEGG, E. K., 1983 - The influence of the static mode I load and R ratio on mode III fatigue crack growth behaviour in mild steel. *Mat. Sci. and Eng.*, **59**, 127 - 137.

108. TSCHEGG, K. E., 1985 - A contribution to mode III fatigue crack propagation. *Mat. Sci. Eng.*, **54**, 127 - 136.

109. TSCHEGG, E. K., MAYER, H. R, CZEGLEY, M., & STANZL, S. E., 1991 - Influence of a constant mode III load on mode I fatigue crack growth

thresholds. Fatigue under Biaxial and Multiaxial loading ESIS10 (Edited by K. KUSSMAUL) 1991. *Mech. Eng. Publications*, London, 213 - 222.

110. VENABLES, R. A., HICKS, M. A. & KING J. K., 1983 - Influence of stress ratio on fatigue thresholds and structure sensetive crack growth in Ni-Base Superalloys. *Proceeding of International Symposium on Fatigue Crack Growth Thresholds.* Philadelphia, Pennsylvania, Oct. 3 - 5 , 1983, Edited by D. L., Davidson and S. Suresh, AIME publications, 341 - 357.

111. WALKER, K., 1970 - The effect of stress ratio during crack propagation and fatigue for 2024 - T3 and 7075 - T6 aluminium. In: Effect of Enviroment and Complex Load History on Fatigue Life. *ASTM STP*, **462**.

112. WANG, T., C., 1977 - Fracture criteria for combined modes cracks, In: Advances in Research on Strength and Fracture of Materials, (Ed. D., M., TAPLING), Vol. 4, *Pergman Press, Oxford.* 135-154.

113. WOOD, W. A., 1958 - Recent observations on fatigue in metals. *ASTM STP* **237**, 110-121.

114. WU, H. C., 1974 - Dual failure criterion for plain concrete. *J. of Eng. Mech., Amer. Soc. of Civ. Eng.*, **100**, 1167 - 1181.

115. XIAOPENG, Z., 1990 - The effects of stress ratio on fatigue threshold. *Int.*

Jour. of Fat., **12**, (2), (1990), 127 - 130.

116. YATES, J. R., 1987 - Fatigue under combined torsion and bending loads. *Ph.D Thesis, Mech. Eng. Dept. Sheffield University.*

117. YATES, J. R., 1987 - Crack tip plastic zone sizes in cylinderical bars subjected to torsion. *Fat. Frac. Eng. Mat. Struct.*, **10**, No. 6, pp. 471-477.

118. YATES, J. R., 1991 - Fatigue threshold under mixed-mode (I& III) loading. *Int. J. of Fatigue*, **13**, No. 5, 383 - 388.

119. YATES, J. R., & MILLER K. J., 1989 - Mixed mode (I+III) fatigue thresholds in a forging steel. *Fat. Frac. Eng. Mat. Struct.*, **12**, (3), 259 - 270.

120. YOSHIOKA, S., WATANABE, K., KITAGAWA, H., INOUE, A., & KUMASAWA, M., 1984 - Fatigue crack growth threshold (ΔK_{th}) under mode III (the effect of stress ratio and mixed mode). In: Fatigue 84 Proceeding, 2nd International Conference on Fatigue and Fatigue Thresholds, Birmingham 1984. Ed. J., BEEVERS, Engineering Materials Advisory Services Ltd., West Midlands, U.K., 241 - 253.

121. ZACHARIAH, K. P., 1974 - *Fatigue crack initiation and stage I propagation.* Ph.D Thesis, Churchill College, Cambridge University.

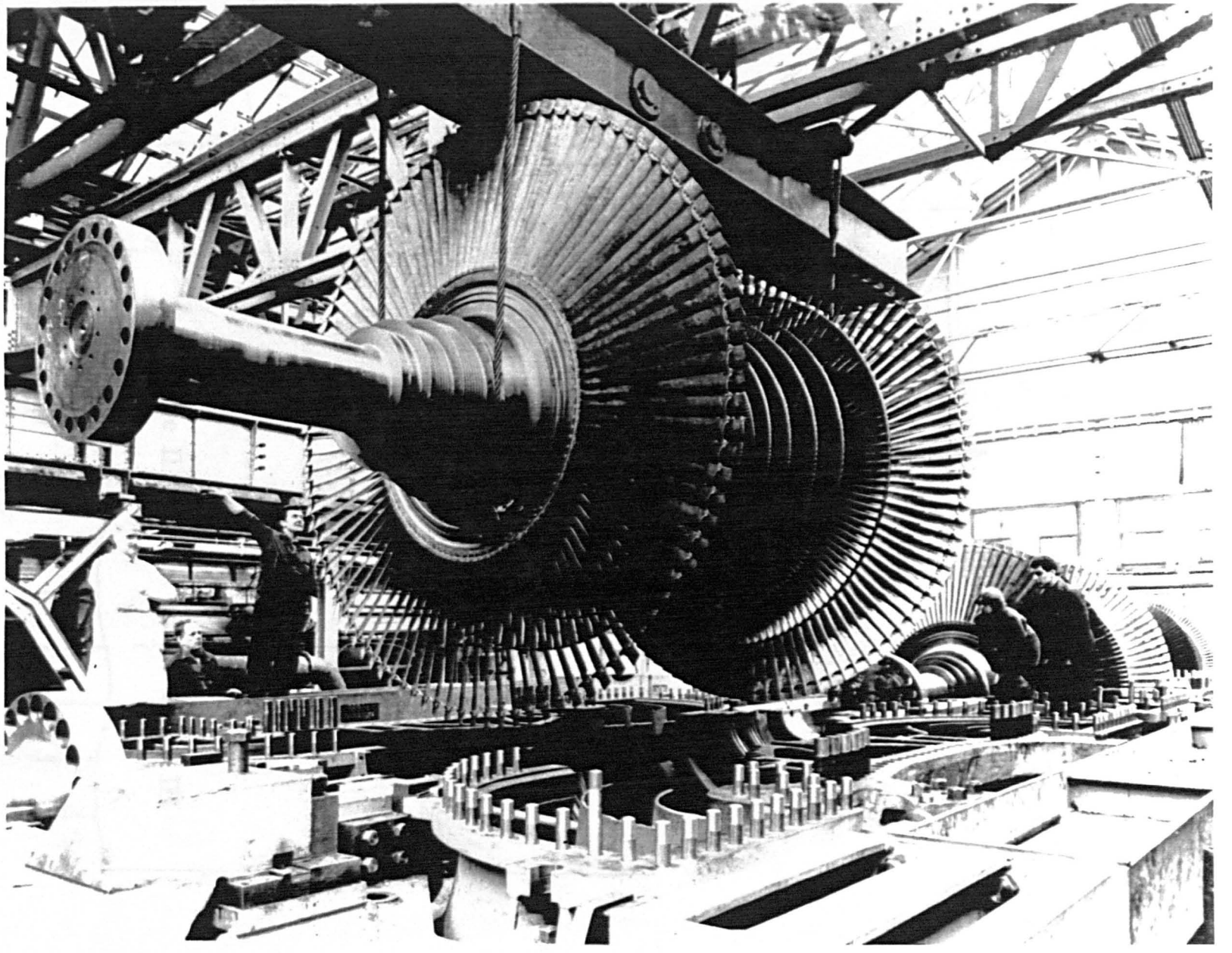

Fig.(1.1) Low Pressure Steam Turbine Rotor (courtesy of NEI Parsons Ltd.)

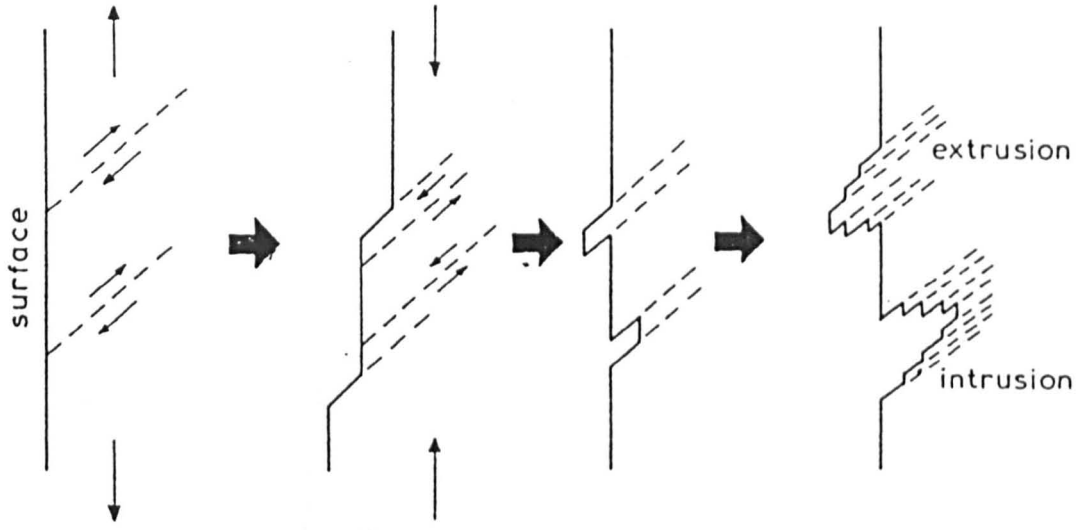

Fig.(2.1) Wood's model for fatigue crack initiation.

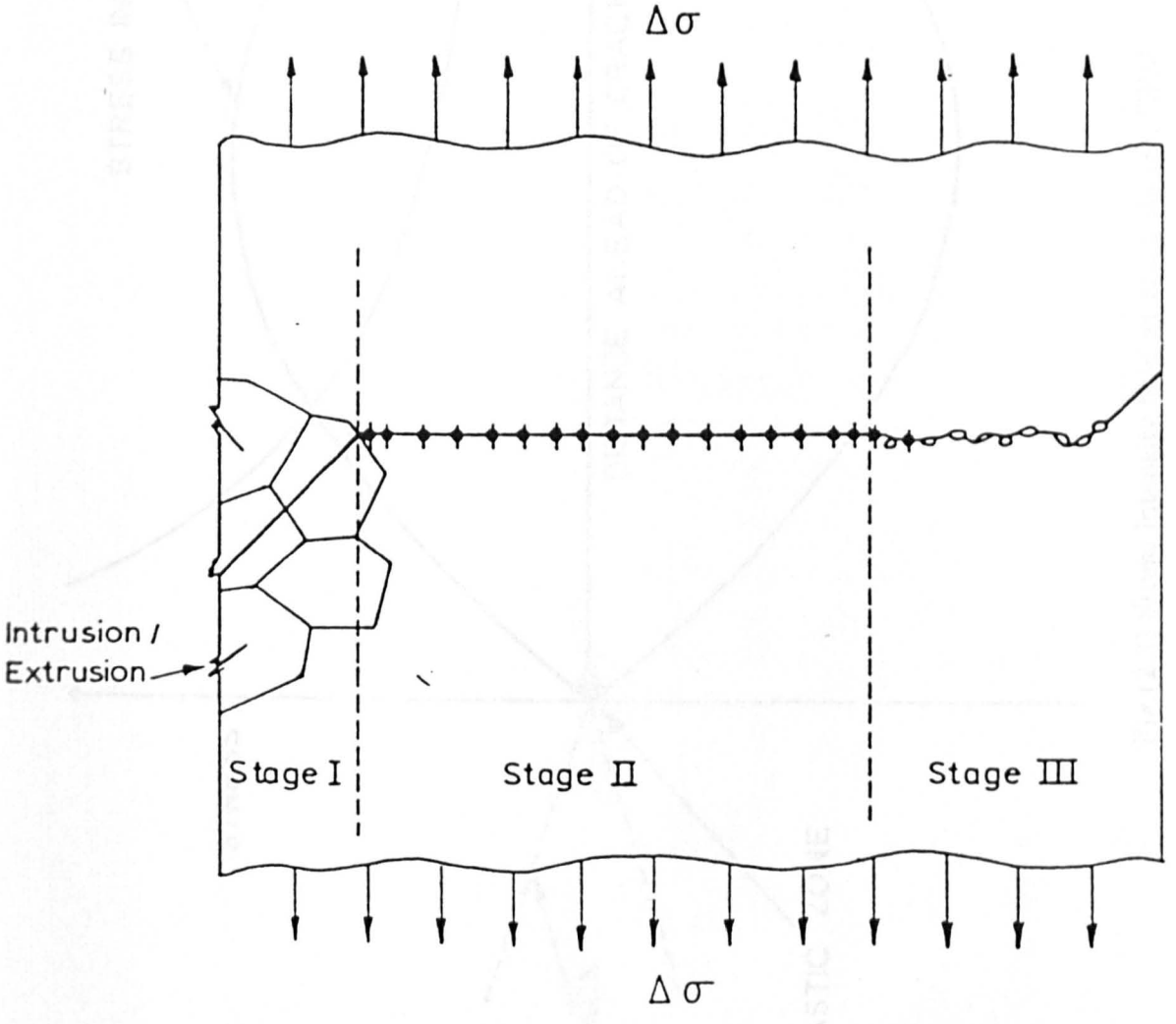

Fig.(2.2) Fatigue crack growth behaviour.

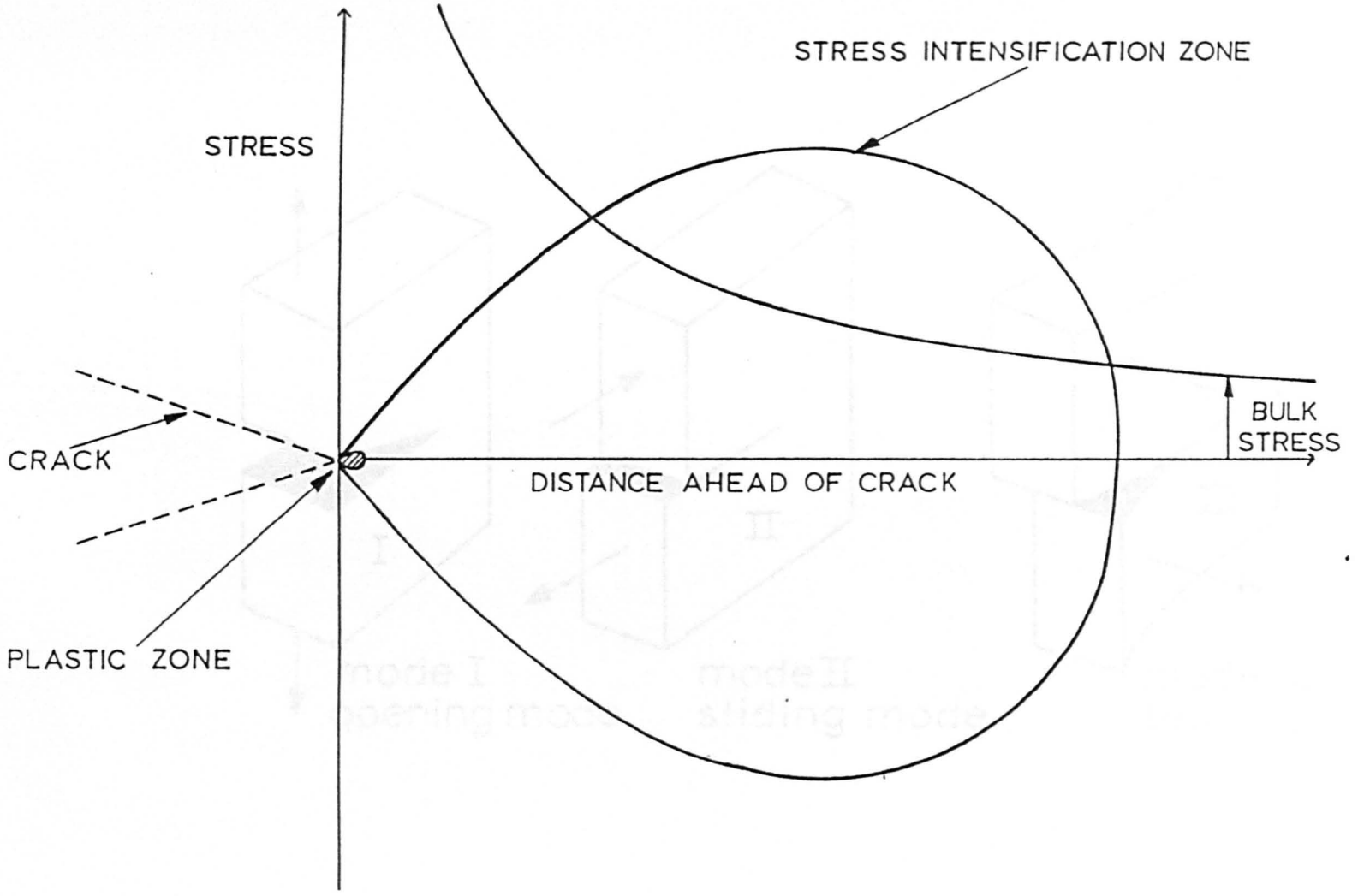

Fig.(2.3) Stress intensity field at crack tip in LEFM.

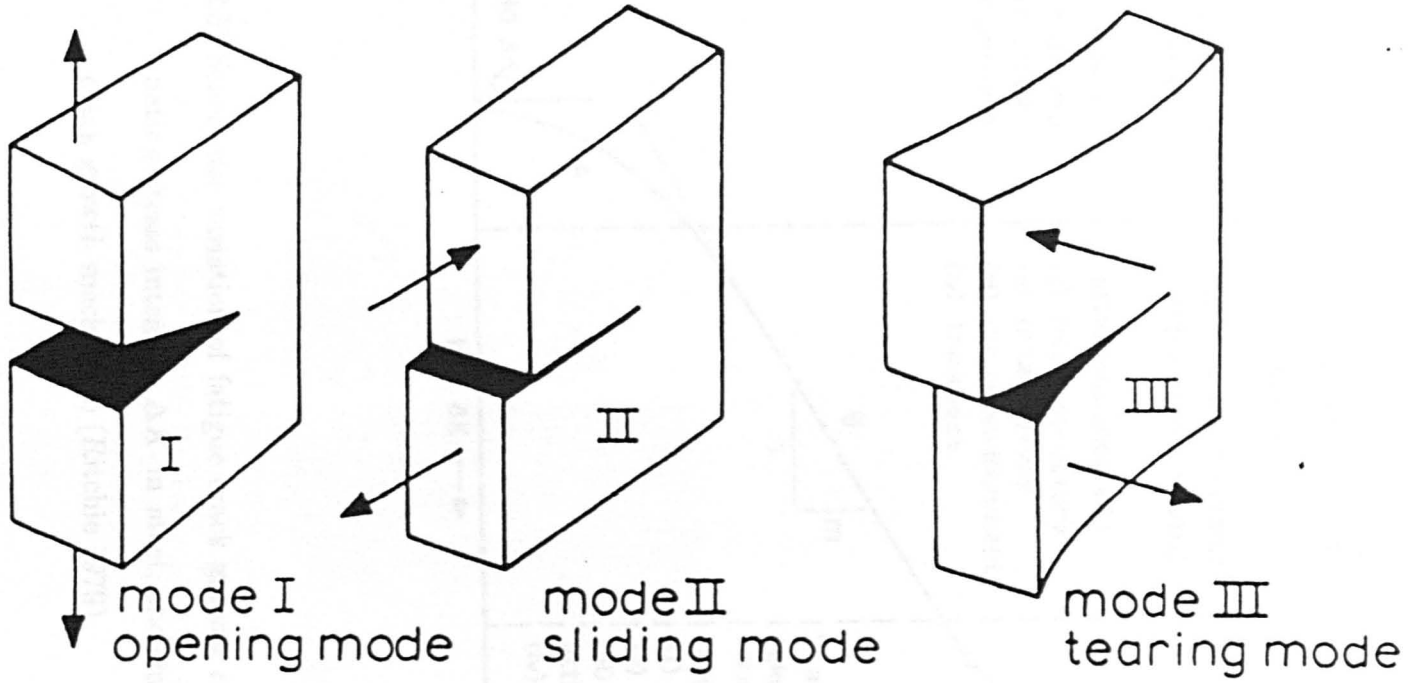

Fig.(2.4) The three modes of crack extension.

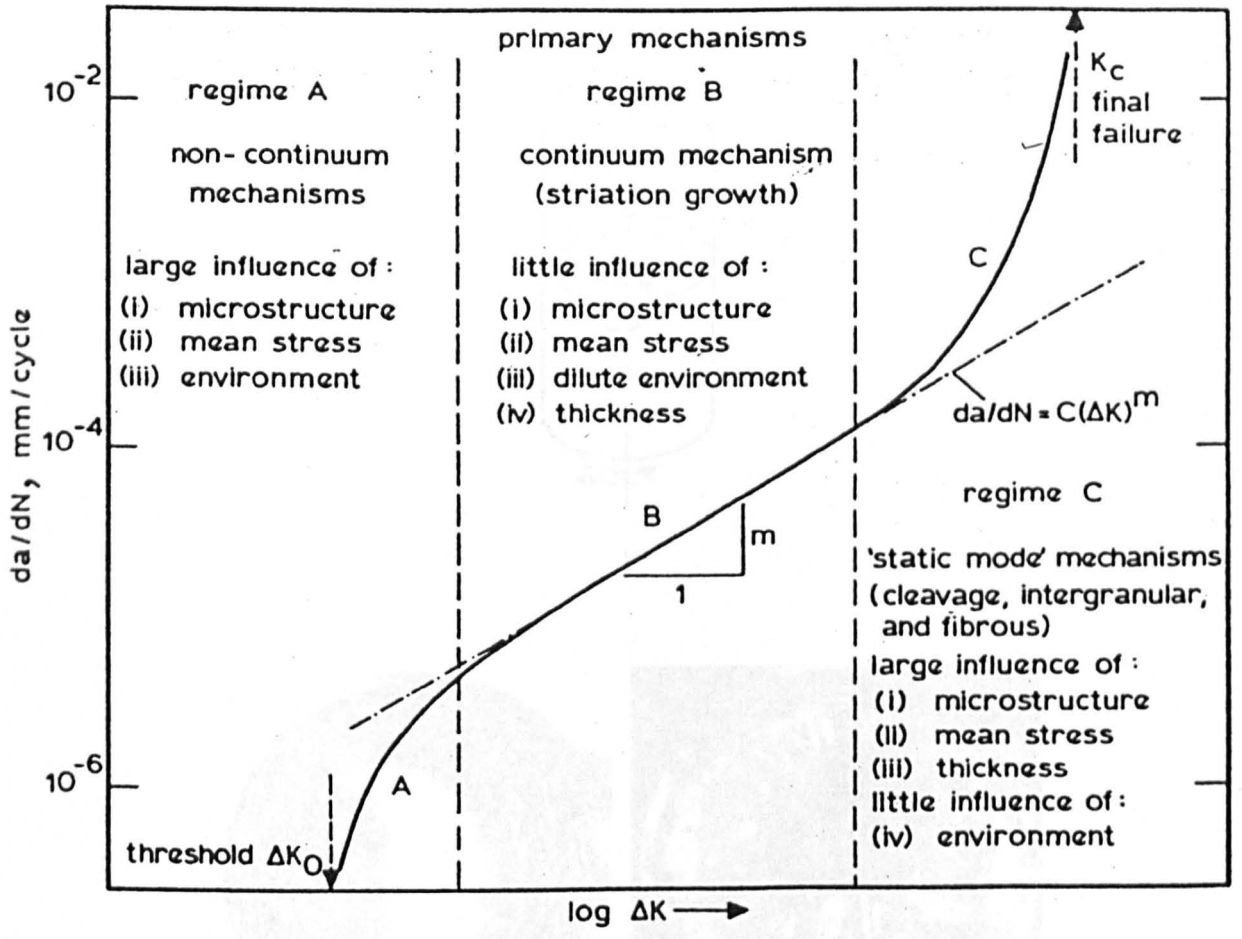

Fig.(2.5) Schematic variation of fatigue crack growth rate da/dN with alternating stress intensity ΔK in steel, showing regimes of primary crack growth mechanism (Ritchie 1979).

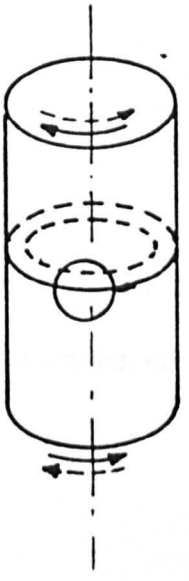

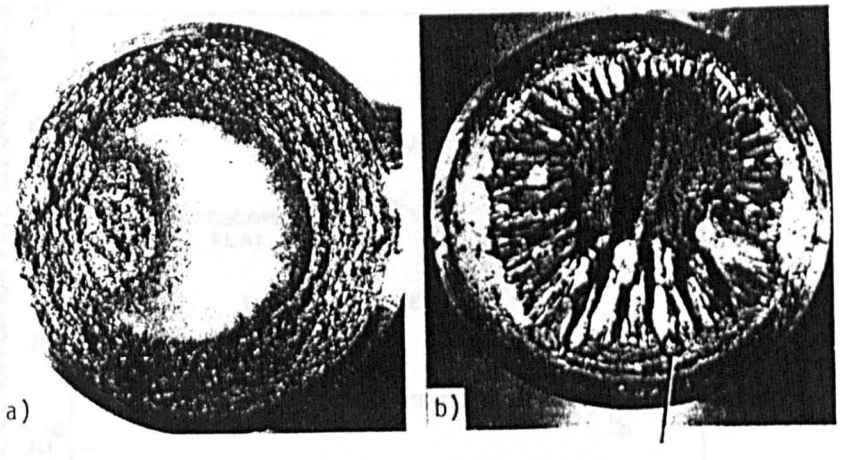

Fig.(2.6) Schematic illustration showing the plane of fatigue cracks in torsion with two types of failures (a) macroscopically-flat mode (pure radial mode III) (b) factory roof fracture (radial mode III with 45° mode I branch crack).

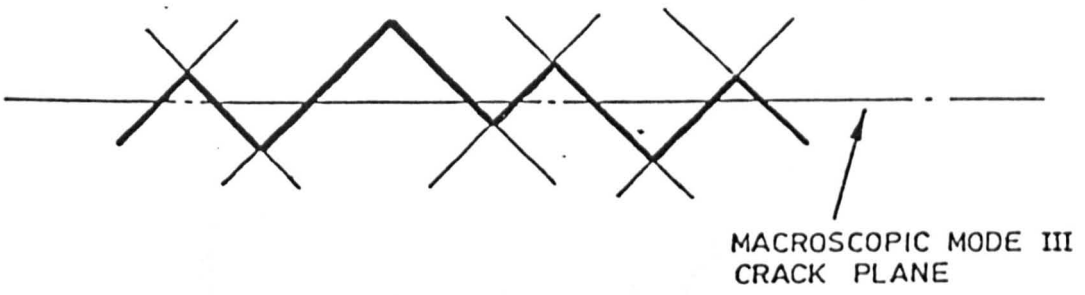

Fig.(2.7) Mode I facet on a complementary planes (Pook 1985a).

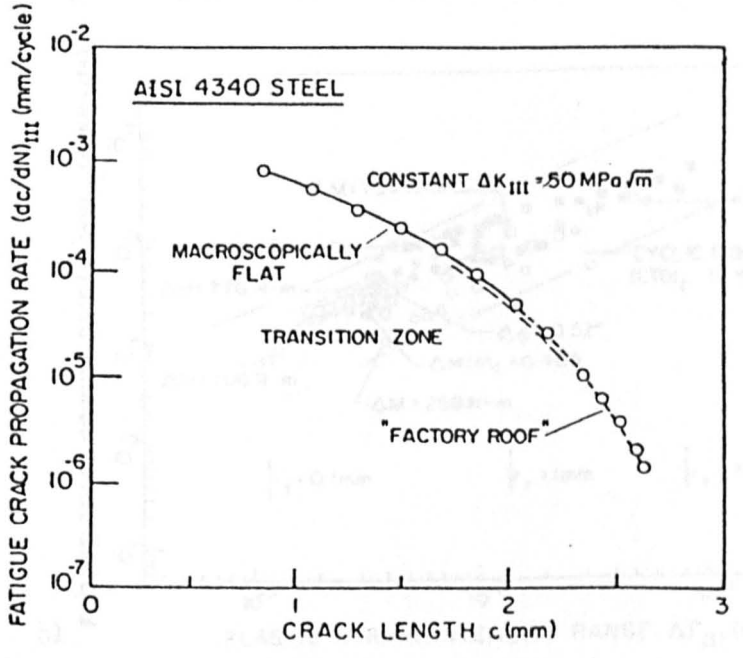

Fig.(2.8) Mode III fatigue crack growth bahaviour at R = -1 in 4340 steel (650° C temper) as a function of crack length for tests at constant ΔK_{III} of 50 $MPa\sqrt{m}$ (Ritchie et al 1985).

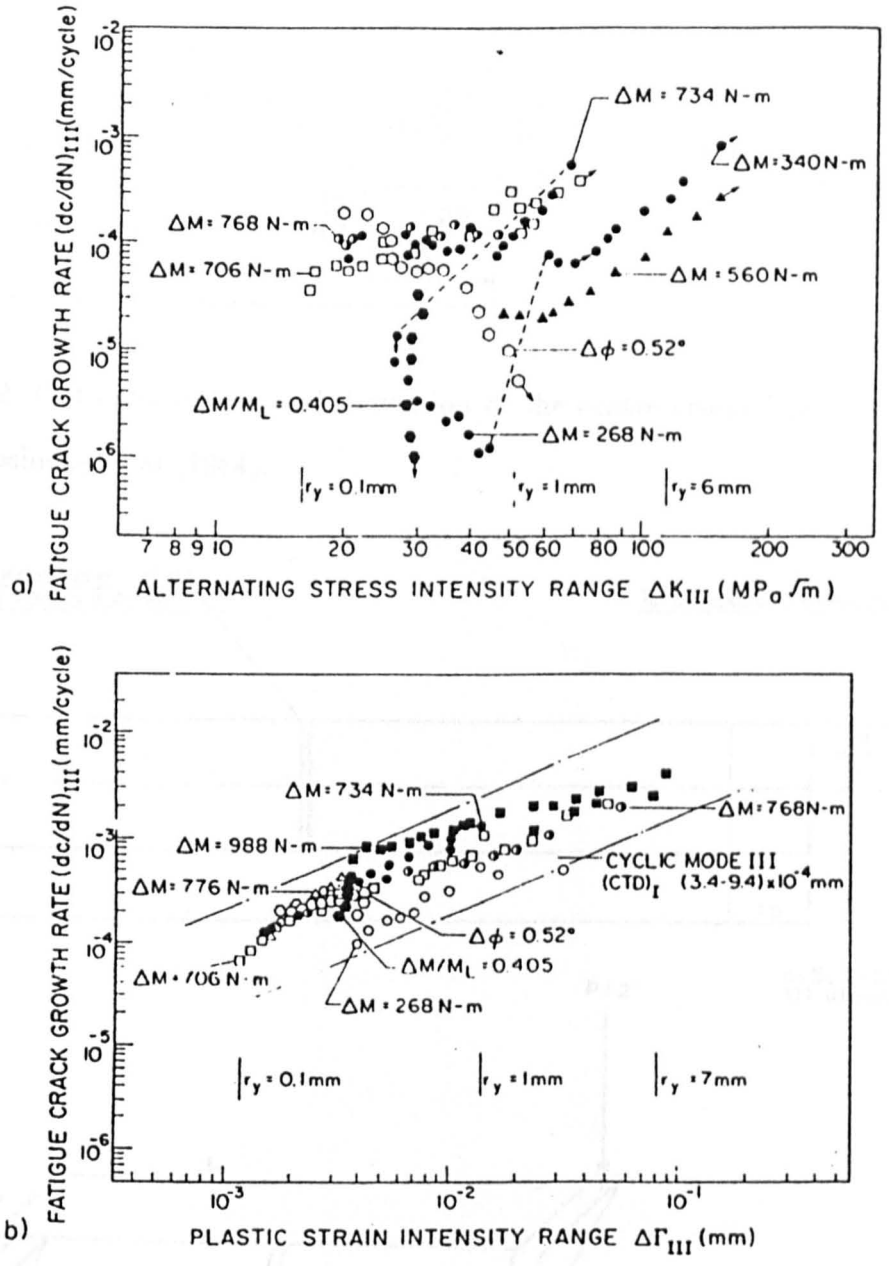

Fig.(2.9) Mode III fatigue crack growth rates (da/dN) at R = -1 in annealed 4140 steel showing (a) behaviour as a function of ΔK_{III} for tests under pure cyclic torsion ($K_I = 0$) and (b) behaviour as a function of plastic strain intensity range $\Delta\Gamma_{III}$ for test under cyclic torsion with small superimposed axial load ($K_I = 6$ *to* $11\ MPa\sqrt{m}\ CTD \approx 0.3$ *to* $0.9\ \mu m$)

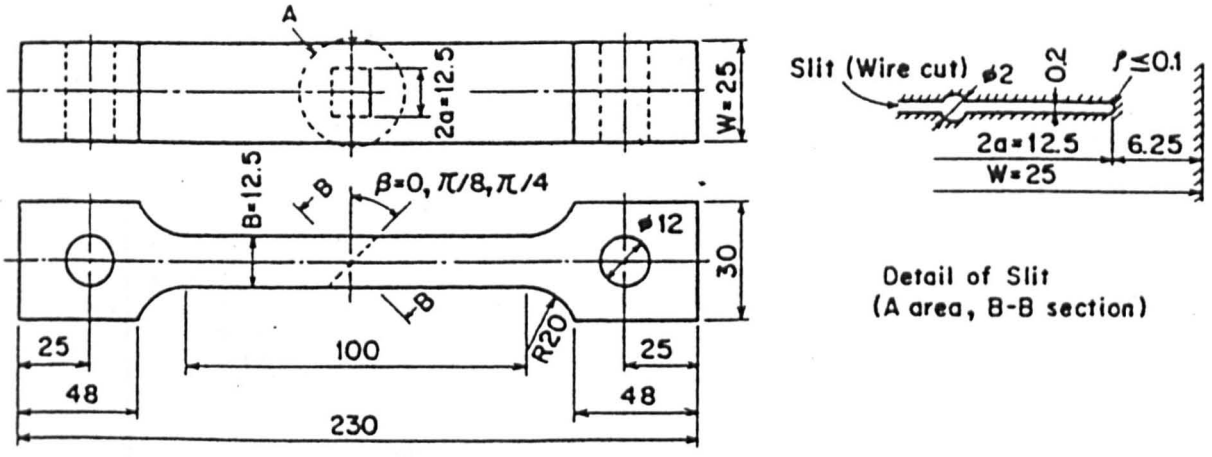

Fig.(2.10) Configuration and dimension of the centre cracked plate specimen used by Yoshioka et al (1984).

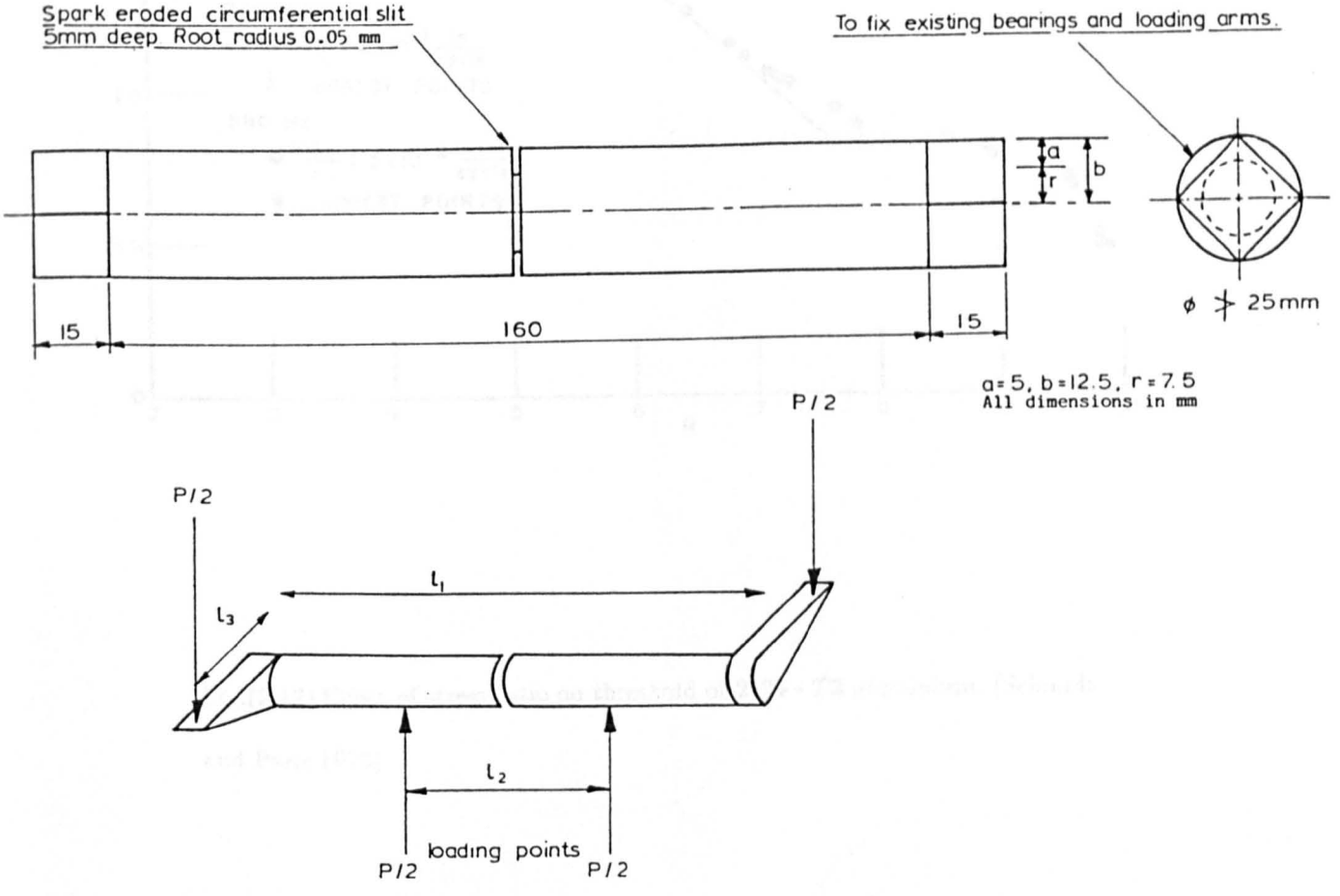

Fig.(2.11) Mixed mode I & III fatigue specimen and loading arrangement used by Yates and Miller (1987).

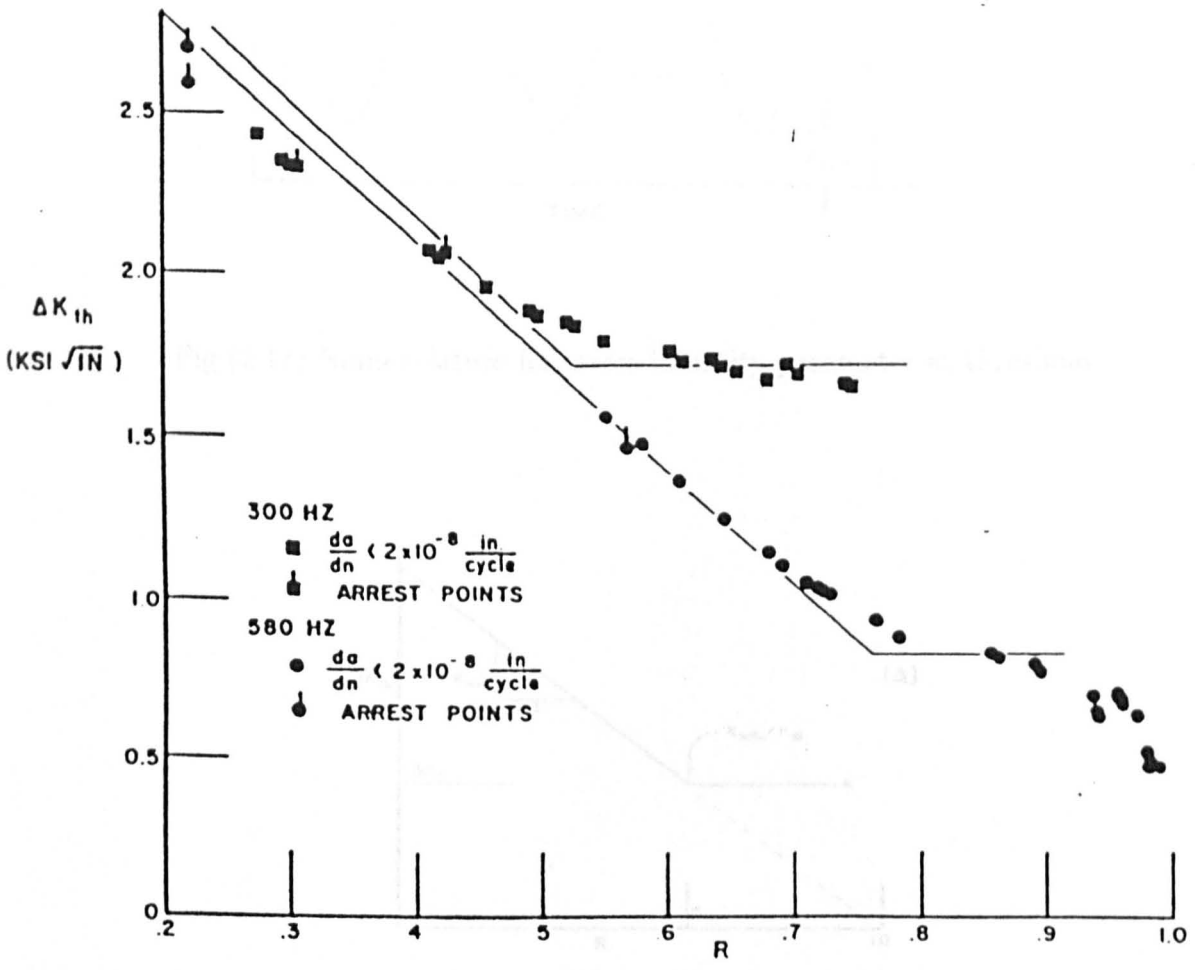

Fig.(2.12) Effect of stress ratio on threshold of 2024 - $T3$ aluminium. (Schmidt and Paris 1973)

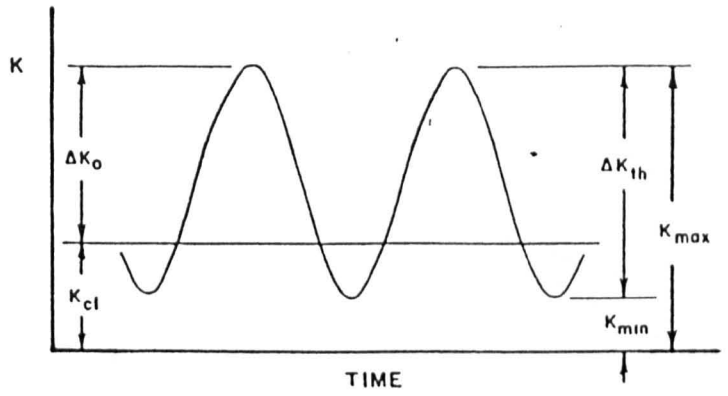

Fig.(2.13) Nomenclature for stress intensity parameter at threshold.

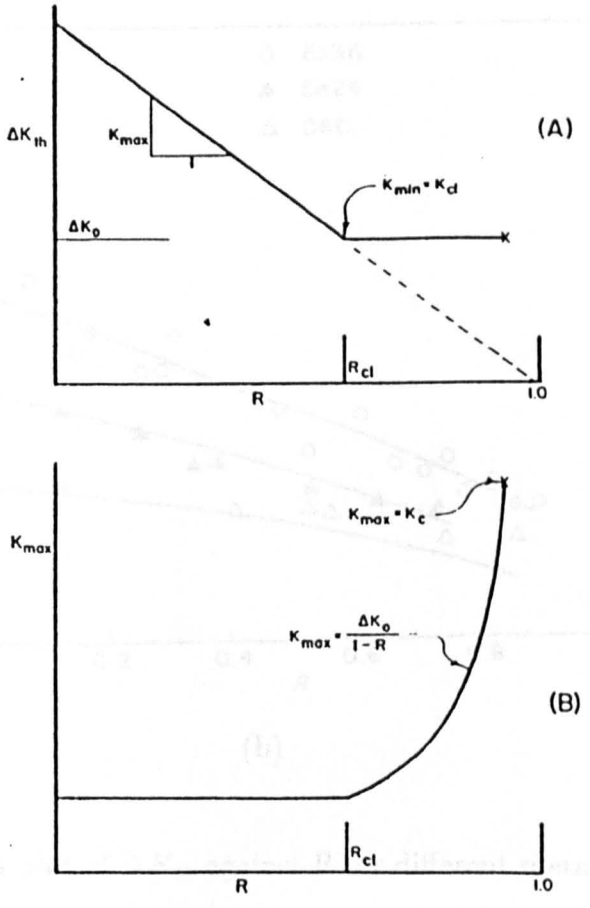

Fig.(2.14) General forms of threshold curves on basis of crack closure.

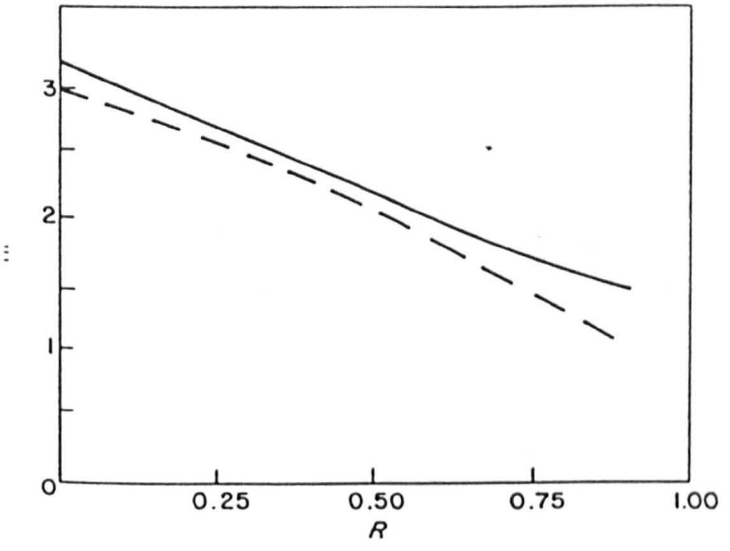

(a)

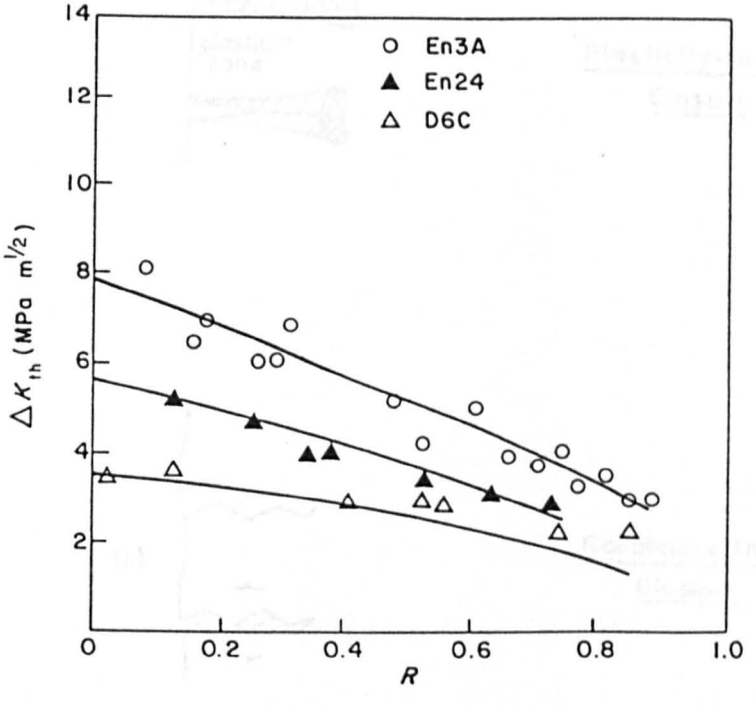

(b)

Fig.(2.15) A plot of ΔK_{th} against R for different metals:

(a) For Ti-6Al-4V. Full curve represents predicted results, broken curve represent experimental results.

(b) For three structural steel EN3A, EN24,D6C (Xiaopeng 1990).

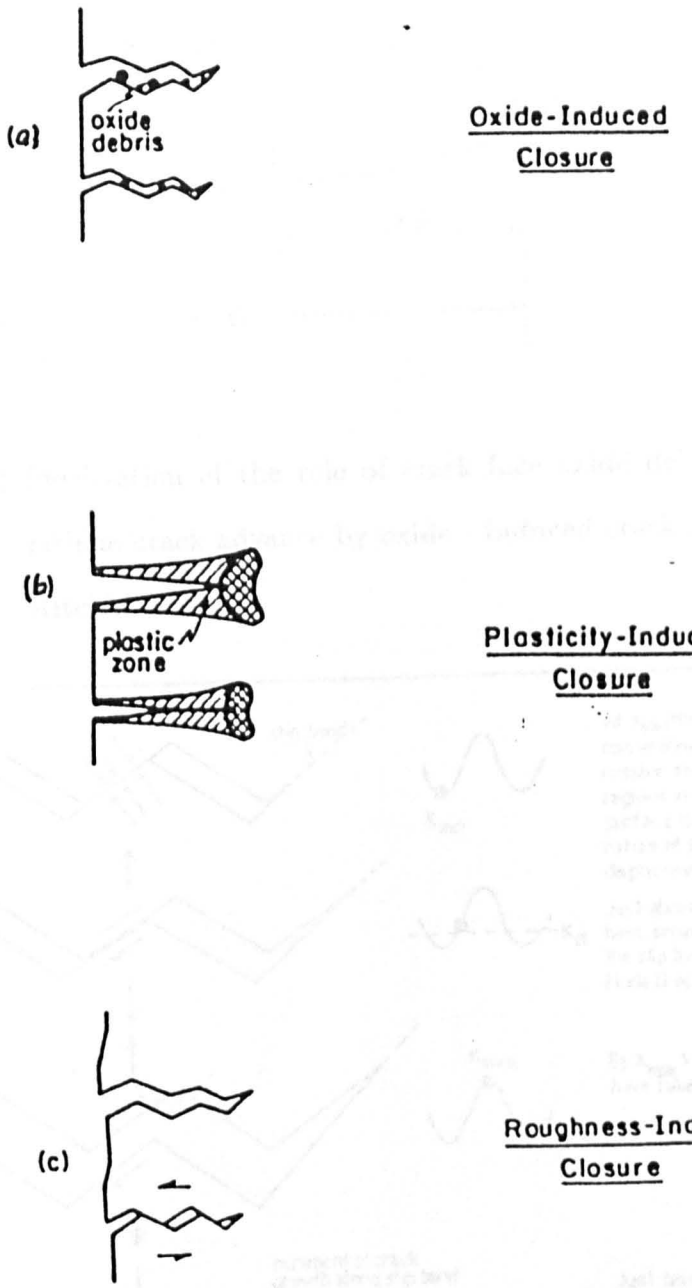

Fig.(2.16) Schematic illustration of the various mechanisim of fatigue crack closure (Suresh & Ritchie 1983).

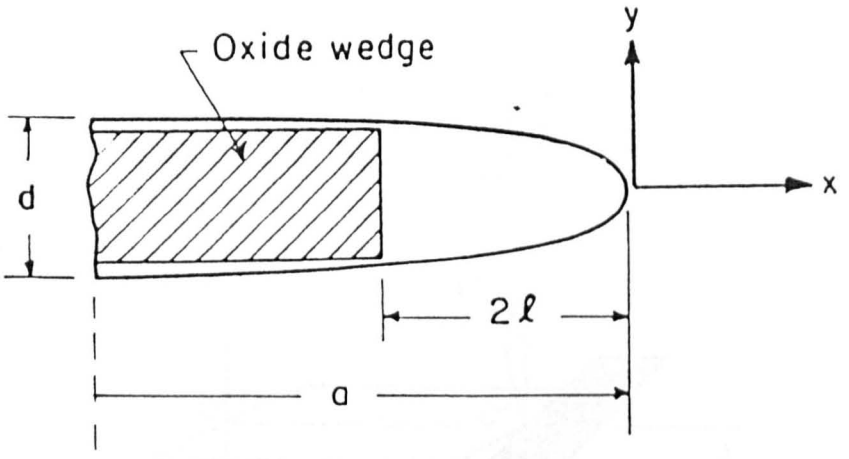

Fig.(2.17) Idealization of the role of crack face oxide debris in influencing fatigue crack advance by oxide - induced crack closure (Suresh & Ritchie 1983).

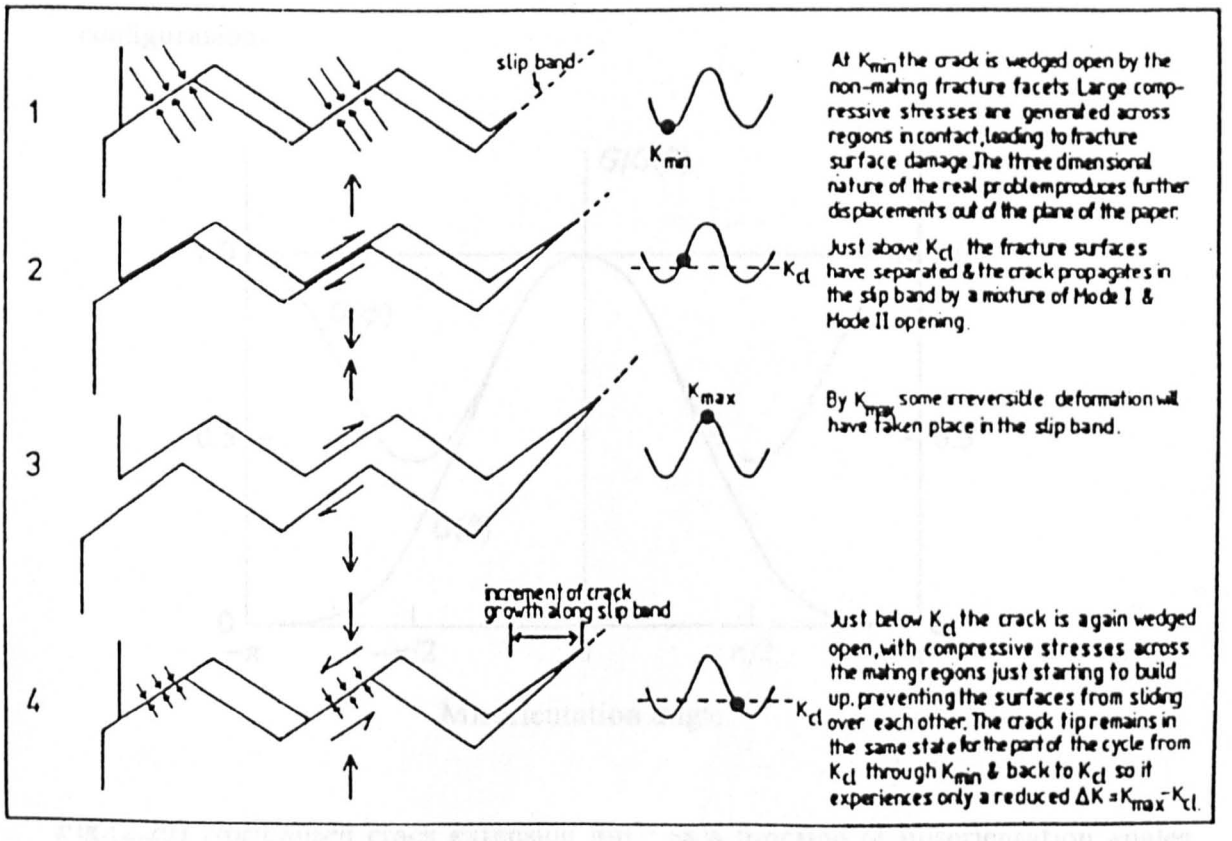

Fig.(2.18) Generation of closure during faceted crack growth (Minakawa & McEvily 1981).

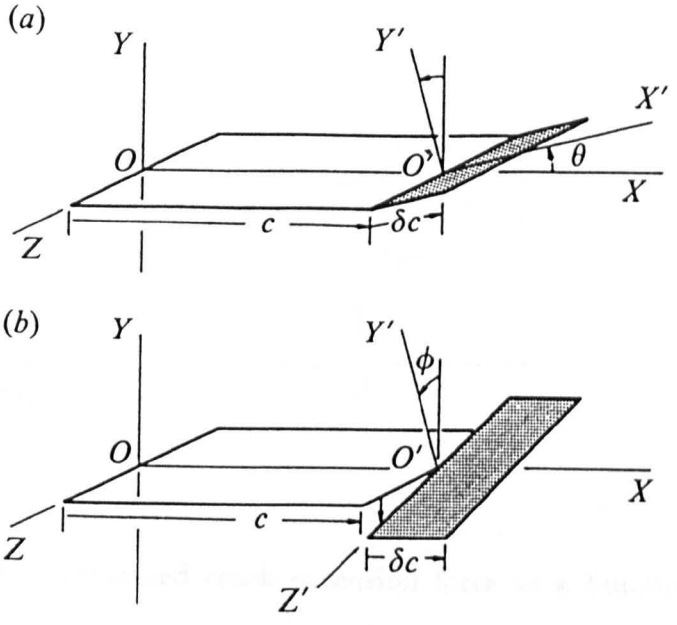

Fig.(2.19) Model for out of plane crack extension: (a) 'tilt' configuration (b) 'twist' configuration.

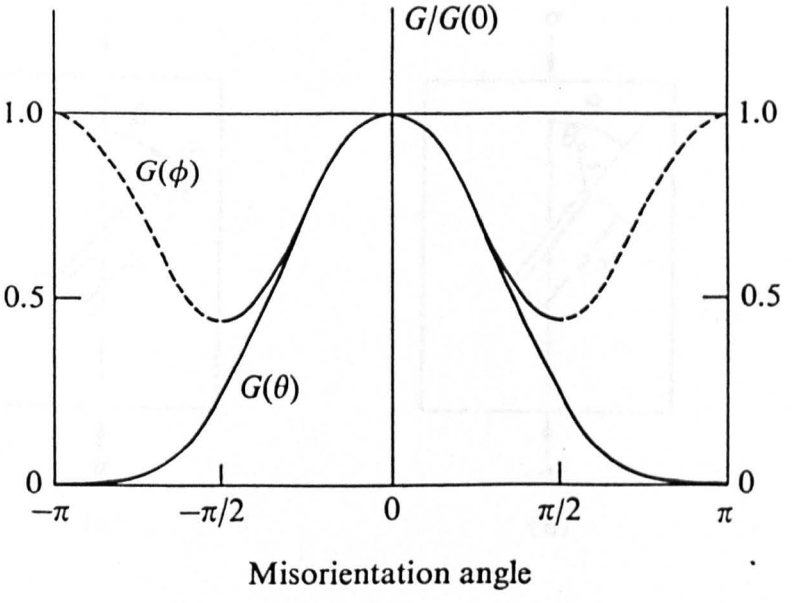

Fig.(2.20) Normalised crack extension force as a function of misorientation angles defined in fig.(2.19) for pure mode I loading (Lawn & Wilshaw 1975)

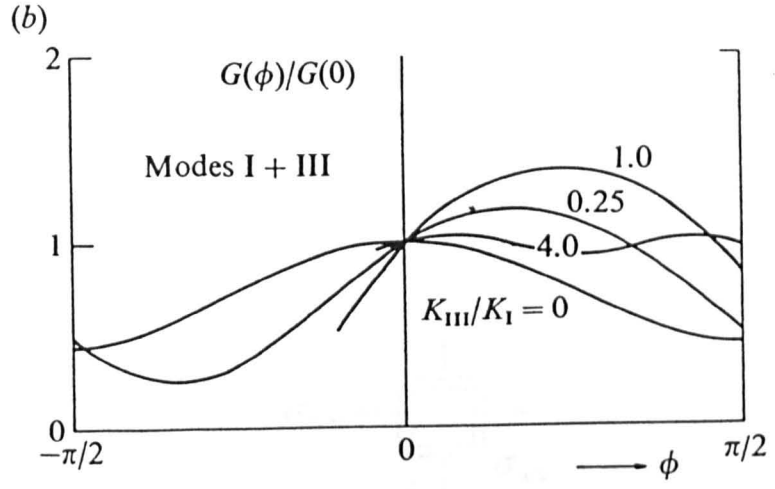

Fig.(2.21) Normalised crack extension force as a function of misorientation angle for super posed modes I & III (Lawn & Wilshaw 1985).

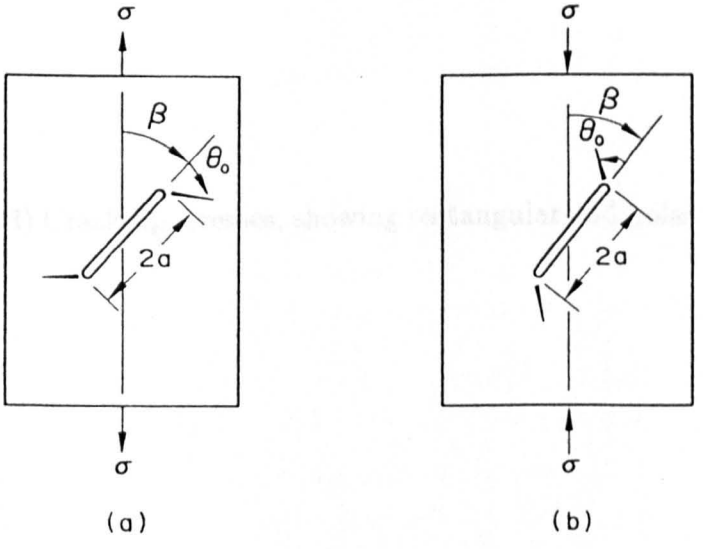

Fig.(2.22) An extension in an inclined crack in a plate under uniform; (a)tension (b) compression.

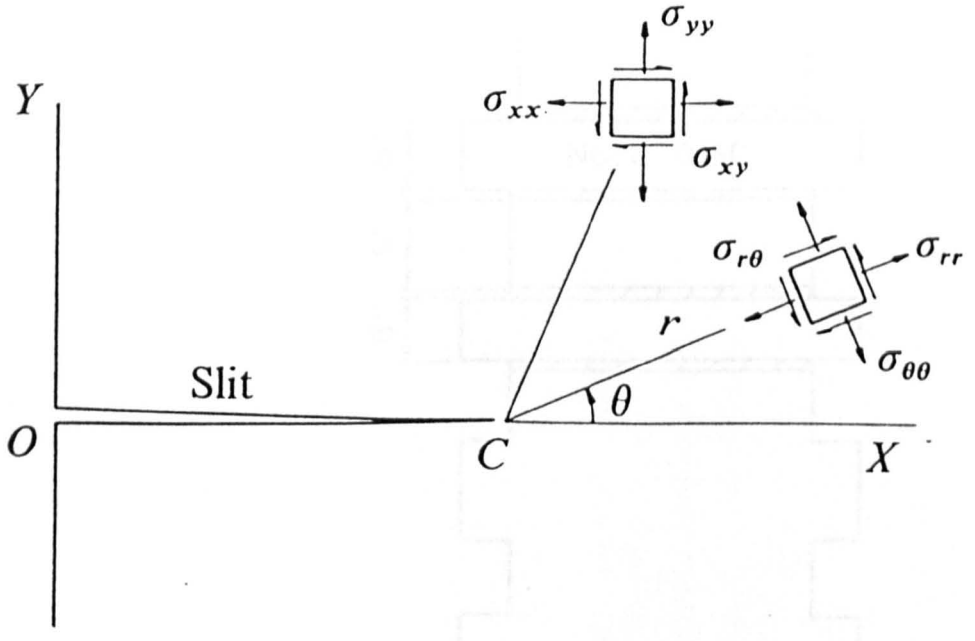

Fig.(2.23) Crack tip stresses, showing rectangular and polar co-ordinate components.

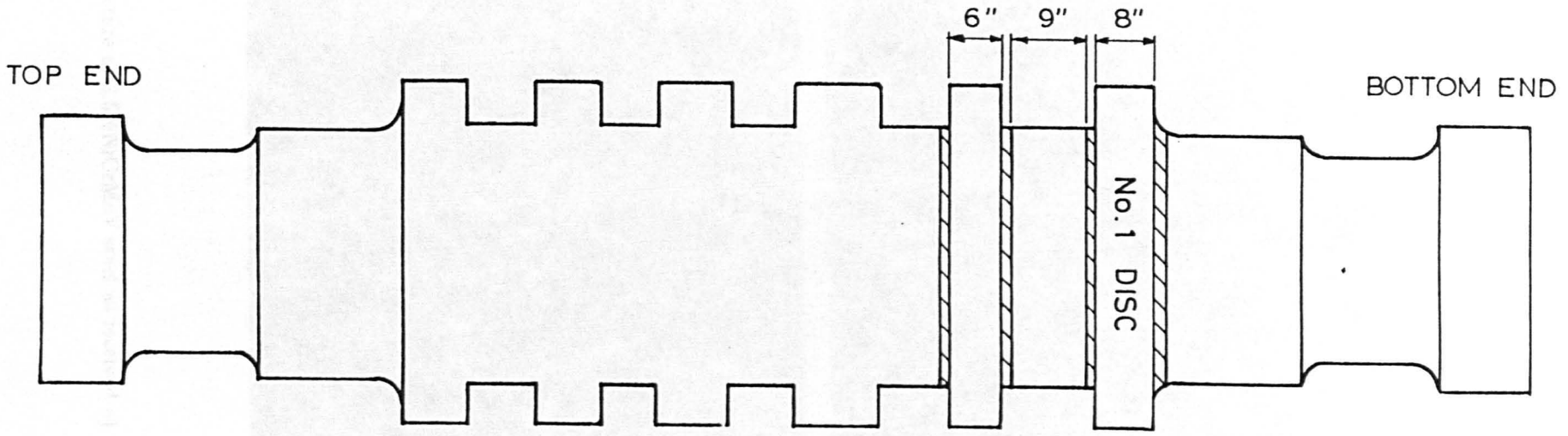

Fig.(4.1) Drawing of a low pressure rotor shaft showing the location of disc No. 1 where all the specimens were taken from with respect to the shaft.

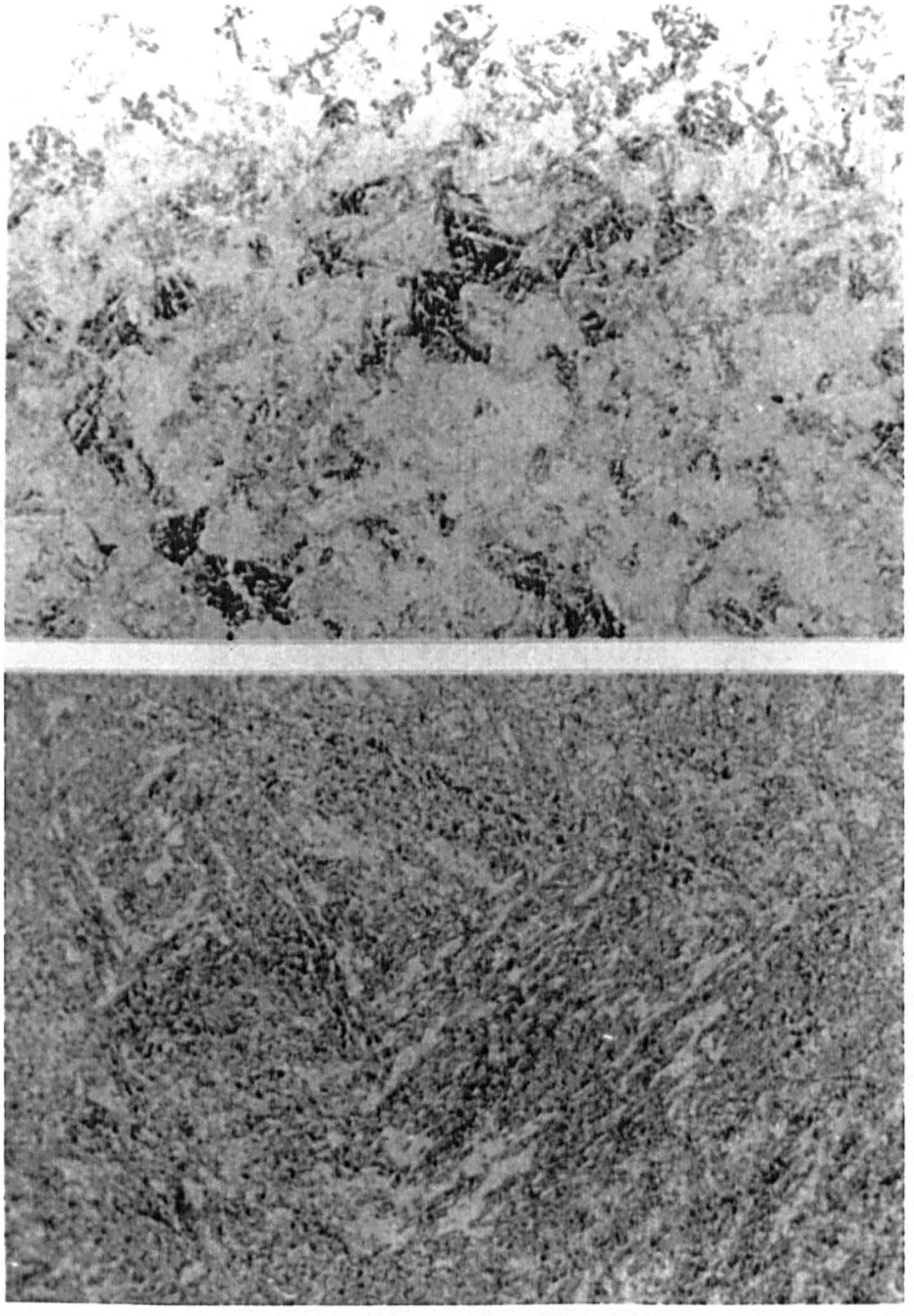

Fig.(4.2) Microstructure of 3.5%NiCrMoV steel as received a) ×70 b) ×700

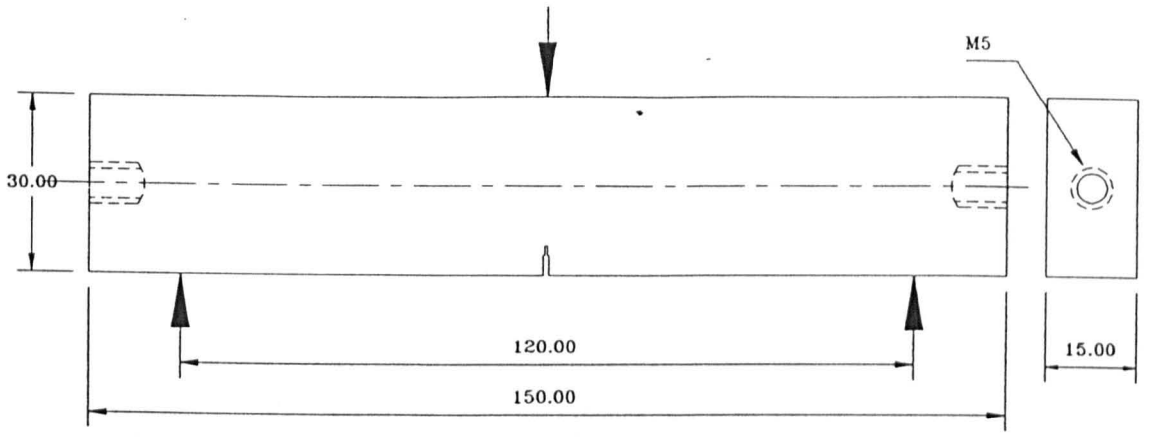

Fig. (4.3) Three points bending specimen used in mode I tests

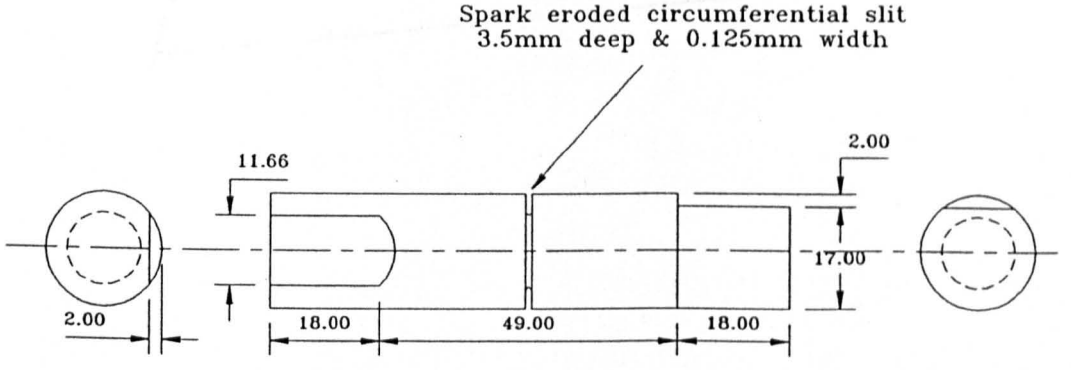

Fig. (4.4) Torsion specimen

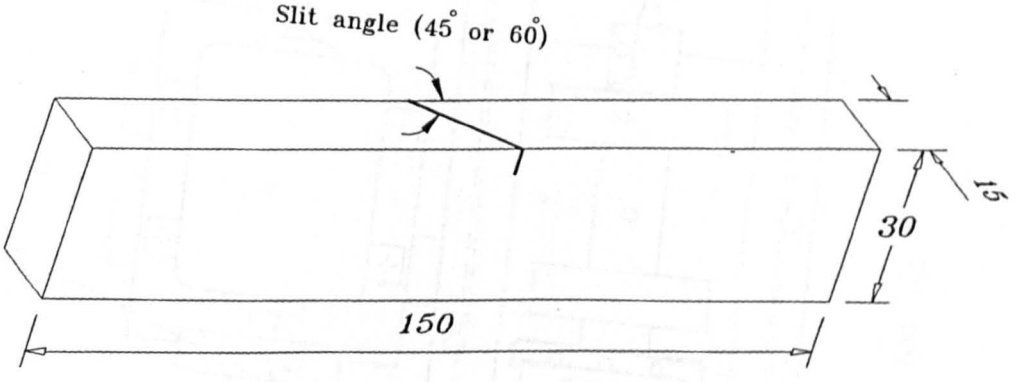

Fig.(4.5) Mixed mode I & III three point bend specimen, slit at an angle.

A- Low Speed Drive Unit.

B- High Speed Drive Unit.

C- A.C. Motor.

D- Reduction Gear.

E- Bearing Housing.

F- Sliding Base Plate.

G- Specimen Holder.

H- D.C. Motor.

J- Counter.

K- Specimen.

L- Torsion Grip.

M- Gides.

N- Load Cell.

P- Adjustable Connecting Rod.

Q- Variable Throw Cranks.

R- Fixed Base Plates.

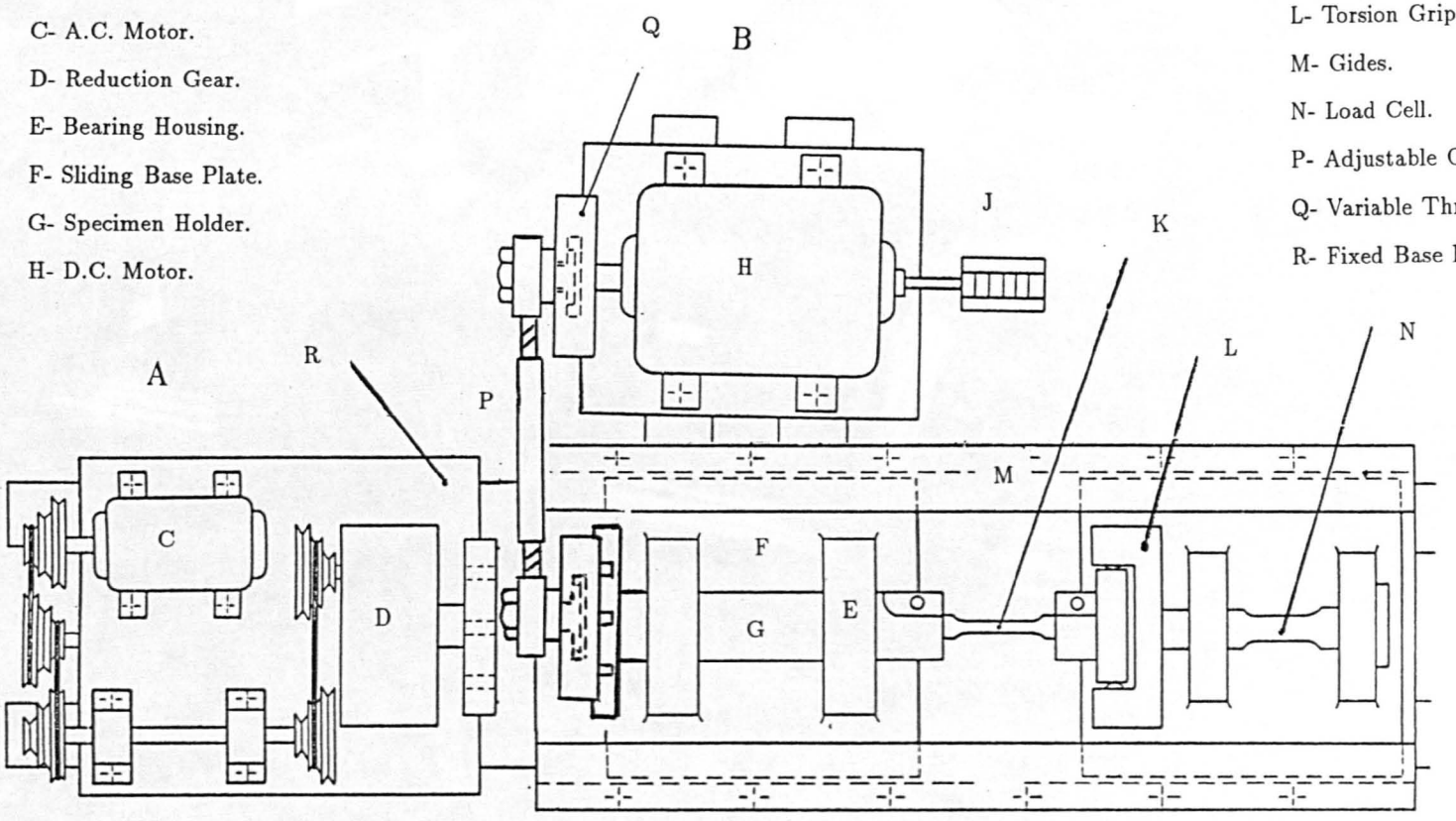

Fig.(4.6) Layout of the torsion test rig.

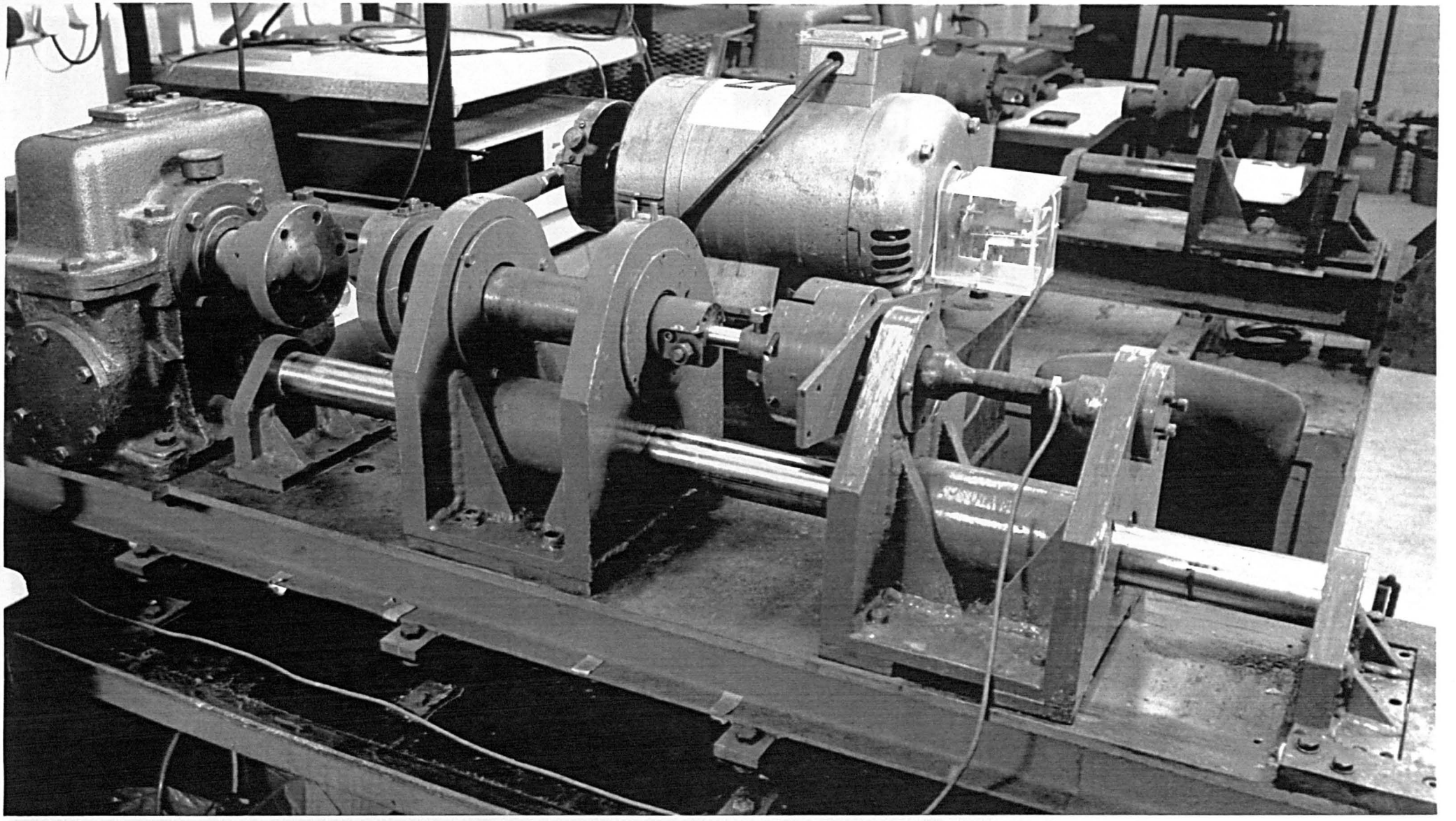

Fig.(4.7) Torsion test rig arrangement.

Fig.(4.8) Mode I and mixed mode I & III test rig.

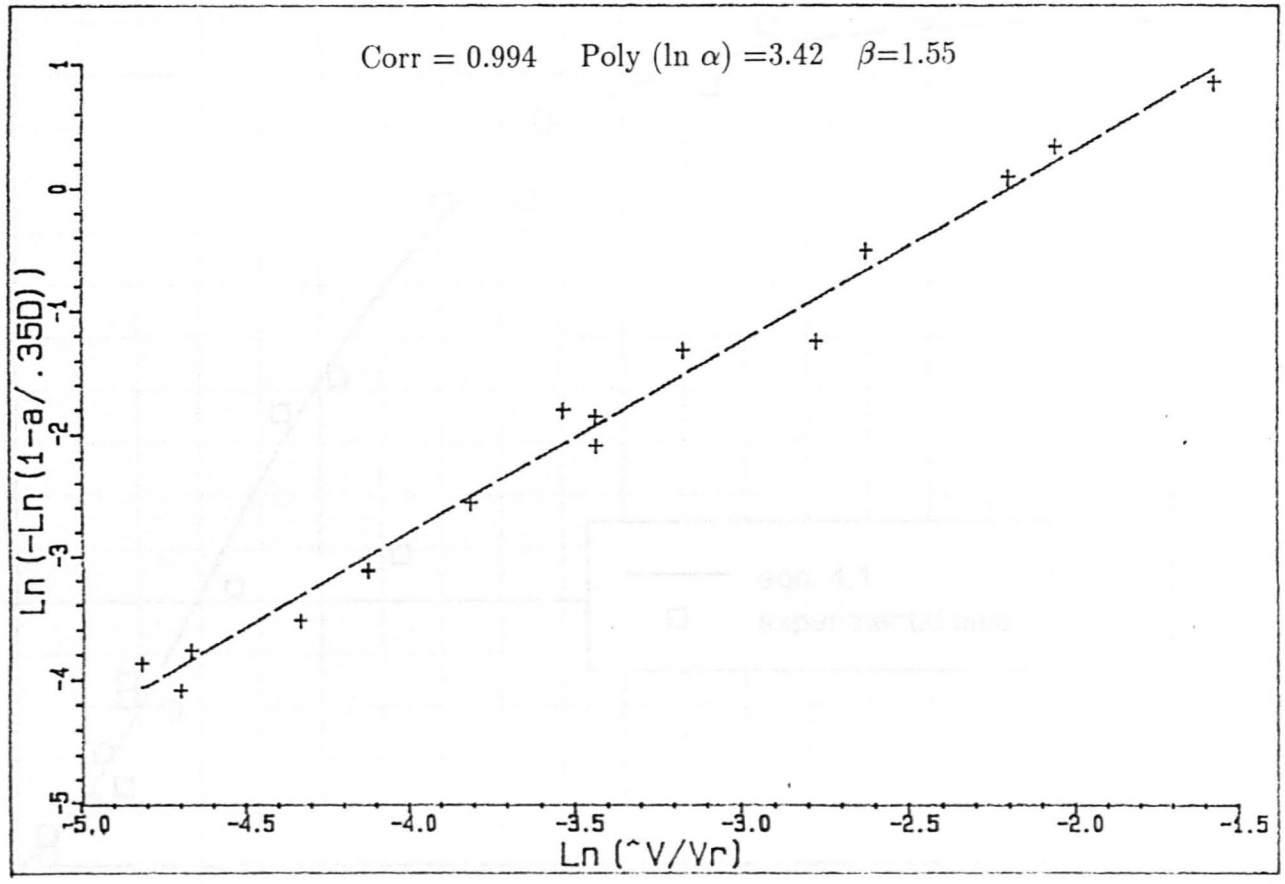

Fig.(4.9) A graph showing the values of (α&β) in equation 4.2.

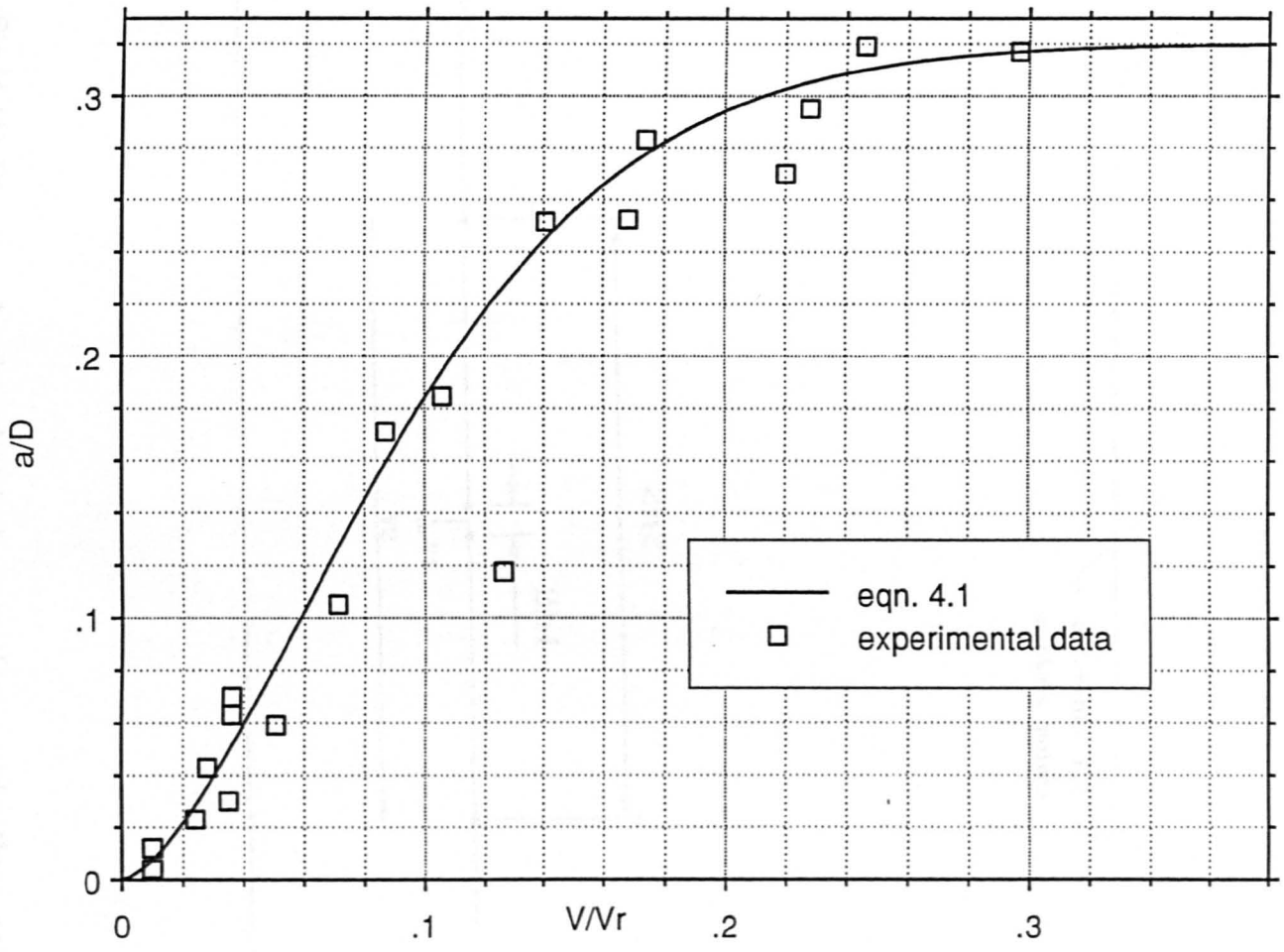

Fig.(4.10) Crack growth calibration curve for torsion specimen.

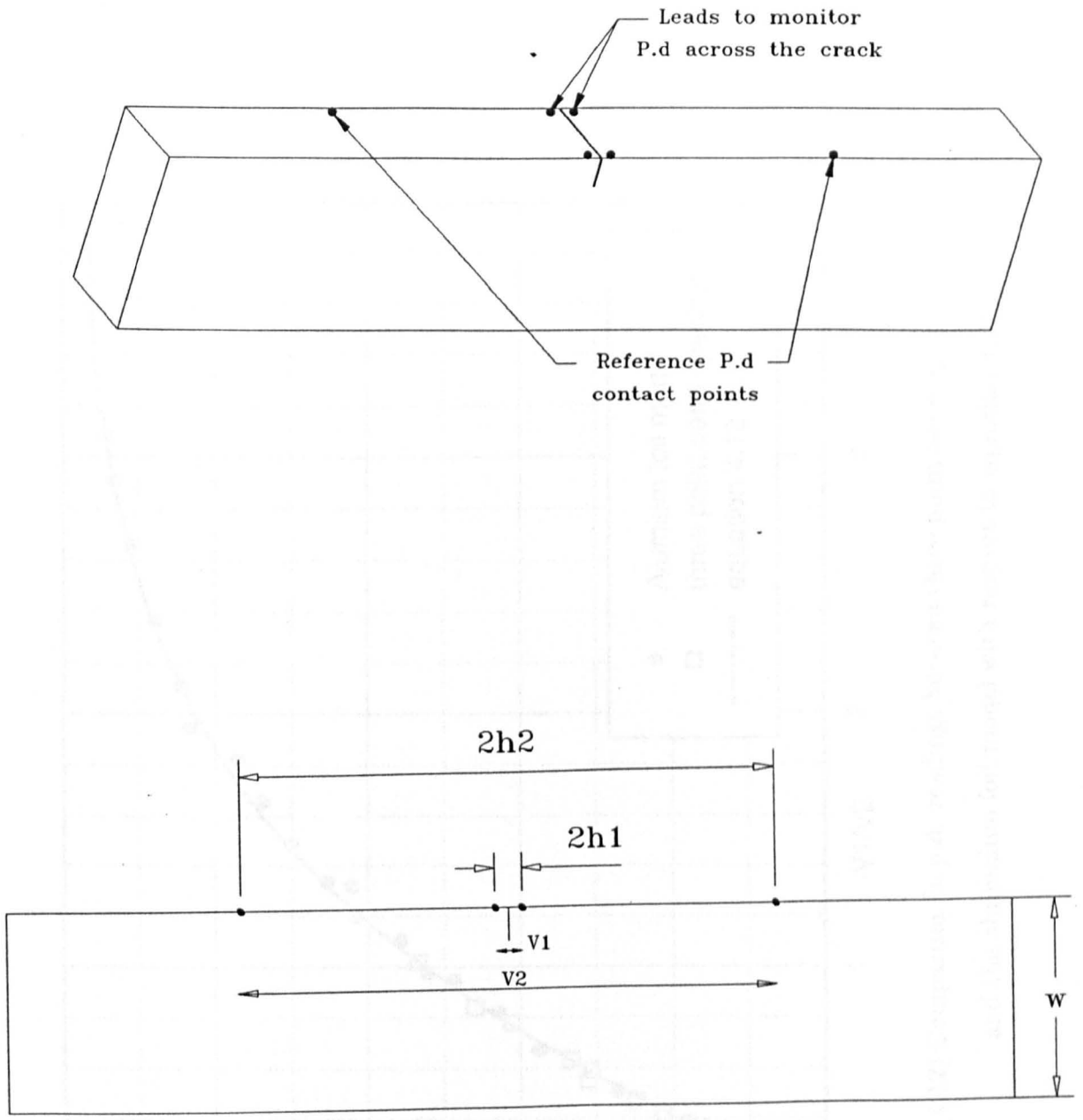

Fig.(4.11) Diagram showing electrical connections on the three point bend specimen.

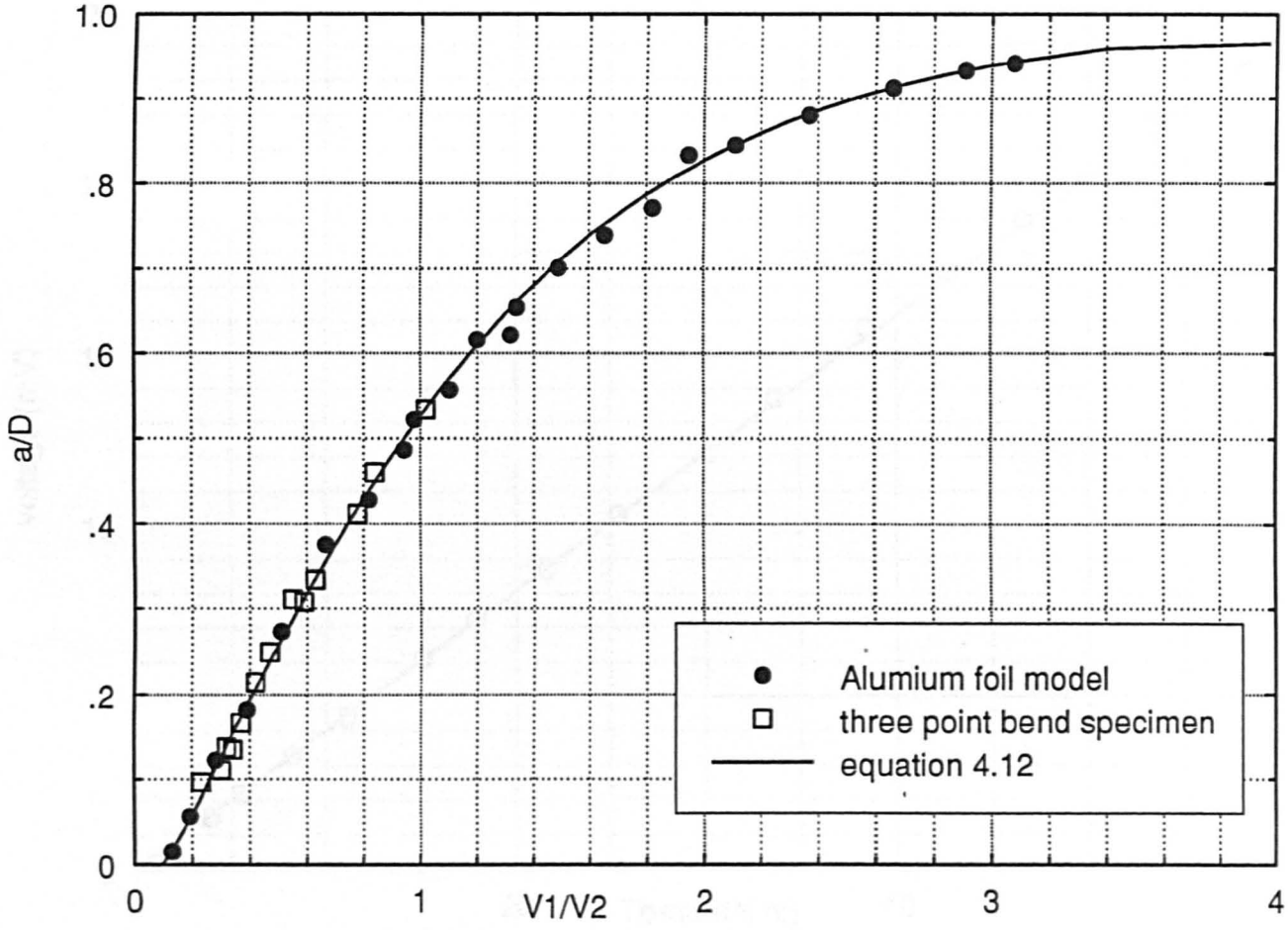

Fig.(4.12) Comparison in p.d. readings between three point bending specimen and the aluminium foil model with respect to equation 4.12.

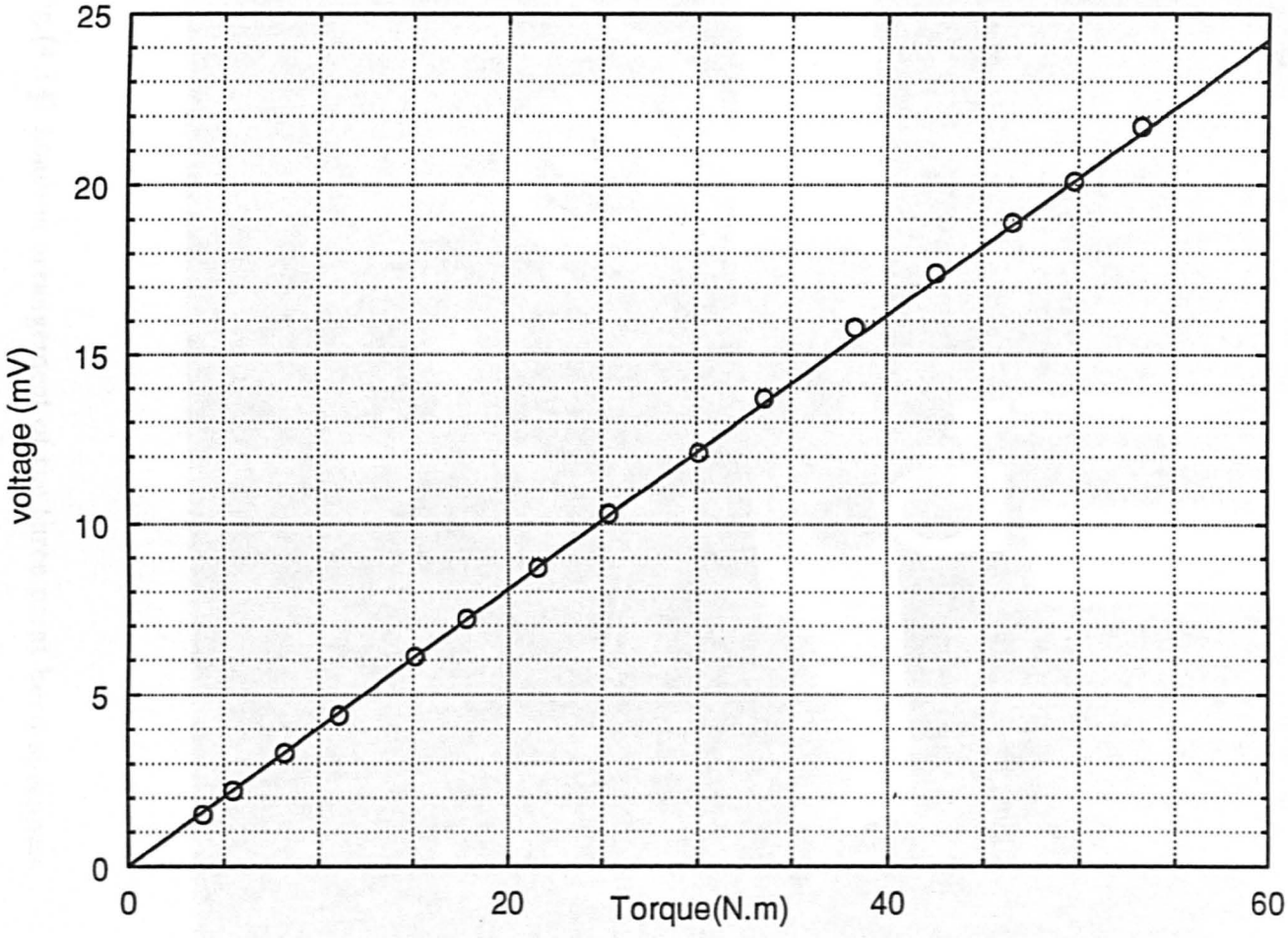

Fig.(4.13) Calibration of the load cell of the torsion test rig.

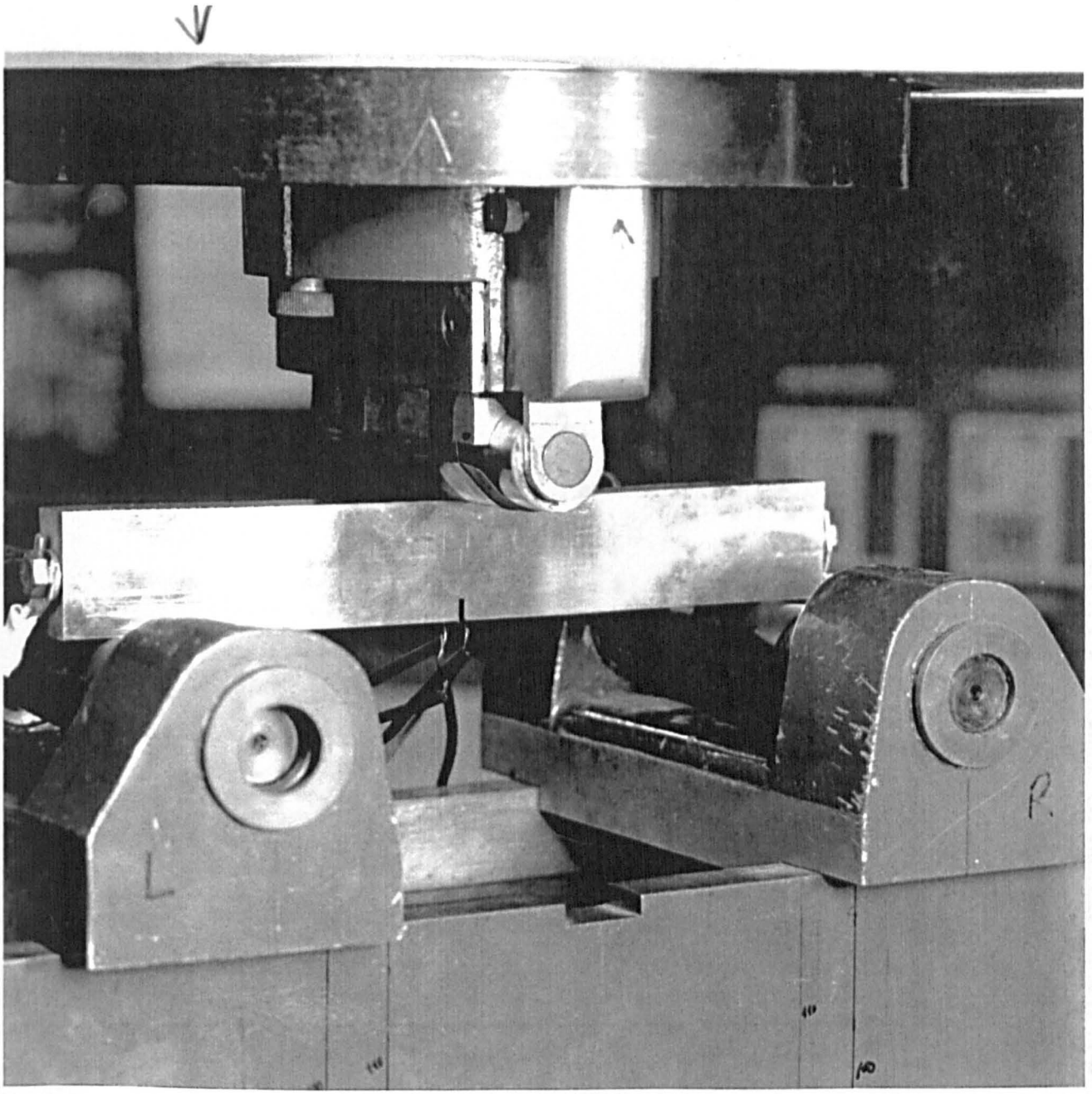

Fig.(4.14) Loading arrangement of the three point bend specimen.

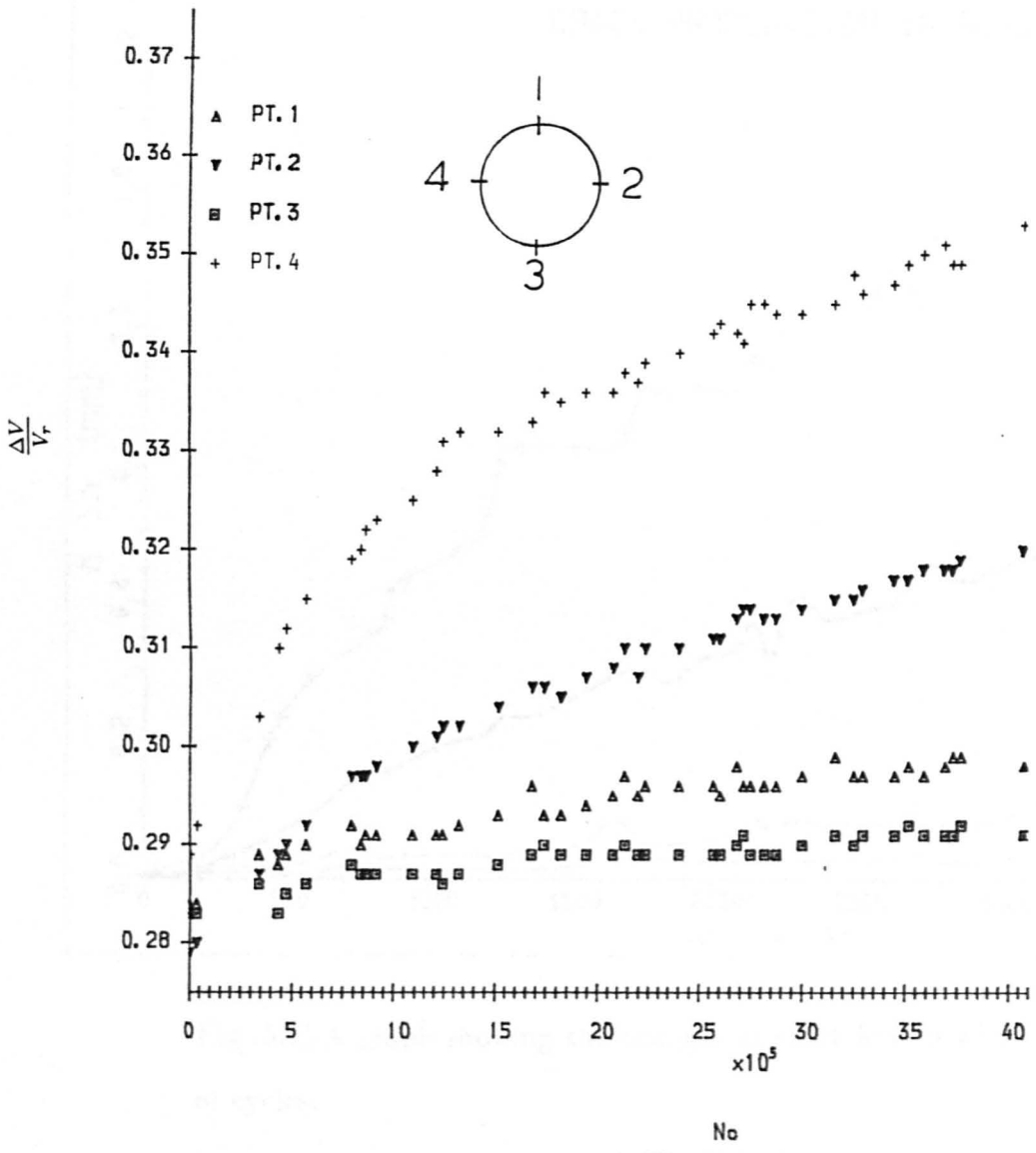

Fig.(5.1) A graph showing the changes in p.d readings of the four measurement points as the crack extends with increase number of cycles.

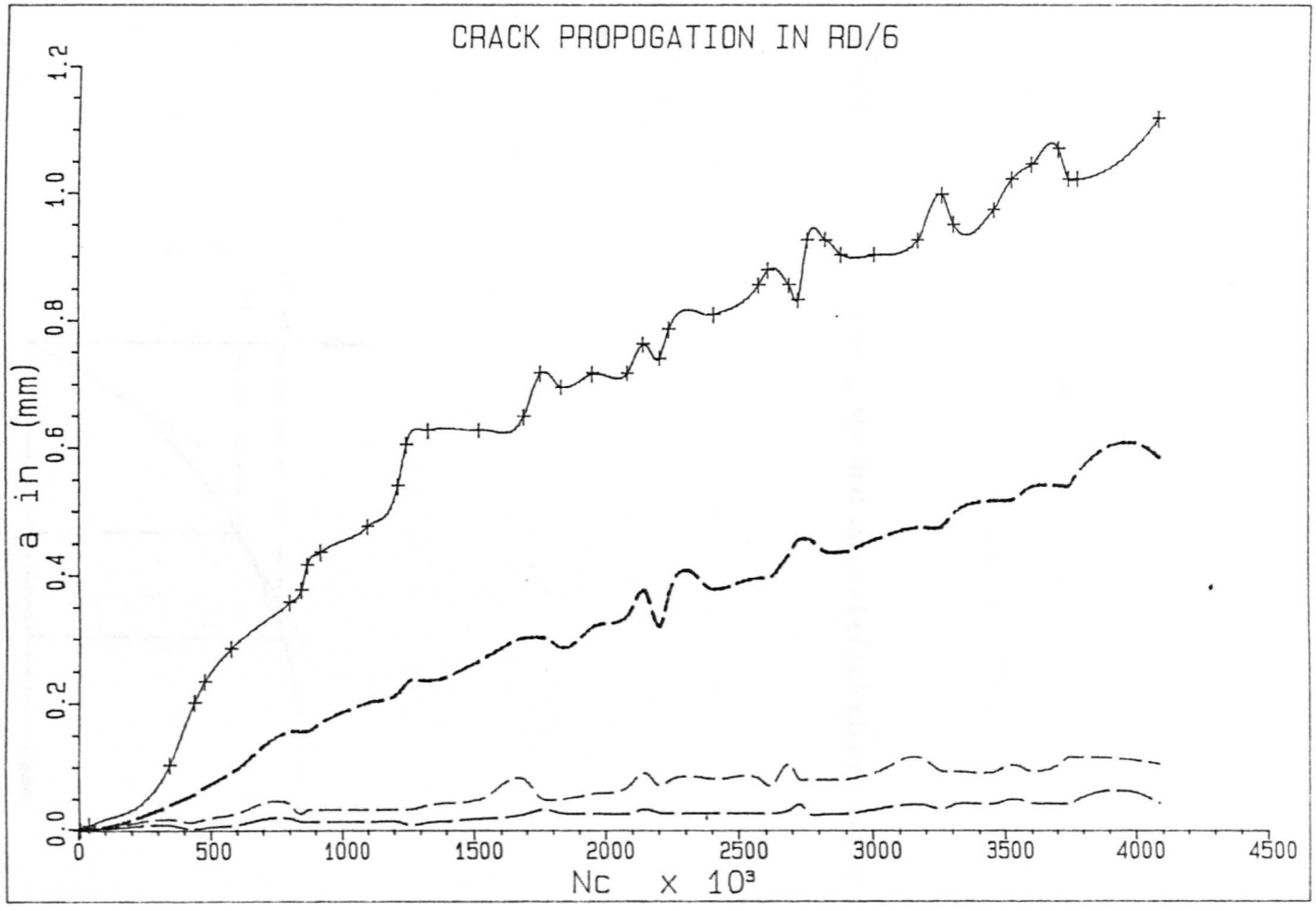

Fig.(5.2) A graph showing the changes in crack length with respect to the number of cycles.

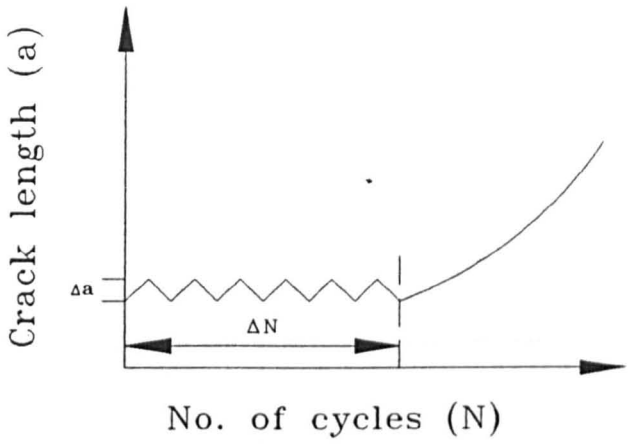

Fig.(5.3) A graph showing the first method of calculating undetected cracks

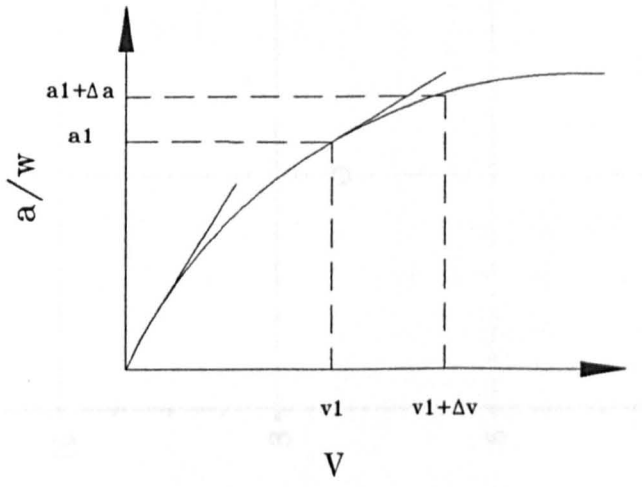

Fig.(5.4) A graph showing the second method of calculating undetected cracks

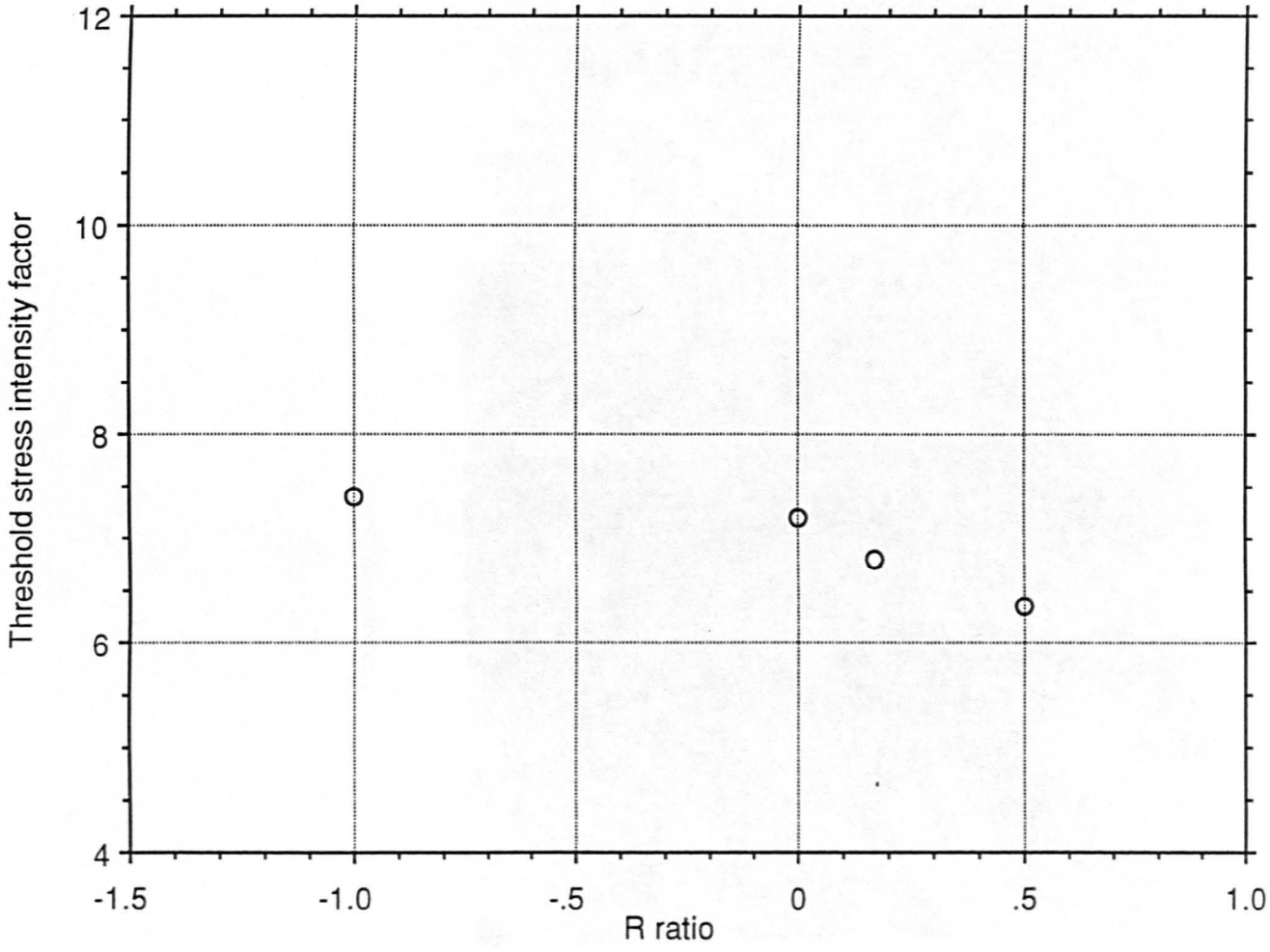

Fig.(5.5) The effect of R ratio on mode III fatigue threshold.

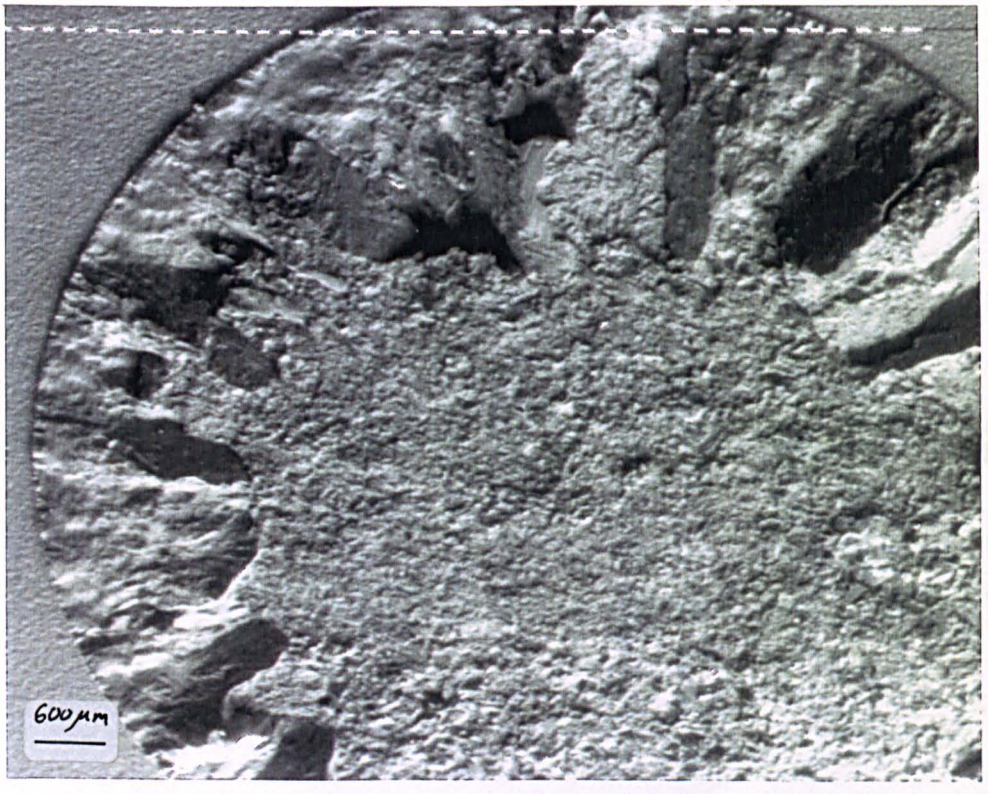

Fig.(5.6) Fracture surface of mode III test specimen.

a

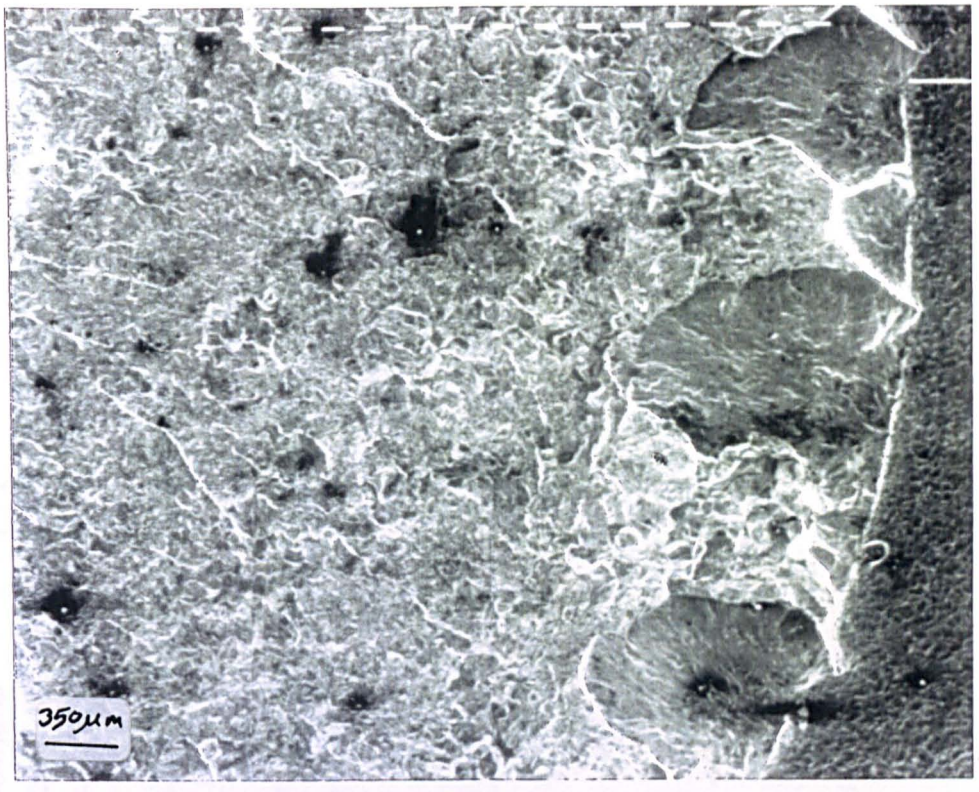

b

Fig.(5.7) a) Separated mode I facets in mode III crack plane. b) Merger of fatigue facets in mode III fracture surface.

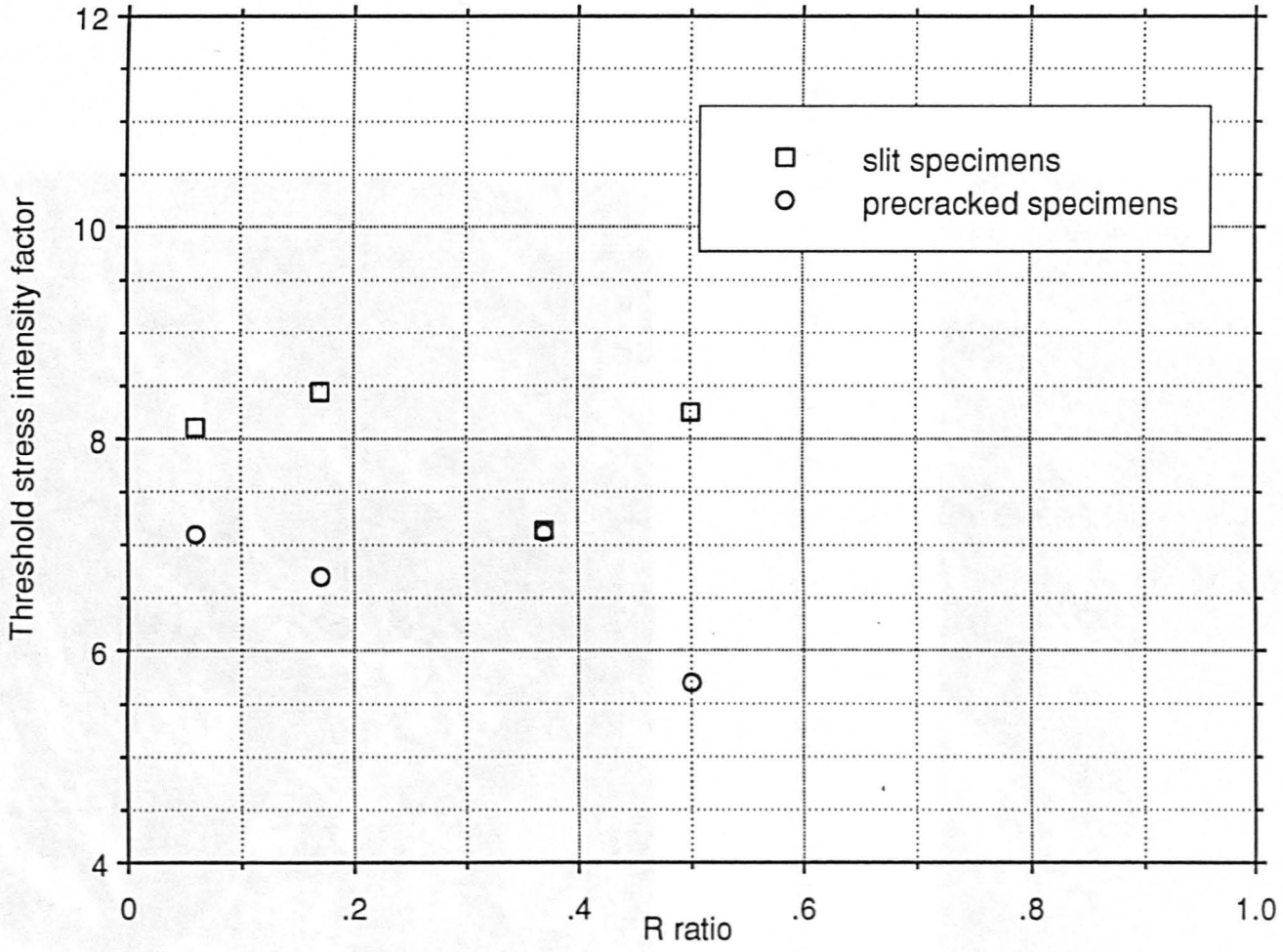

Fig.(5.8) The effect of R ratio on mode I fatigue tests in the slit and precracked specimens.

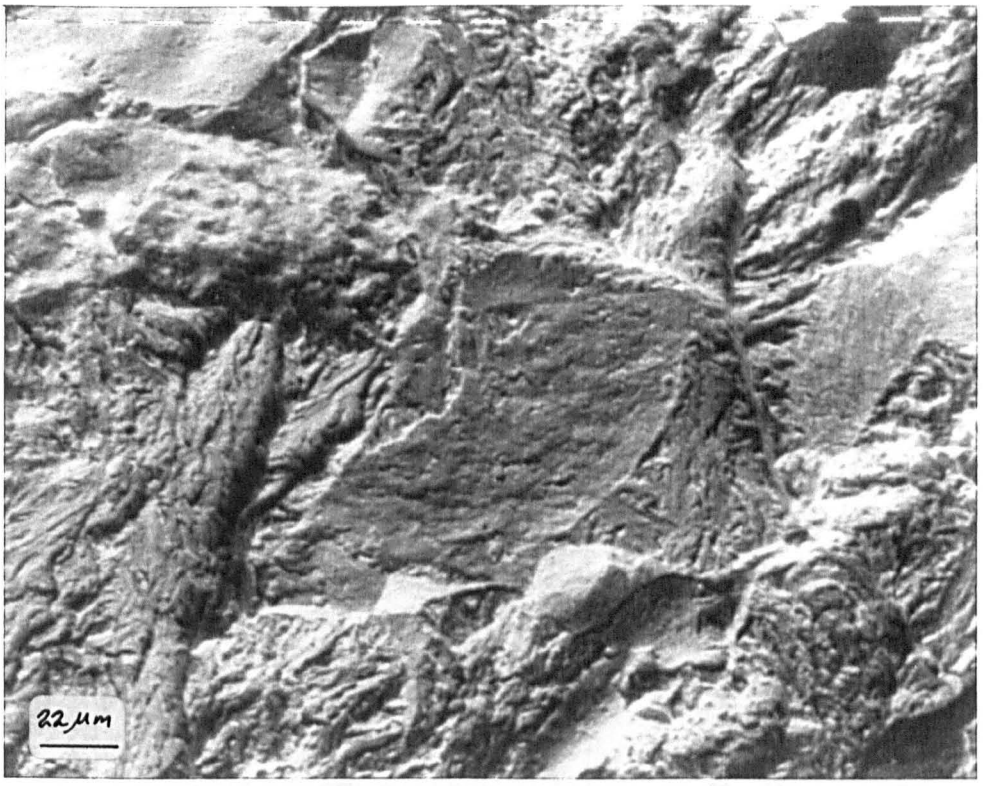

Fig.(5.9) Crystallographic facets at low stress intensity factors in mode I tests.

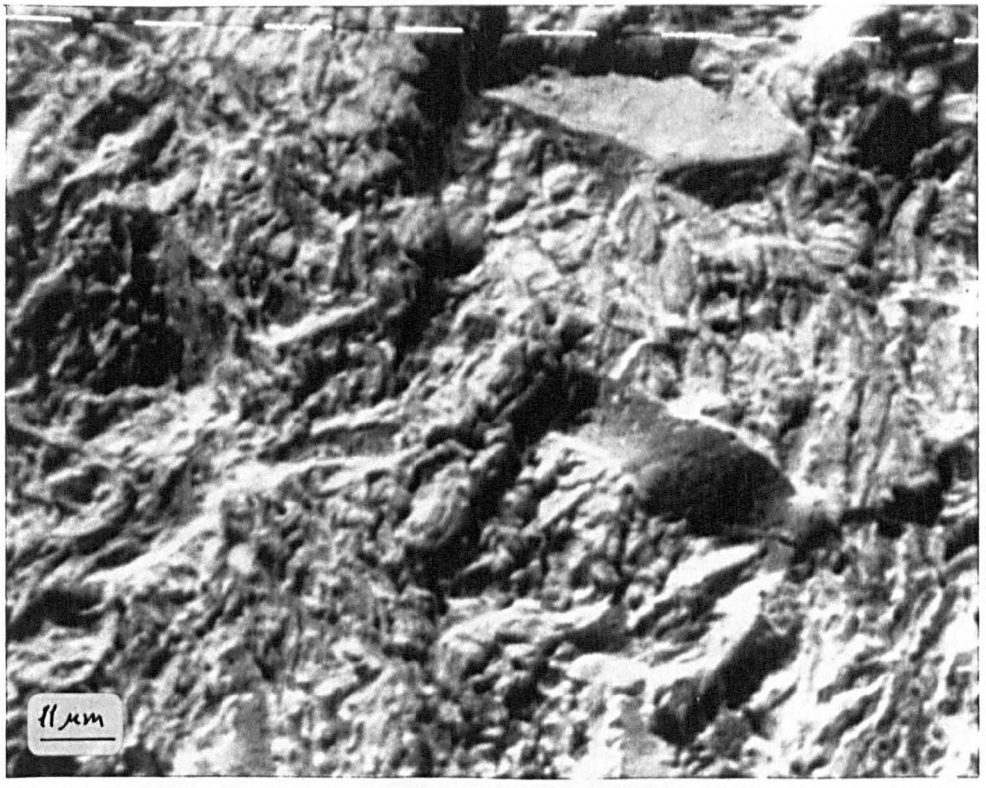

Fig.(5.10) Mode I test specimen at low stress intensity factor.

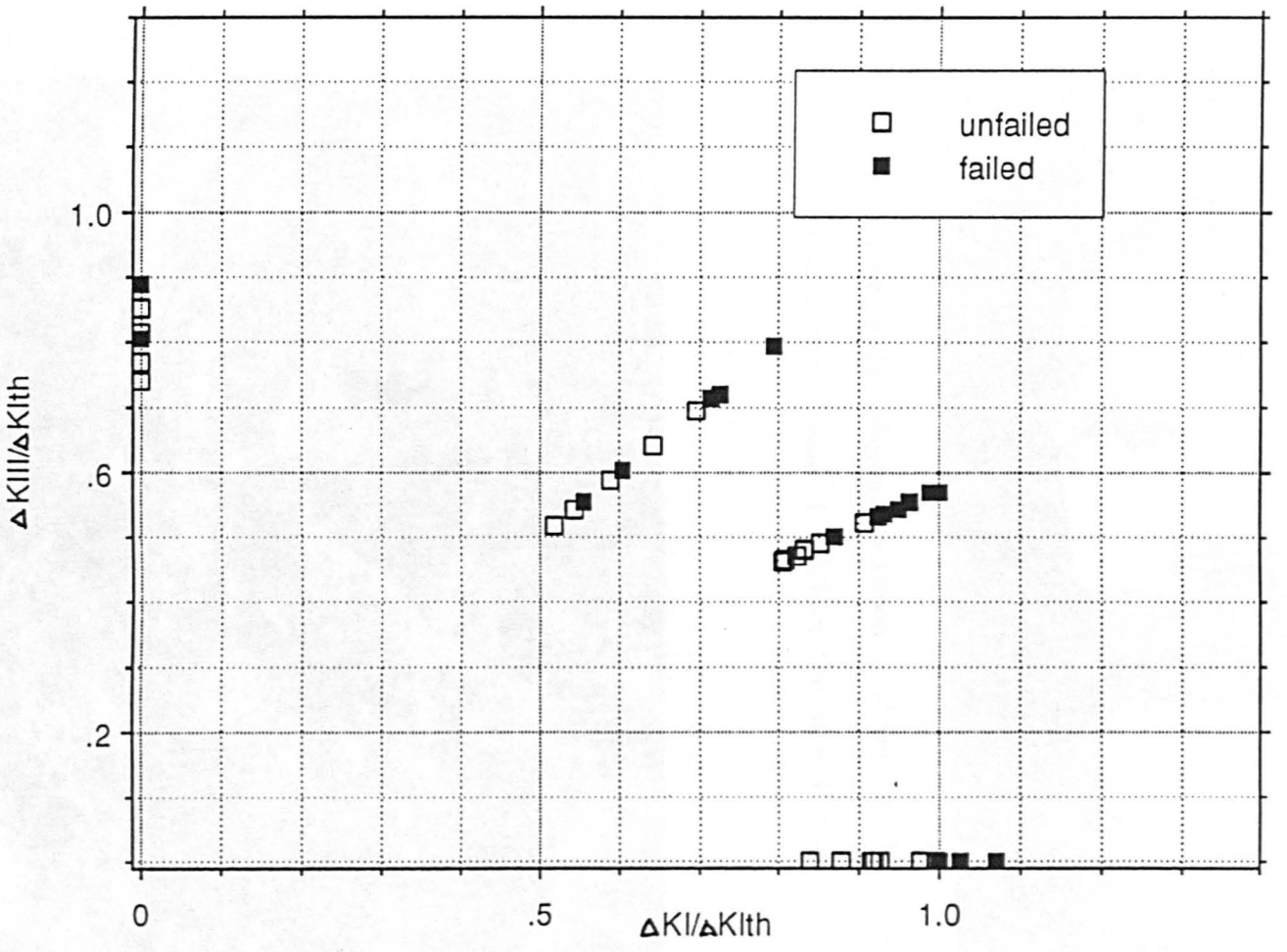

Fig.(5.11) Mixed mode I & III tests results for different R ratios and different slit angles.

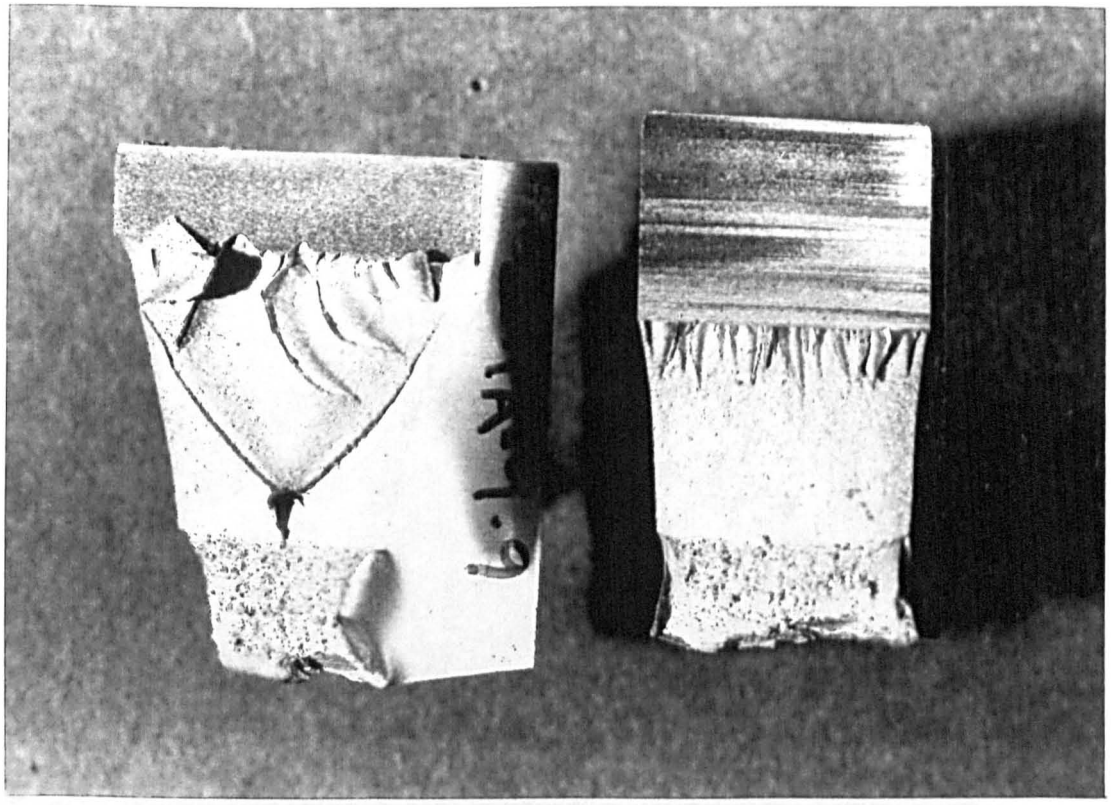

Fig.(5.12) Photograph showing the difference between a 45^o and 60^o slit angles fracture surface in mixed mode I & III for the same R ratio.

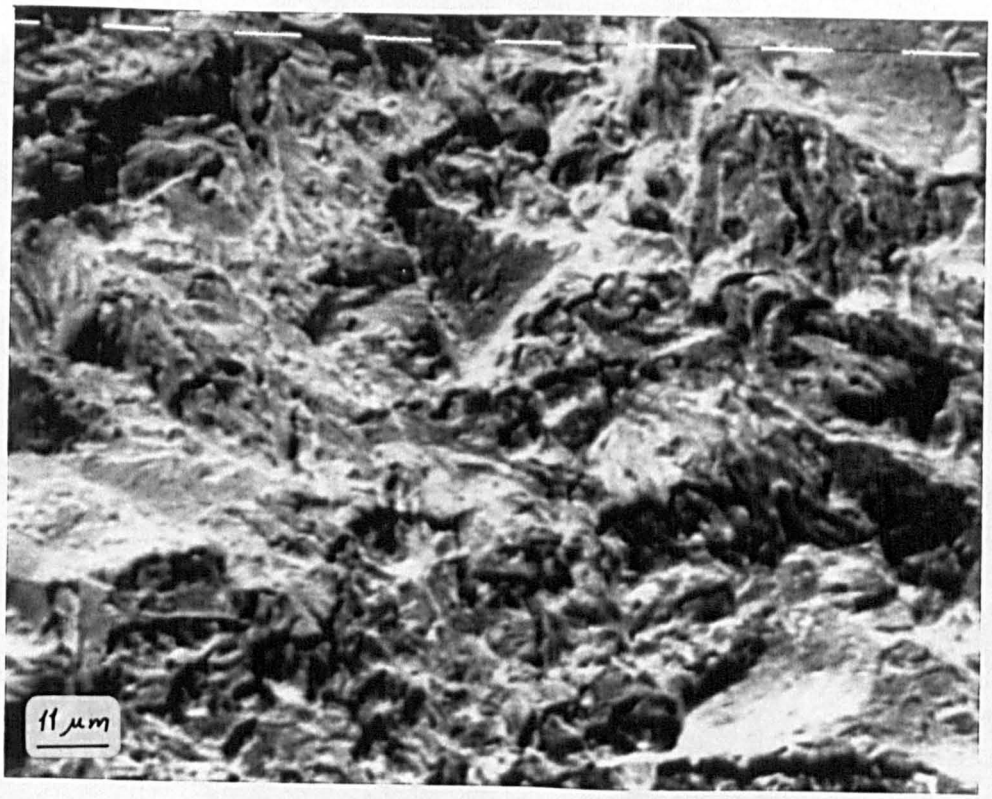

Fig.(5.13) Mixed mode I & III fatigue crack in a 45^o slit specimen for R = 0.5.

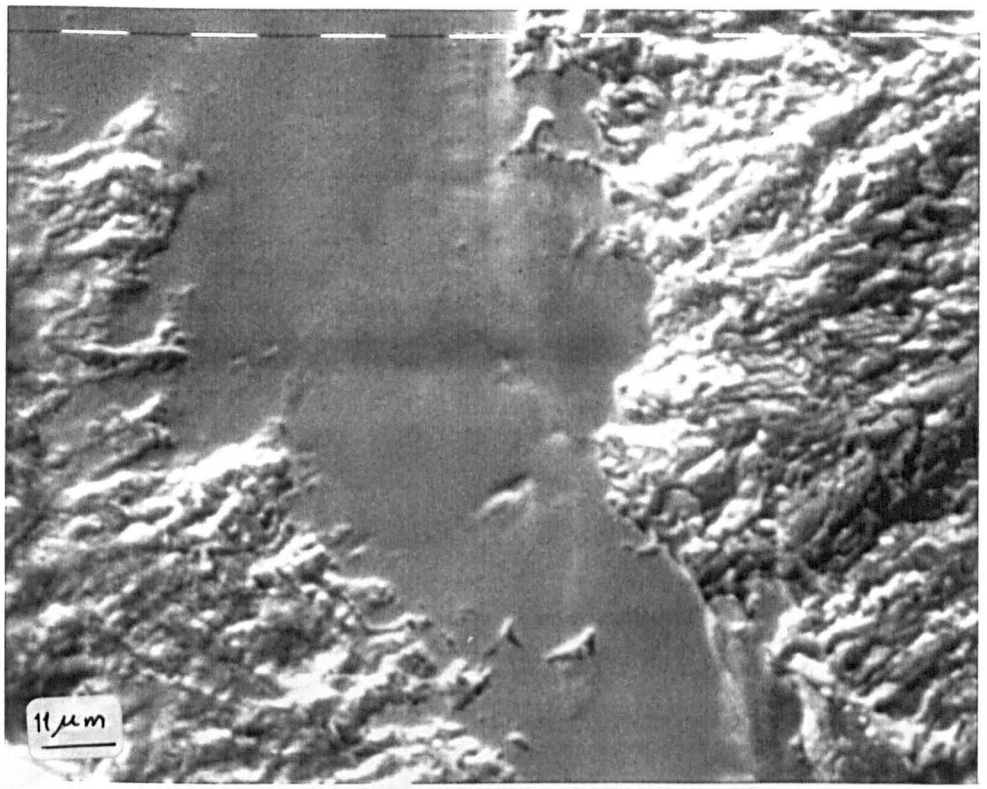

Fig.(5.14) The effect of rubbing due to mode III in mixed mode I & III is shown on top of what used to be a mode I facet.

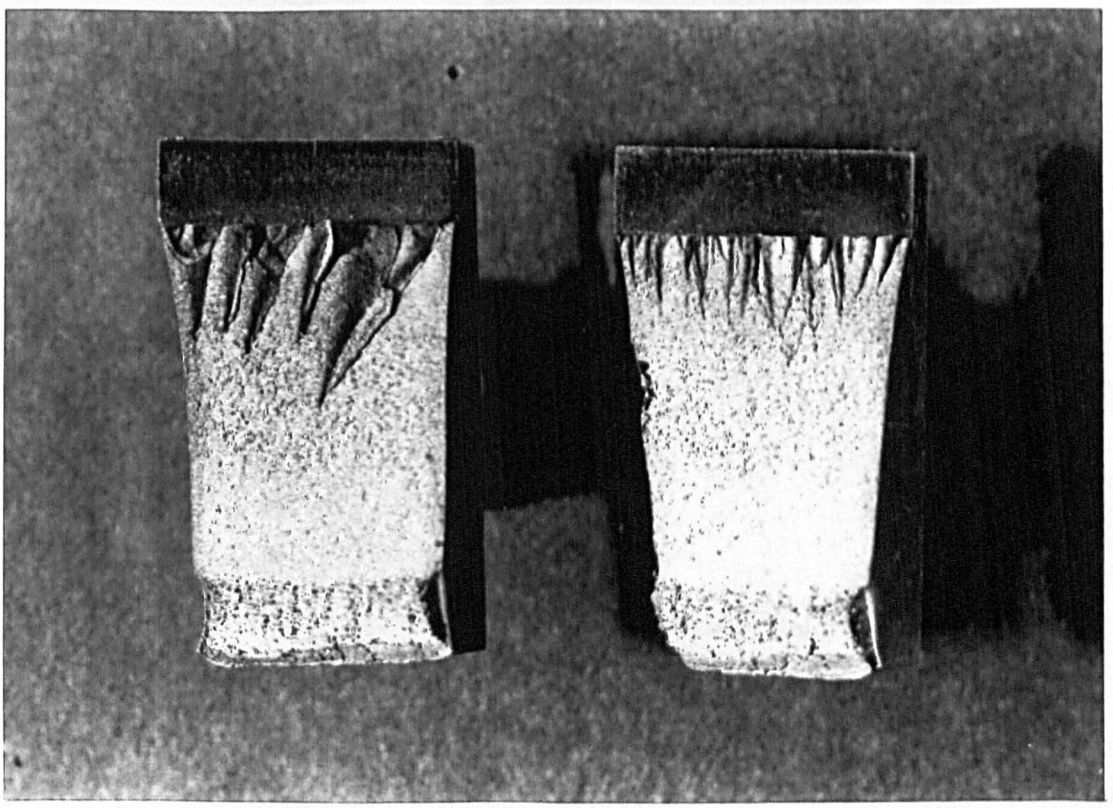

Fig.(5.15) Cross-sections of two mixed mode I & III fatigue specimens with the same slit angle (60^{o}) but different stress intensity factors.

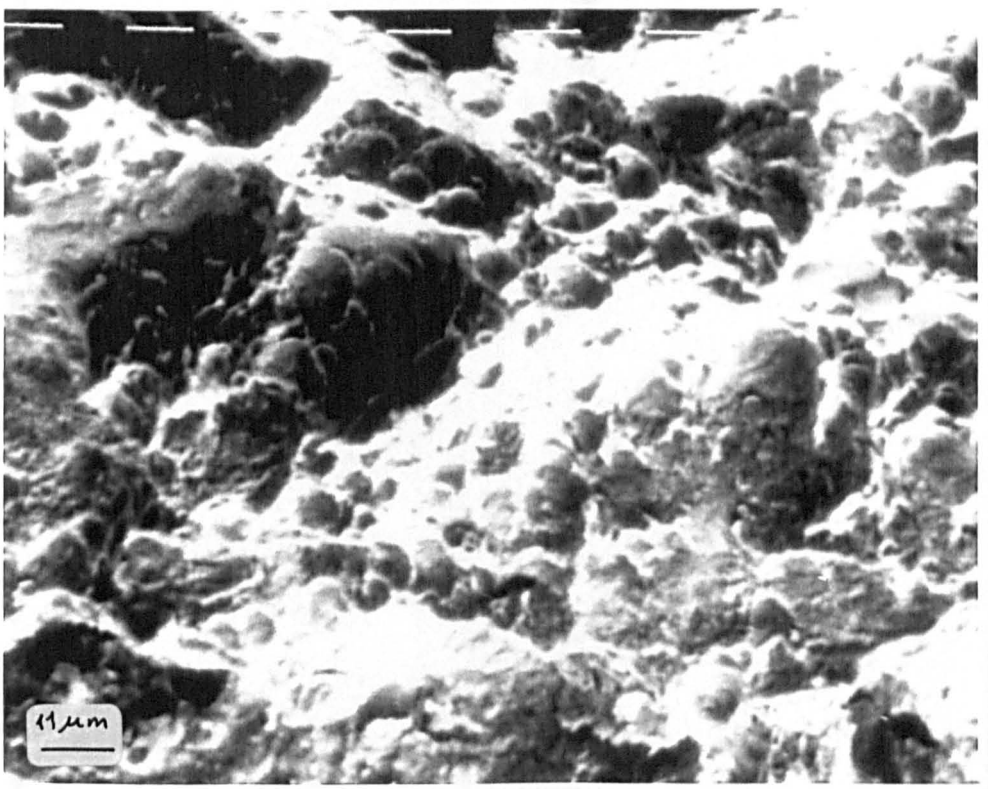

Fig.(5.16) The appearance of voids or dimples due to plastic deformation just before the breakage of the specimen.

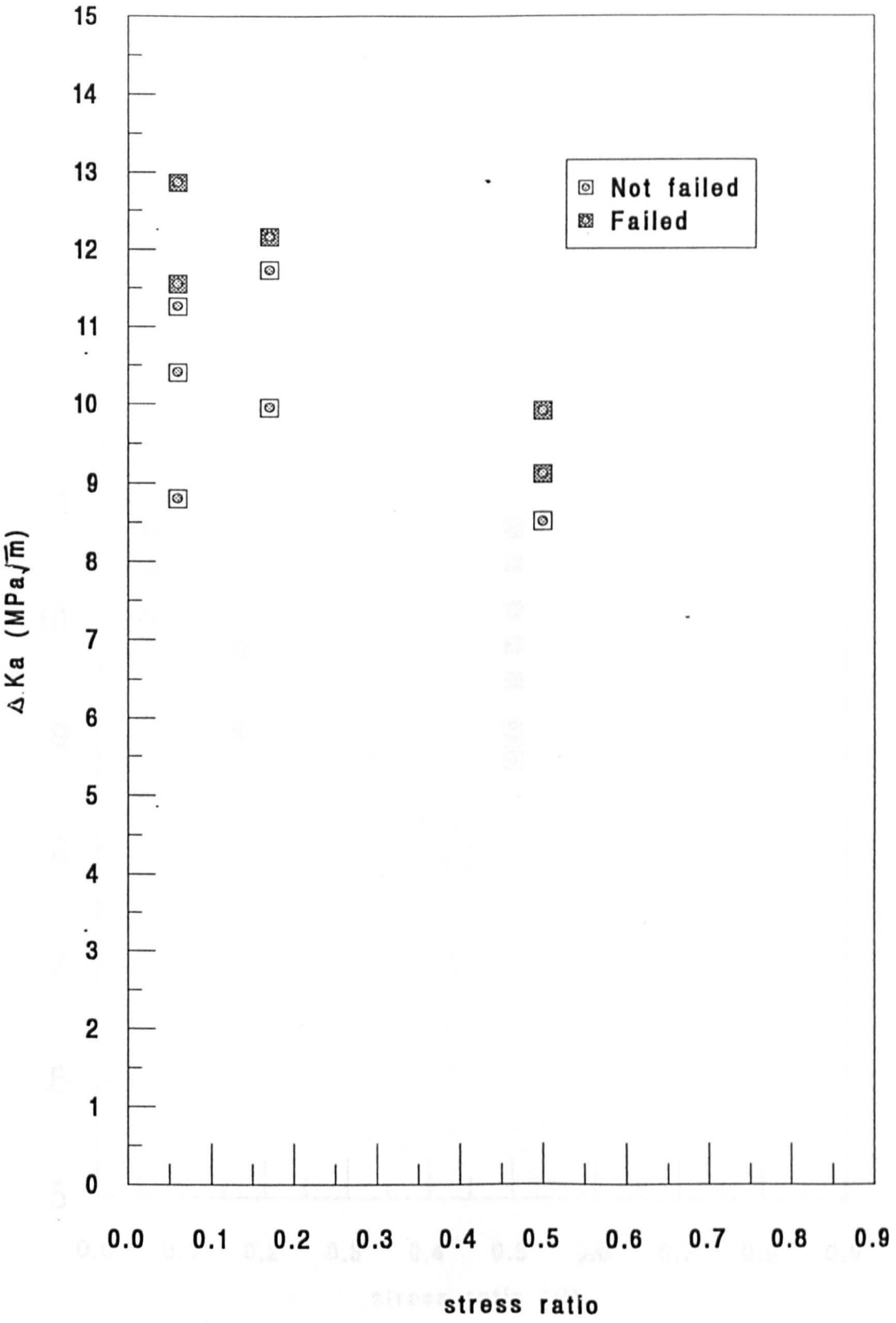

Fig.(5.17) Effect of stress ratio on fatigue threshold behaviour in mixed mode (I & III) tests with 45° slit angle specimens.

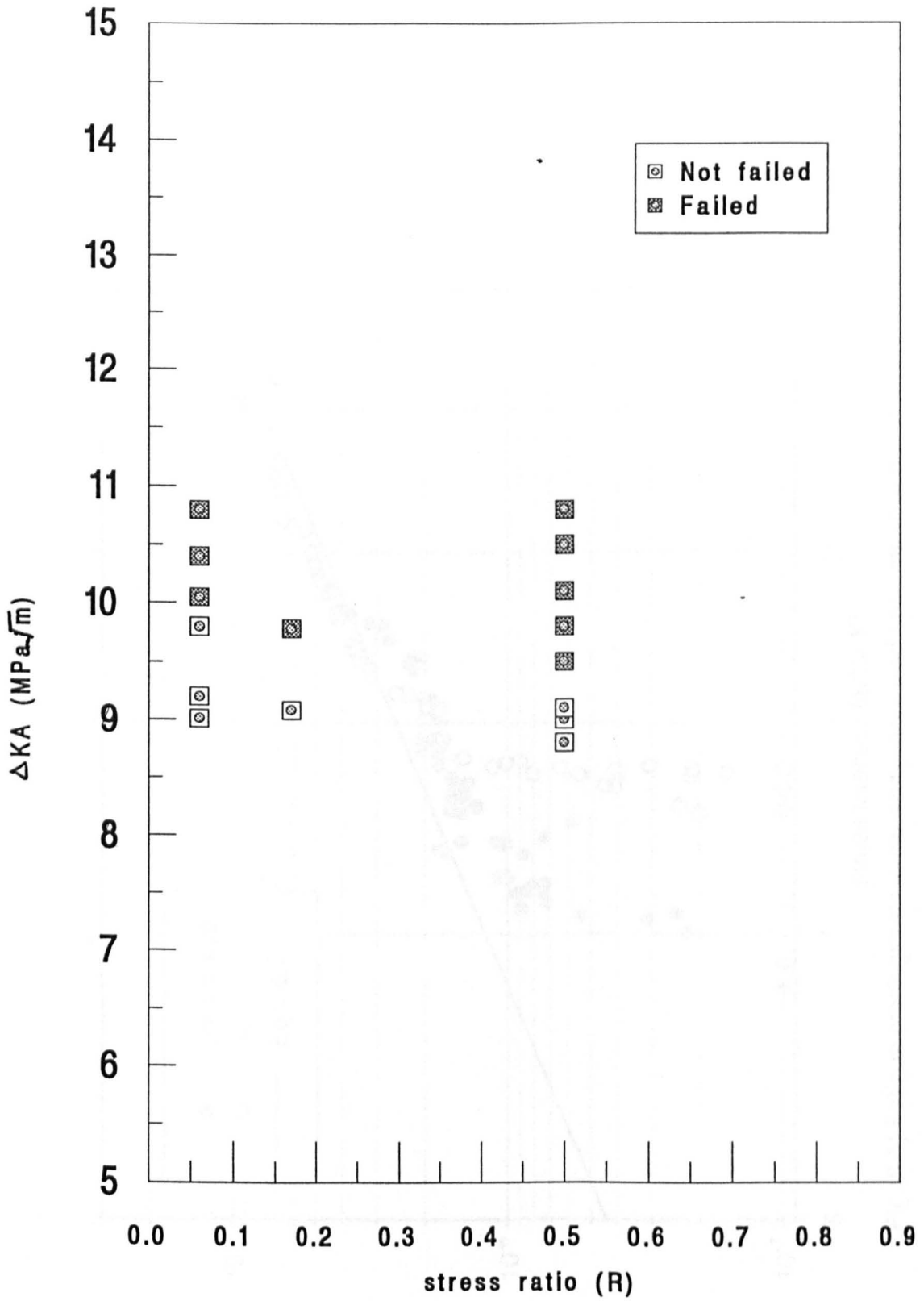

Fig.(5.18) Stress ratio effect on fatigue threshold behaviour in mixed mode I & III with slit angle 60 deg.

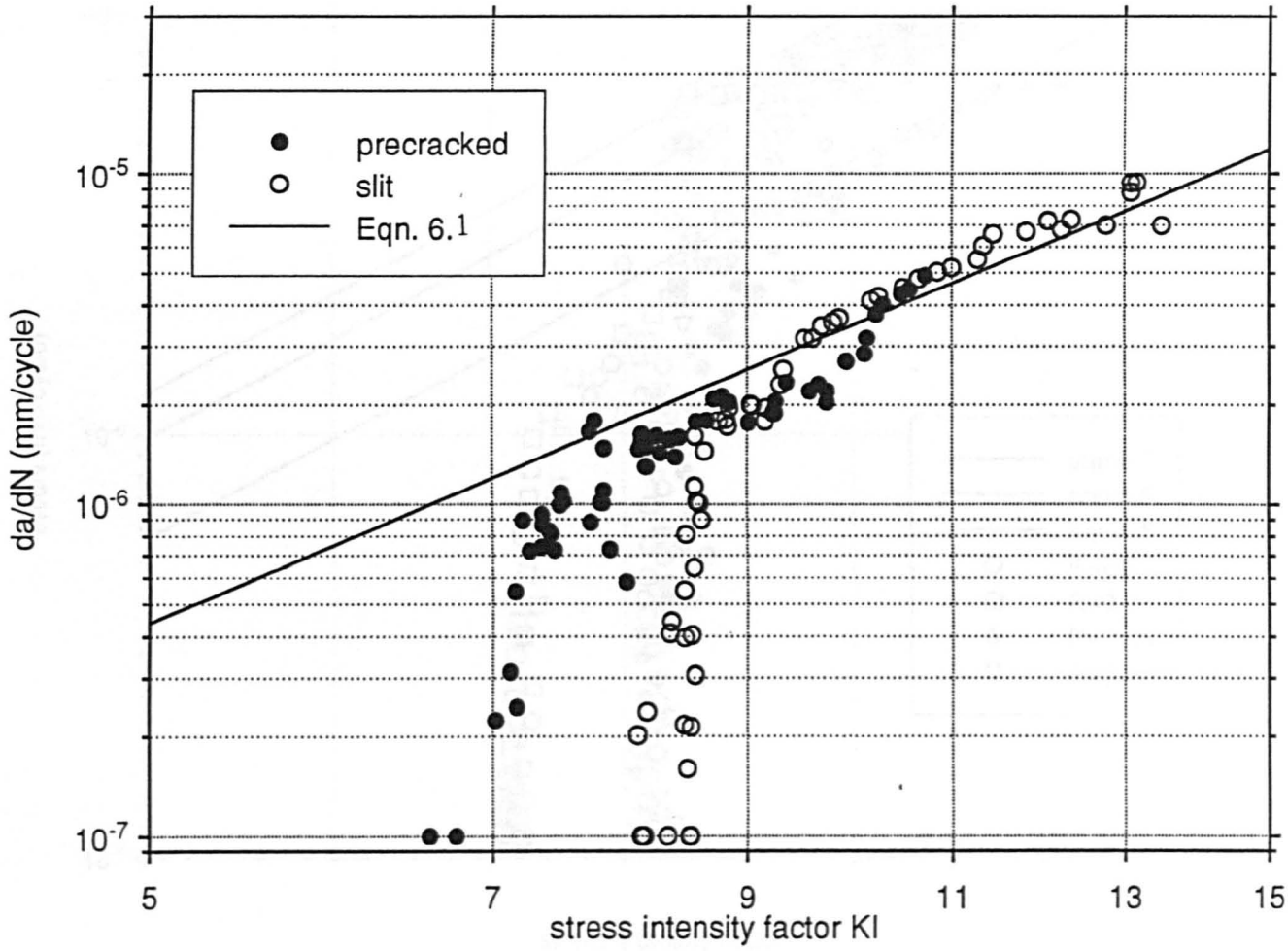

Fig.(6.1) Fatigue crack growth in slit and precracked specimens in mode I tests.

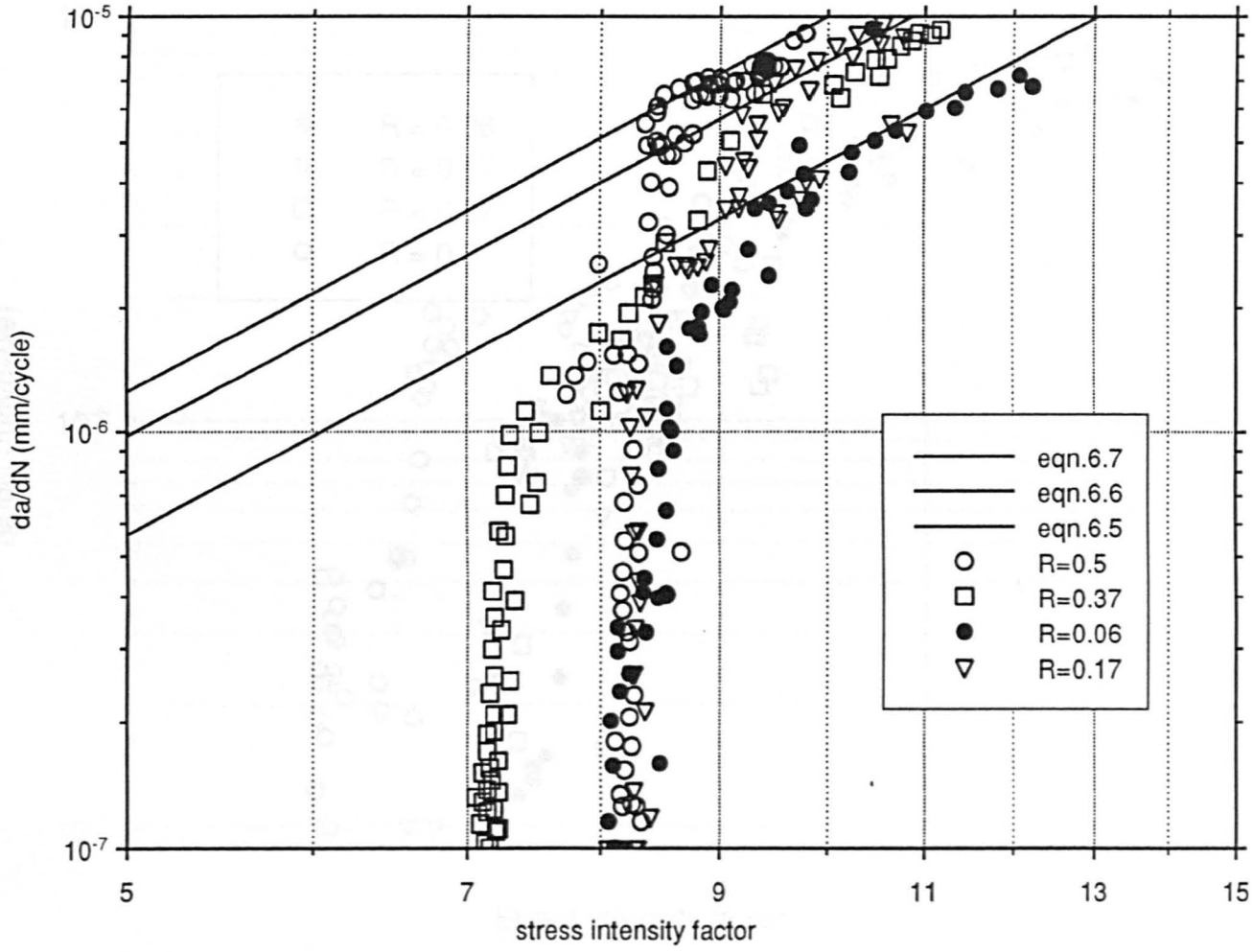

Fig.6.2 Fatigue crack growth in slit specimens at different R ratios in Mode I tests.

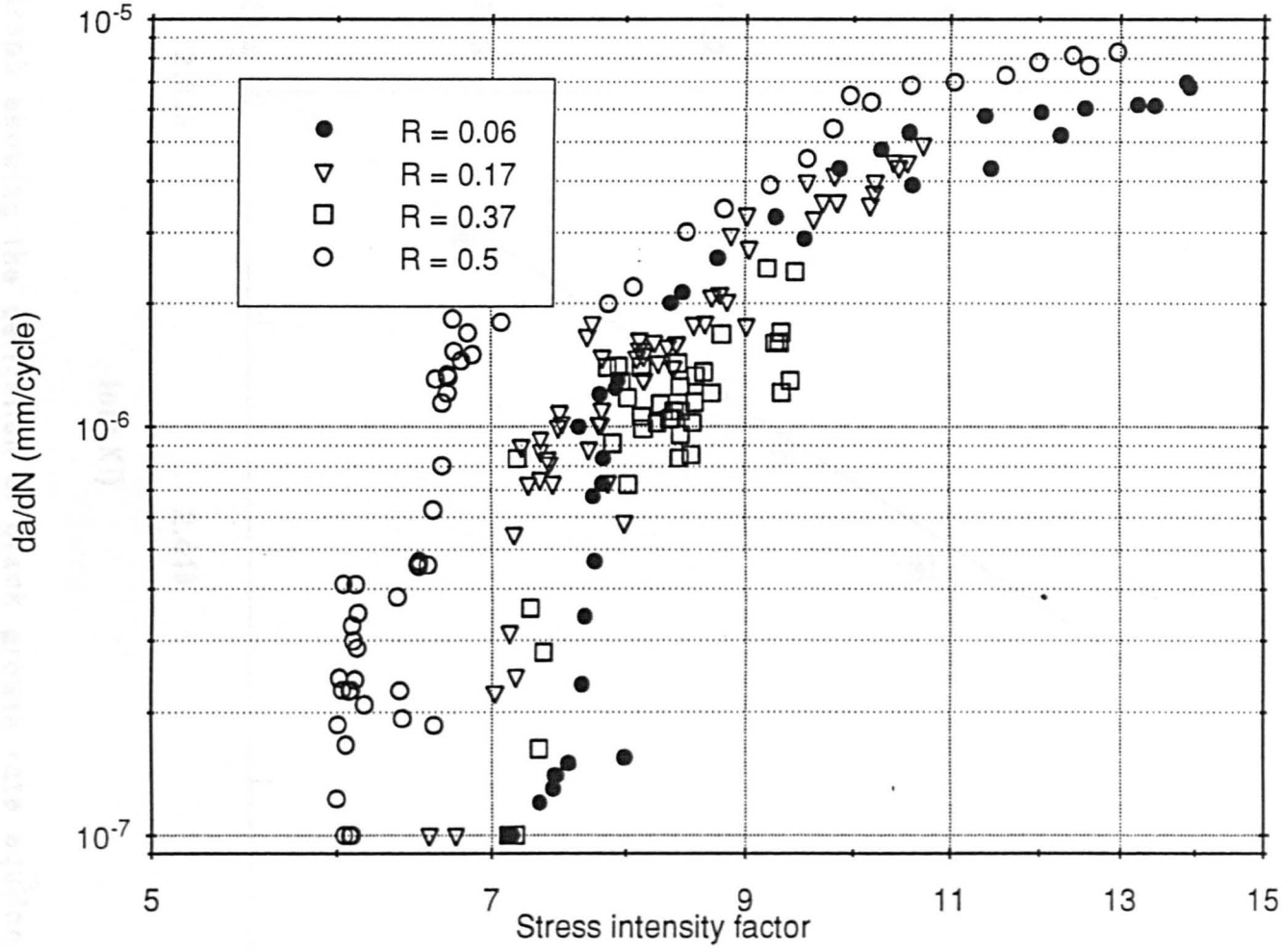

Fig.(6.3) Crack growth rates in fatigue precracked specimens in mode I tests at different R ratios.

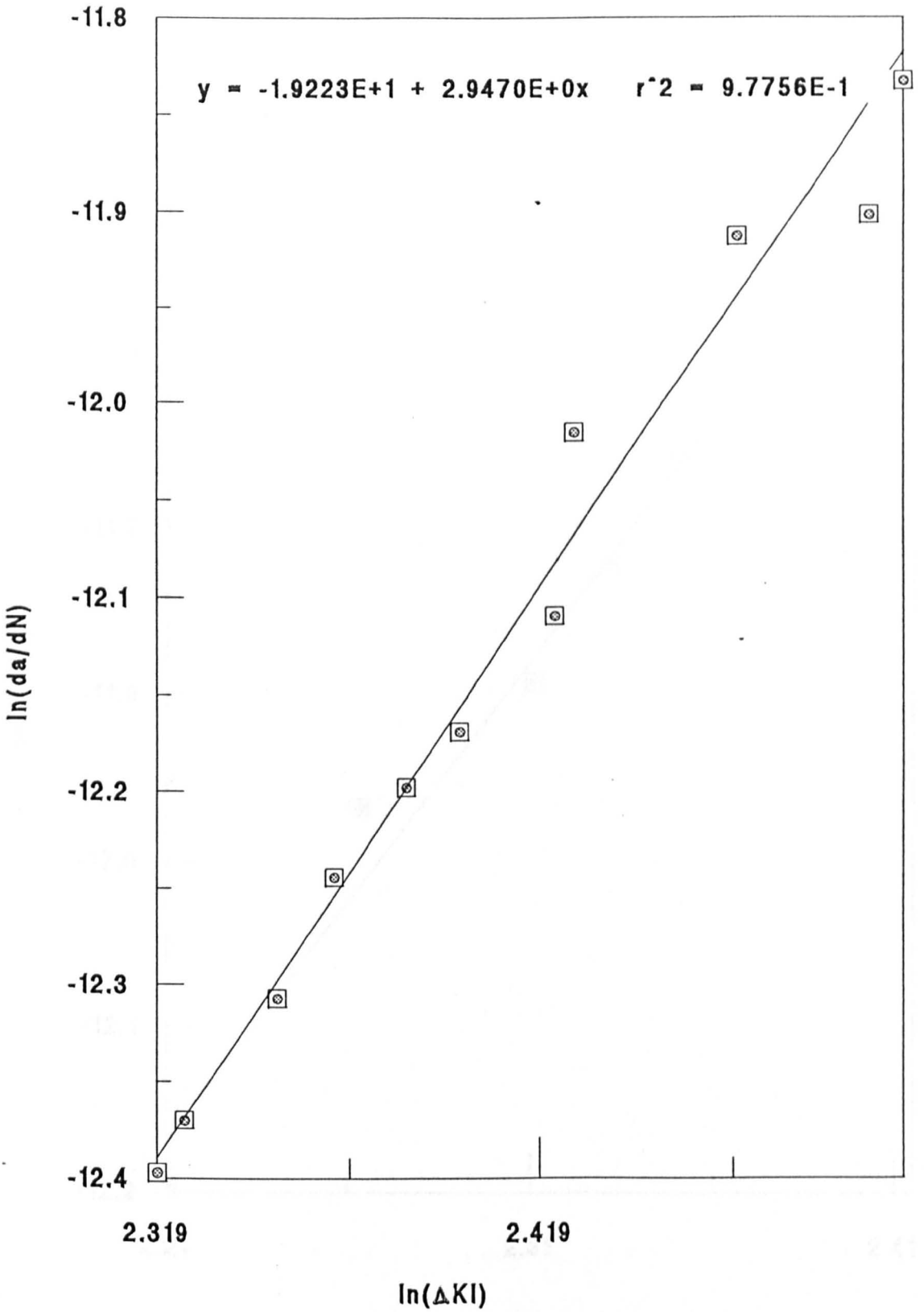

Fig.(6.4)Graph showing the derivation of crack growth rate equation for mode I loading when R = 0.06.

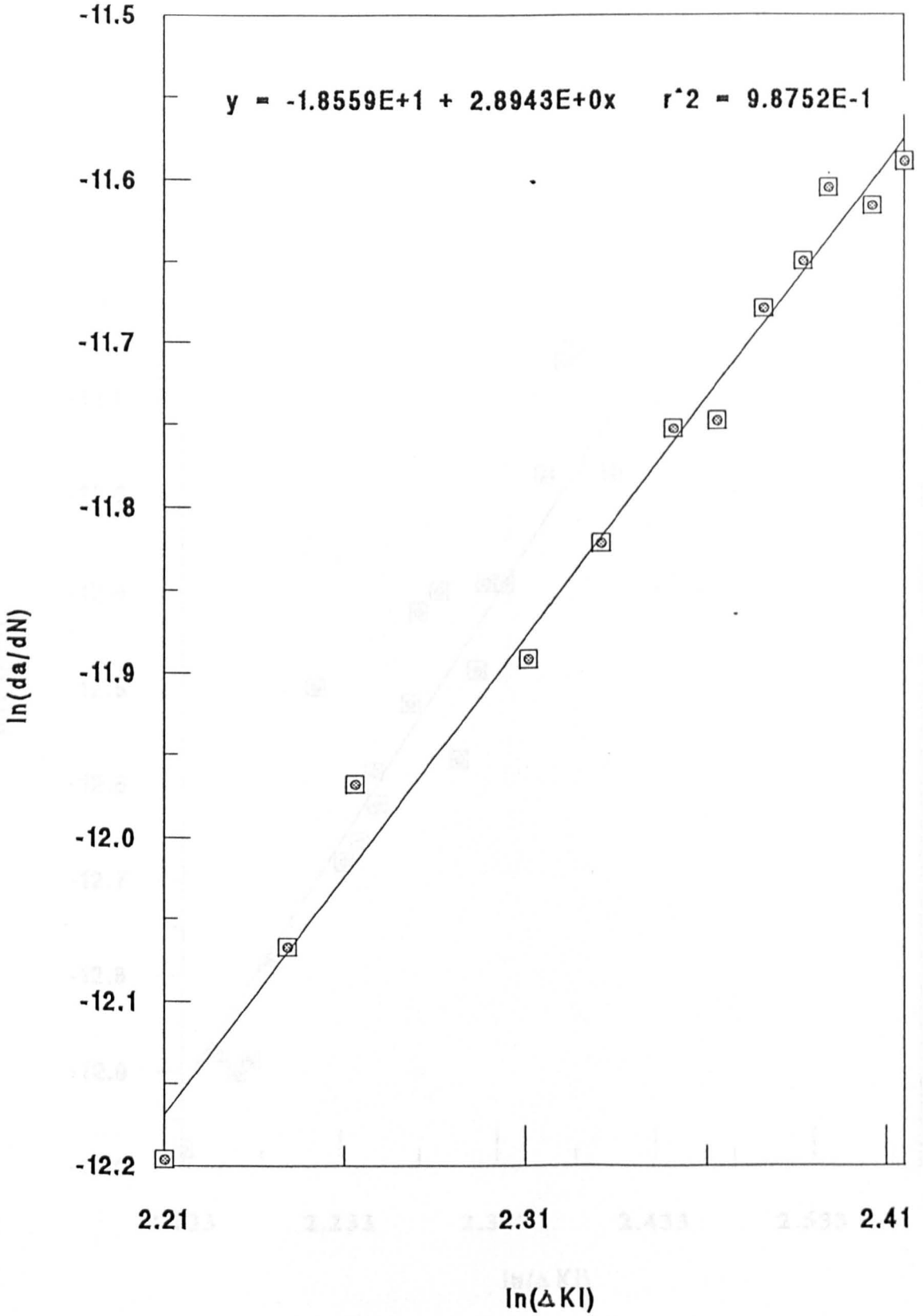

Fig.(6.5) Graph showing the derivation of mode I crack growth rate equation for R = 0.17.

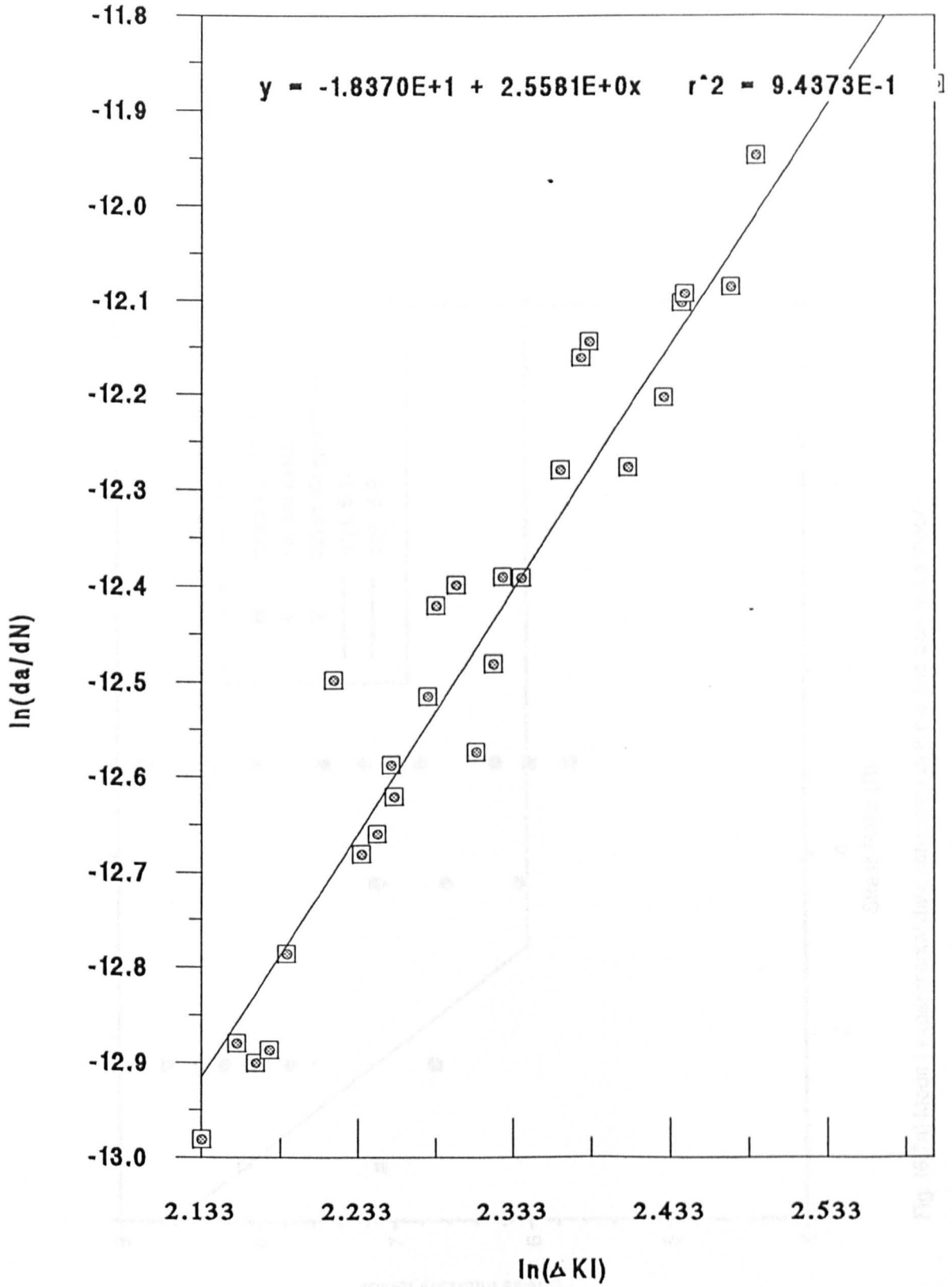

Fig.(6. 6)Graph showing the derivation of crack growth rate equation for mode I loading when R = 0.5.

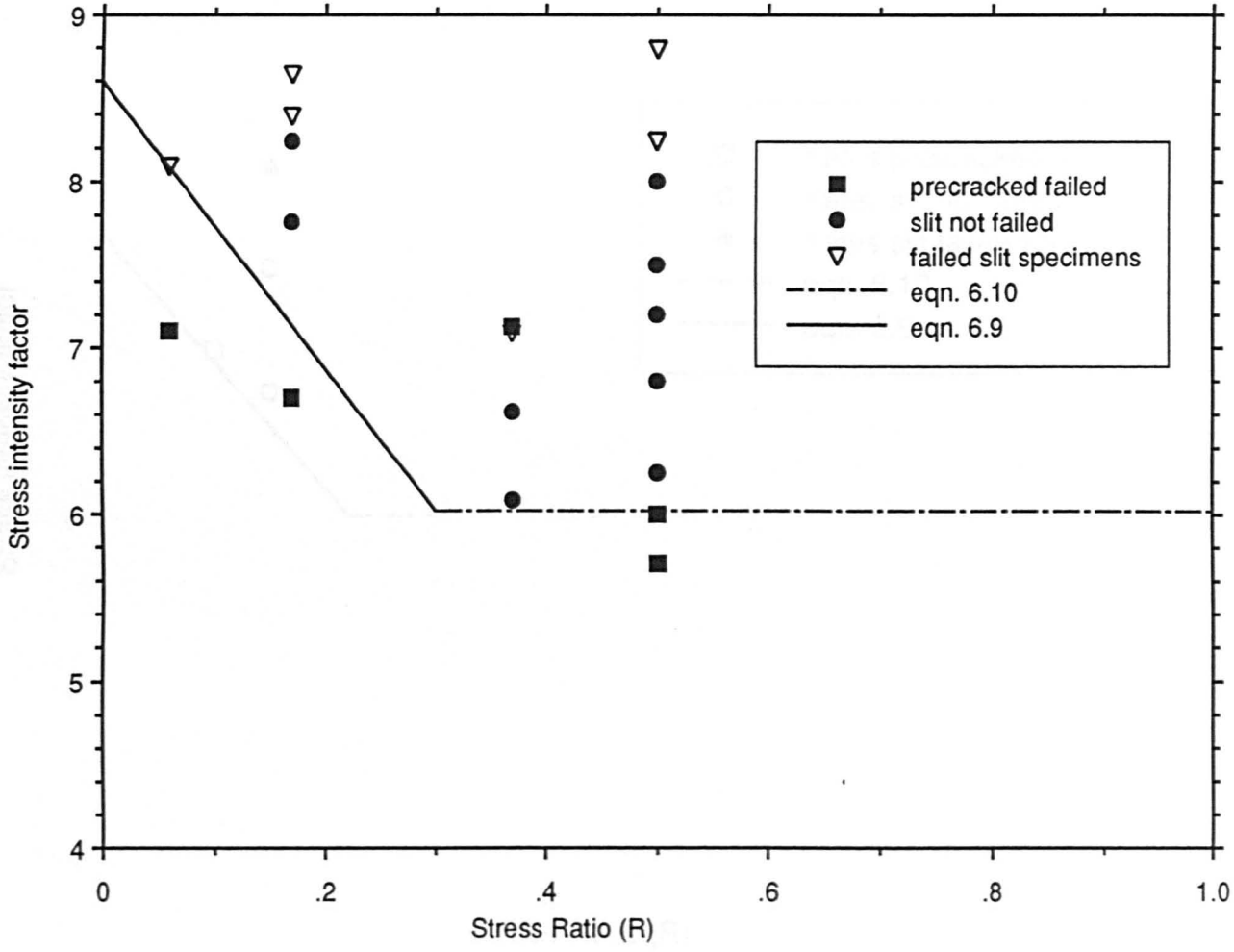

Fig. (6.7a) Mode I experimental data compared to Paris and Schmidt's theory.

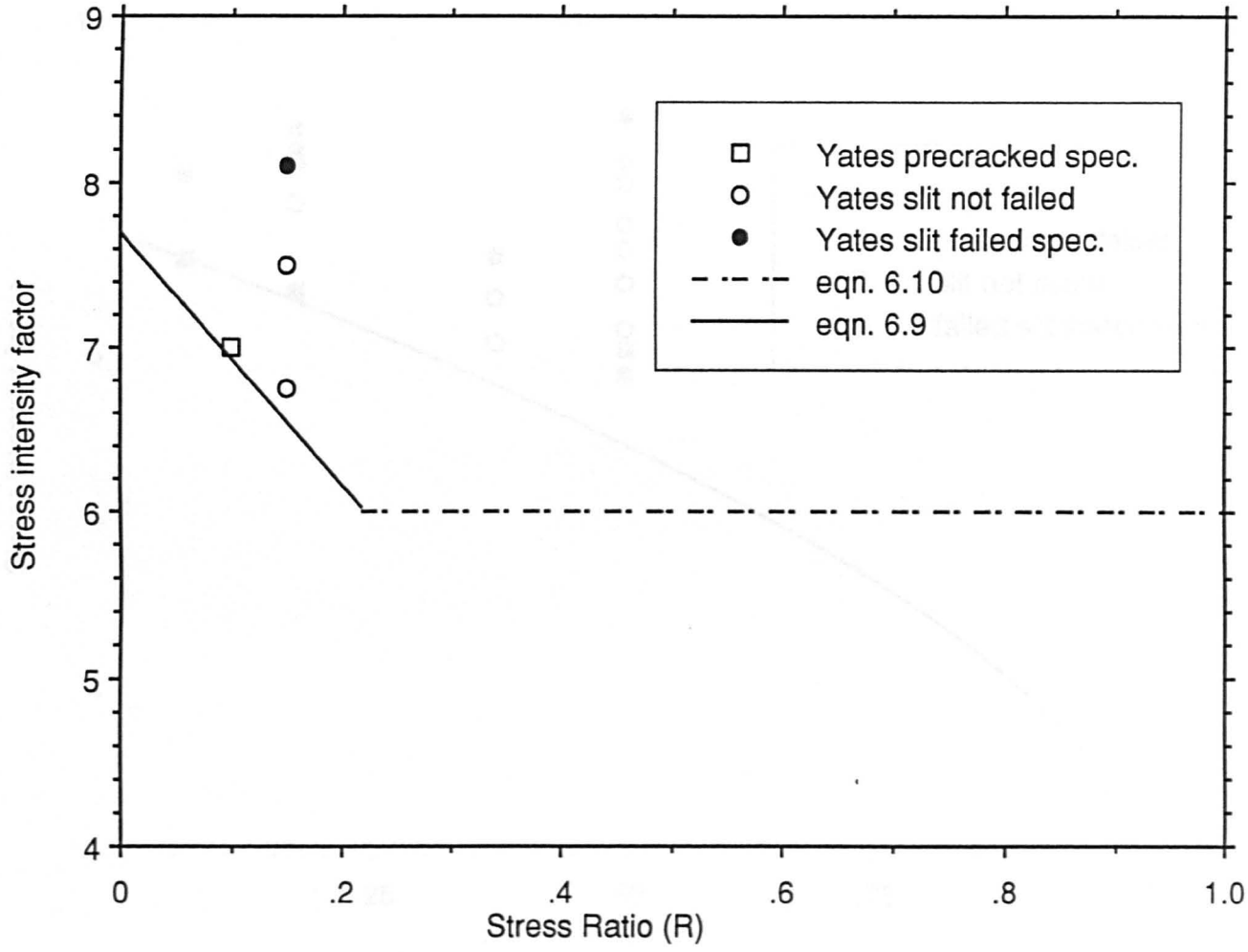

Fig. (6.7b) Yates & Miller experimental Mode I results compared to Paris and Schmidt's theory.

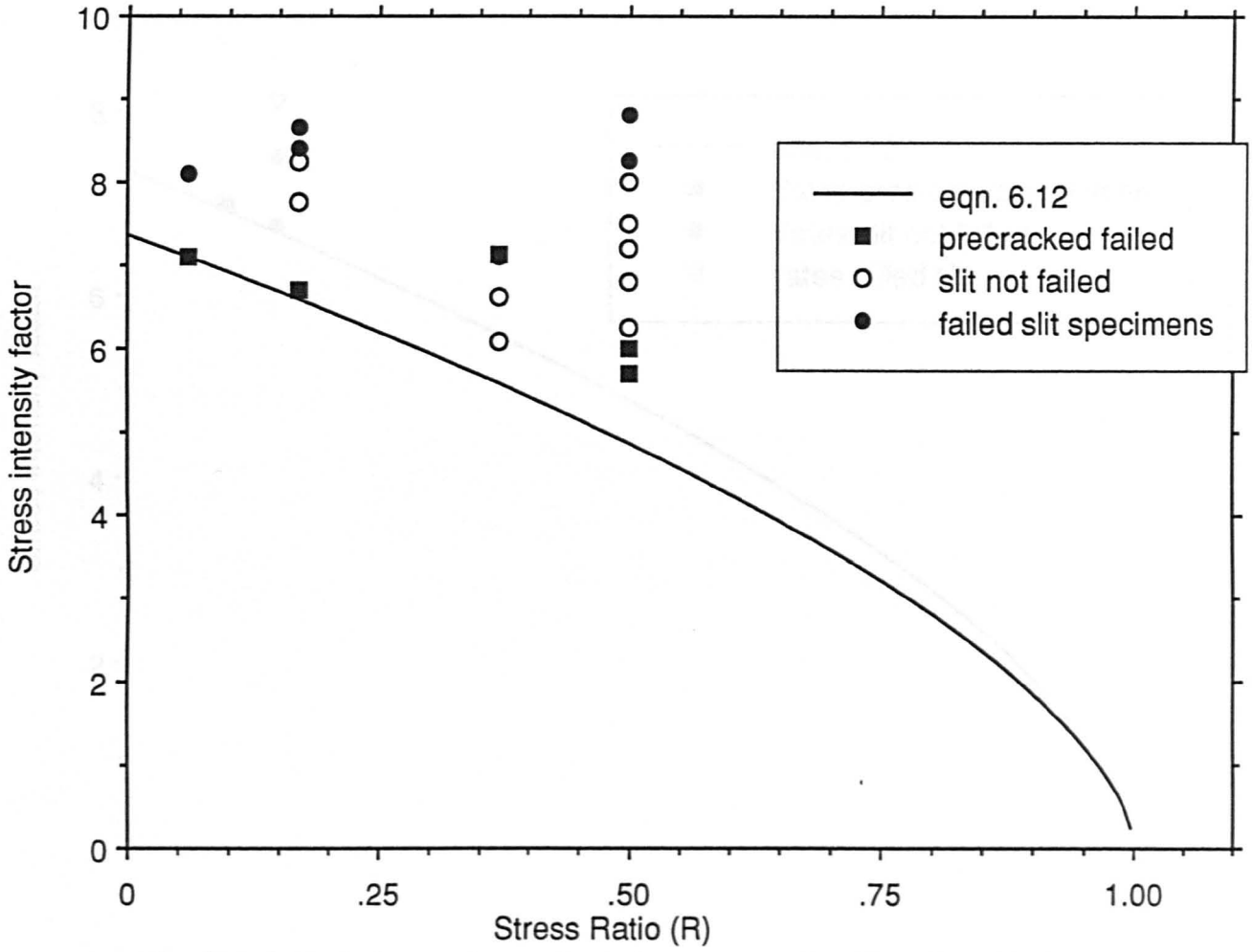

Fig. (6.8a) Mode I experimental results compared to Klensil and Lukas failure prediction theory.

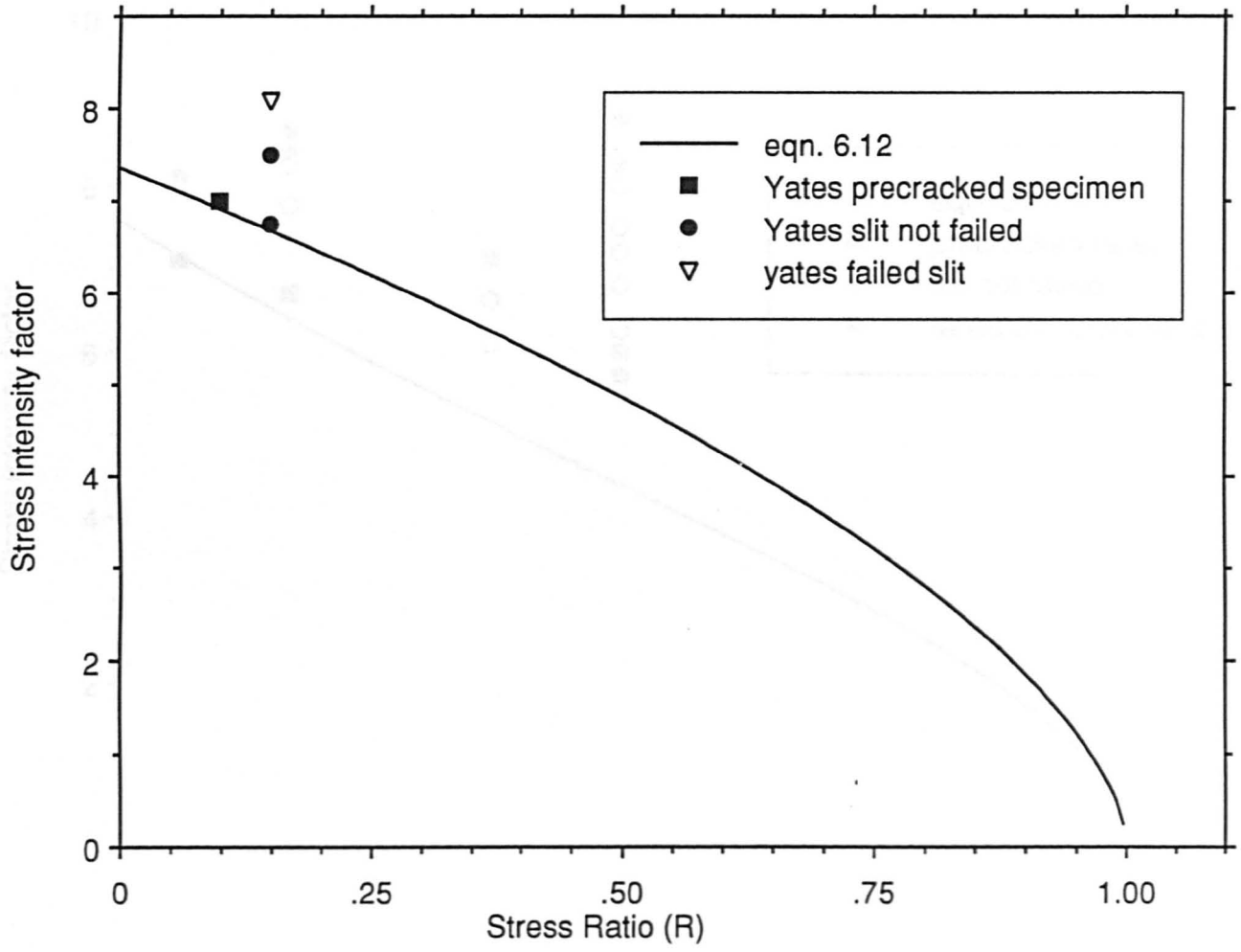

Fig. (6.8b) Yates and Miller experimental results compared to Klensil and Lukas failure prediction theory.

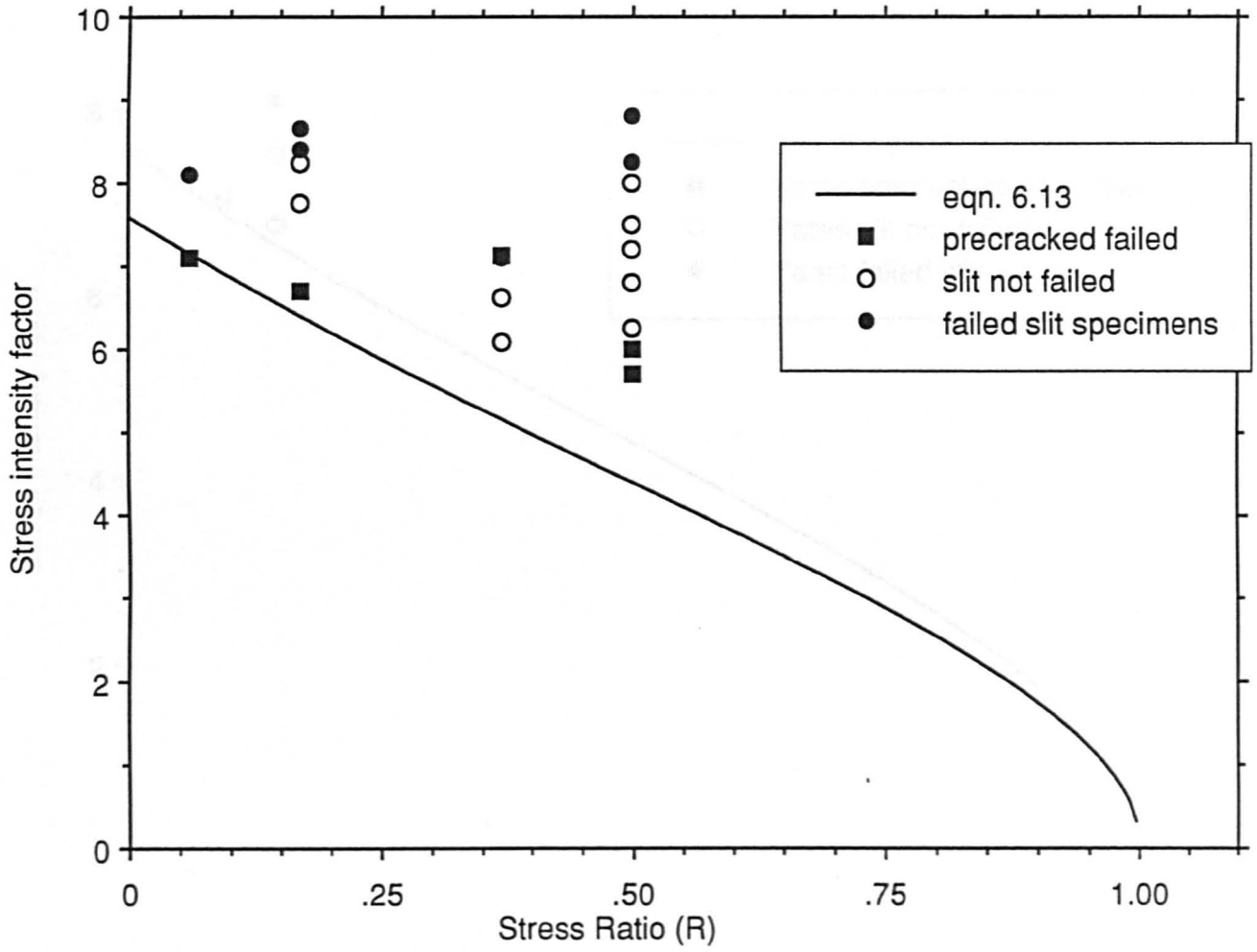

Fig. (6.9A) Mode I experimental results compared to McEvilly and Gregor's failure prediction theory.

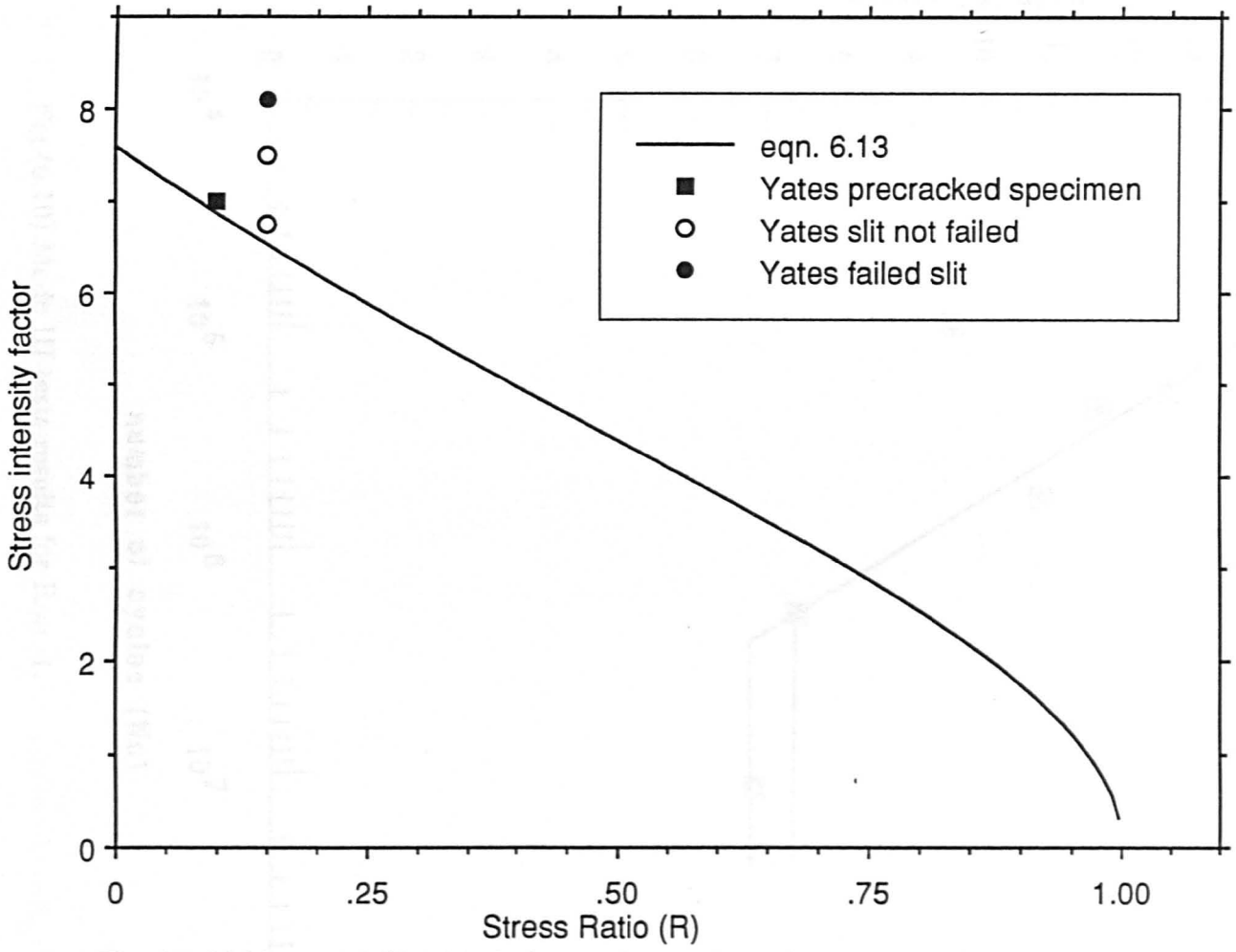

Fig. (6.9b) Yates & Miller Mode I experimental results compared to McEvily & Gregor's failure prediction theory.

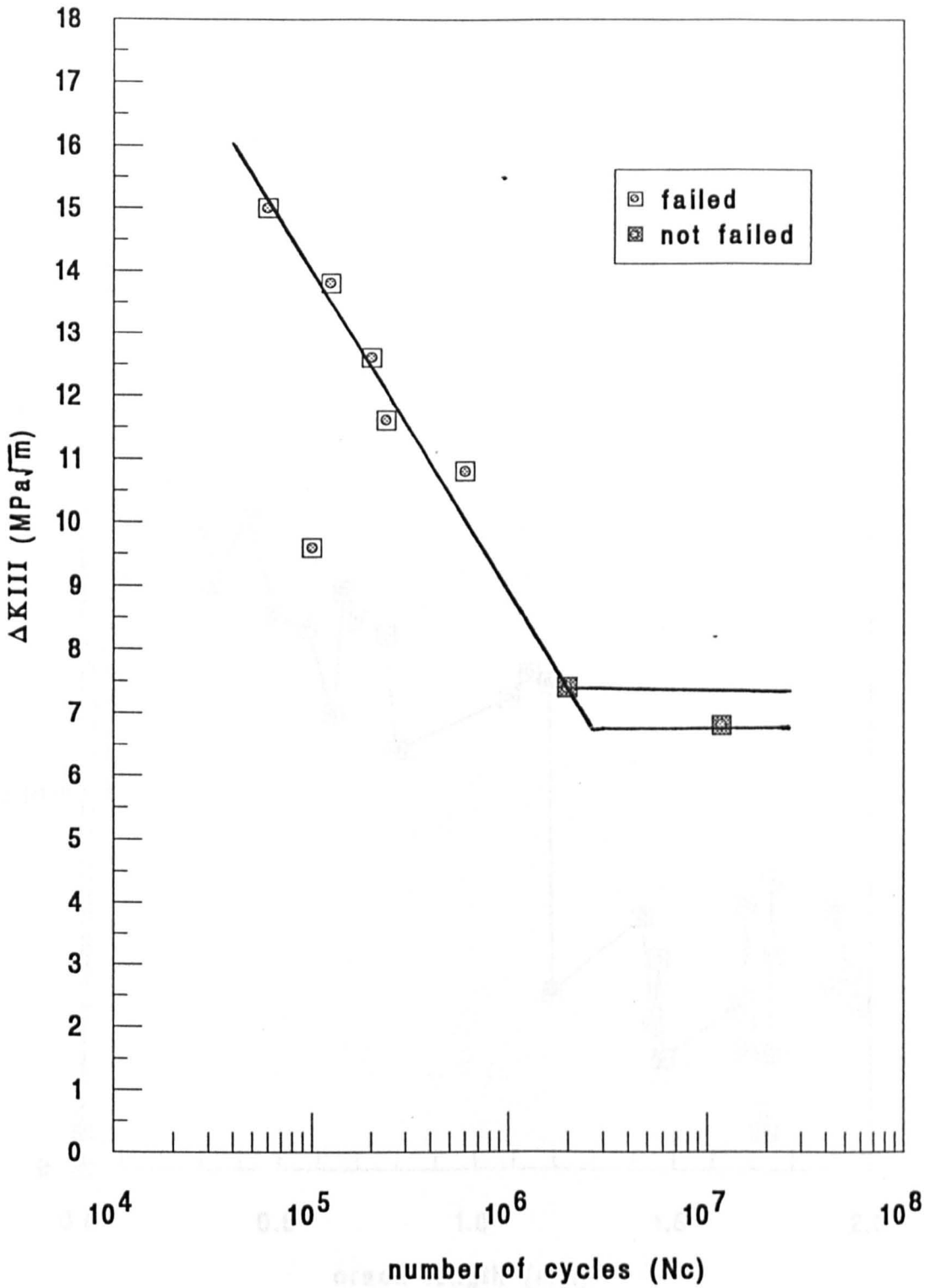

Fig.(6.10) Mode III tests results for R = -1.

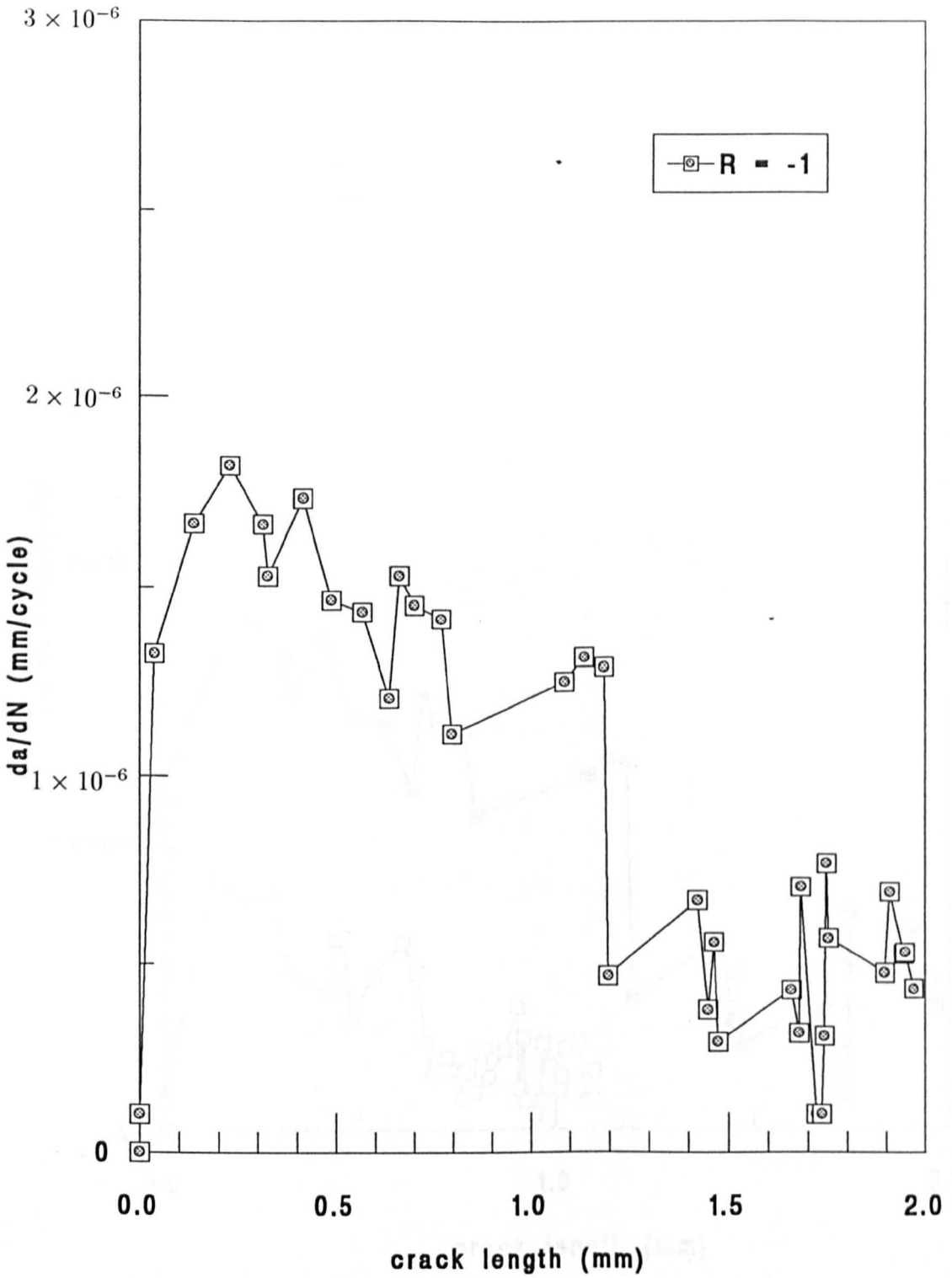

Fig.(6.11)Fluctuation in crack growth rates as the crack length increases in mode III tests for R = -1.

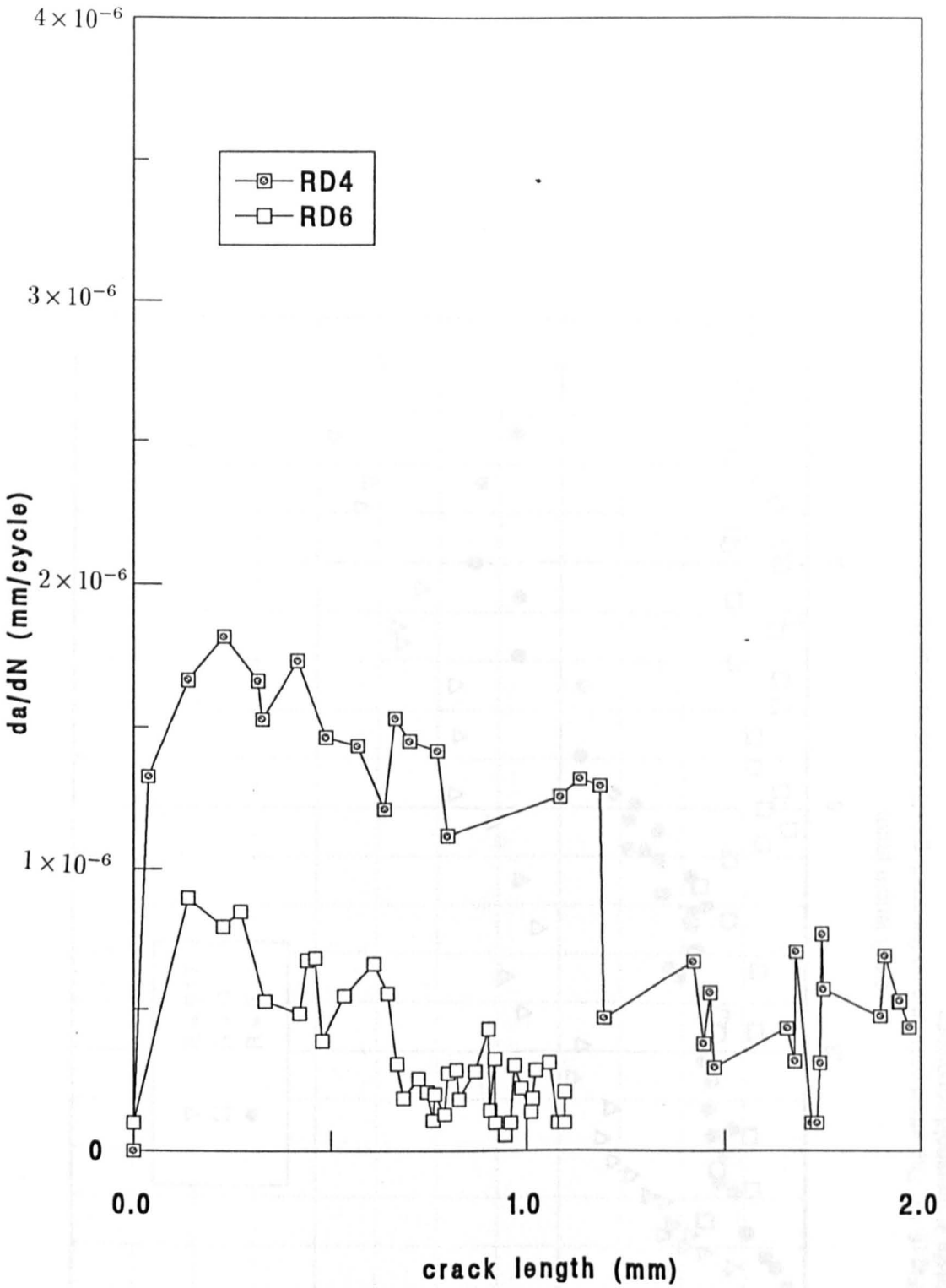

Fig.(6.12) The effect of the applied load on the crack growth rates in mode III tests for different stress intensity ranges. (RD4 = 11.6 $MPa\sqrt{m}$ and RD6 = 9.6 $MPa\sqrt{m}$, R ratio = -1 for both of the specimens.

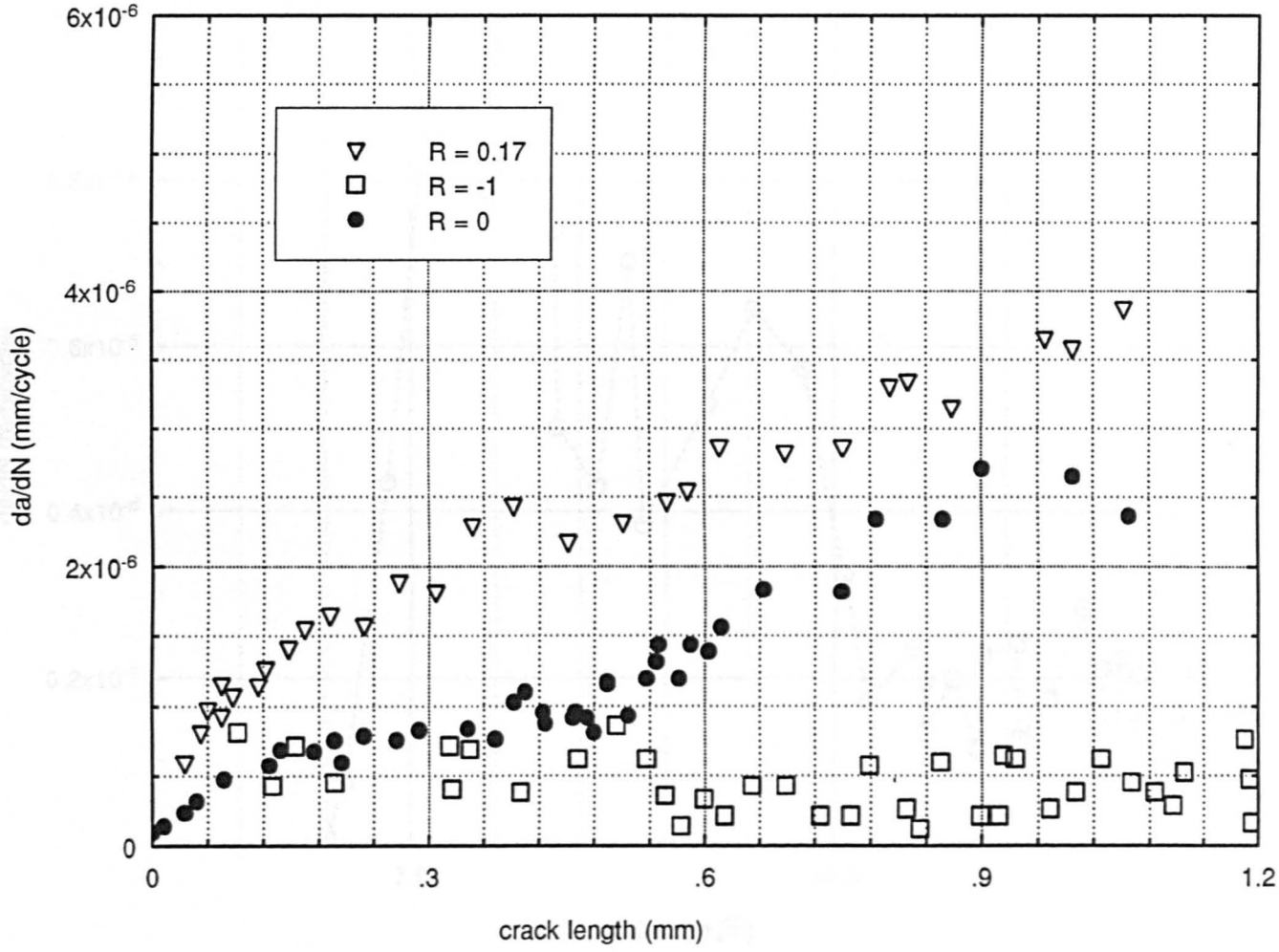

Fig.(6.13) The effect of R ratio on the crack growth rates in mode III tests at threshold conditions.

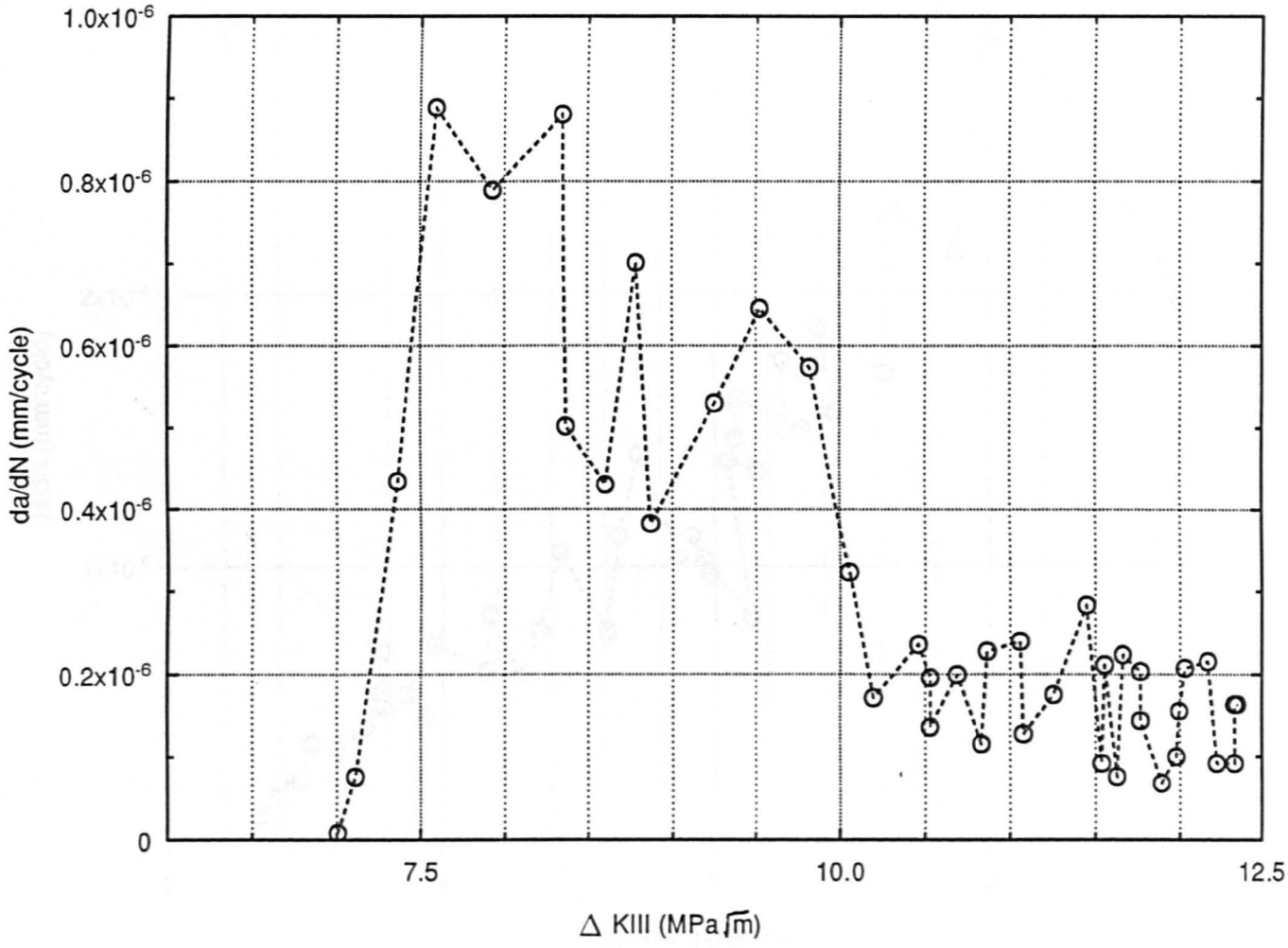

Fig.(6.14) Changes in crack growth rate in mode III test at R = -1.

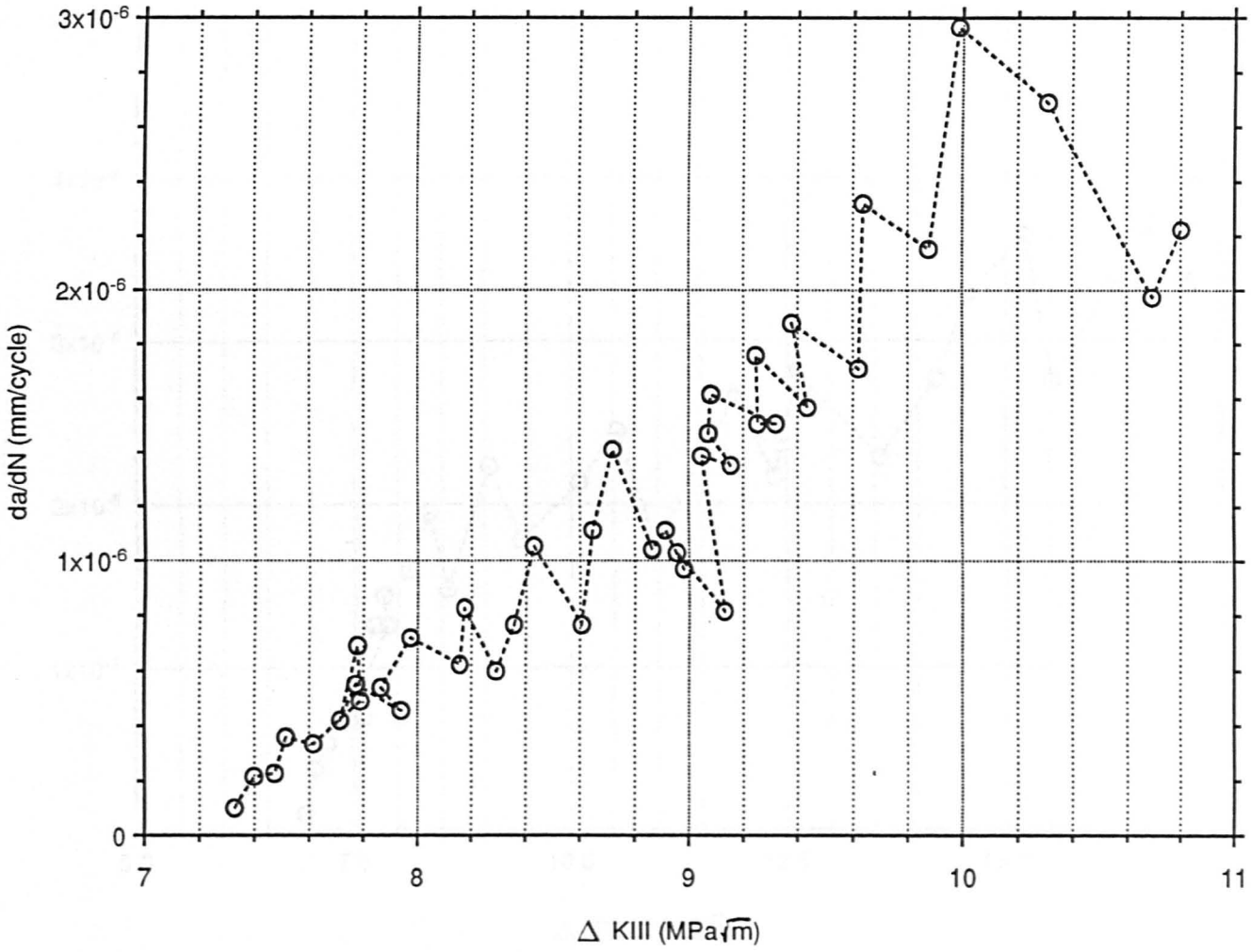

Fig.(6.15) The crack growth increasing rates as the stress intensity factor increases in a mode III test for R = 0.

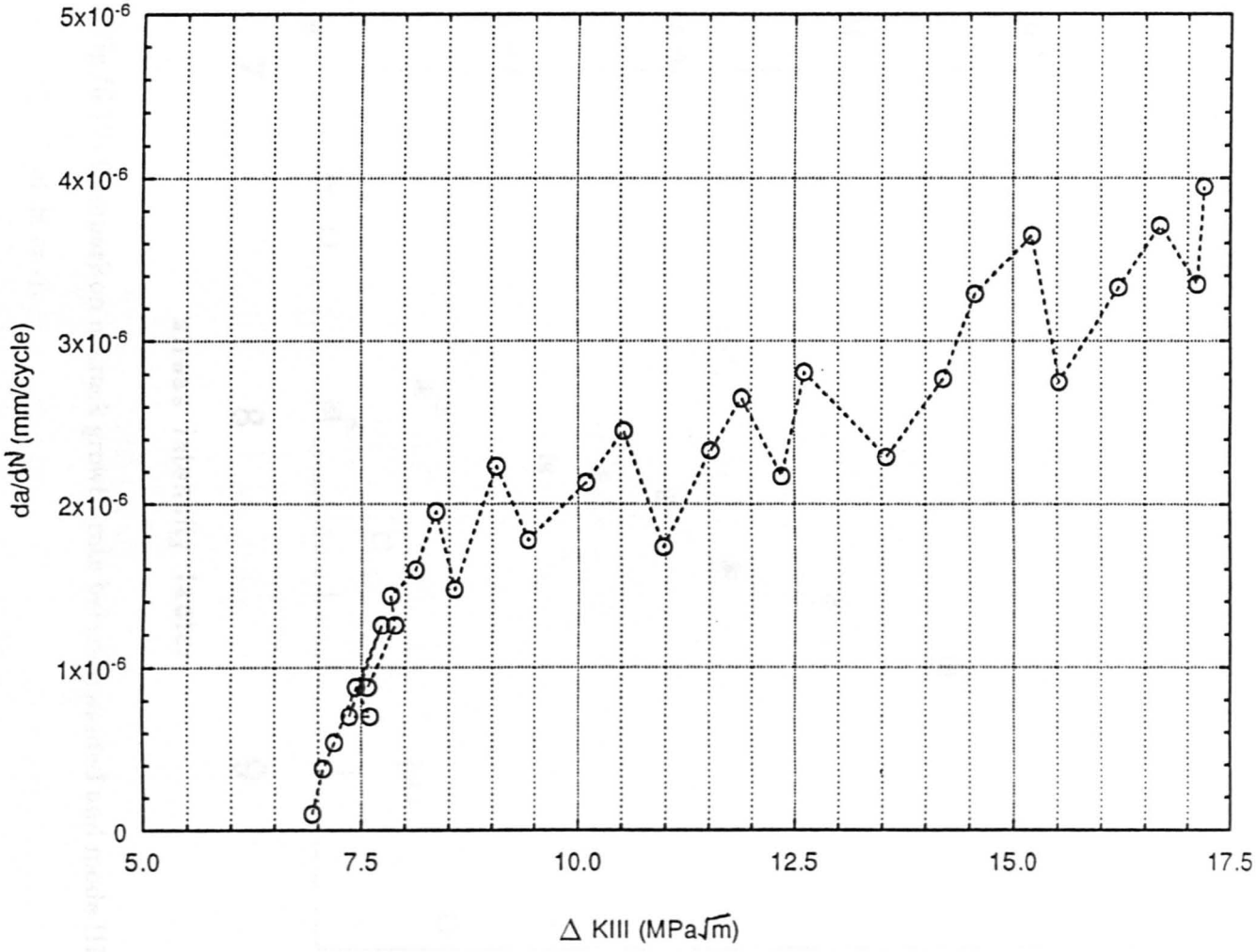

Fig.(6.16) Crack growth rates and its fluctuation as the stress intensity factor increases in mode III tests for R = 0.17.

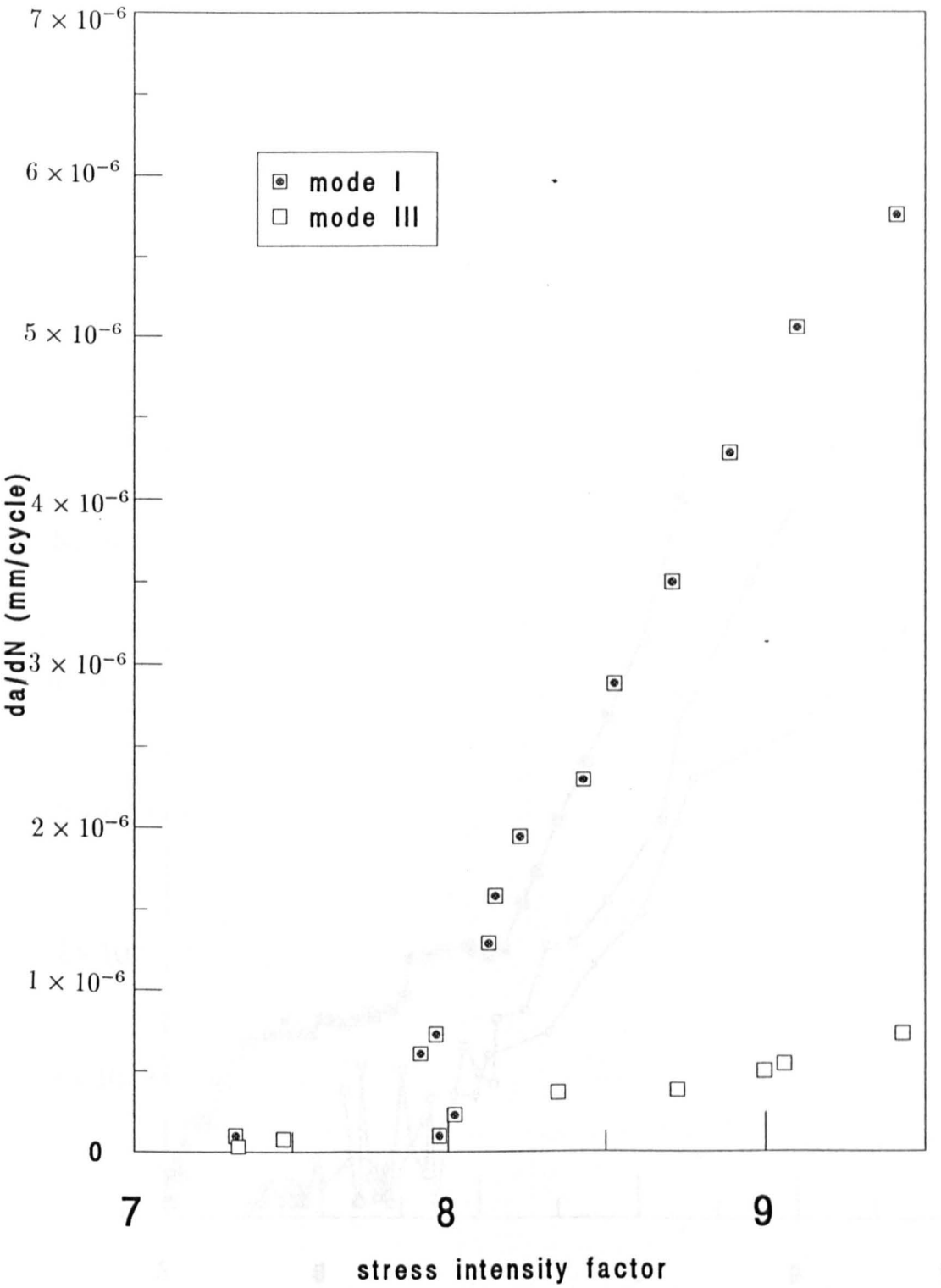

Fig.(6.17) Comparison in crack growth rate between mode I and mode III tests at R = -1.

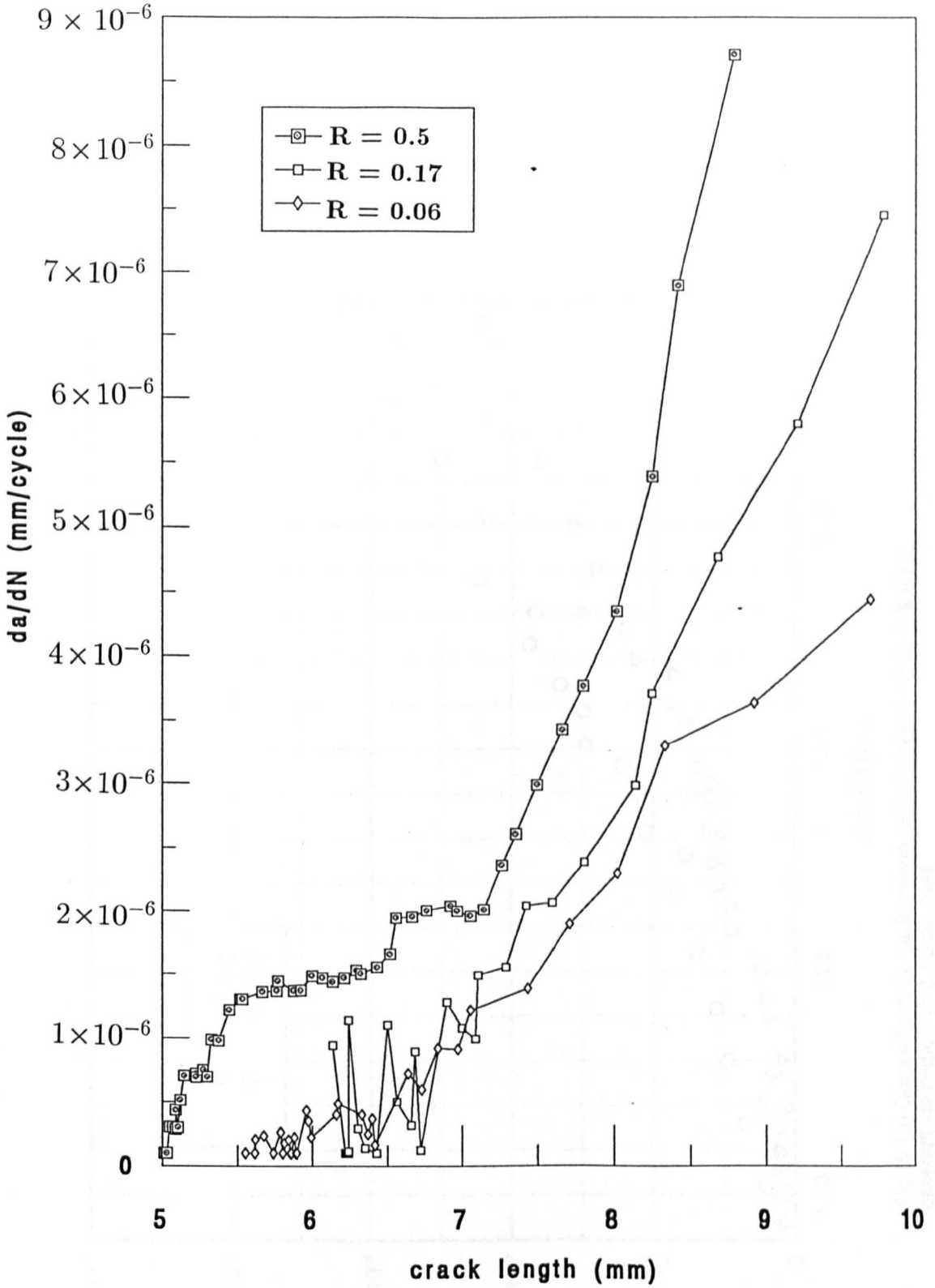

Fig. 6.18 The effect or R ratio on the crack growth rate in mixed modes (I & III) tests for slit angle of 45 deg.

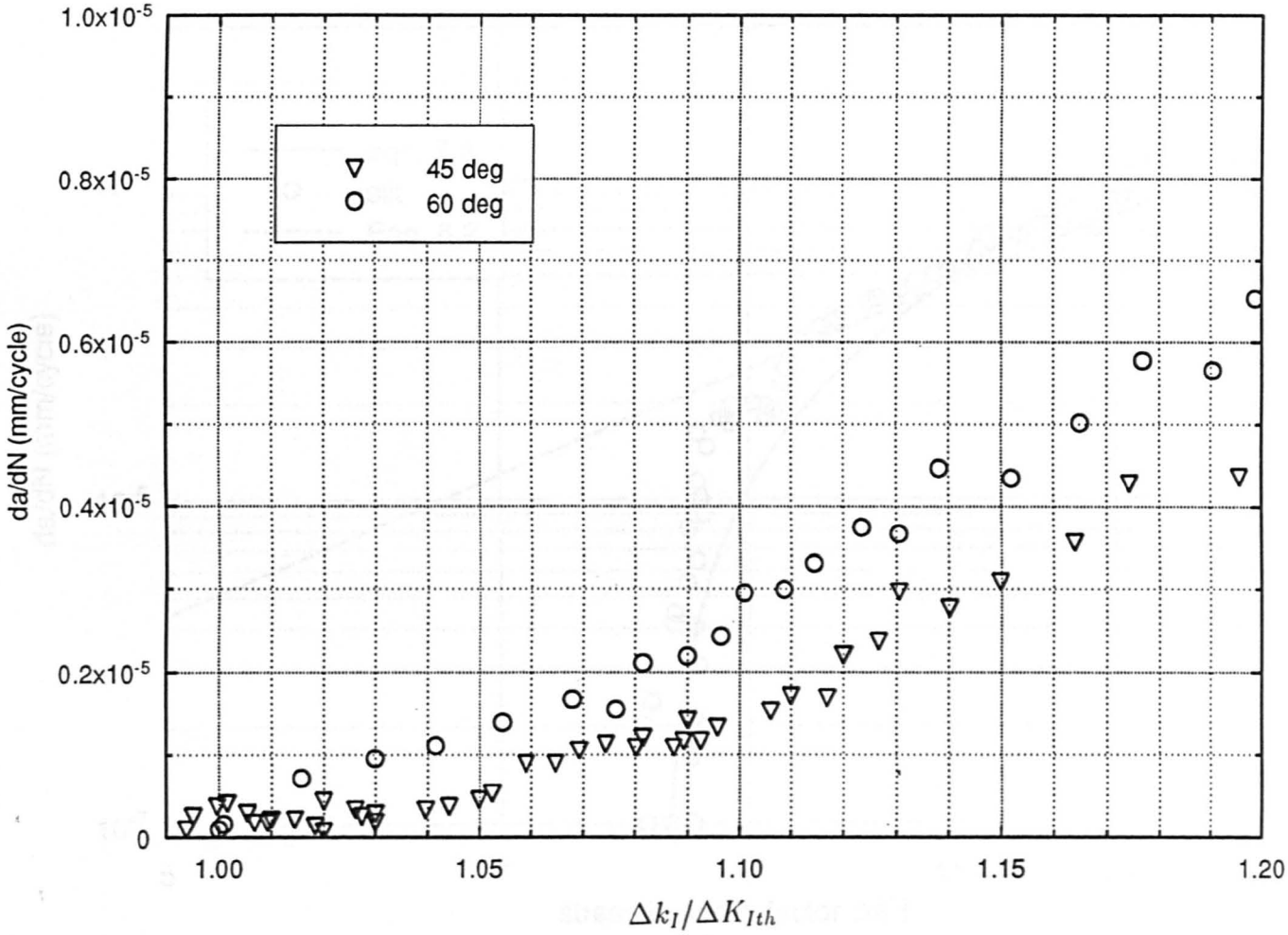

Fig.(6.19) Comparison in crack growth rates in mixed mode (I & III) at different slit angles 45 & 60 degrees.

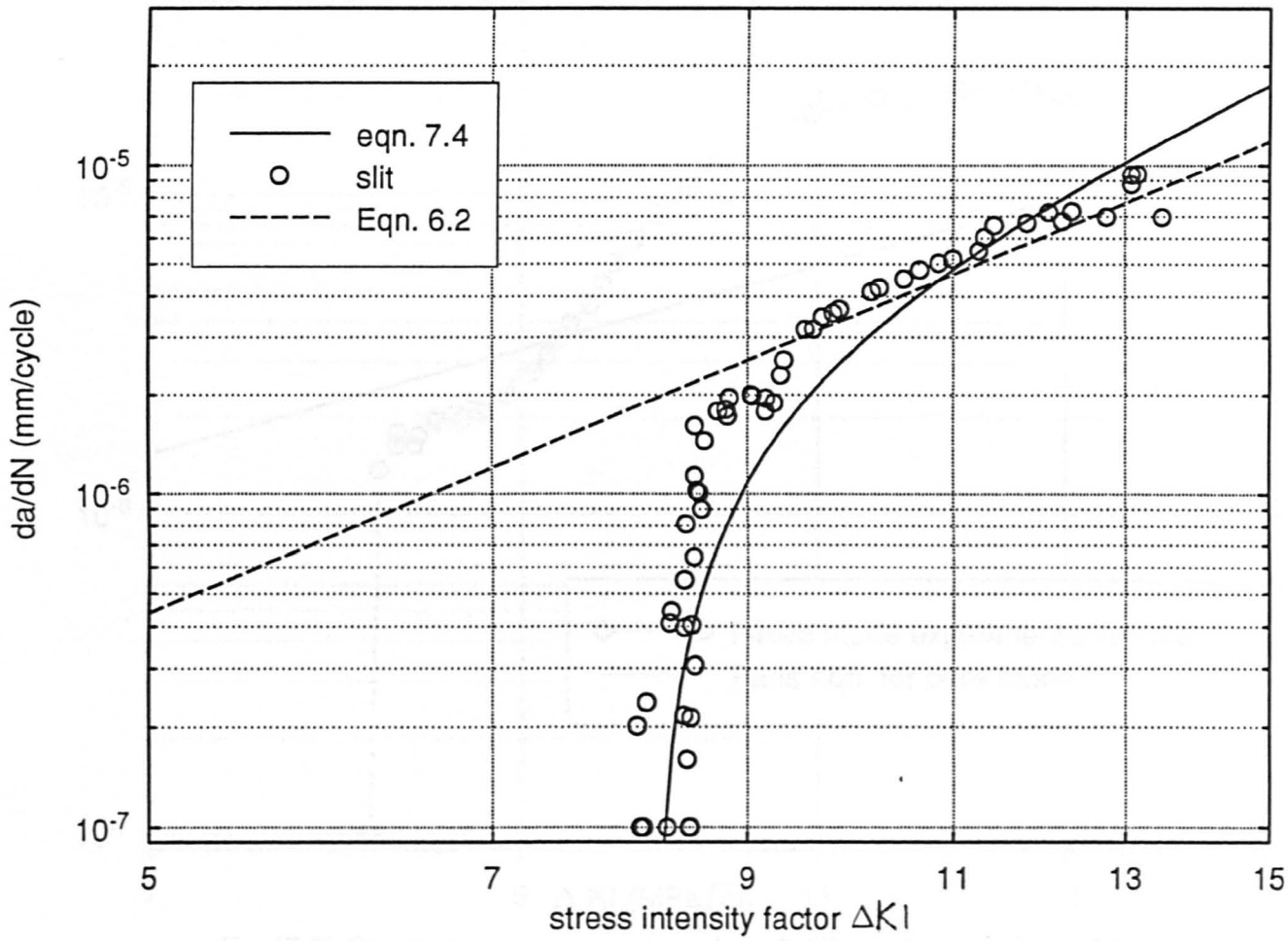

Fig.(7.1) Mode I fatigue crack growth equation (7.4) compared to the present research experimental results and Paris equation.

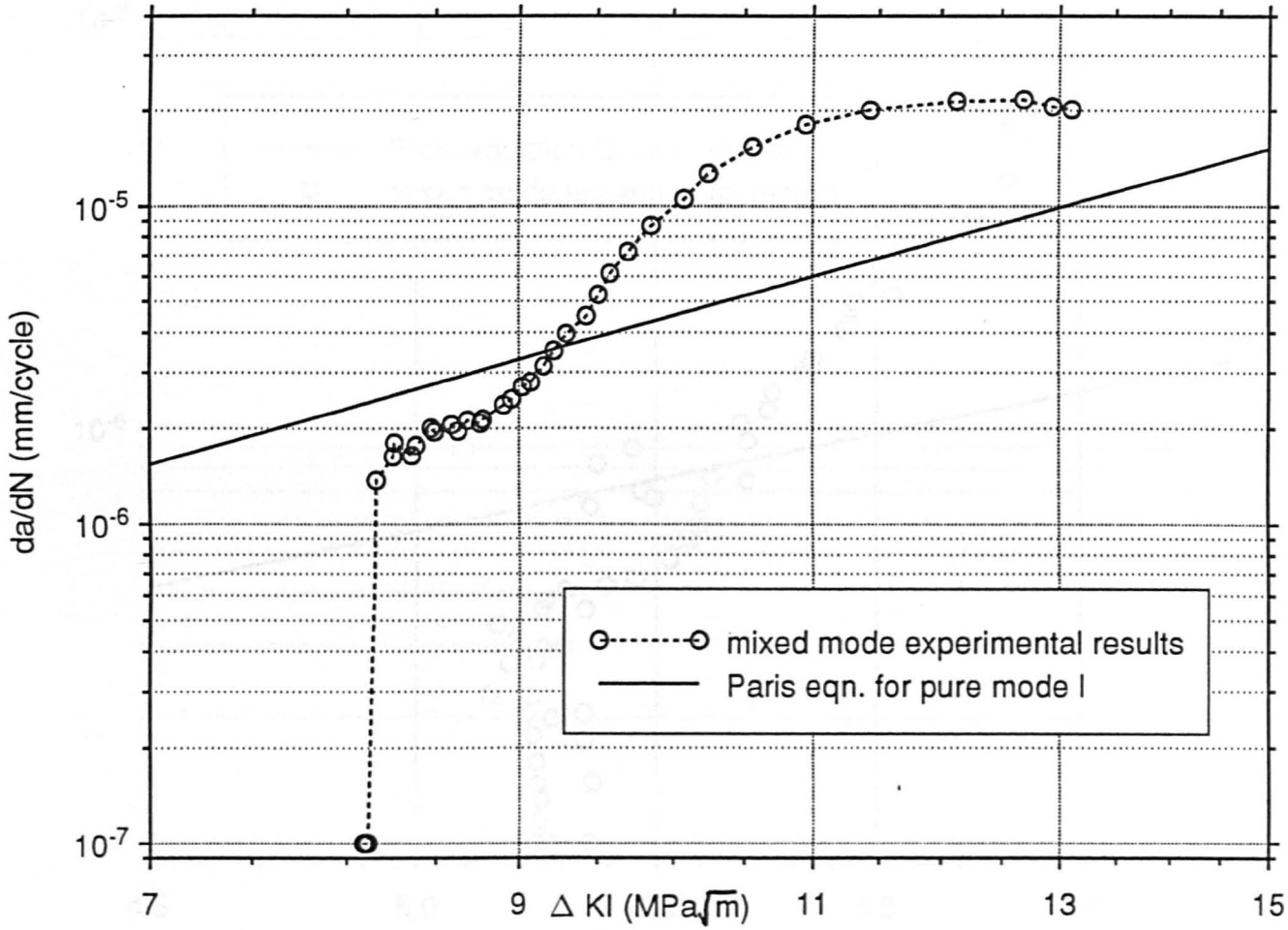

Fig.(7.2) Crack growth in mixed mode (I & III) loading for R = 0.06 and slit angle 60 deg. compared to pure mode I loading for the same R ratio.

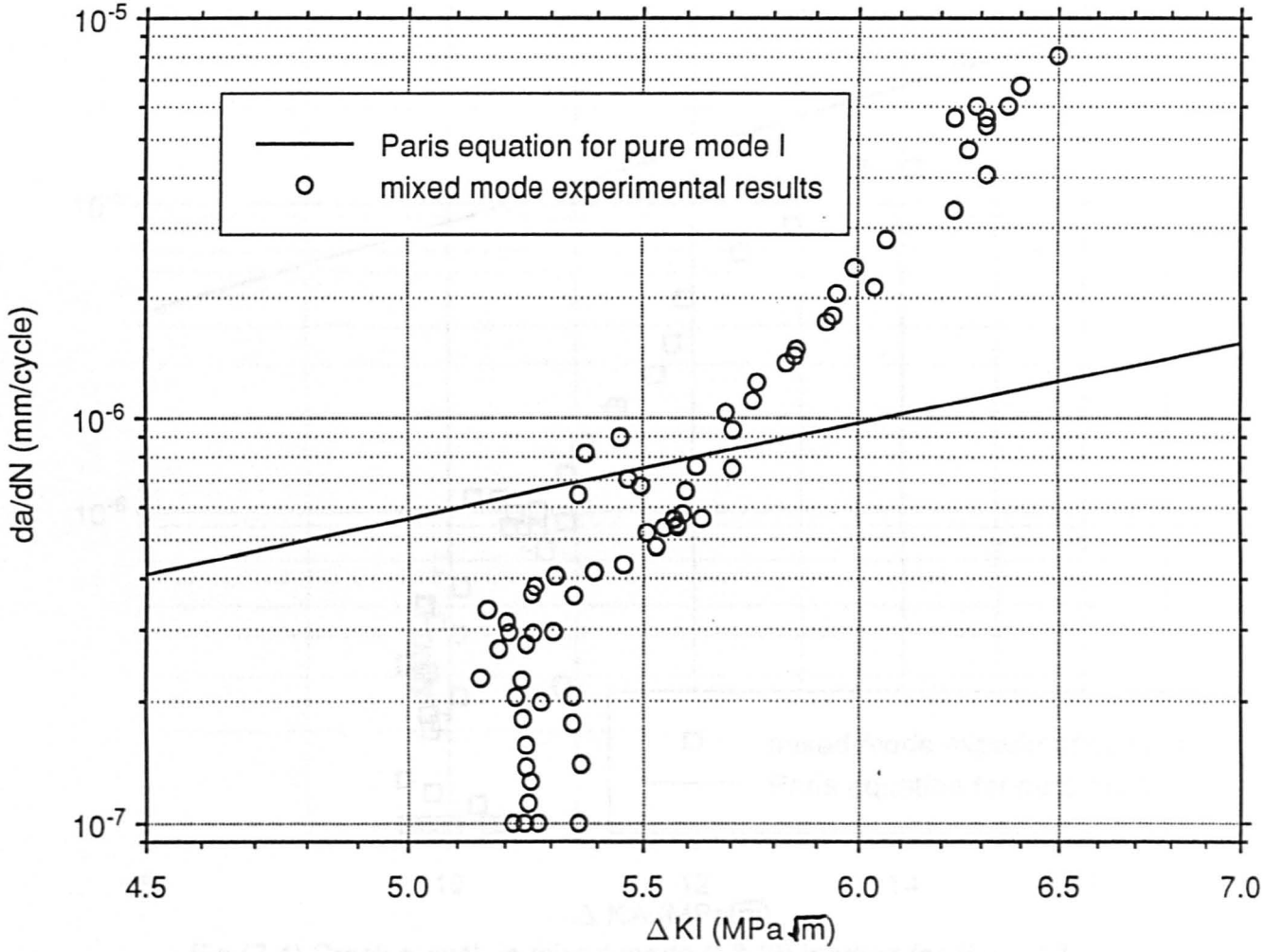

Fig.(7.3) Crack growth in mixed mode (I & III) loading for R = 0.06 and slit angle 45 deg. compared to pure mode I loading for the same R ratio.

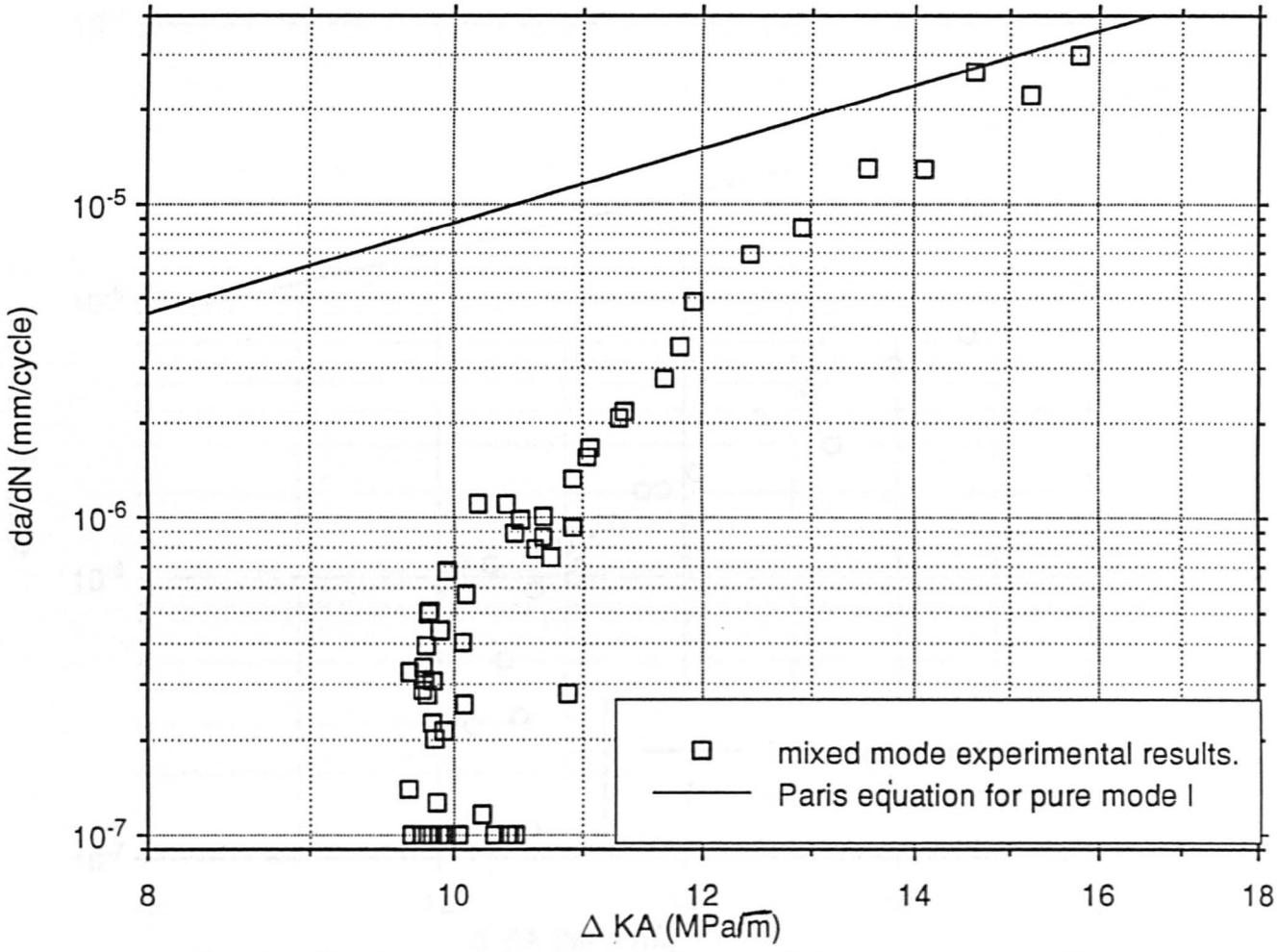

Fig.(7.4) Crack growth in mixed mode (I & III) loading for R = 0.17 and slit angle 60 deg. compared to pure mode I loading for the same R ratio.

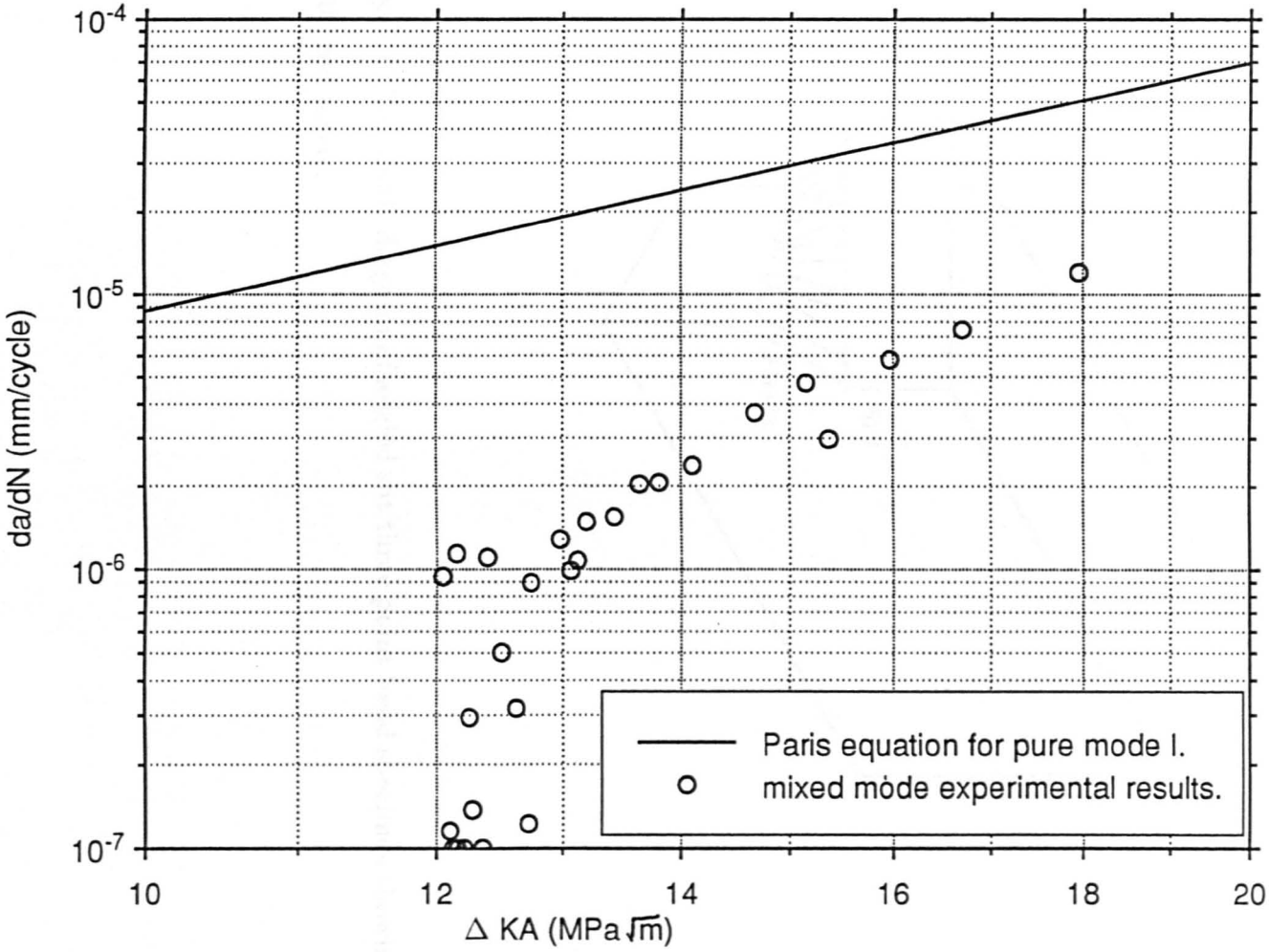

Fig.(7.5) Crack growth in mixed mode (I & III) loading for R = 0.17 and slit angle 45 deg. compared to pure mode I loading for the same R ratio.

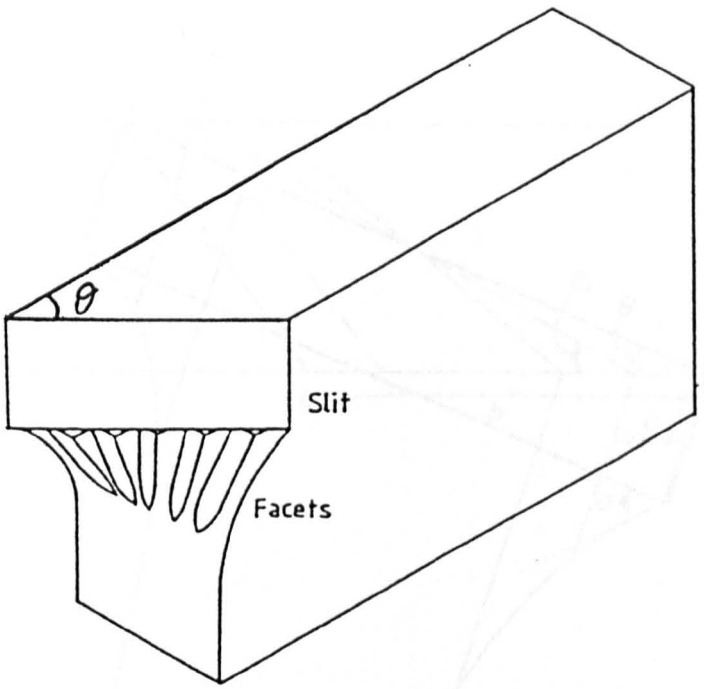

Fig.(7.6) Schematic diagram of angled slit three point bend specimen showing crack path and facets.

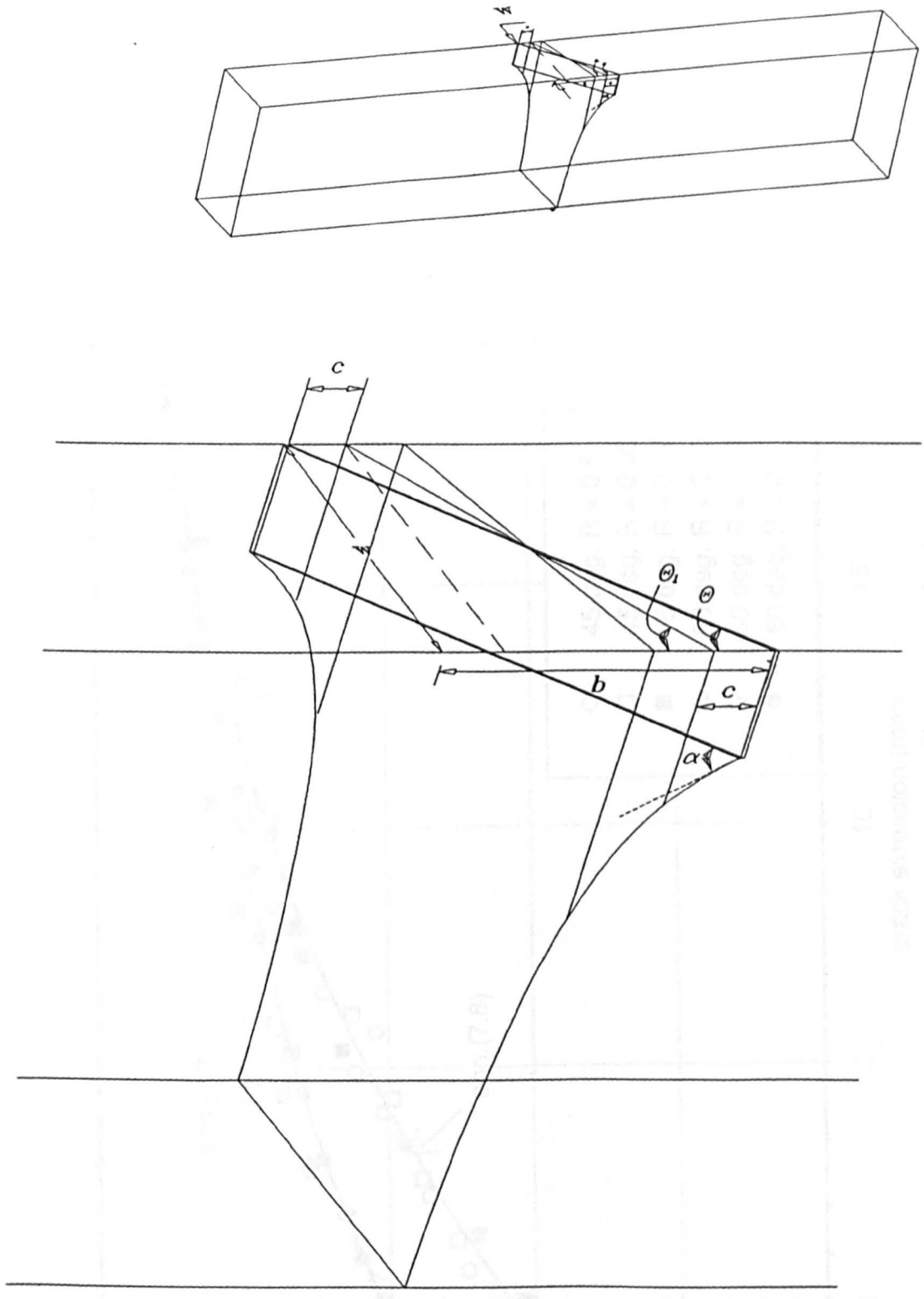

Fig.(7.7) Drawing of fatigue crack path in a three point slit specimen under mixed mode I & III loading showing the changes in the slit angle as the crack extends.

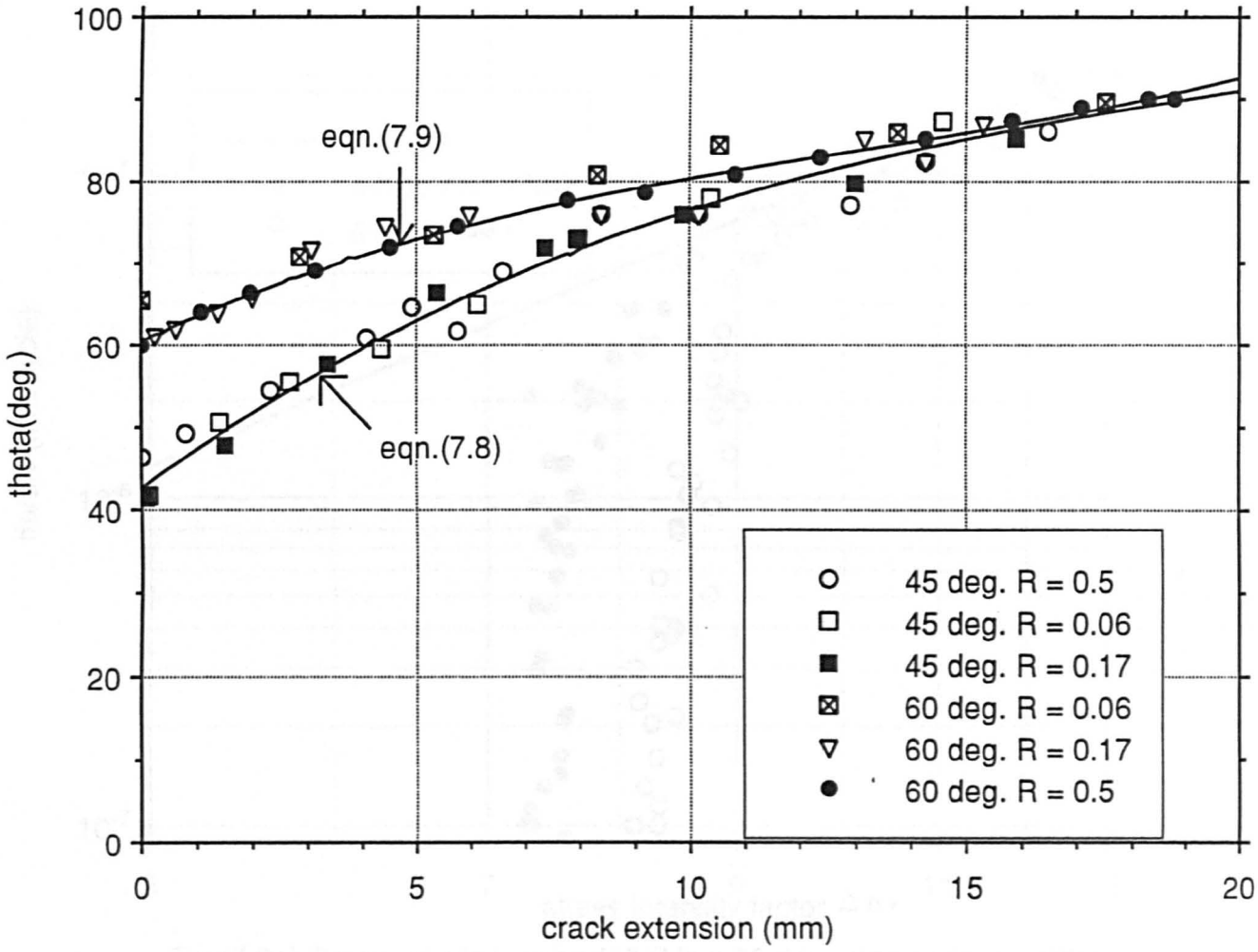

Fig.(7.8) The experimental results of variable measured value of the slit angles in different specimens compared to the predicted theoretical values.

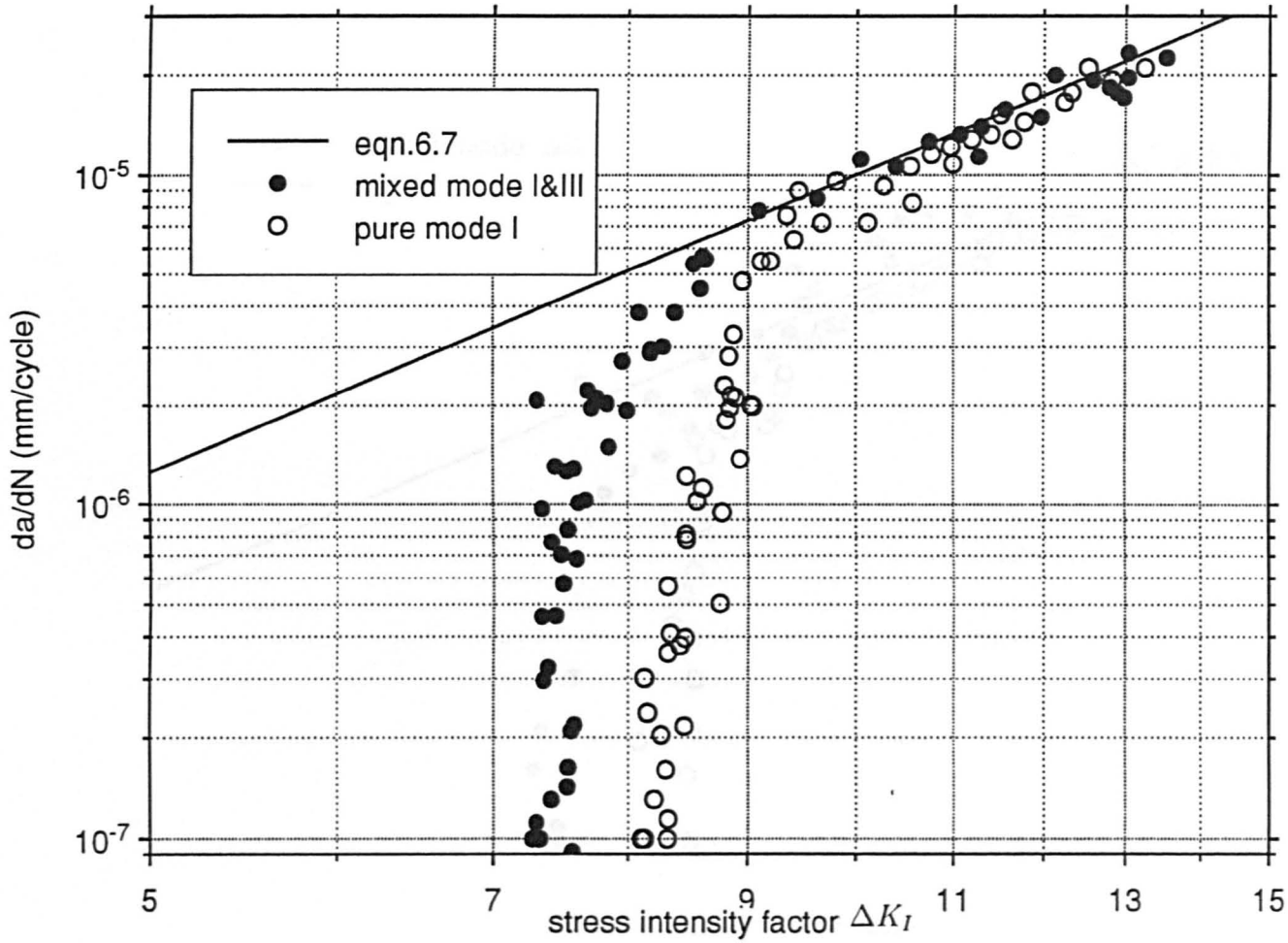

Fig.(7.9a) Crack growth in mixed I&III in a 60 deg. slit specimen with R = 0.5 calculated using the new method compared to pure mode I loading only.

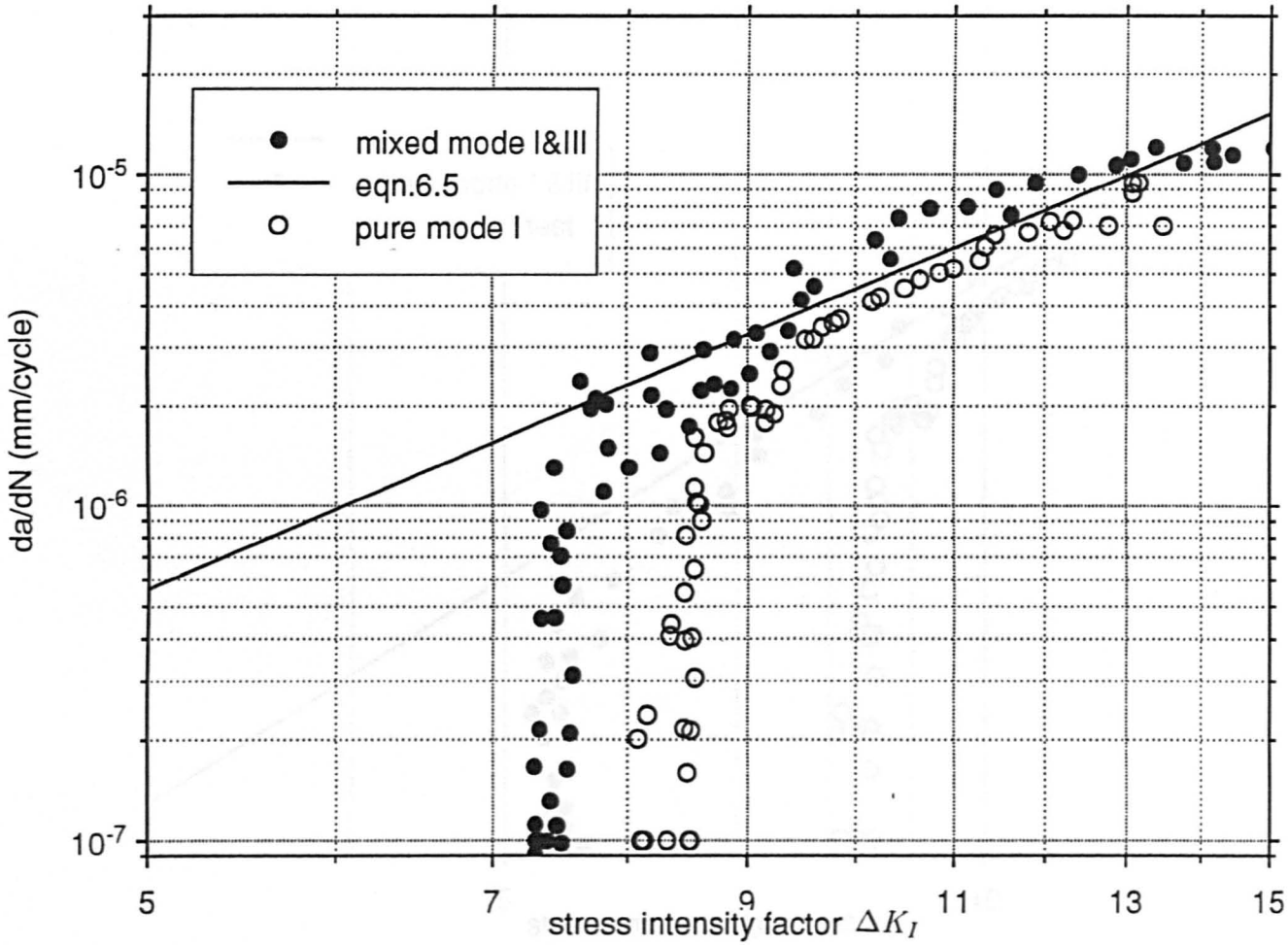

Fig.(7.9b) Crack growth in mixed mode I&III in a 60 deg. slit angle specimen for R = 0.06 calculated using the new method compared to pure mode I test only.

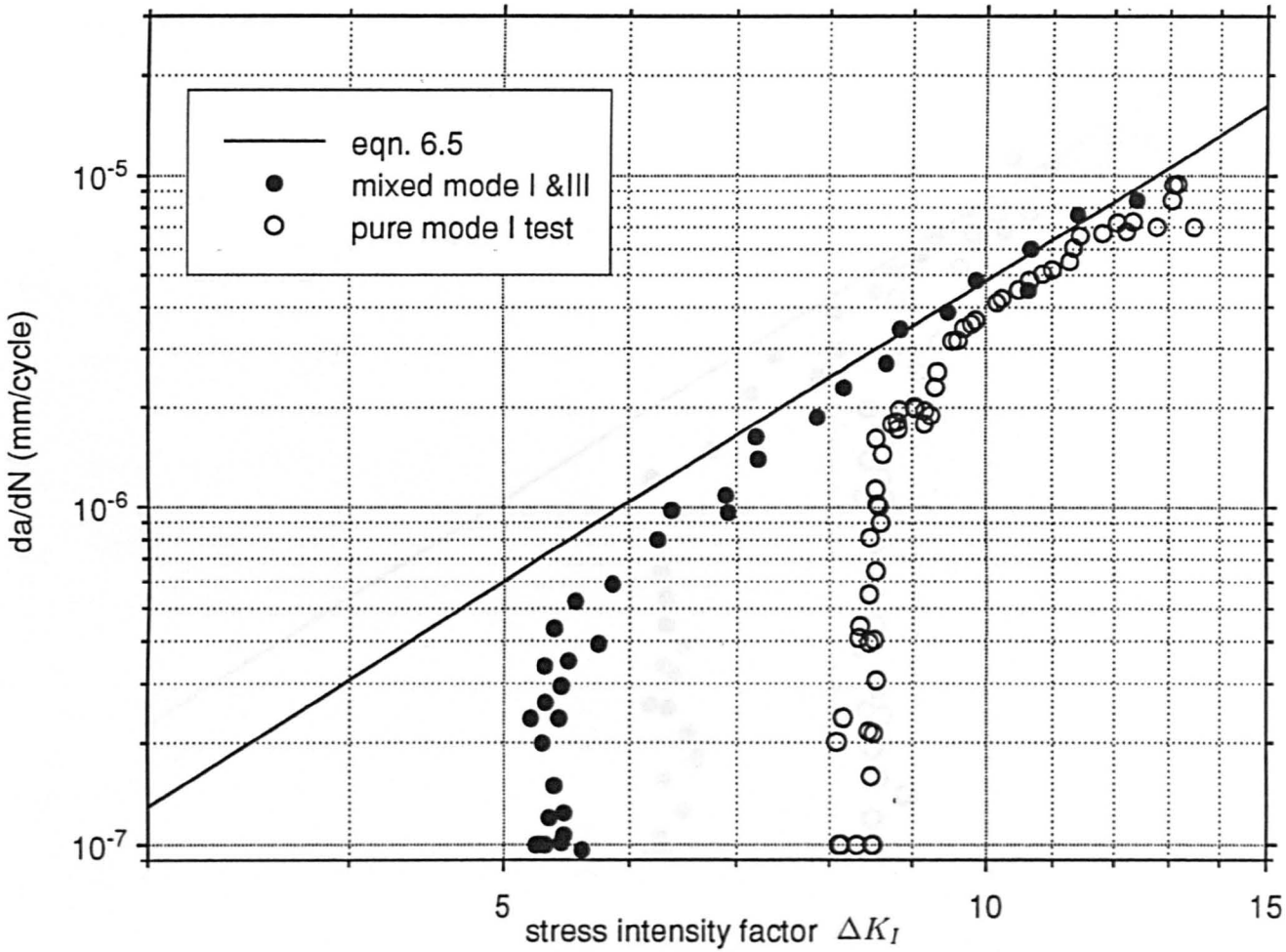

Fig.(7.10a) Crack growth in mixed mode I&III test for R = 0.06 calculated using the new method in a 45 deg. slit specimen compared to pure mode I test on.

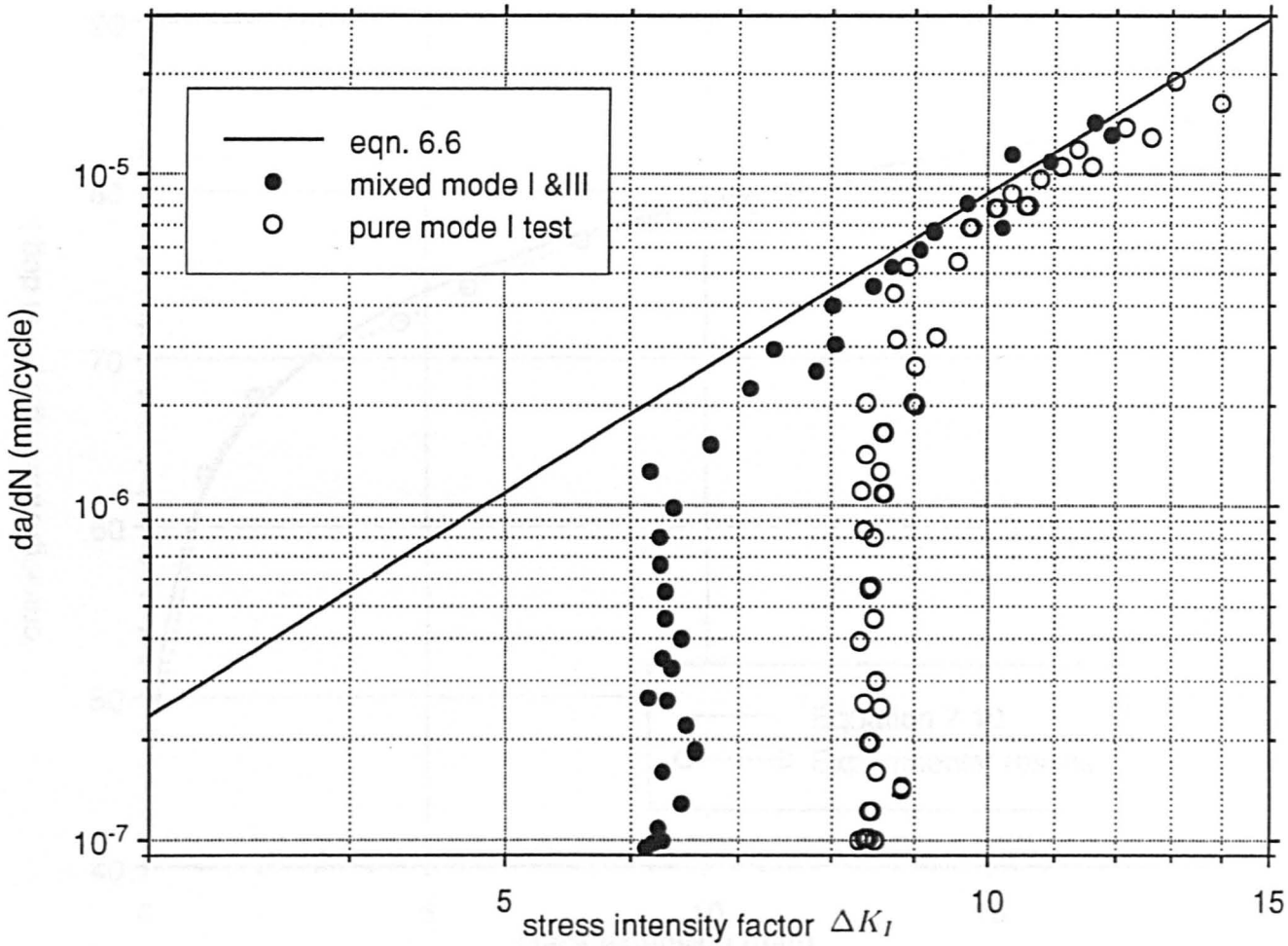

Fig.(7.10b) Crack growth in mixed mode I&III loading for R = 0.17 calculated using the new method in a 45 deg. slit specimen compared to pure mode I only.

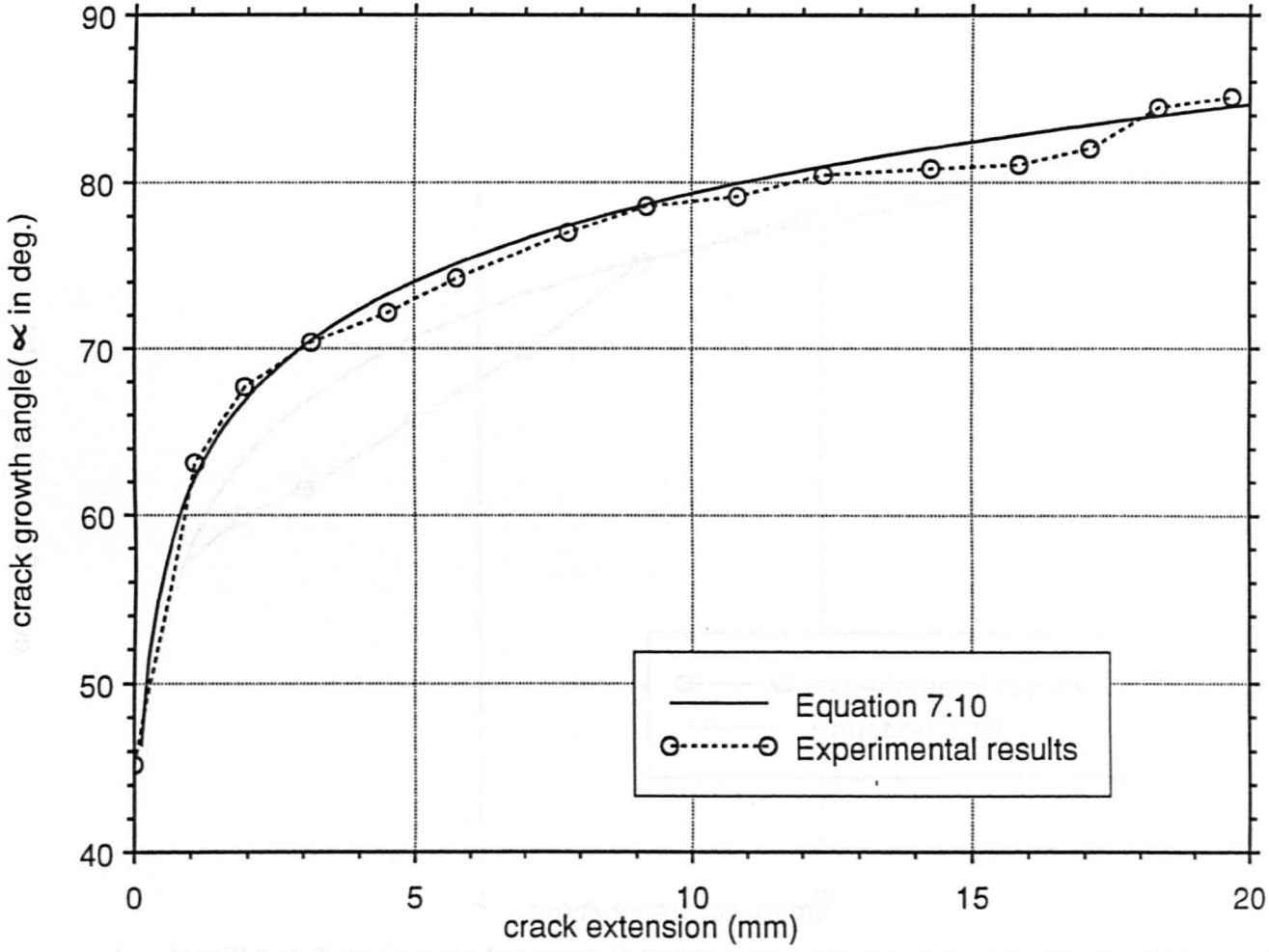

Fig.(7.11) Comparison between the measured experimental values of the crack growth angle and the predicted ones in a 60 deg. slit specimen test with R=0.06

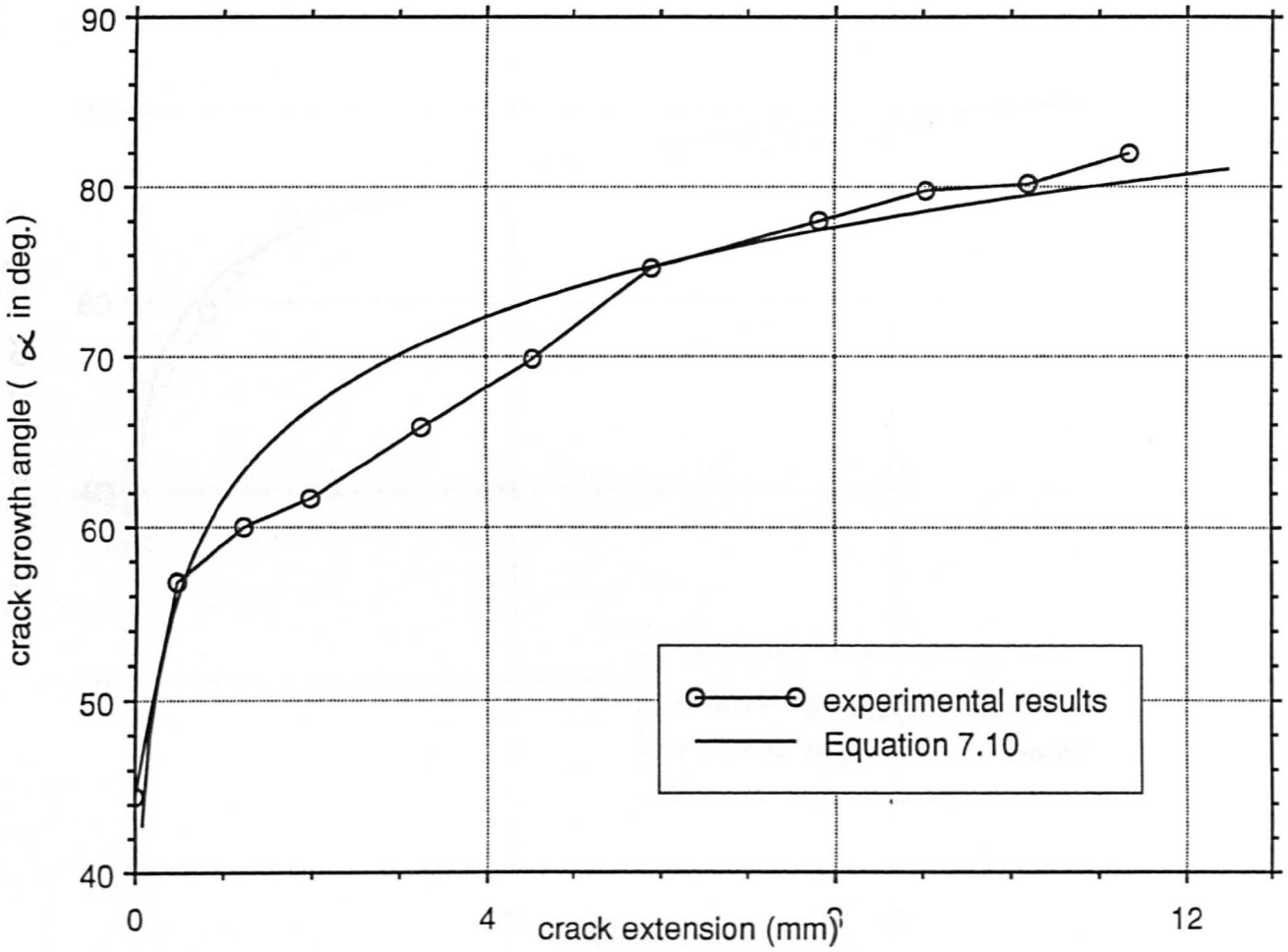

Fig.(7.12) Comparison between the measured values of the crack growth angle in a 60 deg. slit specimen with R = 0.5 and the predicted new model values.

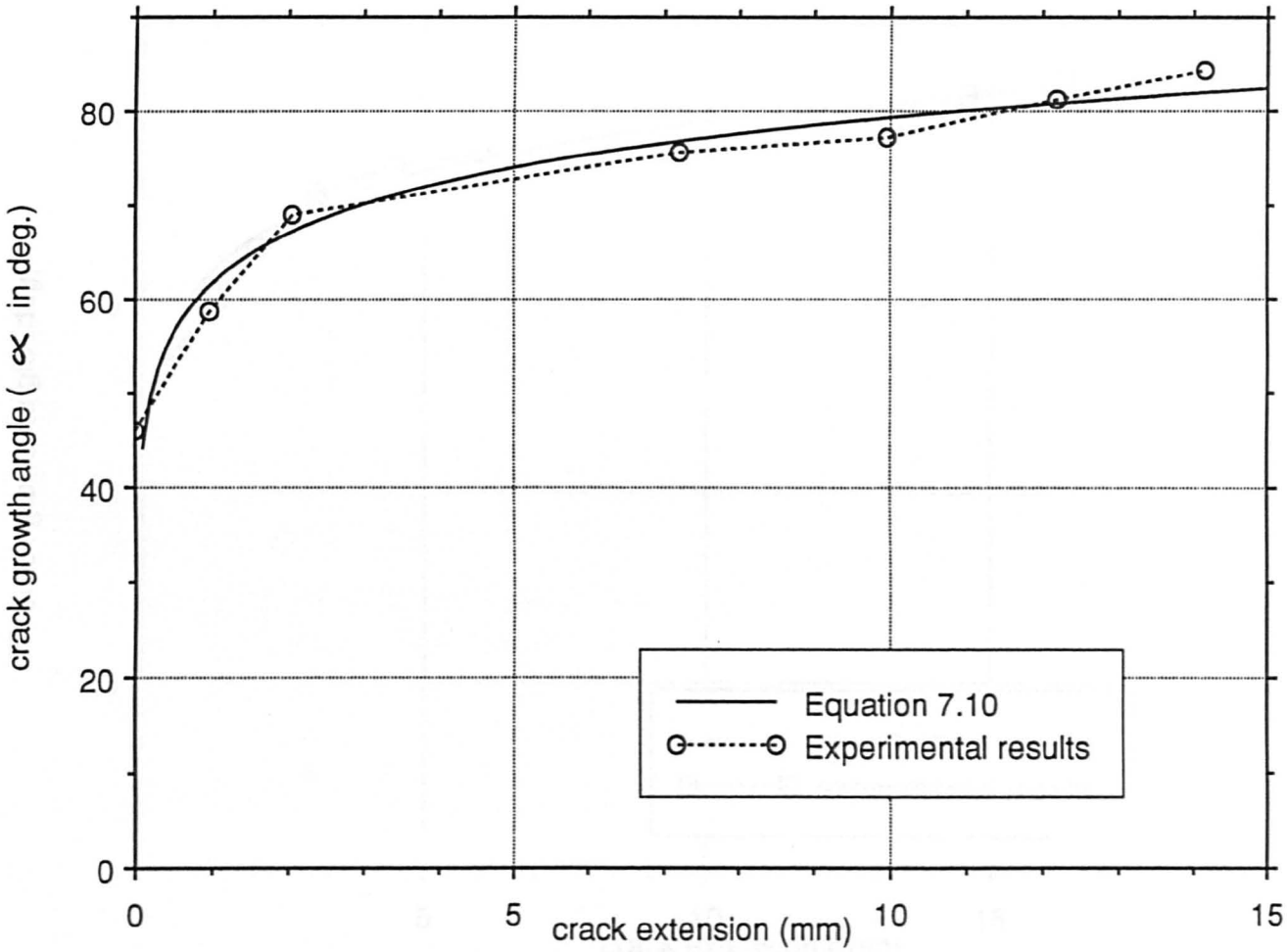

Fig.(7.13)Comparison between the measured values of the crack growth angle and the predicted one by the new model for a 45 deg. slit angle specimen for R=0.5

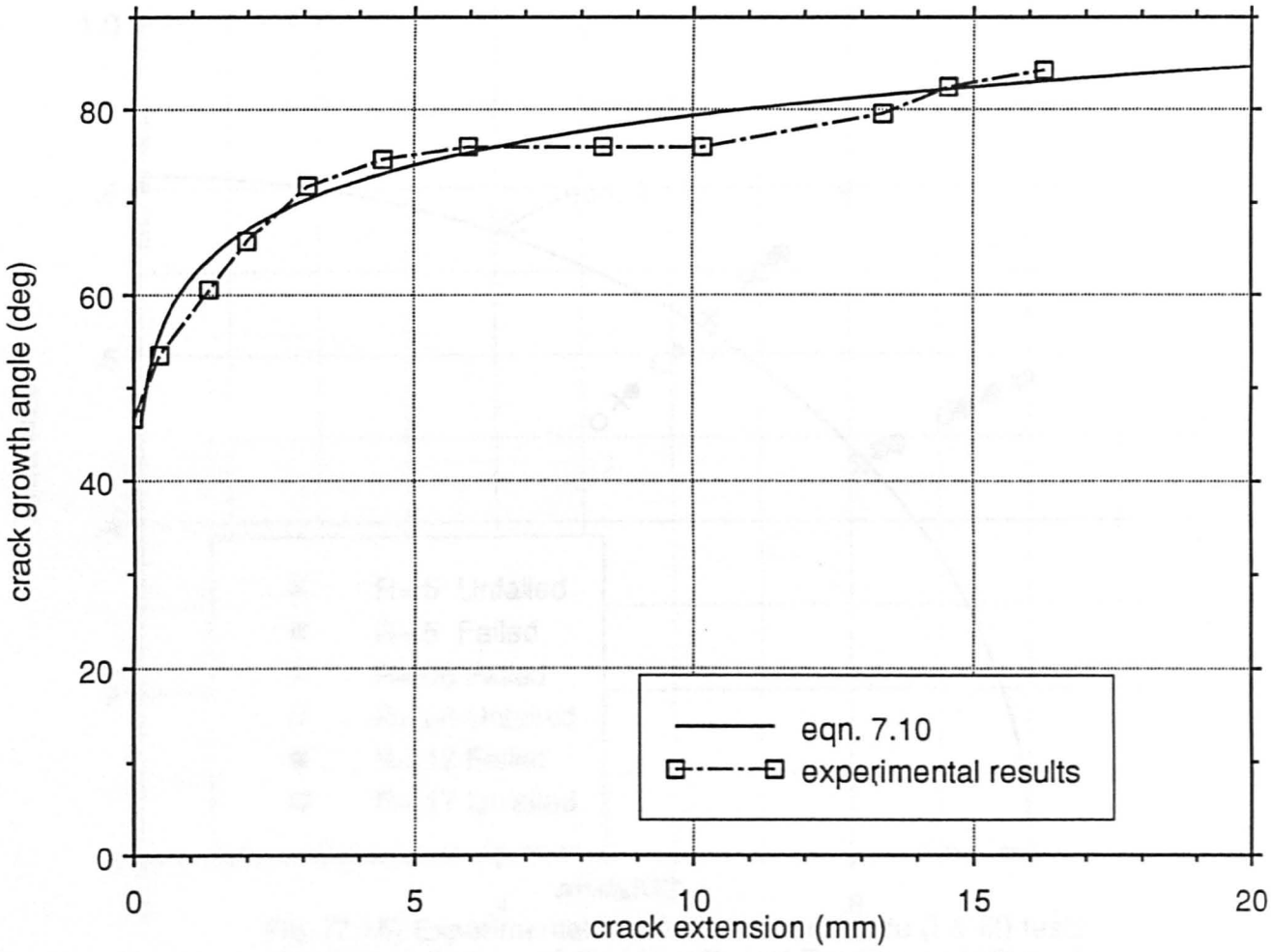

Fig.(7.14) Comparison between the measured values of the crack growth angle and the predicted ones by the new model for a 45 deg. slit specimen with R=0.17

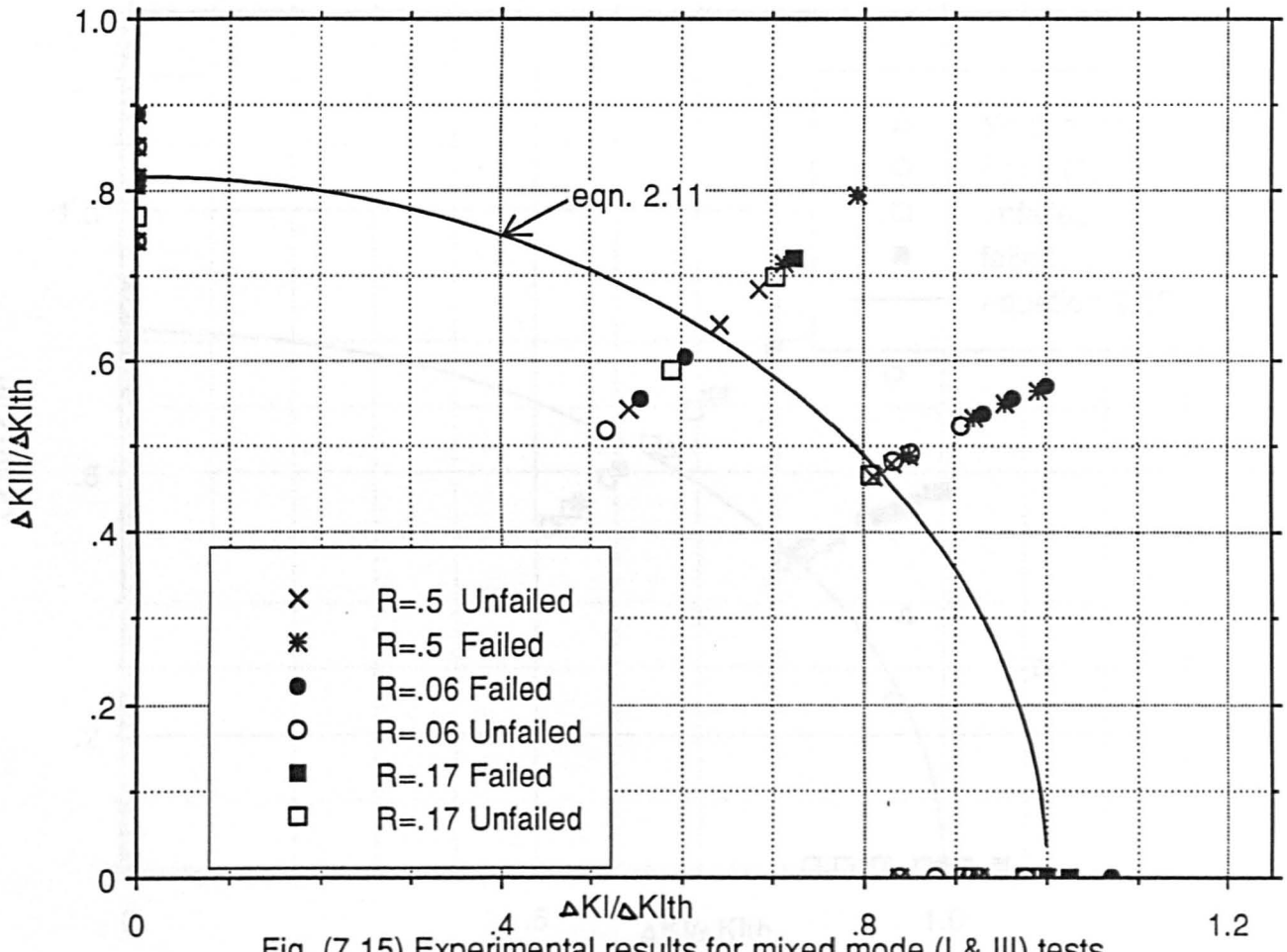

Fig. (7.15) Experimental results for mixed mode (I & III) tests shown as failed or unfailed for different R ratios and slit angles. compared to strain energy release rate failure criteria.

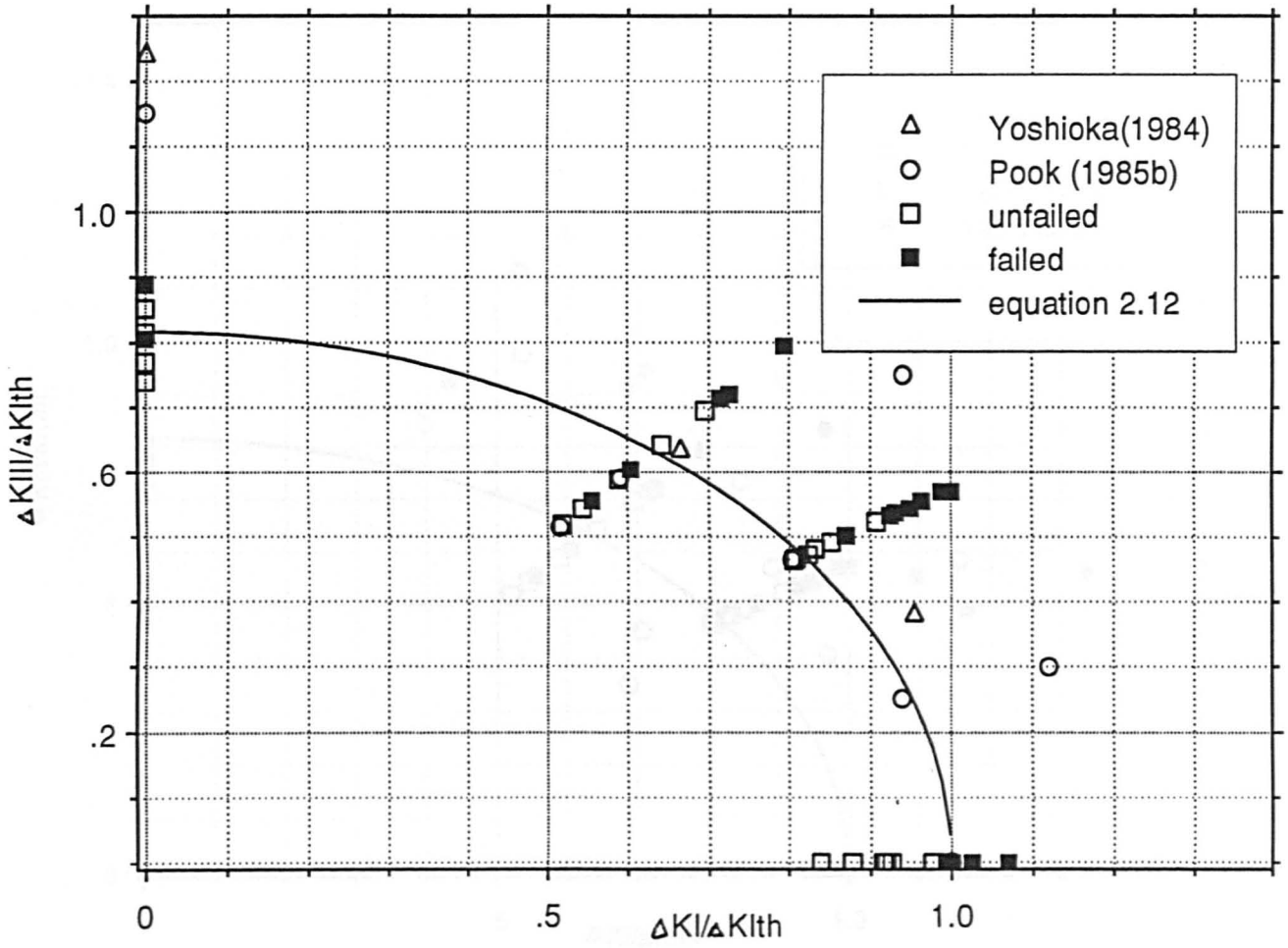

Fig.(7.16) The present research data for mixed mode I & III tests at different R ratios compared to Pook's and Yoshioka's results with respect to strain energy release rate fatigue failure criteria.

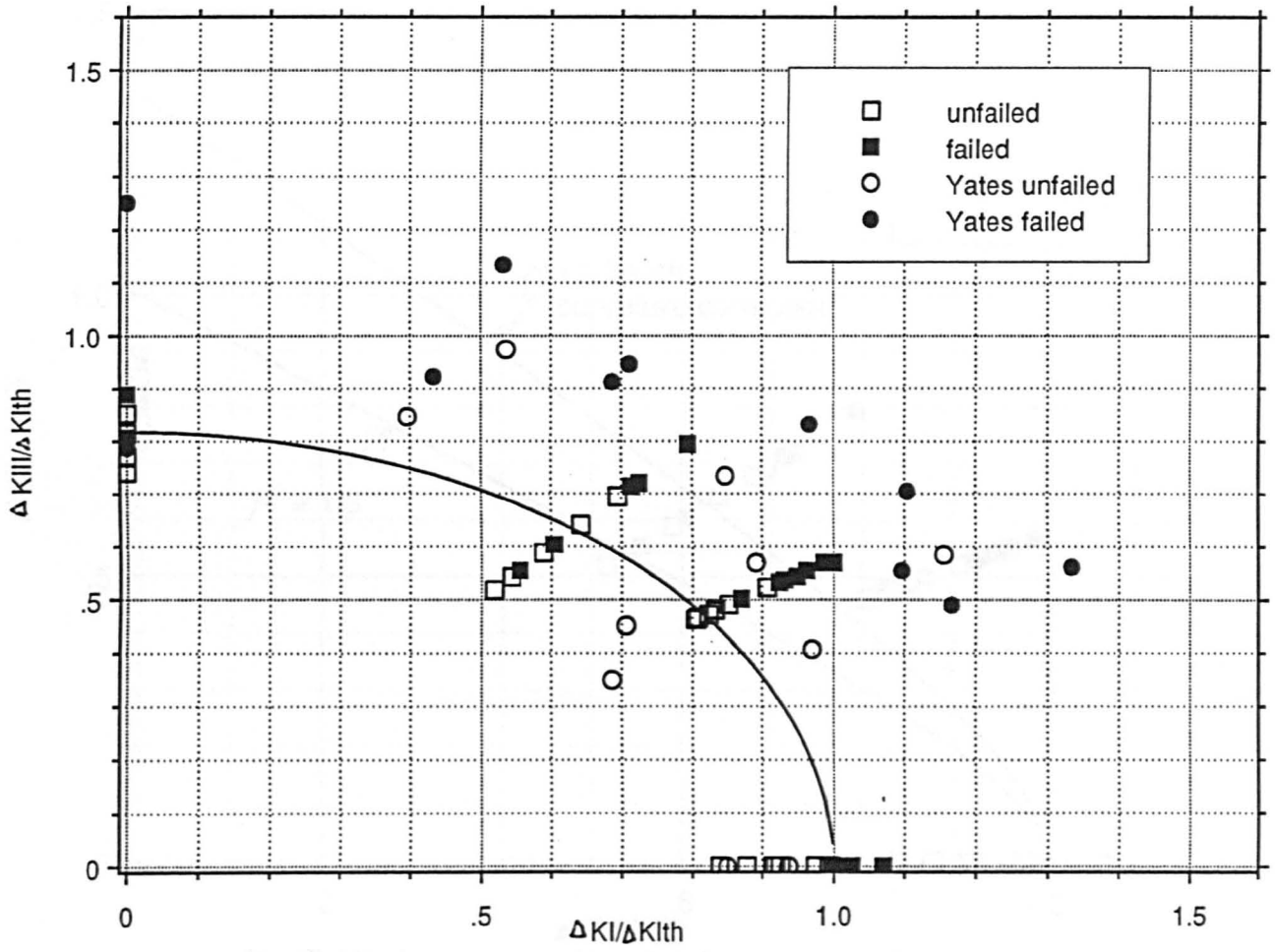

Fig.(7.17) The present research data compared to Yates's results with respect strain energy release rate criteria for predicting fatigue failure in mixed mode I & III.

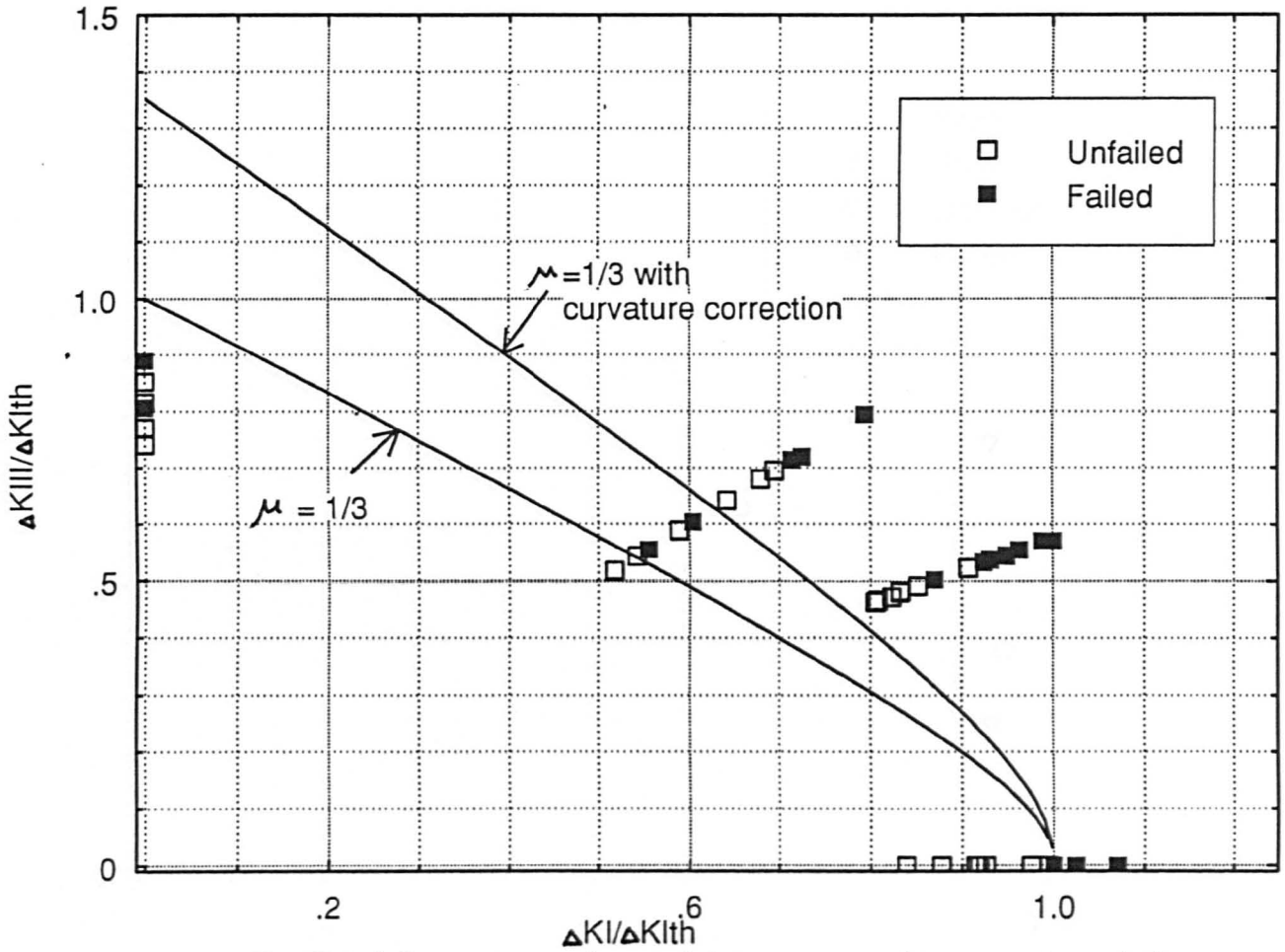

Fig.(7.18) Current experimental data compared to normal crack tip stress and branch crack method of predicting fatigue failure in mixed mode I & III loading.

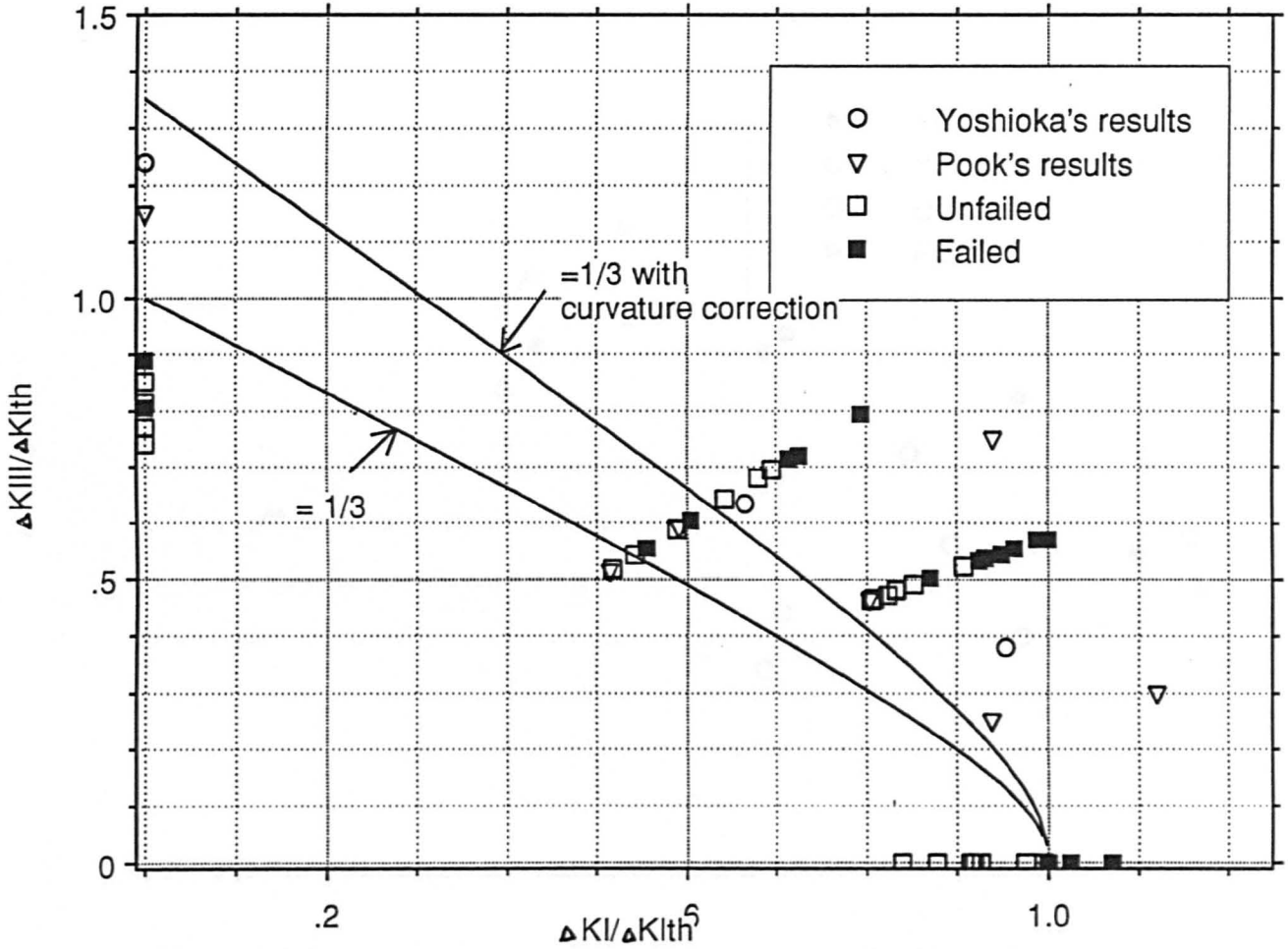

Fig.(7.19) Current experimental data compared to Pook's and Yoshioka's results with respect to the maximum normal crack tip stress and branch crack methods for predicting fatigue failure in mixed mode I & III loading

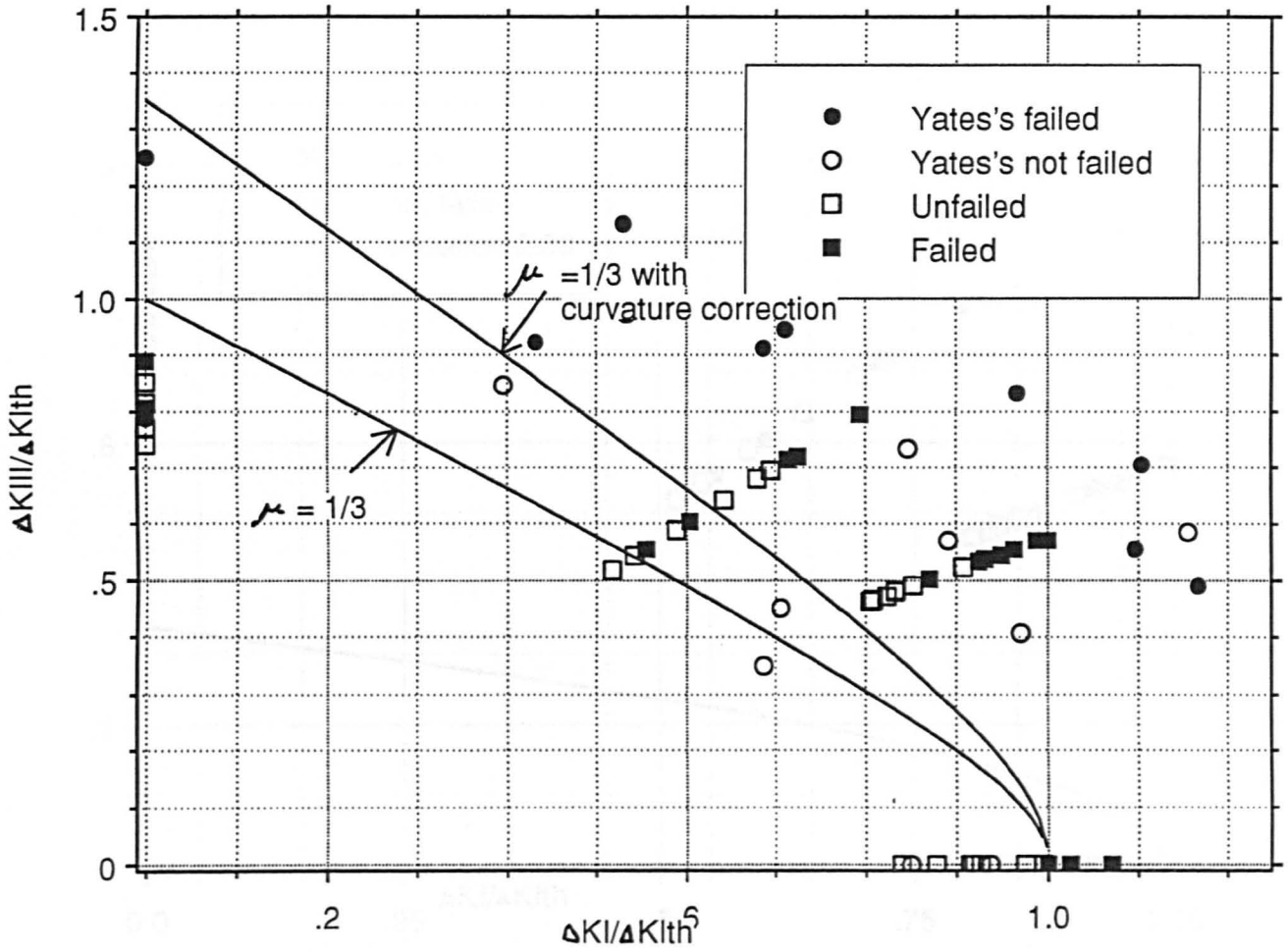

Fig.(7.20) Current experimental data compared to Yates's results with respect to maximum normal crack tip stress and branch crack methods for predicting fatigue failure in mixed mode I & III loading.

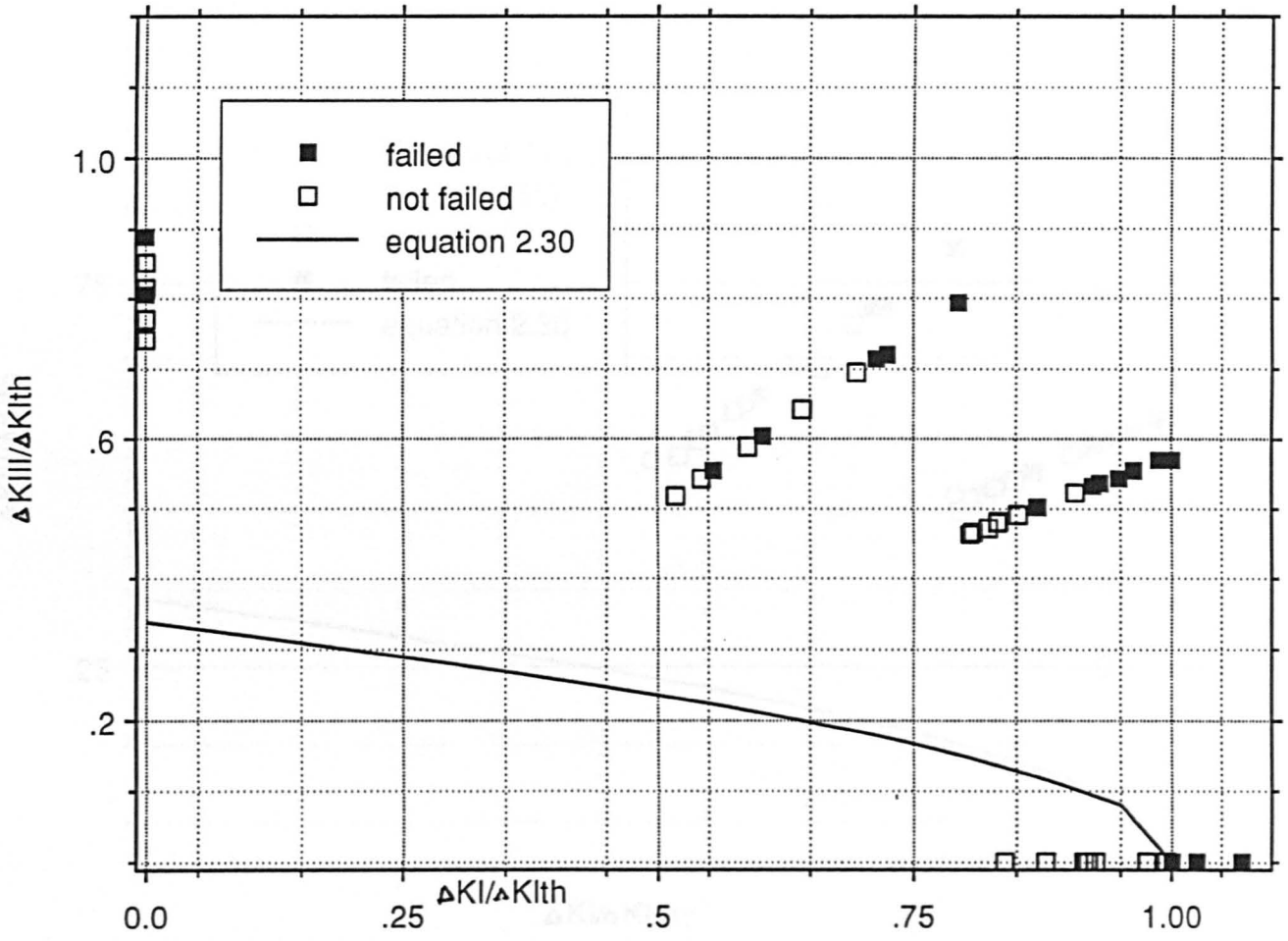

Fig.(7.21) Present results compared to the maximum normal crack tip strain criterion for predicting fatigue failure in mixed mode I & III loading.

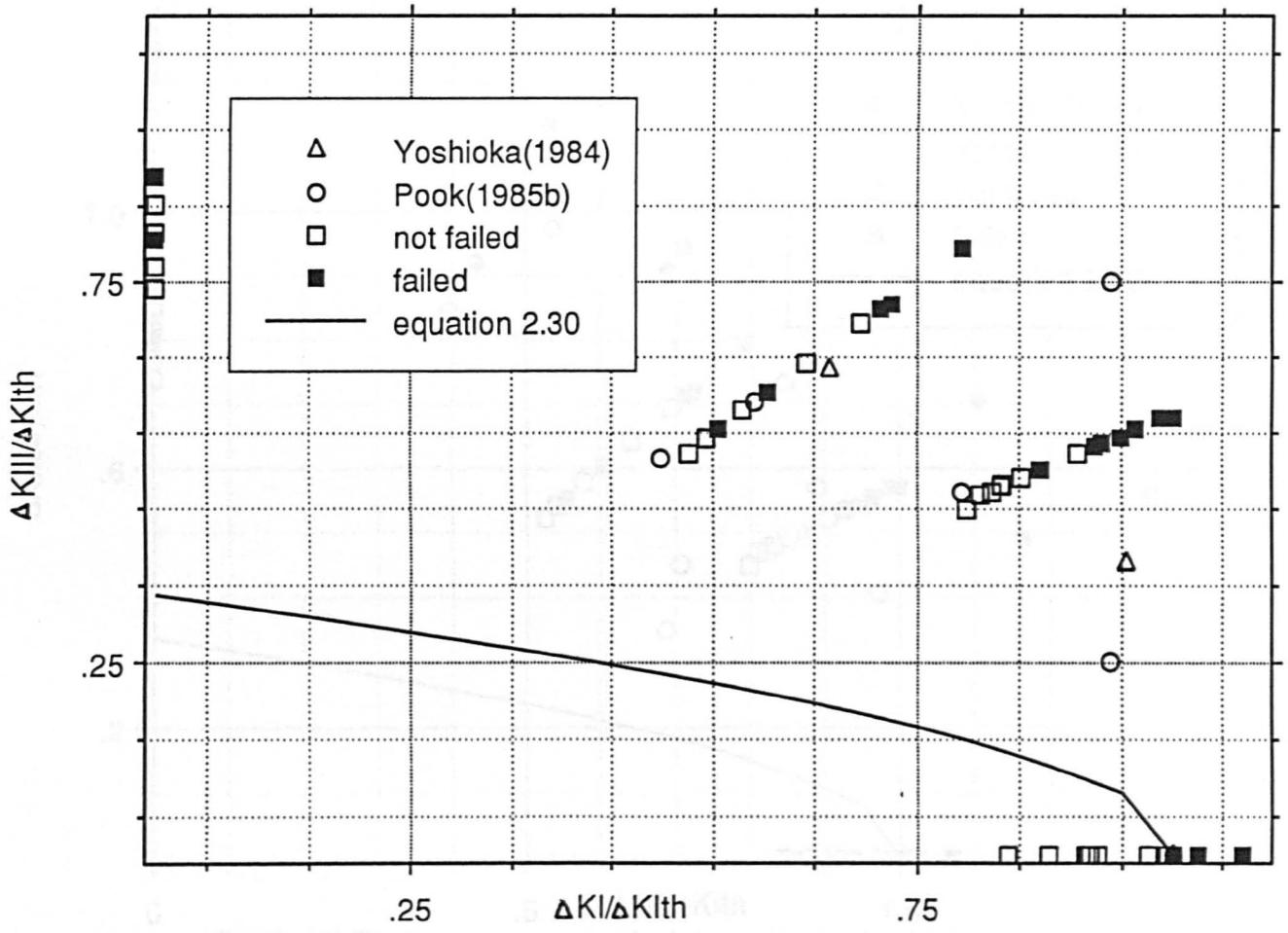

Fig.(7.22) The present research data compared to Pook's and Yoshioka's results with respect to the maximum normal crack tip strain criteion for predicting the mixed mode I & III loading fatigue failure.

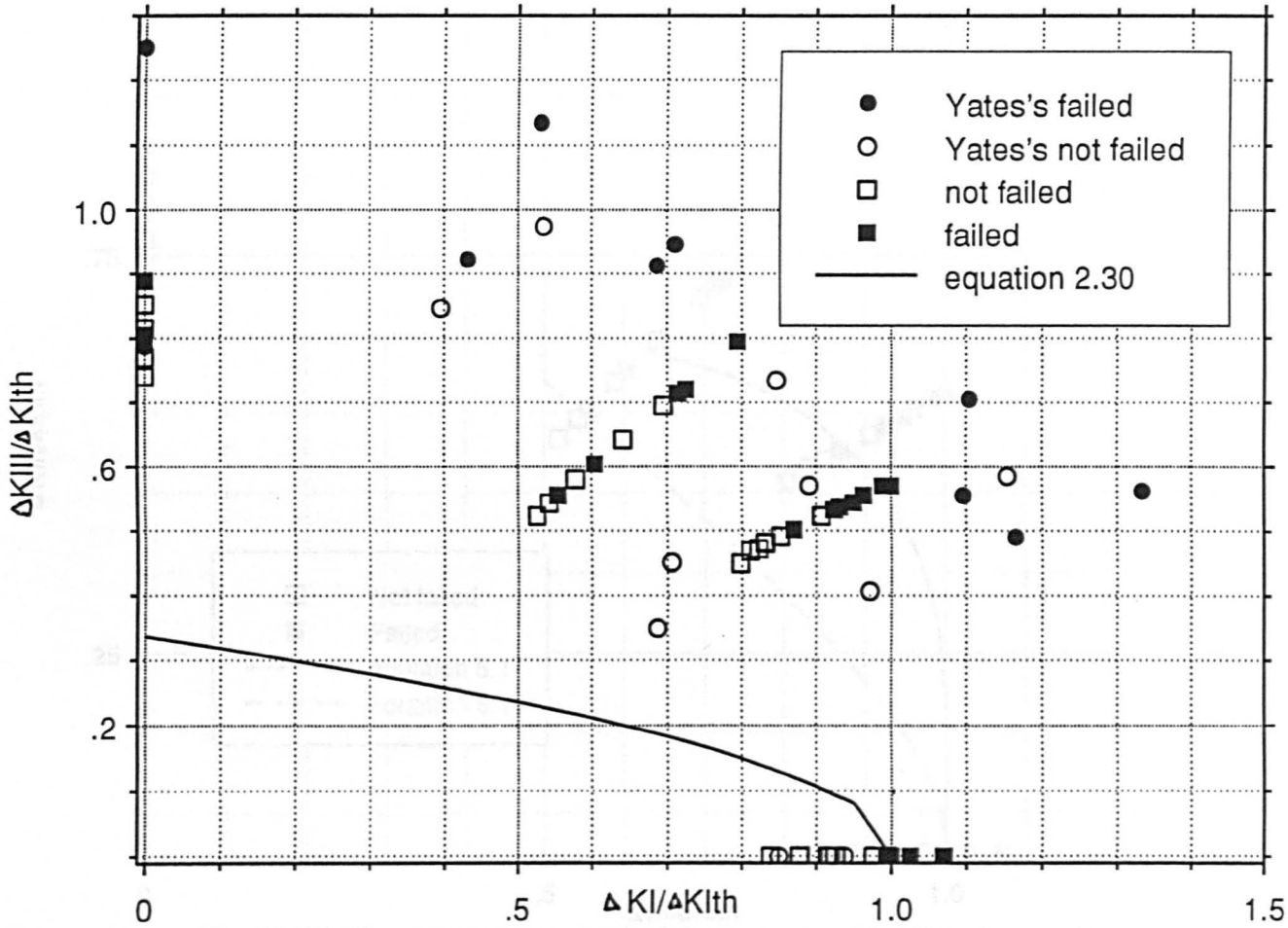

Fig.(7.23) The present research data compared to Yates's results with respect to the maximum normal crack tip strain for predicting failure in mixed mode I & III loading.

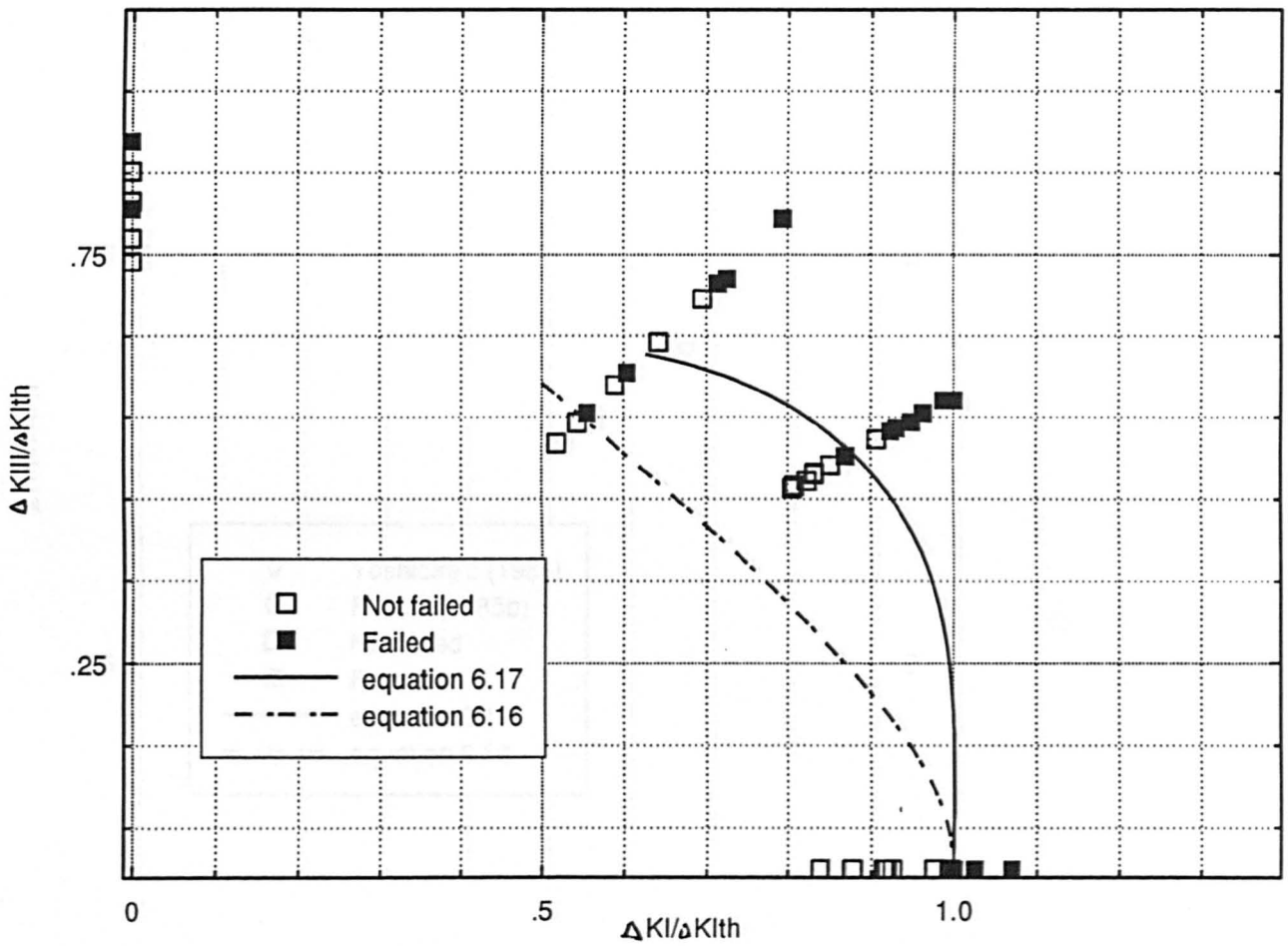

Fig.(7.24) Mixed mode (I & III) results for different R ratios compared to Yates's and Pook's failure criteria.

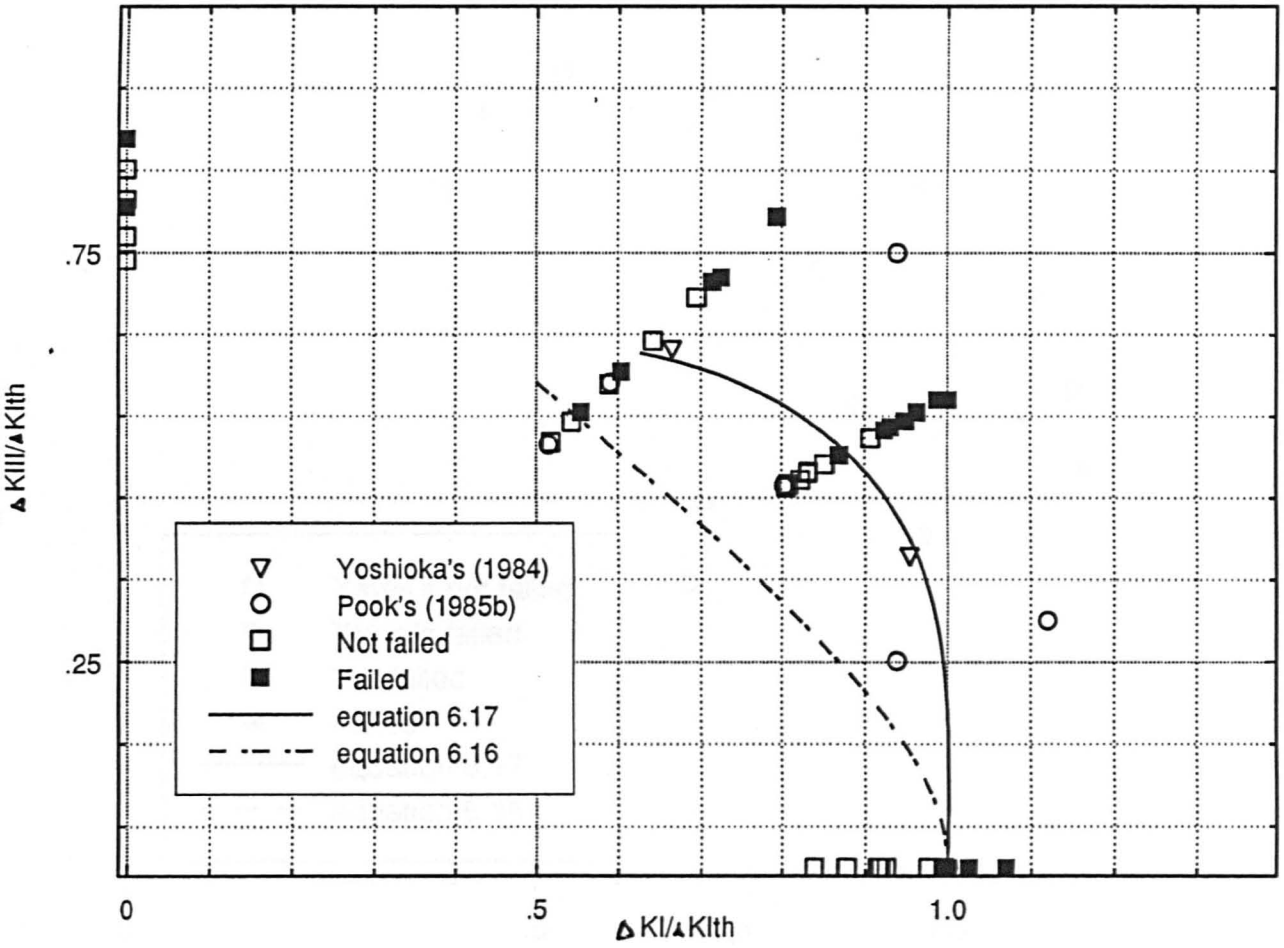

Fig.(7.25) Mixed mode I & III data for different R ratios compared to Yoshioka's and Pook's results with respect to Yates's and Pook's threshold failure criteria.

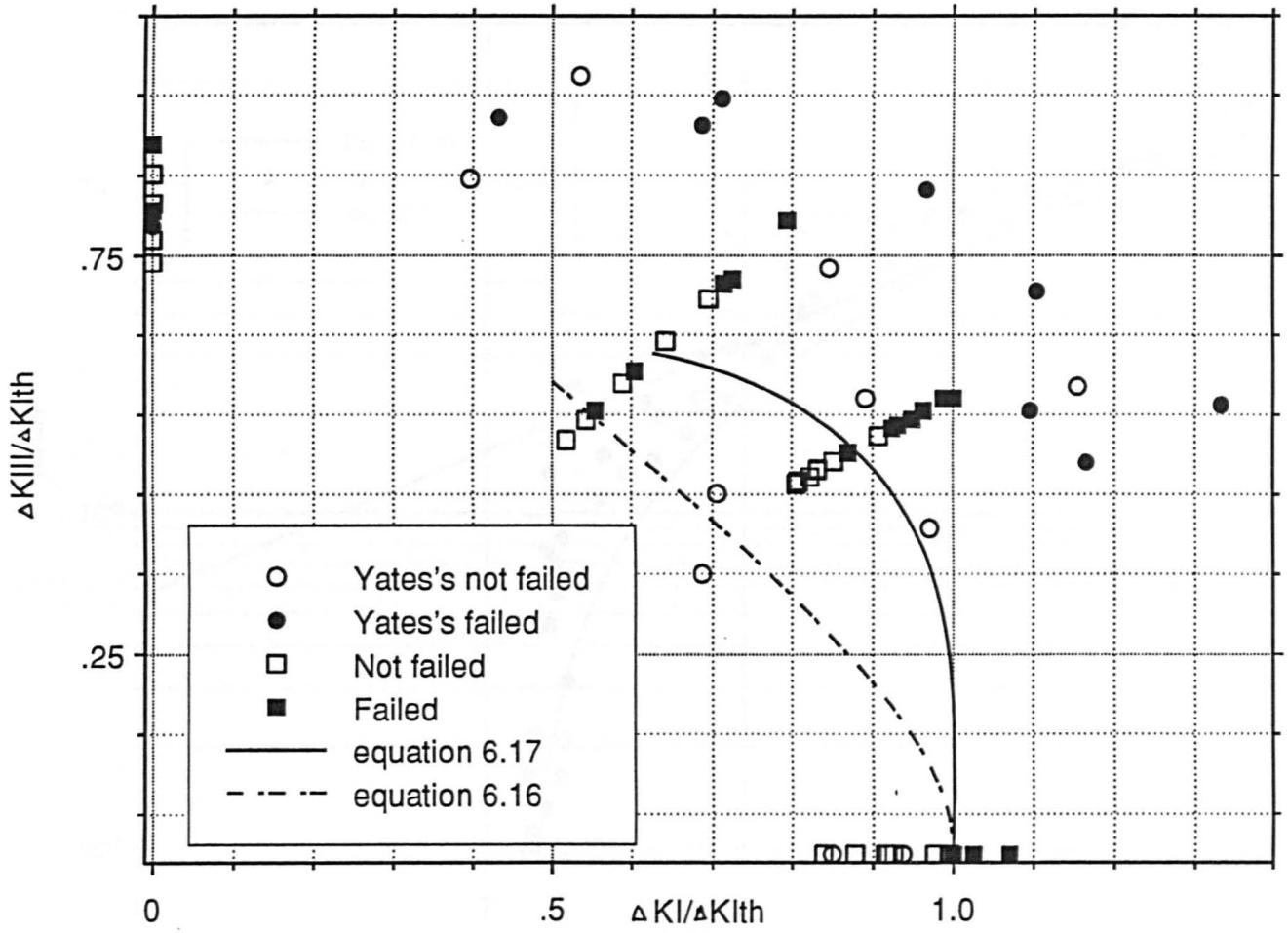

Fig.(7.26) The present research Mixed mode I & III data for different R ratios compared to Yates's results with respect to Pook's & Yates's failure criteria.

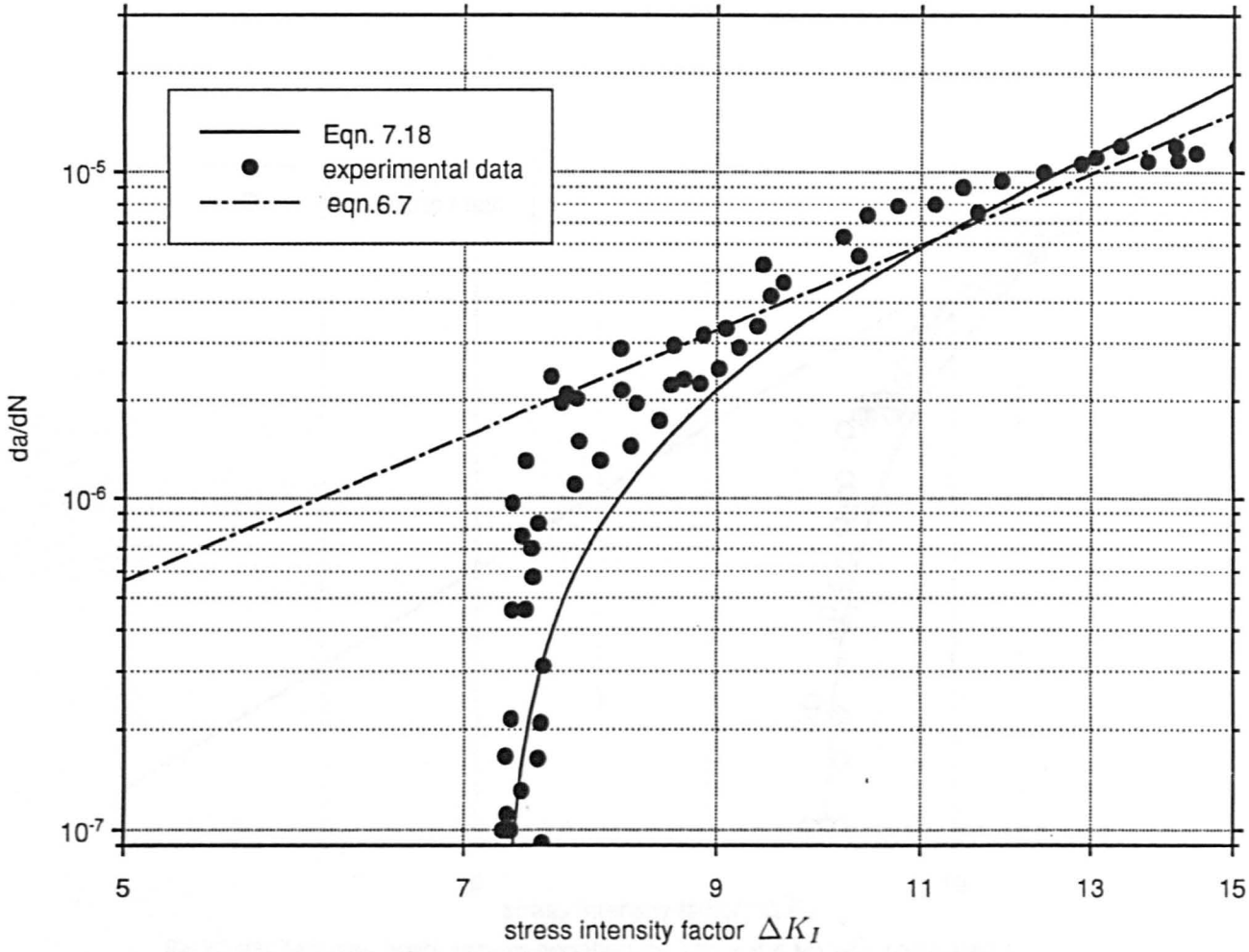

Fig.(7.27) The new crack growth equation compared to mixed mode I & III results (slit angle 60 deg., R = 0.5) and Paris equation.

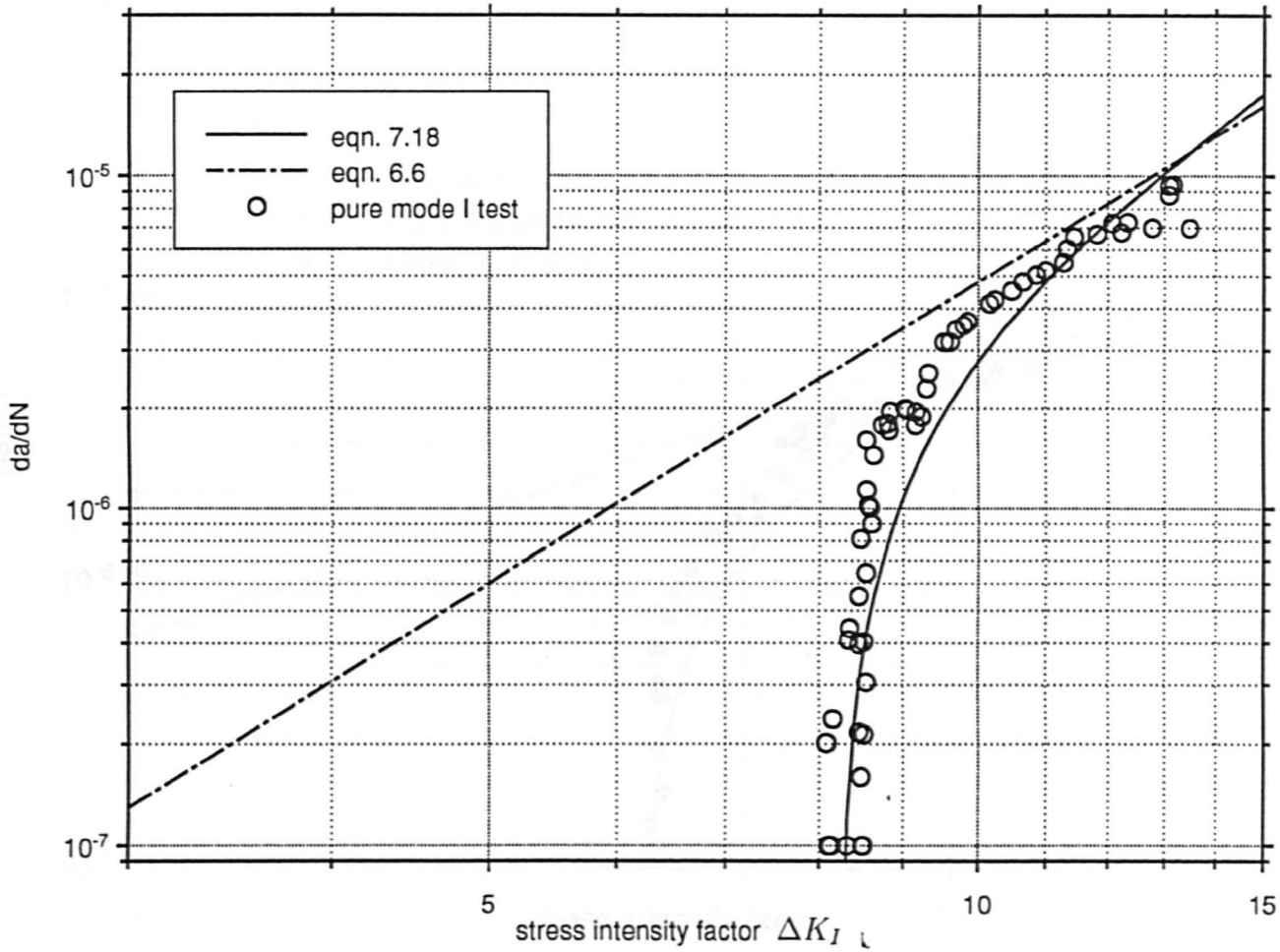

Fig.(7.28) The new crack growth equation for KIth = 8.4 MPa$\sqrt{m}$ compared to mixed mode I & III crack growth in a 45 deg. slit specimen with R = 0.17 and Paris equation for the same test.

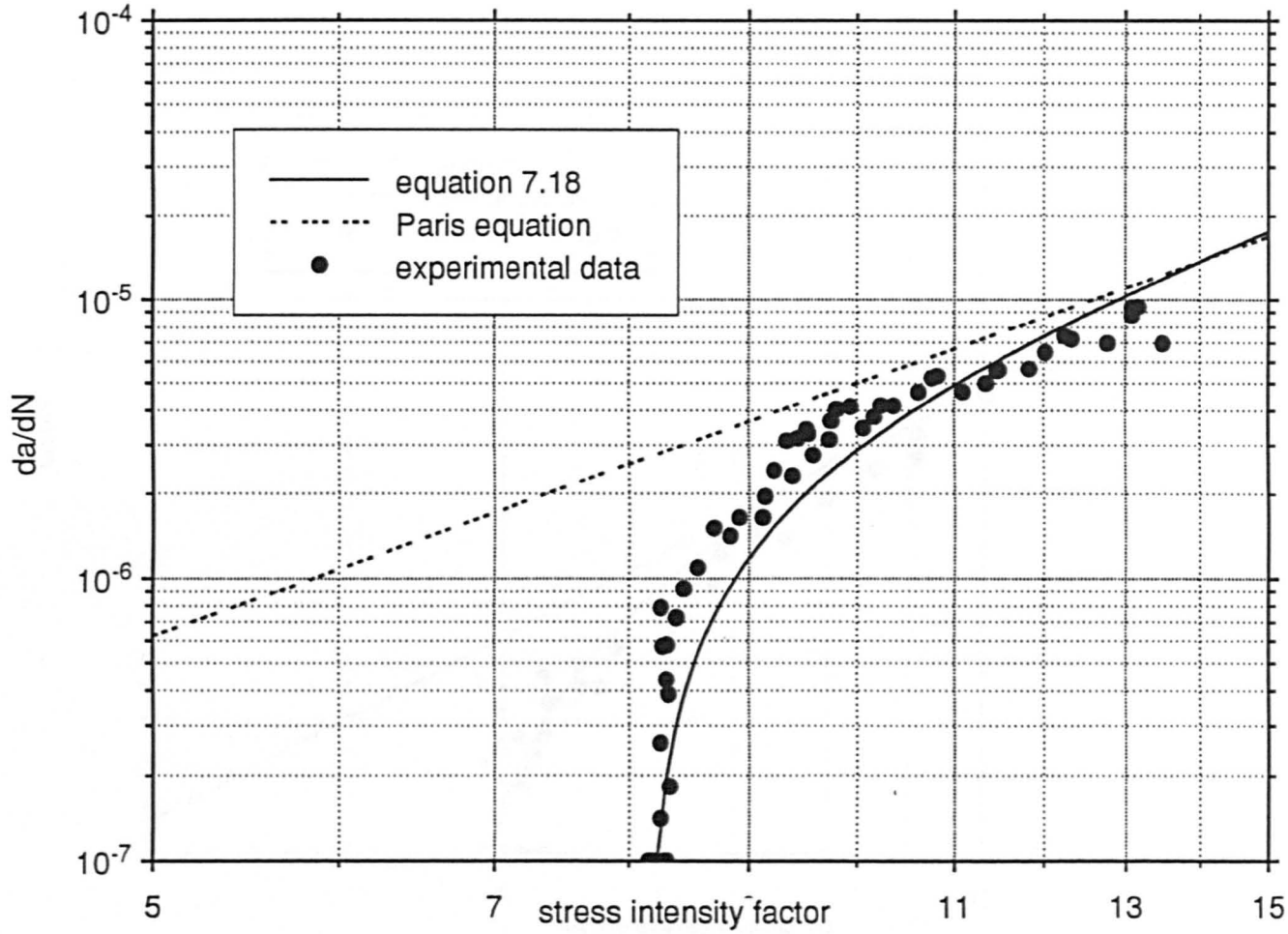

Fig.(7.29) The new crack growth equation applied to a 60 deg. slit specimen with an R ratio = 0.5 under mixed mode I & III loading.

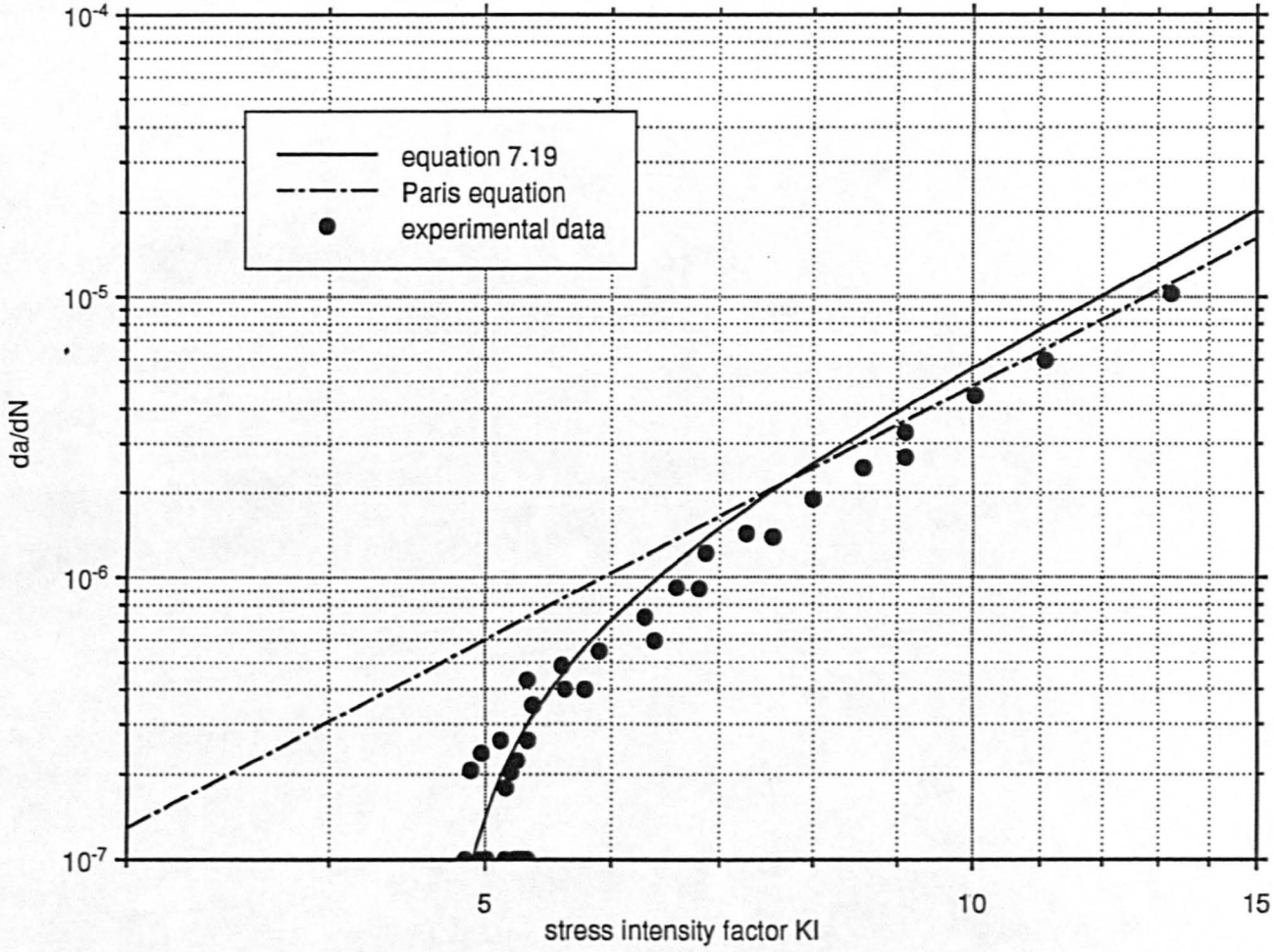

Fig.(7.30) The new crack growth equation applied to a 45 deg. slit specimen with an R ratio = 0.17 under mixed mode I & III loading where the threshold stress intensity factor = 5. MPa$\sqrt{m}$.